

DEVELOPMENT OF AN FT-NIR METHOD TO PREDICT
PROCESS CHEESE FUNCTIONALITY

A THESIS
SUBMITTED TO THE FACULTY OF THE
UNIVERSITY OF MINNESOTA
BY

Lisa Margo Chou

IN PARTIAL FULLFILMENT OF THE REQUIREMENTS
FOR THE DEGREE OF
MASTER OF SCIENCE

Tonya C. Schoenfuss, Ph.D.

February 2021

Acknowledgements

I would like to sincerely thank Dr. Tonya Schoenfuss for her support, knowledge, and patience throughout my graduate research and for sharing her love of dairy products and product development throughout countless dairy product judging trainings and sharing of product development competition advice. I'd also like to thank my committee members, Dr. Pam Ismail and Dr. Craig Hedberg, and the rest of the University of Minnesota (UMN) Food Science and Nutrition department faculty and staff.

There are several other organizations and individuals without whom I couldn't have done this research. I was fortunate enough to receive funding for this work through the UMN Graduate School Diversity Office's Community of Scholars Program and the Midwest Dairy Foods Research Center. I'd also like to thank Ray Miller and Mitchell Maher from the UMN pilot plant, who helped me with the pilot-level production of my process cheese. I'm grateful for AMPI and Tom Berry, who provided cheese when unexpected circumstances almost halted the whole project. Mark Sanders, Mary Brown, and Guillermo Marques from the UMN University Imaging Center were essential resources for my microscopy work. Mark Sullivan and the Büchi Corporation helped with the FT-NIR equipment, software, and calibration development. Lastly, Aaron Rendahl from the UMN College of Veterinary Medicine made completing my statistical analysis more understandable and reproducible.

A special thanks to all of my Lab 107 lab mates, FSCN friends, and lifelong friends who have helped me learn, grow, and have fun throughout my graduate experience. Last but not least, I wouldn't be the person I am now without the amazing role models of my mom, dad, and older brother. Thanks for all your support.

Abstract

Process cheese (PC) production involves using natural cheese, other dairy and non-dairy ingredients, heating, mixing, and cooling to form a final product. The properties of natural cheese, in particular, can be difficult to measure or control, leading to process cheese products with undesirable functional properties that may not be apparent until after cooling. Fourier-Transform Near Infrared (FT-NIR) spectroscopy methods exist for measuring fat and moisture in process cheese (Kapoor & Metzger, 2008) and could be a promising tool for predicting PC properties later in shelf life. In our study, calibrations were developed to correlate FT-NIR spectra of rapidly-cooled PC samples made at benchtop and pilot level production to several functional properties later in shelf life. Properties included heated sauce viscosity, oven melt area, firmness, and fat droplet size. Benchtop and pilot level PC samples were made with cheddar cheese of two different ages, cooked at two mixing speeds, and held at two hold times once final temperature was reached. Sample spectra were collected using a BUCHI NIRFlex N-500 FT-NIR spectrometer (BUCHI Labortechnik AG, CH). NIRCal 5.2 Chemometric Software (BUCHI Labortechnik) was used to correlate the spectra to functional properties using a cross-validation model and partial least squares regression. Across both the benchtop level and pilot level production of PC, 5 and 14 FT-NIR calibration models were created, respectively. Calibration models were developed using the chemometric software calibration wizard and optimized to achieve highest correlation coefficient and minimize standard error by adjusting pretreatments, spectral regions, and quantity of principal components. Many calibration models of different properties (melt area, viscosity, and firmness at different time points) achieved correlation coefficients above 0.6. These findings show that FT-NIR spectroscopy analysis of rapidly-cooled PC samples show potential to be used for predicting fat droplet size, PC sauce viscosity, and oven melt diameter of samples later in shelf life. Further calibrations of molten PC to final properties would show the feasibility of using a rapid, in-line FT-NIR method for process and quality control purposes.

Table of Contents

Acknowledgements	iii
Abstract.....	iv
Table of Contents	v
List of Tables	viii
List of Figures.....	x
CHAPTER 1: INTRODUCTION.....	1
CHAPTER 2. REVIEW OF LITERATURE	2
2.1 Process Cheese History, Economics, & Trends.....	2
2.2 Process Cheese Overview	3
2.2.1 Process Cheese Standards	3
2.3 Composition and ingredient effects on process cheese functionality	4
2.3.1 Natural Cheese	4
2.3.1.1 Milk.....	5
2.3.1.2 Cheese Making.....	5
2.3.1.3 Ripening & Proteolysis	6
2.3.2 Fat	8
2.3.3 Moisture	9
2.3.4 Calcium	9
2.3.5 Emulsifying Salts	9
2.3.5.1 Mechanisms	9
2.3.5.2 Types of emulsifying salts	10
2.3.6 Other Ingredients	13
2.4 Processing effects on process cheese functionality	13
2.4.1 Mixing & Cooking Properties.....	13
2.4.2 Cooling Rate	15
2.4.3 Other factors.....	16
2.5 Process cheese microstructure	16
2.6 Methods of analyzing and predicting functional properties	17
2.6.1 Melt Tests & Rheological Methods	18
2.6.1.1 Arnott	18
2.6.1.2 Schreiber/USDA Melt Test.....	18
2.6.1.3 Microwave Oven Tests	19
2.6.1.4 Differential Scanning Calorimetry (DSC)	19
2.6.1.5 Tube Melt Test.....	19
2.6.1.6 Dynamic Stress Rheometry.....	20
2.6.1.7 Rapid Visco Analyzer (RVA).....	20
2.6.1.8 Micro Visco Amylograph (MVAG)	21
2.6.1.9 Texture Profile Analysis (TA.XT).....	21
2.6.2 Spectroscopic Methods	21
2.6.2.1 Front Face Fluorescence Spectroscopy	22
2.6.2.2 Dielectric Spectroscopy	22

2.6.2.3 Time Domain Nuclear Magnetic Resonance Spectroscopy.....	23
2.6.2.4 Confocal Raman Microscopy	23
2.6.2.5 Confocal laser scanning microscopy (CLSM).....	24
2.6.2.6 Mid-Infrared and Near-Infrared Spectroscopy	27
2.6.2.7 Chemometrics	30
2.7 Conclusion	37

CHAPTER 3: DEVELOPMENT OF A BENCHTOP METHOD TO PRODUCE PROCESS CHEESE USING A THERMOMIX & OF A RAPID METHOD TO PREDICT PROCESS CHEESE FUNCTIONALITY..... 38

3.1 Synopsis	38
3.2 Introduction.....	39
3.3 Materials and Methods.....	40
3.3.1 Thermomix Formula & Method.....	40
3.3.2 Viscosity Analysis	41
3.3.3 Melt Area Analysis	41
3.3.4 NIR Scanning & Chemometric Analysis.....	41
3.3.5 Statistics	42
3.4 Results and Discussion	43
3.4.1 Sauce Viscosity Functional Results.....	43
3.4.2 Sauce Viscosity FT-NIR Calibration Results	44
3.4.2.1 Viscosity at 40°C	44
3.4.2.2 Viscosity at 45°C	48
3.4.2.3 Viscosity at 50°C	50
3.4.3 Melt Area Functional Results	53
3.4.4 Melt Area FT-NIR Calibration	54
3.4.5 Firmness Functional Results	57
3.4.6 Firmness FT-NIR Calibration.....	58
3.4.7 FT-NIR Calibration Summary	61
3.5 Conclusion and Future Research	62

CHAPTER 4: DEVELOPMENT OF A RAPID METHOD TO PREDICT PROCESS CHEESE FUNCTIONALITY..... 63

4.1 Synopsis	63
4.2 Introduction.....	64
4.3 Materials and Methods.....	65
4.3.1 Experimental Design.....	65
4.3.2 Process Cheese Spread Formulation and Manufacture.....	65
4.3.3 Compositional Analysis.....	67
4.3.4 Functional Analysis	68
4.3.4.1 Sauce Viscosity.....	68
4.3.4.2 Melt Area	68
4.3.4.3 Texture Profile Analysis	69
4.3.4.4 Fat Droplet Size Analysis - Confocal Laser Scanning Microscopy	69
4.3.5 Spectroscopic Analysis	71
4.3.6 Statistics	72

4.4 Results and Discussion	73
4.4.1 Compositional Analysis	73
4.4.2 Functional Analysis	74
4.4.2.1 Sauce Viscosity	74
4.4.2.2 Melt Area	78
4.4.2.3 Firmness	79
4.4.2.4 Fat Droplet Size Analysis with CLSM	81
4.4.3 FT-NIR Calibrations	88
4.4.3.1 Sauce Viscosity – 40°C (Time 1)	89
4.4.3.2 Sauce Viscosity – 40°C (Time 2)	91
4.4.3.3 Sauce Viscosity – 45°C (Time 1)	94
4.4.3.4 Sauce Viscosity – 45°C (Time 2)	96
4.4.3.5 Sauce Viscosity – 50°C (Time 1)	98
4.4.3.6 Sauce Viscosity – 50°C (Time 2)	101
4.4.3.7 Melt Area (Time 1)	103
4.4.3.8 Melt Area (Time 2)	106
4.4.3.9 Firmness (Time 1)	108
4.4.3.10 Firmness (Time 2)	110
4.4.3.11 CLSM – Number of Fat Droplets	113
4.4.3.12 CLSM – Average Fat Droplet Volume	115
4.4.3.13 CLSM – Average Fat Droplet Diameter	117
4.4.3.14 CLSM – Median Fat Droplet Diameter	120
4.4.3.14 FT-NIR Calibrations Calibration Summary	122
4.5 Conclusion	122
CHAPTER 5: REFERENCES	124
CHAPTER 6: APPENDIX	140
6.1 Functional Analysis Method SOPs	140
6.1.1 MVAG Viscosity Analysis	140
6.1.2 Schreiber Oven Melt Method	141
6.1.3 TA.XT Firmness Analysis Method	142
6.1.4 CLSM Method	143
Sample staining	143
Sample scanning steps for spectral filters and final image acquisition ..	144
Flow chart for spectral filter development	146
Spectral filter development and application steps	147
Fiji image adjustment & droplet quantification	148
6.2 Statistical Analysis R code	151
6.2.1 R code for two-way ANOVA of Thermomix sample data	151
6.2.2 R code for graphs of Thermomix sample data	153
6.2.3 R code for split-plot ANOVA of Blentech sample data	154
6.2.4 R code for graphs of Blentech data	161
6.3 Supplemental NIR tools	164

List of Tables

Table 1. Pasteurized PC types and standards from 21 CFR 133.169 to 133.180 (FDA, 2018). All values are in the unit of weight/weight of the final product.....	4
Table 2. Emulsifying salts permitted in the US (FDA, 2009).....	11
Table 3. NIRCal tools for PC selection (BÜCHI, 2016).....	36
Table 4. Starting Cheddar composition (left), PC spread target composition (bottom left) standardized for moisture, fat, and protein, and resulting PC formula by percent (bottom right) for Thermomix benchtop level production split by 1-month and 8-month Cheddar.	40
Table 5. Average viscosity results (cP) across the three temperature ranges of 40°C, 45°C, and 50°C. Age = natural cheese age, MS = mixing speed, and HT = hold time. Lowercase letters indicate a difference within the temperature range (P<0.01), n=4. The only difference found was according to age.	43
Table 6. Two-way ANOVA p-value results for average viscosity at 40°C, 45°C, and 50°C across factors and interactions between factors. ** indicates difference (P<0.01). See appendix for exact age p-values. Age = natural cheese age, MS = mixing speed and HT = hold time. n=32.	43
Table 7. Average melt area results (in ²), n=3. Age = natural cheese age, MS = mixing speed, and HT = hold time. No differences were found by age, MS, or HT (P<0.05).	53
Table 8. Two-way ANOVA p-value results for average melt area across factors and interaction between factors. See appendix for exact Age p-values. No differences were found by age, MS, or HT (P<0.05), n=24. Age = natural cheese age, MS = mixing speed, and HT = hold.	53
Table 9. Average firmness results (g), n=2. Age = natural cheese age, MS = mixing speed, and HT = hold time. No differences were found by age, MS, or HT (P<0.05).	57
Table 10. Two-way ANOVA p-value results for average firmness across factors and interactions between factors. No differences were found by age, MS, or HT (P<0.05). Age = natural cheese age, MS = mixing speed, and HT = hold time, n=16.	58
Table 11. Calibration equation statistics using cross-validation and regression model for Thermomix PC sample functional properties. Spectra N indicates the number of spectra used, but there were approximately 3 spectra per unique PC sample. 1°/2° PCs = number of primary/secondary PCs used; PT = pretreatment, SEC = standard error of calibration; SECV = standard error of cross-validation; C r ² = calibration regression coefficient, CV r ² = cross-validation regression coefficient; Q-value = Büchi quality value.	61
Table 12. Original Cheddar composition (left), PC spread target composition by percent standardized for moisture, fat, and total protein (below, left), and resulting PC formula by percent (below, right) for Blentech pilot-level production.	67
Table 13. NIRCal Calibration Properties	72

Table 14. Summary of composition across eight unique samples of cheese (N=2). 3-month & 8-month indicate natural cheese age used to make PC; MS = mixing speed (rpm); HT = hold time (min). Values within a row not sharing a common superscript significantly differed. (P<0.05).....	74
Table 15. Average viscosity results (cP), n=2, across three temperatures of 40°C, 45°C, and 50°C and two shelf life time points (T1 = 2 wks past mfg, T2 = 4 wks past mfg). Superscript lowercase letters indicate a difference across the factor of age (P<0.05).....	76
Table 16. Viscosity split-plot ANOVA p-values, with the averaged 4-sample block for Age and MS factor, and second 8-sample block for HT and interactions. Age = natural cheese age, MS = mixing speed, and HT = hold time. Asterisks indicate a significant p-value (P<0.05).....	76
Table 17. Average melt area values (sq. inches), across two shelf life time points. T1 = 2 weeks past manufacture, T2 = 4 weeks past manufacture, Age = natural cheese age, MS = mixing speed, HT = hold time. No differences were found across factors of age, MS, or HT (P<0.05). N=2.	79
Table 18. Melt area split-plot ANOVA p-values across factors and interaction of factors at two shelf life time points. T1 = 2 weeks past mfg, T2 = 4 weeks past mfg. Age = natural cheese age, MS = mixing speed, HT = hold time. No differences were found (P<0.05).	79
Table 19. Average firmness values (g of force), across two shelf life time points. T1 = 2 wks past mfg, T2 = 4 wks past mfg, Age = natural cheese age, MS = mixing speed, HT = hold time. Superscript lowercase letters indicate a difference across age for T1, but no other differences were found (P<0.05). N=2.	80
Table 20. Firmness split-plot ANOVA p-values across factors and interaction of factors at two shelf life time points. T1 = 2 weeks past mfg, T2 = 4 weeks past mfg. Age = natural cheese age, MS = mixing speed, HT = hold time. Differences were found (P<0.05) for the factor of Age for T1, but not for T2 or any other factors or interactions.	80
Table 21. Average CLSM fat droplet measurements for the number of droplets per 636µm ² image, average volume, average Feret diameter, and median Feret diameter. Age = natural cheese age, MS = mixing speed, HT = hold time. No differences were found (P<0.05). N=2.	82
Table 22. CLSM fat droplet measurement split-plot ANOVA p-values across factors and interactions of factors. Age = natural cheese age, MS = mixing speed, HT = hold time. Asterisk indicates p-value < 0.05.....	82
Table 23. Calibration equation statistics using cross-validation and regression model for Blentech PC sample functional properties. Spectra N indicates the number of spectra used, but there were approximately 3 spectra per unique PC sample. 1°/2° PCs = the quantity of primary and secondary principal components. PT = pretreatments used. SEC = standard error of calibration; SECV = standard error of cross-validation; C r ² = calibration regression coefficient, CV r ² = cross-validation regression coefficient.	88

List of Figures

Figure 1. Example of calcium phosphate salts binding to a protein structure at an oil-water interface (Shimp, 1985).....	10
Figure 2. The model microstructure of (a) natural cheese and (b) process cheese (Kapoor and Metzger, 2008)	16
Figure 4. Büchi N-500 NIRFlex measuring cell designs for different sample modes, including transfectance (above, left and right), diffuse reflection (right), transmission (below, left), and diffuse transmission (below, right). (Büchi, 2017).	28
Figure 3. Büchi N-500 NIRFlex internal assembly (Büchi, 2017).	28
Figure 5. NIR spectra of PC samples (Woodcock et al, 2007)	33
Figure 6. Sample viscosity results as initial MVAG format with both viscosity and temperature on the y-axes and time on the x-axis (left) and adjusted result with time excluded and only viscosity vs temperature (right). Average viscosities at 50C, 45C, and 40C per sample were used for further summaries.	41
Figure 7. CV Group Selector	42
Figure 8. PC sauce viscosity (cP) at 40°C, 45°C, and 50°C (right axis) across samples with different natural cheese age (upper x-axis, 1 & 8 months), mixing speeds (lower x-axis, 410 & 1015 rpm), and hold time (legend, 0.5 & 3 min), n=32. x-points represent mean and error bars represent one standard error. Boxes and asterisks indicate rows with differences according to age (P < 0.05).	44
Figure 9. Viscosity at 40°C CV calibration regression coefficients (left) and standard error of cross-validation (SECV, right). Wavenumber region used for calibration was 5,000-10,000 cm ⁻¹ and 4 PCs were used for primary PC selection.....	45
Figure 10. Viscosity at 40°C CV calibration original spectra (left) and pretreated spectra (right). Pretreated spectra used pretreatments 1st BCAP 5 points (db1), followed by normalization by closure (ncl).	45
Figure 11. Viscosity (cP) at 40°C CV property residuum vs. original property (top), predicted property vs. original property of calibration (middle), and predicted property vs original property of cross-validation (bottom).....	47
Figure 12. Viscosity at 45°C CV calibration original spectra (left) and pretreated spectra (right). Pretreated spectra used pretreatments first derivative BCAP (db1).	48
Figure 13. Viscosity at 45°C CV calibration regression coefficients (left) and standard error of cross-validation (SECV, right). Wavenumber region used for calibration was 4,000-10,000 cm ⁻¹ and 6 primary PCs and 2 secondary PCs used	48
Figure 14. Viscosity at 45°C CV calibration property residuum vs. original property (top) and predicted property vs. original property (bottom).	49
Figure 15. Viscosity at 50°C CV calibration original spectra (left) and pretreated spectra (right). Pretreated spectra used pretreatments normalization by closure (ncl), followed by 1st BCAP 5 points (db1).	51

Figure 16. Viscosity at 50°C CV calibration regression coefficients (left) and standard error of cross-validation (SECV, right). Wavenumber region used for calibration was 4,000-7,144 and 7404-10,000 cm^{-1} and 4 PCs were used for primary PC selection.	51
Figure 17. Viscosity at 50°C CV property residuum vs. original property (top), predicted property vs. original property of calibration spectra (middle), and predicted property vs. original property of CV spectra (bottom).	52
Figure 18. Melt area (sq in) across samples with different natural cheese age (upper x-axis, 1 & 8 months), mixing speeds (lower x-axis, 410 & 1015 rpm), and hold time (legend, 0.5 & 3 min), n=24. X-shaped points represent the mean and error bars represent one standard error.	54
Figure 19. Melt area CV calibration regression coefficients (left) and standard error of cross-validation (SECV, right). Wavenumber region used for calibration was 4,000-7,144 and 7404-10,000 cm^{-1} and 6 PCs used for primary and secondary PC selection.	55
Figure 20. Melt area CV calibration original spectra (left) and pretreated spectra (right). Pretreated spectra used pretreatments of standard normal variate (SNV) and first derivative BCAP (db1).	55
Figure 21. Melt area CV property residuum vs. original property (top), predicted property vs. original property of calibration spectra, n=48 (middle), and predicted property vs. original property of CV spectra (bottom).	56
Figure 22. PC firmness (g) across samples with different natural cheese age (upper x-axis, 1 & 8 months), mixing speeds (lower x-axis, 410 & 1015 rpm), and hold time (legend, 0.5 & 3 min), n=16. X-shaped points represent the mean and error bars represent one standard error.	58
Figure 23. Firmness CV calibration regression coefficient (left) and standard error of cross-validation (SECV, right). Wavenumber region used for calibration was 4,400-4,800, 5,400-6,600, and 7,800-10,000. 4 primary PCs and 3 secondary PCs were used.	59
Figure 24. Firmness CV calibration original spectra (left) and pretreated spectra (right). Pretreatment used was Kubelka Munk (kmu).....	59
Figure 25. Firmness CV calibration property residuum vs. original property (top), predicted property vs. original property for calibration (middle), and predicted property vs. original property for CV (bottom).....	60
Figure 26. Pilot-scale PC spread manufacturing flowchart. Mixing speed 4 and 8 represent 150 and 265 rpms, respectively.....	66
Figure 27. Sample viscosity results as initial output with both viscosity and temperature on y-axes and time on the x-axis (left) and adjusted result with time excluded and only viscosity vs temperature (right). Average viscosities were taken at 50°C, 45°C, and 40°C.	68
Figure 28. CV Group Selector	72
Figure 29. PC sauce viscosity (cP) at three temperatures (right y-axis, 40C, 45C, and 50C), two time points after manufacture (right y-axis, 2 & 4 weeks after mfg) and across samples with different natural cheese age (upper x-axis, 3 & 8 months), mixing speeds	

(lower x-axis, 150 & 265 rpm), and hold time (legend, 1 & 3 min). Rows surrounded by boxes and an asterisk indicate difference across the factor of age (P<0.05). 75

Figure 30. Interaction plots for viscosity at 40°C (T2) (top) and at 50°C (T2) (bottom) across factors of natural cheese age (upper x-axis, 3 & 8 months), mixing speeds (lower x-axis, 150 & 265 rpm), and hold time (legend, 1 & 3 min). 77

Figure 31. PC oven melt area (sq in) at two time points after manufacture (right y-axis, 2 & 4 weeks after mfg) and across samples with different natural cheese age (upper x-axis, 3 & 8 months), mixing speeds (lower x-axis, 150 & 265 rpm), and hold time (legend, 1 and 3 min) 79

Figure 32. Firmness (g), at two time points after manufacture (legend, 2 & 4 weeks after mfg) and across samples with different natural cheese age (lower x-axis, 3 & 8 months), mixing speeds (legend, 150 & 265 rpm), and hold time (upper x-axis, 1 and 3 min). Asterisk and box indicate a difference (P<0.05) across the factor of age. N=2. 81

Figure 33. Examples of differences in diameter measurements for non-spherical shapes, such as the difference between maximum Feret diameter (Fmax) and minimum Feret diameter (Fmin). Spherical shapes have the same diameter (d) regardless of the angle of measurement. 81

Figure 34. CLSM measurements across samples with different natural cheese age (upper x-axis, 3 & 8 months), mixing speeds (lower x-axis, 150 & 265 rpm), and hold time (legend, 1 and 3 min). Individual graphs represent the number of fat droplets within a 636µm² image (top) and average fat droplet volume (bottom). 83

Figure 35. CLSM measurements across samples with different natural cheese age (upper x-axis, 3 & 8 months), mixing speeds (lower x-axis, 150 & 265 rpm), and hold time (legend, 1 and 3 min). Individual graphs represent average Feret diameter (µm, top) and median Feret diameter (µm, bottom). 84

Figure 36. CLSM fat droplet images for 8 unique cheese samples (numbers 1-8), with the red and black original lipid-stained images (A) and multi-color Fiji-adjusted images for fat droplet quantification (B). Images here are of a single z-plane from a collected z-stack of 20-30 images. Full stacks were used for quantification purposes. Scale bar in lower right corners represents 50µm. Identical samples are grouped vertically (1A + 1B, 2A+2B, etc)..... 85

Figure 37. Fat droplet Feret diameter distribution curves across the 8 unique PC samples, with the number of droplets across each diameter range. Depending on the shape of the distribution curve, the median diameters (triangles) and average diameters (circles) are often different..... 86

Figure 38. Interaction plots for viscosity at 40°C (T2) (top) and at 50°C (T2) (bottom) across factors of natural cheese age (upper x-axis, 3 & 8 months), mixing speeds (lower x-axis, 150 & 265 rpm), and hold time (legend, 1 & 3 min). 87

Figure 39. Viscosity at 40°C (Time1) CV calibration original spectra (left) and pretreated spectra (right). Pretreated spectra used pretreatments standard normal variate (snv). 89

Figure 40. Viscosity at 40°C (Time1) CV calibration regression coefficients (left) and standard error of cross-validation (SECV, right). Wavenumber region used for calibration was 5,000-10,000 cm⁻¹ and 6 PCs used for primary and secondary PC selection. 89

Figure 41. Viscosity at 40°C (Time1) CV calibration property residuum vs. original property (top), predicted property vs. original property of calibration (middle), and predicted property vs original property of CV (bottom).....	90
Figure 42. Viscosity at 40°C (Time2) CV calibration original spectra. No pretreatments were used for final calibration.	92
Figure 43. Viscosity at 40°C (Time2) CV calibration regression coefficients (top) and standard error of cross-validation (SECV, bottom). Wavenumber region used for calibration was 4,000-7,144 and 7404-10,000 cm^{-1} and 2 PCs used for primary and secondary PC selection.	92
Figure 44. Viscosity at 40°C (Time2) CV calibration property residuum vs. original property (top), predicted property vs. original property of calibration (middle), and predicted property vs original property of CV (bottom).....	93
Figure 45. Viscosity at 45°C (Time1) CV calibration original spectra (top) and pretreated spectra (bottom). No pretreatments were used for final calibration.	94
Figure 46. Viscosity at 45°C (Time1) CV calibration regression coefficients (top) and standard error of cross-validation (SECV, bottom). Wavenumber region used for calibration was 4,000-7,144 and 7404-10,000 cm^{-1} and 3 PCs used for primary PC selection.	94
Figure 47. Viscosity at 45°C (Time1) CV calibration property residuum vs. original property (top), predicted property vs. original property of calibration (middle), and predicted property vs original property of CV (bottom).....	95
Figure 48. Viscosity at 45°C (Time2) CV calibration original spectra (top) and pretreated spectra (bottom). Pretreated used include 1st BCAP 5 points (db1), followed by normalization by closure (ncl).	96
Figure 49. Viscosity at 45°C (Time2) CV calibration regression coefficients (top) and standard error of cross-validation (SECV, bottom). Wavenumber region used for calibration was 4,000-10,000 cm^{-1} and 2 PCs used for primary PC selection.....	96
Figure 50. Viscosity at 45°C (Time2) CV calibration property residuum vs. original property (top), predicted property vs. original property of calibration (middle), and predicted property vs original property of CV (bottom).....	97
Figure 51. Viscosity at 50°C (Time1) CV calibration regression coefficients (top) and standard error of cross-validation (SECV, bottom). Wavenumber region used for calibration was 5,000-10,000 cm^{-1} and 7 PCs used for primary PC selection.....	99
Figure 52. Viscosity at 50°C (Time1) CV calibration original spectra (top) and pretreated spectra (bottom). Pretreated used was normalization by closure (ncl).	98
Figure 53. Viscosity at 50°C (Time1) CV calibration property residuum vs. original property (top), predicted property vs. original property of calibration (middle), and predicted property vs original property of CV (bottom).....	100
Figure 54. Viscosity at 50°C (Time2) CV calibration original spectra (top) and pretreated spectra (bottom). No pretreatments were used for final calibration.	101

Figure 55. Viscosity at 50°C (Time2) CV calibration regression coefficients (top) and standard error of cross-validation (SECV, bottom). Wavenumber region used for calibration was 4,000-10,000 cm ⁻¹ and 2 PCs used for primary PC selection.....	101
Figure 56. Viscosity at 50°C (Time2) CV calibration property residuum vs. original property (top), predicted property vs. original property of calibration (middle), and predicted property vs original property of CV (bottom).....	102
Figure 57. Melt area (Time1) CV calibration regression coefficients (top) and standard error of cross-validation (SECV, bottom). Wavenumber region used for calibration was 4,000-7,144 and 7404-10,000 cm ⁻¹ and 3 PCs used for primary PC selection.	104
Figure 58. Melt area (Time1) CV calibration original spectra (top) and pretreated spectra (bottom). Pretreated used include 1st BCAP 5 points (db1), followed by normalization by closure (ncl).	104
Figure 59. Melt area (Time1) CV calibration property residuum vs. original property (top), predicted property vs. original property of calibration (middle), and predicted property vs original property of CV (bottom).....	105
Figure 60. Melt area (Time2) CV calibration original spectra (top) and pretreated spectra (bottom). Pretreatment used was 1st BCAP 5 points (db1).	106
Figure 61. Melt area (Time2) CV calibration regression coefficients (top) and standard error of cross-validation (SECV, bottom). Wavenumber region used for calibration was 5,000-10,000 cm ⁻¹ and 2 PCs used for primary PC selection.	106
Figure 62. Melt area (Time2) CV calibration property residuum vs. original property (top), predicted property vs. original property of calibration (middle), and predicted property vs original property of CV (bottom).....	107
Figure 64. Firmness (Time1) CV calibration regression coefficients (top) and standard error of cross-validation (SECV, bottom). Wavenumber region used for calibration was 4,400-4,800, 5,400-6,600, and 7,800-10,000 cm ⁻¹ and 2 PCs used for primary PC selection.	108
Figure 63. Firmness (Time1) CV calibration original spectra (top) and pretreated spectra (bottom). Pretreatment used was Kubelka Munk (kmu).....	108
Figure 65. Firmness (Time1) CV calibration property residuum vs. original property (top), predicted property vs. original property of calibration (middle), and predicted property vs original property of CV (bottom).....	109
Figure 67. Firmness (Time2) CV calibration original spectra (top) and pretreated spectra (bottom). Pretreatment used was Kubelka Munk (kmu).....	111
Figure 66. Firmness (Time2) CV calibration regression coefficients (top) and standard error of cross-validation (SECV, bottom). Wavenumber region used for calibration was 5,000-10,000 cm ⁻¹ and 2 PCs used for primary PC selection.	111
Figure 68. Firmness (Time2) CV calibration property residuum vs. original property (top), predicted property vs. original property of calibration (middle), and predicted property vs original property of CV (bottom).....	112

Figure 69. CLSM average number of fat droplets CV calibration original spectra (top) and pretreated spectra (bottom). Pretreated used include normalization by closure (ncl), followed by 1st BCAP 5 points (db1).....	113
Figure 70. CLSM average number of fat droplets CV calibration regression coefficients (top) and standard error of cross-validation (SECV, bottom). Wavenumber region used for calibration was 4,000-10,000 cm^{-1} and 2 PCs used for primary PC selection.	113
Figure 71. CLSM average number of fat droplets CV calibration property residuum vs. original property (top) and predicted property vs. original property (bottom).	114
Figure 72. CLSM average fat droplet volume CV calibration original spectra (top) and pretreated spectra (bottom). Pretreatment used was Savitzky-Gola 9 points (sg9).	115
Figure 73. CLSM average fat droplet volume CV calibration regression coefficients (top) and standard error of cross-validation (SECV, bottom). Wavenumber region used for calibration was 5,000-10,000 cm^{-1} and 2 PCs used for primary PC selection.....	115
Figure 74. CLSM average fat droplet volume CV calibration property residuum vs. original property (top), predicted property vs. original property of calibration (middle), and predicted property vs original property of CV (bottom).	116
Figure 75. CLSM average fat droplet Feret diameter CV calibration original spectra (top) and pretreated spectra (bottom). Pretreated used include standard normal variate (SNV), followed by 1st BCAP 5 points (db1).6.....	118
Figure 76. CLSM average fat droplet Feret diameter CV calibration regression coefficients (top) and standard error of cross-validation (SECV, bottom). Wavenumber region used for calibration was 5,000-10,000 cm^{-1} and 3 PCs used for primary PC selection.	118
Figure 77. CLSM average fat droplet Feret diameter CV calibration property residuum vs. original property (top), predicted property vs. original property of calibration (middle), and predicted property vs original property of CV (bottom).	119
Figure 78. CLSM median fat droplet Feret diameter CV calibration original spectra (top) and pretreated spectra (bottom). Pretreatment used was Savitzky-Golay 9 points (sg9).	120
Figure 79. CLSM median fat droplet Feret diameter CV calibration regression coefficients (left) and standard error of cross-validation (SECV, right). Wavenumber region used for calibration was 5,000-7,144 and 7404-10,000 cm^{-1} and 3 PCs used for primary PC select.....	120
Figure 80. CLSM median fat droplet Feret diameter CV calibration property residuum vs. original property (top), predicted property vs. original property of calibration (middle), and predicted property vs original property of CV (bottom).	121
Figure 81. NIR Band Assignment Table (Bruker, 2009).....	164

CHAPTER 1: INTRODUCTION

Process cheese (PC) manufacturers face an ongoing challenge: the ability to produce a final product with a stable emulsion and within specifications for functional properties. The causes of an unstable emulsion vary across ingredients, processing conditions, and even storage conditions. When unstable, the emulsion formed by the end of PC manufacture is not static and can continue to change in the subsequent weeks and months following manufacture (Kapoor and Metzger, 2008). The outcome of this ongoing challenge is inconsistent PC quality, high amounts of rework, wasted product, and overall lost profits. Many researchers have attempted to solve different parts of the challenge, from stronger ingredient and composition control (Adams et al., 1999, Biswas et al., 2004, Blazquez et al., 2004, Ma et al., 2019), improved processing control (Curda and Kukackova, 2004, Garimella Purna et al., 2006), and methods of predicting the final properties (Amamcharla and Metzger, 2015). In a PC manufacturing setting, rapid analysis methods are most desirable to allow for process or ingredient modification as early as possible. Many spectroscopic methods, such as fluorescence (Garimella Purna et al., 2005), MIR (Fagan et al., 2007a, Fagan et al., 2007b), NIR (Kapoor and Metzger, 2008, Ma et al., 2019), and dielectric spectroscopy (Amamcharla and Metzger, 2015) offer rapid results and have been explored for analysis and prediction of PC composition and properties. However, exact methods for analyzing PC after being rapidly cooled and correlating those spectra to functional properties later in shelf life has not yet been completed. With this background, we hope to investigate the ability of FT-NIR to scan rapidly-cooled spectra and use chemometrics to correlate those spectra to functional properties and emulsion structure later in shelf life. This goal is broken into two objectives: the first is to use FT-NIR spectroscopy to predict PC functionality produced at the benchtop-level; the second is to accomplish the same with PC produced at the pilot level. If methods for predicting PC functionality are successful, the impact of this research could allow for greater process control and increased quality across the approximately \$3 billion PC produced in the US (Cheese, US, October 2019).

CHAPTER 2. REVIEW OF LITERATURE

2.1 Process Cheese History, Economics, & Trends

Process cheese originated slightly over 100 years ago and is a fairly modern food product relative to natural cheese, which has existed for thousands of years. It was originally made in Germany in 1895, made in Switzerland in 1911, and made popular in the United States starting in 1916 by J. L. Kraft (Meyer, 1973, Berger et al., 1989, Guinee et al., 2004, Kapoor and Metzger, 2008). The invention of process cheese occurred as a way to extend the shelf life of natural cheese, to utilize cheese that could not be sold due to defects, and for increased trade (Meyer, 1973, Guinee et al., 2004). In the mid-1940s, process cheese became widely used as military rations due to its dense nutrient value and stability under adverse storage conditions (Price and Bush, 1974). Between 1977-1981, federal subsidies for the dairy industry led to surplus milk production and a 500 million pound government-owned stockpile of Cheddar cheese, which ultimately became 300 million pounds of process cheese distributed to low-income people and organizations (Donnelly, 2016, Blakemore, 2018). In fact, in the communities that received the process cheese, it became known as “government cheese” (Roots, 1999, Carter, 2013, Blakemore, 2018). The production of process cheese is likely to increase with the USDA’s \$12 billion farmer relief package announced in 2018 and with the current government stockpile of cheese reaching the largest in history at 1.4 billion pounds (Dewey, 2018, Hirtzer et al., 2018).

Process cheese sales and production trends have differed by geography throughout time. At the consumer level, total US retail sales of process cheese have decreased from \$4.16 billion in 2014 to \$3.67 billion in 2019 and are forecasted to fall 5% to be \$3.47 billion by 2024, despite continuous growth in sales of cheese products as a general category. As of August 2019, 34% of consumers claim to have consumed process cheese multiple times a week, while 55% have consumed it in the past three months (Cheese, US, October 2019). One theory for declining sales of process cheese within the US is a perception by as high as 77% of consumers that natural cheese is healthier than process cheese (Cheese, US, October 2019). Despite decreases in US consumer purchasing, the US continues to be the largest exporter of cheese, in

combination with global food service and fast food placing a growing demand for process cheese. The growing fast food demand for process cheese is especially prominent in the Asia/Pacific regions and Latin America, where the versatility of process cheese merges well with the fast food cuisines (M2-Presswire, 2015).

2.2 Process Cheese Overview

Process cheese is made by mixing natural cheeses, emulsifying salts, and other dairy and non-dairy ingredients, heating until melted, and then cooling into molds or slices. The conversion of natural cheese, emulsifying salts, and other ingredients to process cheese generates a longer shelf life and unique melting and flow characteristics that can be used in various food applications (Meyer, 1973). Controlling ingredients, process parameters, and storage conditions allow manufacturers to create process cheeses with their desired functional properties, including specific textures, melting points, flow properties, and flavors. However, controlling ingredients can be challenging when ingredients have high variability in properties, as is the case with natural cheese. By understanding more of the ingredients and process parameters and developing more rapid analytical methods, some of those challenges may be overcome.

2.2.1 Process Cheese Standards

Most types of process cheese are made using hard and semi-hard cheeses like Cheddar, gouda, and Emmental (Swiss), with an average age of three months (Tamime, 2011, Tunick, 2014). Although the term “processed cheese” is used most widely by consumers, the United States Food and Drug Administration Code of Federal Regulations (CFR) divides “process cheese” into seven types of process cheese products (FDA, 2009). The most common products include pasteurized process cheese, pasteurized process cheese food, and pasteurized process cheese spread. The CFR distinguishes products according to the levels of fat, moisture, pH, and the addition of other ingredients in the finished product (Table 1) and defines them all as “food prepared by comminuting and mixing, with the aid of heat, one or more cheese for manufacturing with an emulsifying agent into a homogenous plastic mass” (FDA, 2018). CFR section 133.169 also defines American cheese as process cheese containing “Cheddar cheese, washed

curd cheese, Colby cheese, or granular cheese” (FDA, 2018). Other countries have varying categories and definitions of similar products (Tamime, 2011).

Table 1. Pasteurized PC types and standards from 21 CFR 133.169 to 133.180 (FDA, 2018). All values are in the unit of weight/weight of the final product.

Category	Cheese	Ingredients & level Other ingredients	Moisture (%w/w)	Fat (%w/w)	pH
Process cheese	% not specified	$\leq 3\%$ emulsifying agents acidifying agent $\leq 5\%$ cream, anhydrous milk fat, dehydrated cream $\leq 0.03\%$ water, salt, colors, spices or flavorings, enzyme-modified cheese, mold inhibitors $\leq 0.03\%$ anti-sticking agent	≤ 40	≥ 30	≥ 5.3
Process cheese food	$\geq 51\%$	All ingredients allowed in process cheese Milk, skim milk, buttermilk, and cheese whey	≤ 44	≥ 23	≥ 5.0
Process cheese spread	$\geq 51\%$	All ingredients allowed in process cheese food Food gums, sweetening agents $\leq 250\text{ppm}$ nisin	44 - 60	≥ 20	≥ 4.0

2.3 Composition and ingredient effects on process cheese functionality

2.3.1 Natural Cheese

Natural cheese is considered cheese made from milk, salt, enzymes, and flavorings, and makes up 50-75% by weight of process cheese. It is one of the most challenging ingredients to control due to its variability in properties such as age, pH, and moisture content (Kapoor and Metzger, 2008). This variability can exist on a batch per batch basis, from the outside to the center when the cheese is formed in larger units like 640 lb. blocks or 500 lb. barrels, and through storage time for a single batch. Therefore, the chemistry of natural cheese and its components of milk proteins, carbohydrates, and minerals are important to consider. Natural cheese is a dynamic product, with numerous biochemical reactions occurring from its production throughout the ripening process until its final use. Because of this, the age of the natural cheese and product size are important to consider when selecting natural cheese to be used for process cheese manufacture.

2.3.1.1 Milk

Milk is the starting material for natural cheese, so its properties are important to understand. Cow's milk is made up of approximately 87.1% water, 4.0% fat, and 8.9% solids-not-fat, including 4.6% lactose, 3.3% protein, and 0.7% minerals (Walstra, 2006). The proteins in milk are divided into casein proteins (primarily α_{s1} -caseins, α_{s2} -caseins, β -caseins, and κ -casein) and whey proteins (primarily α -lactalbumin and β -lactoglobulin). Casein proteins make up 80% of the total protein content, are mostly hydrophobic under normal conditions, and are present in milk in the form of a casein micelle (Swaisgood, 1996). Whey proteins compose the remaining 20% of protein content and are also hydrophobic. However, they contain more secondary structure which increases their solubility.

The structure of casein micelles has been deeply studied but the exact internal structure has yet to be uncovered (Creamer and MacGibbon, 1996, Horne, 1998). Micelles range from 40-300 nm in diameter, are stabilized by colloidal calcium phosphate, and have a net negative charge (Walstra, 2006). As the only polar component of the various caseins, portions of κ -casein reside on the outside of the micelle, forming a "hairy" layer. The remaining non-polar portion of κ -casein and the rest of the α_{s1} -caseins, α_{s2} -caseins, and β -caseins reside on the interior of the micelle. These matrices, called paracaseinate, have particularly low solubility when bound to calcium ions. This paracaseinate-calcium interaction is transformed by emulsifying salts during process cheese-making (Fox et al., 2017), which will be discussed later in the *Emulsifying Salts* section. Under normal conditions, the "hairy" surface of casein micelles creates steric repulsion and prevents the aggregation of micelles. During cheese-making, however, aggregation is induced using rennet and acidification, which will be discussed next (Swaisgood, 1996).

2.3.1.2 Cheese Making

When manufacturing cheese, the fat and protein, especially casein, are concentrated into a solid form leaving cheeses such as Cheddar with approximately 39% water, 25% protein, and 31% fat (Walstra, 2006). The general steps for cheese-making involve first adding a starter culture, then adding rennet as a coagulant, followed by

forming and cutting the gel, removing the whey, and shaping. The starter culture is used to lower the pH of the system, while the rennet enzymatically cleaves the “hairy” κ -casein fragments, eliminating steric and electrostatic repulsion of the micelles and inducing coagulation (Dalgleish, 1997). As coagulation occurs, syneresis follows, leading to curd formation. Although these steps may vary widely across cheese types, this outlines the main steps for making Cheddar, one of the most common types used for making PC (Tamime, 2011).

The process of making Cheddar cheese follows unique steps after curd formation and whey drainage. These steps are appropriately called “Cheddaring,” and involve continuous heating of the curds while allowing them to mat together. Once adequate matting of the curds occurs, the slabs are cut into blocks and stacked upon each other, rotating the stacks over time. This allows further draining of whey and lowering of the pH. Lastly, the slabs are milled into curds – forming what Midwesterners know as “cheese curds” – before being salted, drained once more, and pressed into forms and stored for ripening (FDA, 2016).

2.3.1.3 Ripening & Proteolysis

Proteolysis is one of the biochemical processes occurring in natural cheese that is most influential on process cheese properties. As natural cheese ages, the protein structure is broken down by bacteria, fungi, and other sources (Shimp, 1985), and breakdown occurs at different rates in different types of cheeses (Berger et al., 1989). This is important because proteolysis and intact casein content, necessary for forming an effective emulsion in process cheese, are inversely proportional (Fenelon and Guinee, 2000). Intact casein, the portion of casein not hydrolyzed, is necessary for the stabilization of fat molecules in processed cheese, and lower levels of intact casein lead to process cheese that is softer and more meltable due to fewer protein-protein and protein-fat interactions (Berger et al., 1989, Garimella Purna et al., 2006, Henderson, 2012).

The three main sources of proteolysis are the indigenous and endogenous milk proteinases, clotting enzymes, starter cultures, and non-starter cultures (McSweeney and Fox, 1997). The two proteinases found in milk that can withstand heat treatments like

pasteurization are plasmin and acid proteases (Walstra, 2006). Clotting enzymes like rennet are added during cheesemaking and may retain their proteolytic activity during ripening if medium or low cook temperatures are used. Enzymes originating from lactic acid bacteria starter culture also contribute to the proteolytic activity during cheese ripening but vary widely based on the strain. Lastly, the presence of non-starter organisms can occur through contamination of the milk or cheese and can also lead to proteolysis (Walstra, 2006).

Although proteolytic enzymes can target a variety of cheese proteins during ripening, caseins are the most important protein class for process cheese manufacture. Young cheeses with high intact casein content can lead to process cheese that is firmer and less meltable (Templeton and Sommer, 1930, Henderson, 2012), while older cheeses can lead to process cheese with softer and more meltable (Berger et al., 1989, Garimella Purna et al., 2006, Henderson, 2012). The decrease of intact casein in Cheddar cheese is not linear, however, and was found to decrease the fastest between 6 to 12 weeks of ripening and then stabilize from 12 to 18 weeks of ripening (Garimella Purna et al., 2006).

Although proteolysis is a key factor in process cheese functionality, the quantification of intact casein continues to be a challenging task. Traditional analysis using Kjeldahl is time-consuming and reagent-intensive while using more rapid methods requires calibration. Some of the rapid methods that have been developed utilize spectrophotometric tools (Samples et al., 1984) and infrared and fluorescence spectroscopy (Karoui et al., 2006, Kokawa et al., 2015, Ma et al., 2019). Further discussion on the mechanisms, advantages, and challenges of spectroscopic methods can be found in the *Spectroscopic Methods* section.

Because intact casein content varies in natural cheese, natural cheese suppliers may provide processors information of the type, age, and weight of cheese, but may not always provide chemical properties such as moisture, fat, salt, or pH (Zehren and Nusbaum, 1992). Some process cheese plants submit samples for laboratory testing to determine these properties, but selecting a representative sample is challenging since natural cheese is often packaged in 640- to 700-pound blocks (Sommer, 2016). As a result, cheese graders primarily rely on their own sensory and texture analyses to choose

blocks for use based on flavor, texture, consistency, and level of acidity and often mix blocks with varying properties to achieve the desired characteristics (Zehren and Nusbaum, 1992, Kapoor and Metzger, 2008).

2.3.2 Fat

Whether originating from natural cheese or separate dairy and non-dairy ingredients, fat begins as large droplets and is converted to an emulsified system of small uniform droplets in process cheese. In natural cheese, fat droplets are an average of 4 μm in diameter (Lopez, 2005, Walstra, 2006). During the mixing that occurs at ambient and high temperatures of process cheesemaking, the fat droplets are reduced in size by shear force, melted by heat, and stabilized at their surface by the casein in the system (Zehren and Nusbaum, 1992). By the time process cheese cools, fat droplets reach an average of 1-10 μm in finished process cheese (Pereira et al., 2001). The formation and stabilization of small fat droplets are affected by the amount of fat, the protein-to-fat ratio, and the mixing properties.

The amount of fat may vary in process cheese but must be no less than 30% w/w to achieve the standard of identity for process cheese or lower for process cheese food or process cheese product (Table 1). The protein-to-fat ratio in particular can be used to determine the functionality of the emulsion since casein surrounds the surface of fat droplets throughout process cheese (Shimp, 1985, Fox et al., 2017). If too low of a protein-to-fat ratio exists or too small of fat droplets are formed from overmixing, there may not be enough protein to stabilize the entire surface area formed, leading to an unstable emulsion. The potential effects of this include oiling off of fat or “overcreaming,” where too many interactions in the caseins lead to a thick pudding-like consistency (Garimella Purna et al., 2006). Conversely, too low a fat content relative to protein, such as in reduced-fat PCs, can lead to increased protein-protein cross-linking, higher firmness, and decreased meltability since fat is less able to interfere with cross-linking (Subramanian et al., 2006). When manufacturing fat-free PC spreads, adjustments in emulsifying salts, hydrocolloids, cook time, cook temperature, and pH are necessary to reach the desired functional properties (Swenson et al., 2000, Brickley et al., 2008).

Although already mentioned in reference to overcreaming, mixing properties are also key to properly break the fat droplets down by force and distribute the emulsifying salts and casein adequately through the system to coat all the fat droplets (Zehren and Nusbaum, 1992). Further discussion on the effects of mixing properties can be found in the *Mixing Properties* section.

The degree of lipolysis of fat in the starting natural cheese may not affect functionality, but it does affect the flavor of the final process cheese. Since using higher amounts of aged natural cheese to achieve desired flavor properties may not be feasible due to increased proteolysis, flavors from ingredients such as enzyme-modified cheeses may be added to compensate for the weaker flavor in younger cheeses (Hassan et al., 2007).

2.3.3 Moisture

Moisture is easy to adjust in process cheese formulas and is chosen based on the type of process cheese being produced (Table 1). Water can be added as a liquid in the ambient mixing step or as steam during mixing. Process cheese with lower moisture is typically more firm than products with higher moisture (Zehren and Nusbaum, 1992). Having high moisture and not enough other ingredients to depress the water activity can also lead to a greater risk of pathogen growth (Glass and Ellin Doyle, 2013).

2.3.4 Calcium

Although the major sources of calcium in PC are from natural cheese, calcium's specific effects are worth discussing. During manufacturing the calcium content affects formulation and ES in particular, since higher calcium requires additional ES to adequately sequester calcium from paracaseinate (Kapoor and Metzger, 2008).

2.3.5 Emulsifying Salts

2.3.5.1 Mechanisms

No emulsifying salts were used when the Germans first made process cheese in 1895, while the Swiss are known to have used citric acid when they made Swiss cheese-based process cheese. Shortly after, American producers like Kraft developed the use of

citrates and phosphates as emulsifying salts for Cheddar-based process cheese production independently from European producers (Meyer, 1973). The idea of adding emulsifying salts may have arisen through the practice of mixing Swiss fondue cheese with wine during heating, where tartrates in wine act as emulsifying agents (Caríc and Kaláb, 1993).

When natural cheese is heated and sheared without emulsifying salts, it leads to phase separation by oiling off of the fat and changes to the protein network. This occurs as a result of the fat liquifying from heat and coalescing from the loss of the milk fat globule membrane, while the proteins constrict due to increased hydrophobic interactions and precipitation of soluble calcium and phosphate (Fox et al., 2017).

When used, emulsifying salts affect the chemical, physical, and microbiological properties of process cheese by developing the emulsifying properties of the natural cheese proteins. Although the term emulsifiers are considered compounds that stabilize the interfaces of emulsions, emulsifying salts are not surface-active themselves but are ionic compounds that have the overall effect of increasing the solubility of casein by removing the calcium through ion exchange and contributing a net negative charge (Shimp, 1985) (see Figure 1).

2.3.5.2 Types of emulsifying salts

Currently, thirteen emulsifying salts are approved for use by the FDA (2009) (Table 2). The most commonly used emulsifying salts are trisodium citrate and disodium phosphate (Kapoor and Metzger, 2008). Emulsifying salts contain a monovalent cation and polyvalent anions, including variations of sodium and potassium phosphates and sodium citrate.

Emulsifying salts are chosen primarily based on the extent that they alter the pH of the process cheese and their ability to sequester calcium, as well as the functional

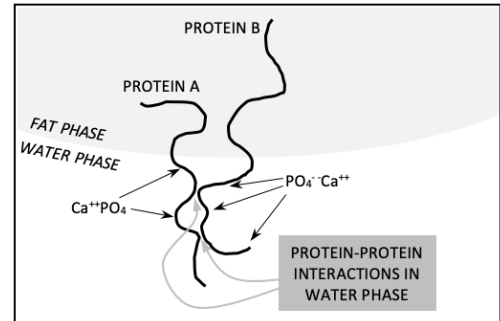


Figure 1. Example of calcium phosphate salts binding to a protein structure at an oil-water interface (Shimp, 1985)

Table 2. *Emulsifying salts permitted in the US (FDA, 2009)*

Trisodium citrate	Monosodium phosphate	Dipotassium phosphate
Potassium citrate	Disodium phosphate	Sodium metaphosphate
Calcium citrate	Trisodium phosphate	Sodium acid pyrophosphate
Sodium tartrate	Sodium aluminum phosphate	Tetrasodium pyrophosphate
Sodium potassium tartrate		

properties desired in the final process cheese (Shimp, 1985). Emulsifying salts increase the pH of process cheese through their buffering capacity from about 5 to 5.5 for natural cheeses like Cheddar, Emmental, and Gouda, to 5 to 6.5 in process cheese (Zhong, 2003, Walstra, 2006). This is important since the water-binding ability of proteins changes with pH. Furthermore, while the pH of process cheese ranges from 5 to 6.5, most desired properties are only possible in the center of that range. Process cheeses with pH close to 5 are dry and crumbly, whereas those close to pH of 6.5 are soft and sticky. Using disodium phosphate as an emulsifying salt leads to cheese in the center of that pH range, which is why it's one of the most commonly used ingredients (Shimp, 1985). The way emulsifying salts alter pH is important, but their most significant property is their ability to sequester calcium.

As mentioned in the previous 2.3.1.1 *Milk* section, casein micelles in milk and natural cheese are stabilized by calcium phosphate, which is bound to the non-polar portion of κ -casein and the rest of the α_{s1} -caseins, α_{s2} -caseins, and β -caseins on the interior of the micelle. During process cheese-making, emulsifying salts target these particular proteins by exchanging calcium for sodium or binding to calcium directly. This mechanism establishes the partial solubility of those caseins necessary for emulsification (Shimp, 1985). Once paracaseinate is solubilized, its ability to act as an emulsifier at the oil-water interface stabilizes the fat globules in the emulsion (Meyer, 1973, Caric and Kaláb, 1993). As a result, the emulsifying salts have a direct effect on the final fat globule size distribution of process cheese, which then affects the texture and melting properties (Shimp, 1985, Fox et al., 2017). Emulsifying salts that bind calcium the weakest (sodium citrate, sodium aluminum phosphate, disodium phosphate, and trisodium phosphate) lead to cheeses that are soft and easily melted, while those that bind

calcium the strongest (tetrasodium pyrophosphate, sodium tripolyphosphate, and sodium hexametaphosphate) lead to firm, poorly-melting cheeses (Templeton and Sommer, 1936). The former group is more desirable for achieving soft process cheeses and sauces, while the latter is useful for products like Cheddarwurst (sausage with Cheddar cheese inside) and other processed foods where less melt or no melt is preferred. Furthermore, combinations of emulsifying salts were found to be most effective in forming process cheese with stable emulsions (Caric et al., 1985). The maturity of the starting natural cheese can sometimes influence the ES chosen. One study that examined how blends of ES affected Swiss-type cheese within a range of maturity showed that a 1:1 ratio mixture of disodium phosphate and tetrasodium diphosphate led to the hardest PC samples, while other rheological properties were affected by other composition factors (Salek et al., 2016). An additional factor in choosing the right ES is whether PC slices, loaves, or sauces are being manufactured, and the most appropriate ES is used to achieve the desired functional properties. Trisodium citrate is common for slice applications, for example (Shirashoji et al., 2006).

Although emulsifying salts mainly influence emulsification, they can also have some small microbiological effects. Some emulsifying salts, such as orthophosphates, can inhibit *Clostridium botulinum* in cheese spreads (Tanaka et al., 1979, Tanaka et al., 1986). The models developed by Tanaka in combination with other studies are widely used to predict the safety of process cheese formulations and processing parameters (Glass and Ellin Doyle, 2013).

Since the majority of emulsifying salts are sodium salts, manufacturing reduced-sodium PCs can be a challenge. Gupta et al. explored the textural and flavor properties of sodium-reduced PCs and found that blends of potassium salts such as tripotassium citrate, dipotassium phosphate, and tetrapotassium pyrophosphate all led to PCs with a wide range of functional properties (1984). Another study by Cernikova et al. replaced emulsifying salts with hydrocolloids but found that several hydrocolloids yielded poor PC properties (2010).

Overall, a wide variety of individual emulsifying salts and their combinations can have some effect and potential control over the manufacture of PC and its final properties, but many other factors still have significant effects as well.

2.3.6 Other Ingredients

Besides natural cheese and emulsifying salts, other ingredients and additives may be added to process cheese. These include dairy ingredients (whey protein, lactose, nonfat dried milk, dried whey), additives (flavors, preservatives, colors), other ingredients (hydrocolloids, meat inclusions, spices), and rework (process cheese that does not meet specifications). Other dairy ingredients are added to change the functional or sensory properties. For example, the addition of ingredients containing whey protein has been shown to build a stronger protein structure, increasing firmness and decreasing meltability of the process cheese (Thapa and Gupta, 1992, Kapoor and Metzger, 2008). Rework can be formed intentionally – through surplus product made within a batch, or unintentionally – through product that doesn't meet the specifications. Either way, it cannot be sold due to problems during manufacturing, such as excessive heating due to delays or stoppages in manufacturing (Kalab et al., 1987). Depending on the properties, it can be added back as an ingredient but variations in properties may make formulation difficult (Meyer, 1973). In one study, Cernikova et al. found that adding rework up to 20% wt/wt led to process cheese with smaller fat globule sizes (2018) so care must be taken to ensure overemulsification doesn't occur when adding rework (Shimp, 1985). Overall, other ingredients added to PC can have some effect on properties but vary widely across the industry.

2.4 Processing effects on process cheese functionality

In addition to ingredient selection, processing parameters also play a large role in affecting the final properties of process cheese. The major parameters include the amount of mixing, cook temperature, hold time, and rate of cooling.

2.4.1 Mixing & Cooking Properties

Since mixing and cooking can occur simultaneously in the manufacture of PC, they are discussed together. The effect of mixing properties on PC can be divided into ambient mixing and heated mixing, as well as both the speed of mixing and the duration of the mixing step. Mixing helps distribute the emulsifying salts, hydrate the proteins, and decrease fat globule size (Guinee et al., 2004). Although other equipment may be used

for mixing, cookers are often used. There is a wide variety of cookers and operating conditions used by process cheese manufacturers to achieve different types and quantities of process cheese. Modes of heat transfer in cookers may include indirect heating or direct steam injection (Berger et al., 1989, Zehren and Nusbaum, 1992). Indirect heating passes heat through steam-jacketed walls or other elements of a cooker, while direct steam injection transfers heat and water into the product directly via steam (Kosikowski, 1982).

High-speed mixing can be achieved with cutting blade-type mixers, such as a Thermomix (Vorwerk & Co., GmbH, Wuppertal, Germany) or Rapid Visco Analyzer (RVA; Newport Scientific Pvt. Ltd., Warriewood, Australia) for bench-top production or a Stephan cooker (Stephan Machinery Corporation, Columbus, OH, U.S.A.) for pilot-level production. Mixing speeds with these cookers can range from 300 to 3000 rpm and from 1 to 5 minutes of mixing and cooking (Garimella Purna et al., 2006, Kapoor and Metzger, 2008). Low-speed mixing can occur using single screw cookers (Damrow cooker, Damrow, Fond du Lac, WI, U.S.A.), twin screw cookers (Blentech Cooker, Blentech Corp., Rohnert Park, Calif., U.S.A.) and other cookers (Keebler Engineering, Chicago, Ill., U.S.A.) at pilot-scale manufacture, with mixing speeds ranging from 50 to 150 rpm and 3 to 15 minutes of mixing and cooking (Swenson et al., 2000, Glenn et al., 2003, Hassan et al., 2007, Kapoor and Metzger, 2008). Another processing factor is the difference between batch and continuous cookers. While the previously-mentioned models are batch cookers, Rota Therm is a new type of continuous cooker developed by Gold Peg (Gold Peg International Pty Ltd., Victoria, Australia) which can achieve 600 to 1000 rpm mixing speeds (Guinee et al., 2004, Kapoor and Metzger, 2005).

Overall, studies show that high-speed, high-shear cookers lead to decreased fat globule size (Lee et al., 2003a), which then correlate to higher firmness and decreased flow and melt properties once cooled (Tamime, 2011). Conversely, Swenson et al. found that increased cook time led to decreased firmness in fat-free PC spreads (2000). Additionally, undermixing and overmixing can result in undesirable properties. Undermixing can result in too large of fat droplets, inadequate dispersal of emulsifying salts, and an overall poor emulsion, while overmixing can lead to overcreaming, a

phenomenon previously mentioned in the *Fat* section and *Other Ingredients* section regarding rework (Meyer, 1973, Garimella Purna et al., 2006).

Although the minimum cook temperature indicated by the CFR is 150°F (65°C) for a minimum of 30 seconds, industry cook temperatures range from 70-100°C and are determined based on the ingredients, cooking equipment, and type of process cheese being produced (Kapoor and Metzger, 2008, Tamime, 2011, FDA, 2018). When exploring the effects of cook temperature on fat-free PC spreads, Swenson et al. found that increased cook temperature led to decreased firmness, increased meltability, and increased spreadability when measuring cook temperatures ranging from 60-90°C (2000). Generally, higher temperatures are used for PC blocks (80-85°C) versus a lower and slightly wider temperature range for slices (78-85°C) (Caríc and Kaláb, 1993).

2.4.2 Cooling Rate

The rate of cooling of PC is impacted both by the duration of cooling and the temperature of the cooling environment and is unique to the PC product being made. For example, differences in surface-area-to-volume ratios cause blocks to undergo slower, more moderate cooling while slices are cooled more rapidly. Different cooling properties impact emulsions by affecting the fat crystallization, protein-protein interactions, and protein-fat interactions (Zhong et al., 2004). Earlier research in fat crystallization suggested that faster cooling rates lead to smaller fat crystal size in model milk fat emulsions (Lopez et al., 2002), while in an oil-in-water emulsified product like PC, maximum fat crystal size is already limited by the droplet size (Bot et al., 2007). Additional work by Zhong et al. (2004) and Piska & Stetina (2004) both found that faster cooling led to softer PC texture, which was consistent with the converse industrial observation of slower cooling leading to firmer PC (Caríc and Kaláb, 1993). Furthermore, the rapid cooling rates had larger impacts on texture than the maturity of natural cheese (Piska and Stetina, 2004). In PC manufacturing, adjusting cooling rates could be a potential tool for overcoming emulsification challenges in the ingredient and cooking steps, although not much research has been done outside of the work of Piska and Stetina (2004). Barriers to exploring this option may be due to a lack of flexibility in production equipment and processes in PC factories.

2.4.3 Other factors

Other factors that affect PC production may be less obvious or widespread within the PC industry but are just as significant. One of these includes the buildup of process cheese on equipment and pipes over a long shift. This causing the pumping ability and functional pipe diameter to decrease over time (Brandsma, 2019).

2.5 Process cheese microstructure

The microstructure of finished process cheese is an emulsion of oil in water, with fat globules ranging in size around one to ten microns suspended in water within a cross-linked protein matrix (Shimp, 1985). This arrangement and size have been observed using various imaging techniques, including scanning electron microscopy (Cernikova et al., 2017), transmission electron microscopy (Caric et al., 1985), light microscopy, nuclear magnetic resonance (NMR) (Chen and Liu, 2012), near-infrared (NIR) spectroscopy, and Raman spectroscopy (Smith et al., 2017).

Natural cheese has a similar structure but contains larger fat globules surrounded by globule membranes (Caric et al., 1985, Shimp, 1985) as well as a higher quantity of coalesced or clumped globules (Kapoor and Metzger, 2008) (Figure 2). During the mixing, heating, and melting steps of process cheese manufacture, the fat globules of natural cheese decrease in size as the emulsifying salts solubilize para-casein strands and destabilize the fat globule membranes (Caric and Kaláb, 1993). The rate and characteristics of the formation of this microstructure are affected in various ways by many of the previously mentioned process cheese ingredients.

The microstructure of processed cheese is generally considered stable and final once the sample is stored and cooled (Berger et al., 1989), however, changes may still

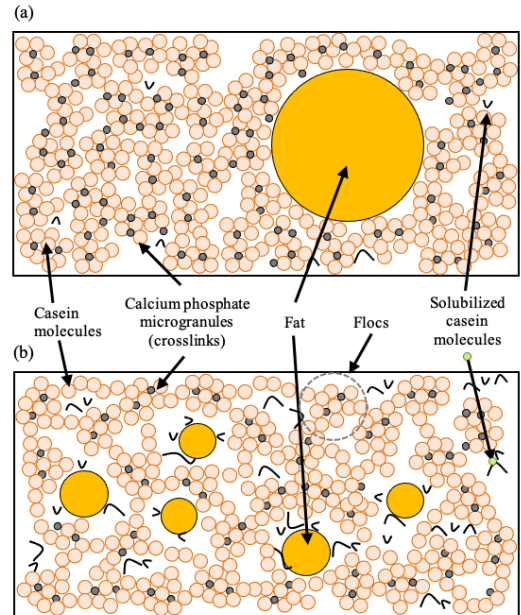


Figure 2. The model microstructure of (a) natural cheese and (b) process cheese (Kapoor and Metzger, 2008)

occur over the following weeks and months of storage depending on the length of time, storage conditions, and packaging properties (Cernikova et al., 2018). One fundamental challenge with the production of process cheese is that problems with the microstructure and emulsion stability of production batches aren't known until processing is over and defects cannot be fixed. Ideally, a sample of molten process cheese could be tested for desired final characteristics before batches are allowed to cool and stabilize. This would allow for adjustments in process parameters to achieve the desired characteristics if a predicted defect is likely to occur. Although studies have been completed which compare specific ingredients or processing parameters with final properties, predicting the outcome of complex formulas or varying process parameters is much more challenging in realistic manufacturing settings, especially when the raw ingredient of natural cheese may not be consistent. As a result, many studies have explored ways to predict emulsion stability and functional characteristics of process cheese, but each has its drawbacks for its use in applied manufacturing settings.

2.6 Methods of analyzing and predicting functional properties

Most past studies on process cheese can be grouped into those that (i) test effects of natural cheese, (ii) effects of other ingredients, and (iii) effects of varying processing parameters on final functional properties. These findings have greatly helped manufacturers to achieve desirable properties and to produce more consistent processed cheese across production runs. However, challenges still exist to produce stable and consistent processed cheese despite the high variability of natural cheese blends. Furthermore, in-process characteristics of processed cheese do not necessarily represent the finished structure, and problems with emulsion stability may not be seen until production is complete (Caríc and Kaláb, 1993). Because of this, a rapid, in-process technique for determining the emulsion stability of processed cheese is needed. Nonetheless, the following sections describe the existing melt tests, rheological methods, and spectroscopic methods used for analyzing functional properties.

2.6.1 Melt Tests & Rheological Methods

One of the unique characteristics of PC over natural cheese is its versatile physical characteristics, including smooth melting properties. Furthermore, many of the melting and rheological characteristics can be used as a quality metric unique to each product application (Park et al., 1984). Melting and rheological tests range from measuring the final spread or flow of a sample to precise changes throughout a temperature gradient. The wide variety of methods reflects the interdependence and transience of the PC properties, sample geometries, and external heat transfer properties.

2.6.1.1 Arnott

The Arnott test involves measuring the difference in height of unmelted versus melted cheese samples cut into cylinders of equal height and width, such as 17mm wide by 17mm diameter. The difference in center height is converted to a percent length decrease and is reported as the Arnott meltability, ranging on a scale of 0 to 100 (Arnott et al., 1957). Although this method is one of the most commonly reported methods historically, it has not been standardized and many researchers have made adjustments to it over time (Park et al., 1984).

2.6.1.2 Schreiber/USDA Melt Test

Instead of measuring the height difference, the Schreiber test and USDA melt test measure the diameter or area of spread of a melted cheese sample. Like the Arnott test, the Schreiber test is also one of the most commonly reported methods historically and has been adjusted by researchers over time. Modifications include the starting disc dimensions, temperature and duration of heating, cover and tray material (Altan et al., 2005), and method of measuring the diameter or area of melt. Muthukumarappan, et al. (2004) modified the original Schreiber test by adjusting oven temperature, heating surface, and measurement unit and found that 5 min at 90°C on aluminum plates was ideal for analyzing the surface area of mozzarella cheese melt. The USDA melt test is identical to Schreiber in melting procedure but uses a different standard guide for diameter measurement (Zehren and Nusbaum, 1992). When it comes to PC, Blazquez et al. followed a similar method by measuring the area of melt of a 25 mm wide x 5 mm tall

cylinder. Amamcharla & Metzger (2015) continued with a similar method but with 34 mm wide x 7 mm tall PC cylinders on aluminum plates with glass Petri dish covers and a 30-min tempering step before melting. When comparing uncovered to covered samples of PC and Cheddar samples, the data from covered samples were more statistically robust (Altan et al., 2005). More detailed descriptions for area measurement using computer vision were described by Wang & Sun (2002) and Everard et al. (2005).

2.6.1.3 Microwave Oven Tests

Microwave oven tests are similar to the Schreiber method with a PC sample of specific dimensions being melted in a microwave and the final diameter or area spread used for analysis. It is faster than the Schreiber method, but heat transfer is less dependent on heat transfer to the surface than on sample geometry and rheological properties (Park et al., 1984).

2.6.1.4 Differential Scanning Calorimetry (DSC)

DSC has often been used to monitor thermal properties of milk fat across dairy products, using slow heating and cooling gradients to measure precise phase change properties (Lopez et al., 2006). One of the advantages of DSC is the negligible heat transfer effects since small sample sizes are used and that it depicts very specific microstructural properties. However, it is worse at distinguishing larger differences in meltability across samples (Park et al., 1984).

2.6.1.5 Tube Melt Test

The tube melt test, sometimes called the Olson and Price test, also involves melting cheese in an oven but inside of a sealed glass tube tilted horizontally to allow for one-directional flow. This was created as an alternative to the Schreiber method to overcome challenges with surface film formation and uneven flow (Olson and Price, 1958). After removing from the oven and cooling to room temperature, the length of melted cheese is recorded and the difference between final vs original length is the final meltability (Mounsey and O'Riordan, 1999, Everard et al., 2005). Tube melt test has been

shown to have a high correlation with dynamic stress rheometry (DSR) and rapid visco analyzer (RVA) melt time for PC samples (Prow and Metzger, 2005).

2.6.1.6 Dynamic Stress Rheometry

Unlike the simple melt tests previously discussed, large-strain and small-strain dynamic stress rheometry use assorted motions on cylindrical cheese samples to measure rheological properties. Large-strain rheometry uses a slow twisting motion of cheese between two parallel plates to measure the precise force required for fracture of the gel structure. Where melt properties are associated with functionality, fracture properties are important in sensory perception (Bowland and Foegeding, 1999). Although measuring different properties than the tube melt test, DSR melt temperature is correlated to it (Prow and Metzger, 2005).

Conversely, small-strain rheometry and small amplitude oscillatory shear rheology (SAOSR) use smaller motions to explore viscoelastic properties without disrupting the gel structure. The outcomes of this method indicate the strength of the para-casein network and other interactions at the molecular level (Bowland and Foegeding, 2001). Specific methods for small-strain rheometry and SAOSR involve the motion of a bob in a sample-filled cup (Zhong et al., 2004), as well as parallel flat plates moving at defined amplitudes and frequencies at various temperatures (Piska and Stetina, 2004). These methods were used to explore model PC microstructure (Bowland and Foegeding, 2001, Joshi et al., 2004), commercial PC microstructure (Lu et al., 2007), and the effects of phosphate ES's on PC (Sadlikova et al., 2010).

2.6.1.7 Rapid Visco Analyzer (RVA)

The RVA is a viscometer capable of measuring viscosity across time, temperature, and stir speeds for cheese and other foods. When analyzing PC, it is best for measuring the functional properties of melt temperature and viscosity (Perten Instruments Application Note: RVA Method 30.04, Prow and Metzger, 2005), and has also been used for small-scale benchtop PC production (Metzger et al., 2002, Kapoor et al., 2004, Kapoor and Metzger, 2005, Trivedi et al., 2008). As mentioned before, RVA results are correlated to some properties of tube melt test and DSR (Prow and Metzger, 2005).

2.6.1.8 Micro Visco Amylograph (MVAG)

The MVAG is very similar to the RVA except for a few mechanical differences. While the RVA has a dynamic spindle and static cup, the MVAG has a static spindle and rotating cup. The MVAG also has a temperature probe positioned in the center of the cup while the RVA measures the temperature along the perimeter of the cup. With this difference, one benefit of the MVAG over the RVA is its ability to measure the real-time temperature of the cheese sample without the unknown temperature gradient from the center of the sample to the outside of the sample cup where the heat is being measured in RVA.

2.6.1.9 Texture Profile Analysis (TA.XT)

Numerous instruments are equipped to analyze the texture of PC and other food products, including Brookfield and TA.XT2i (Lee et al., 1978). Although both types of equipment can measure several functional properties in PC such as firmness/hardness, fracturability, adhesiveness, springiness, cohesiveness, and gumminess, TA.XT has been used much more widely for TPA of PC (Tunick et al., 1990, Tunick, 2000, Biswas et al., 2004, Joshi et al., 2004, Piska and Stetina, 2004, Amamcharla and Metzger, 2015). A double-compression profile of a small cylindrical PC sample such as that described by the standard method ISO 17996, (ISO 17996, 2006), Joshi et al. (2004), and Piska and Stetina (2004) are the most commonly used method for PC analysis. Further analysis of the compression ratio for a TPA method found that 80% compression was best for American cheese (Imoto et al., 1979). The ISO 17996 method serves as a reference for height-to-diameter ratios of 1.1 to 1.5 for cheese test portion geometry and additional method suggestions (ISO 17996, 2006).

2.6.2 Spectroscopic Methods

There are several spectroscopic techniques useful for analyzing the chemical structures, droplet sizes, and generating spectral “fingerprints” of colloidal systems like cheese and other dairy products. Some examples discussed below include fluorescence, dielectric, nuclear magnetic resonance (NMR), Raman, infrared techniques, and confocal, but additional less-studied methods include diffusing wave spectroscopy and ultrasonic

spectroscopy (Alexander and Corredig, 2014). Spectroscopic methods have several advantages, including a short scan time, non-targeted data collection, and non-destructive nature (Alexander and Corredig, 2014). Some are techniques better at providing concrete results, such as NMR for droplet size, while others generate spectroscopic results that require chemometrics to fully understand.

2.6.2.1 Front Face Fluorescence Spectroscopy

Front face fluorescence spectroscopy (FFFS) is a fairly recently-developed spectroscopic method where the surface is observed instead of higher-depth observation with traditional fluorescence spectroscopy (Zaïdi et al., 2007). Because of the shallower depth of measurement, analysis of pastes, powders, and other opaque food samples is possible. In addition to FFFS being a suitable method for PC analysis since food products often contain fluorophores from proteins and other compounds, it has additional benefits of higher sensitivity than other spectroscopic methods (Strasburg and Ludescher, 1995) and the ability to detect fluorophore changes in food proteins in response to thermal effects or interactions with other food components (Zaïdi et al., 2007). FFFS has been primarily used for food analysis in milk and cheese applications to measure things such as the extent of thermal processing in milk (Dufour and Riaublanc, 1997, Kulmyrzaev et al., 2005), cheese compositional and structural changes in fat and protein (Dufour et al., 2000, Mazerolles et al., 2001, Karoui et al., 2003), cheese identification (Dufour et al., 2000, Herbert et al., 2000), light-induced oxidation (Wold et al., 2002), Maillard browning reactions (Schamberger and Labuza, 2006), and PC properties (Garimella Purna et al., 2005).

2.6.2.2 Dielectric Spectroscopy

Dielectric spectroscopy (DS) measures the interactions between an applied electrical field and the food products tested – primarily water and other charged compounds – and has all the similar benefits of other spectroscopic methods such as rapid scan time, high precision for identification, and is non-destructive (Skierucha et al., 2012). DS is distinguished from ordinary dielectric analysis through its use of broad ranges of frequency (Nelson, 2005). While the use of DS in food is relatively new, it may

be useful for measuring maturity in fruits and vegetables or dry matter content in food products (Nelson, 2005). One recent study by Amamcharla & Metzger showed that DS could successfully predict melt time, melt diameter, and hardness in PC (2015).

2.6.2.3 Time Domain Nuclear Magnetic Resonance Spectroscopy

The use of NMR analysis for emulsion applications began in the 1970s (Packer and Rees, 1972). Time Domain Nuclear Magnetic Resonance (TD-NMR) spectroscopy works by applying a magnetic gradient to samples and monitoring the relaxation back to its original state. It has greater potential for food analysis than regular NMR spectroscopy since it measures less chemical information and more signal amplitude, bulk quantification, solid vs liquid identification, and morphology (Bruker, 2015). With oil- and water-based components relaxing at different rates, NMR is ideal for characterizing the interfaces of emulsions and analyzing droplet sizes in foods (Bruker, 2016). As the diffusion of oil and water molecules is limited by droplet interfaces, the output can indicate interface barriers. This is extremely useful since it can be difficult to observe emulsion structures without altering the sample, differentiate between clusters and individual droplets, or analyze concentrated emulsions, all of which TD-NMR can do (Goudappel et al., 2001, Johns and Hollingsworth, 2007). Some drawbacks of TD-NMR compared to other spectroscopic methods is that it has a slightly longer analysis time of approximately 22 minutes per sample, requires costly equipment for high magnetic field strengths, and is limited by its assumptions of lognormal unimodal droplet size distribution and spherical droplets (Deublein et al., 2015, Bruker, 2016). Pulsed-field gradient NMR has been shown to effectively measure fat globules in Cheddar and Swiss cheeses (Callaghan et al., 1983), butter (Van Lent et al., 2008). Additional food applications for NMR include solid fat content, shelf-life stability, moisture and fat content, and functionality (van Duynhoven et al., 2010).

2.6.2.4 Confocal Raman Microscopy

Confocal Raman spectroscopy is based on Raman scattering, where the inelastic scattering of excitation light can serve as an indicator of chemical bonds and broader compositions within samples (WITec). It is a complementary method to infrared

spectroscopy since they're both based on vibrational transitions in molecules, with Raman depending on polar groups and infrared depending on nonpolar groups and dipole moments (Li-Chan, 1996, Chalmers et al., 2012). One of the benefits of Raman over other microscopy techniques like confocal, or in some cases of FFFS, is that samples don't need to be labeled before scanning since Raman scattering is caused by intrinsic molecular signatures (Roefsaers et al., 2011). Some disadvantages of Raman spectroscopy include the costly equipment needed, slow and tedious sample image collection needed for high-resolution images, and shallow depth of sample analysis. For example, one study using Raman to analyze PC required up to 60 min to scan a sample area of 50 x 50 μ m (Smith et al., 2017). In addition to PC, other products that have been analyzed by Raman spectroscopy combined with chemometric tools include spreadable cheese (Oliveira et al., 2016), cheese and cheese analogs (Sowoidnich and Kronfeldt, 2016), and milk (Gallier et al., 2011).

2.6.2.5 Confocal laser scanning microscopy (CLSM)

Background

Confocal laser scanning microscopy (CLSM) is a newer method of conventional light microscopy techniques where a laser is used instead of a light source and images are collected by a scanning unit above the sample as well as a pinhole in the back of the focal plane (Dürrenberger et al., 2001). The term *confocal* refers to the common focus on the sample by the illumination pinhole and the detection pinhole (Brakenhoff et al., 1988). Images of desired regions of samples are captured by labeling with fluorescent markers, exciting fluorophores at unique laser wavelengths, and collecting emitted light. Additional advantages of CLSM include its ability to analyze multiple labels in a sample at once (Hibbs, 2004), measure fluorescence both along and through the focal plane, and measure in high resolution (Brakenhoff et al., 1988). Although samples must be small and thin for CLSM labeling steps, CLSM's ability to measure fluorescence through the focal plane allows observation of the food structure at an area relatively undisturbed by sample preparation as well as undisturbed by the out-of-focus regions above and below the plane (Everett et al., 1995). Sample areas can reach as small as 0.2 x 0.2 μ m with 0.25 μ m distance between each focal plane (Brakenhoff et al., 1988, Dürrenberger et al.,

2001). Three-dimensional images are created by combining multiple images collected at defined steps through the focal plane (Lichtman, 1994). Overall, the properties of CLSM are very useful for observing the 3-dimensional microstructure of many foods, including cheeses and process cheeses where various sizes of fat globules and air bubbles are trapped within a continuous matrix (Dürrenberger et al., 2001).

Dairy product & cheese applications

CLSM has been used to measure fat globule size and distribution in fat spreads and emulsions (Van Dalen, 2002, Van Duynhoven et al., 2002, Van Lent et al., 2008), Cheddar cheese (Everett et al., 1995, Guinee et al., 2000), swiss cheese (Huc et al., 2013b), semi-hard cheeses (Huc et al., 2013a), and process cheese (Pereira et al., 2001, Lopez and Briard-Bion, 2007). These studies show that the fat droplets are mostly spherical and range in diameter from 1-20 μm in natural cheese (Everett et al., 1995) and 3-6 μm in process cheese (Pereira et al., 2001).

Spectral Filtering Techniques

Although numerous varieties of fluorescent dyes have been developed for modern microscopy and multiple probes are often used together, challenges with overlapping signals can be a barrier to effective separation of signals and subsequent quantitative analysis (Marqués, 2020). Overlapping signals are more specifically divided into cross talk, or the overlapping emission spectra, and cross-excitation, a similarity in excitation maximums (Zimmermann et al., 2014). To overcome this overlap between dyes, two options exist. One is to choose the dyes more carefully, and the other is to utilize spectral filtering with linear unmixing (Marqués, 2020). Spectral filtering combined with linear unmixing can minimize fluorophore cross-talk and cross-excitation and more reliably separate fluorescence signals and identify sample components (Zimmermann et al., 2014). This separation allows for increased contrast in the final images (Mansfield et al., 2008). As implied in the name, spectral filtering is performed by creating individual filters for individual dyes. Filters are created by imaging samples with single fluorophores, generating filters for each, and then combining the filters to one filter set. (Zimmermann et al., 2014). The second component, linear mixing, uses algebra to derive

the individual filter components from the combined spectra when applying the filters to an image containing multiple dyes together (Marqués, 2020). Valm, Oldenbourg, and Borisy (2016) demonstrated the ability to spectrally filter several fluorophores that previously would have been indistinguishable and described the best methods for image acquisition.

Quantitative Image Analysis Techniques Using Fiji

After the steps of sample prep and image acquisition comes qualitative or quantitative or image analysis. Several types of imaging analysis software exist, but Fiji is a widely-used free and open-source program with a diverse array of tools and plugins that can analyze multidimensional images like those produced from CLSM. When it comes to quantification of lipid droplets, the most useful tools and order of processing steps include splitting multi-channel images to the channels of the desired component (lipids), utilizing a median filter, thresholding to set binary pixel values, applying a 3D watershed split, and measuring the final components using the 3D ROI manager (Brown, 2020a, 2020b, Brown, 2020c). Splitting the channels in an image helps to isolate the sample components, such as lipids, needed for quantification from the other components and speed up image processing. A median filter helps to remove noise and establish clearer boundaries of droplets. Thresholding is needed to enable quantification by setting binary pixel boundaries of the lipid droplets. 3D watershed split uses binary images combined with Euclidean distance transform to identify boundaries between what appears to be aggregated droplets (Brown, 2020b, Brown, 2020c). Measuring the components with a 3D ROI manager allows for simple geometric, shape, and intensity measurements of the regions of interest (ROIs) created through the previous steps (Brown, 2020c). Alternative imaging processing and quantification methods were described by Bowland and Foegeding (2001).

Limitations

One of the major limitations of CLSM is that sample treatment is required before imaging, which can alter the product composition (Dürrenberger et al., 2001). Other challenges are choosing the best dyes, image acquisition strategies, and image analysis

steps. With small image areas, it is important to have a representative sample, otherwise low homogeneity in sample collection may lead to low reproducibility (Van Lent et al., 2008). Overall, CLSM can be a labor-intensive, time consuming, and expensive analysis method.

2.6.2.6 Mid-Infrared and Near-Infrared Spectroscopy

The overall mechanism of mid-infrared spectroscopy (MIR) and near-infrared spectroscopy (NIR) is the measurement of the amount of energy absorbed when electromagnetic radiation is transmitted through the sample (López et al., 2013). When electromagnetic radiation reaches the bonds in a sample, those vibrational movements are measured in the form of spectra (Chalmers et al., 2012). They are often described in wavelength units of nm but are also shown in wavenumber format, where the unit is cm^{-1} , such as $400\text{-}4000\text{ cm}^{-1}$ for MIR and $4000\text{-}12,800\text{ cm}^{-1}$ for NIR (Chalmers et al., 2012). With the wave range region of $4000\text{-}200\text{ cm}^{-1}$ and $2,500\text{-}50,000\text{ nm}$, MIR spectroscopy is best for identifying organic and organometallic molecules (Woodcock et al., 2008).

It also helps to explain a bit about the NIR instrumentation to better understand the mechanisms, advantages, and disadvantages. The specific internal assembly and process of spectra collection of a Büchi N-500 NIRFlex are shown in **Figure 3**. The black numeric symbols indicate the path of light, with the process beginning with the lamp on the right (1), beam splitting, polarization, phase shifting, and recombination (2-6), sample scanning (7), and ending with the detector and sample spectra on the left (8) (Büchi, 2017). The white numeric symbols represent the reference laser beam path. These components start with the laser beam being coupled to the NIR beam (1-2), being analyzed by the intensity sensor (3), while also being decoupled (4), and sent to the laser feedback sensor (5), which controls the shifting linear drive velocity (6) (Büchi, 2017).

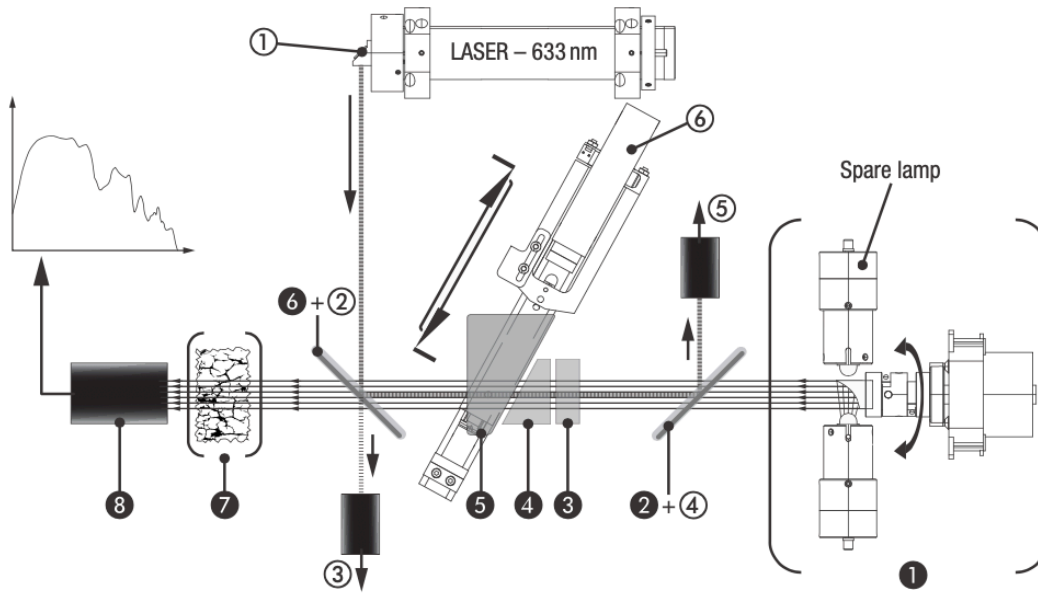


Figure 3. Büchi N-500 NIRFlex internal assembly (Büchi, 2017).

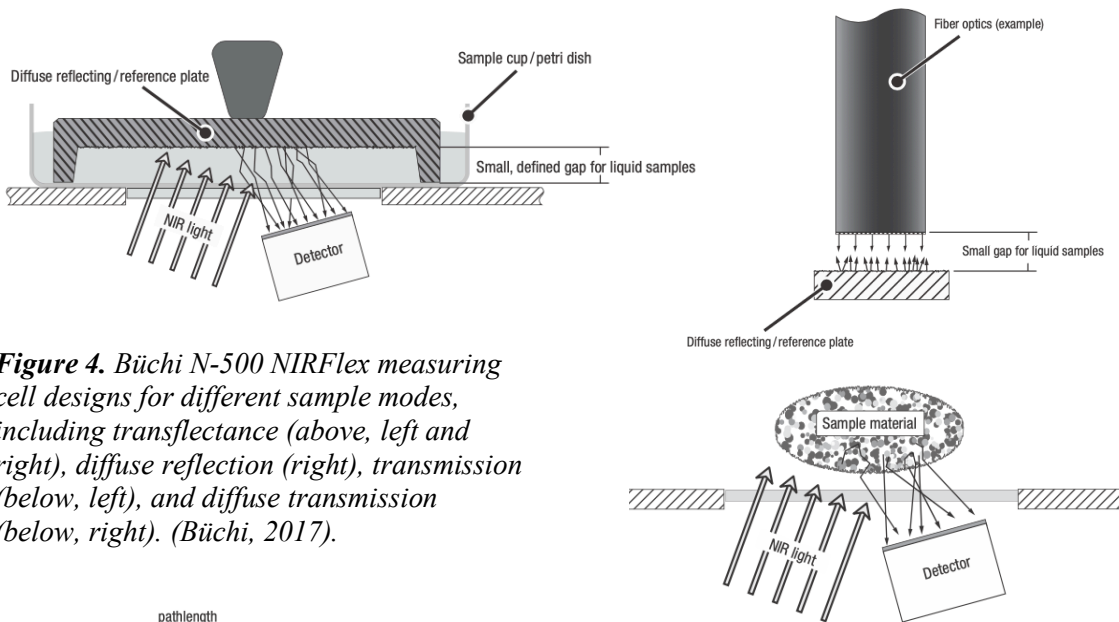
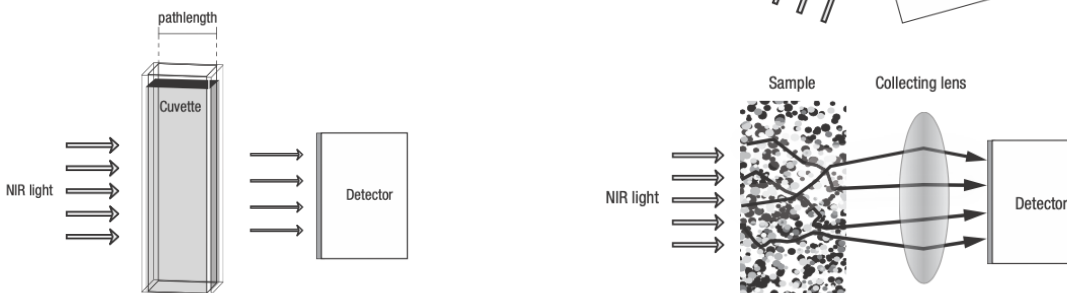


Figure 4. Büchi N-500 NIRFlex measuring cell designs for different sample modes, including transflectance (above, left and right), diffuse reflection (right), transmission (below, left), and diffuse transmission (below, right). (Büchi, 2017).



The multiple measuring cell designs are shown in **Figure 4**. The transreflectance mode is best for translucent and opaque liquids, the diffuse reflection is best for solids, and the transmission and diffuse transmission modes are ideal for liquids (Büchi, 2017).

The growth of Near-Infrared (NIR) spectroscopy technology began in the 1930s with the development of the programmable computer, further progressed in the 1960s and 70s with USDA's development of NIR methods and multiple linear regression analysis, and has continued to evolve rapidly in recent decades with new food industry applications being recognized (Burns and Ciurczak, 2008, Pasquini, 2018). NIR spectroscopy measures reflected light within wavelengths of 750 to 2500 nm, or wavenumbers of 4,000 – 10,000 cm^{-1} , which is between the ranges of visible and infrared light (Buning-Pfaue, 2003). At a chemical level, those wavelength ranges ^{indicate} the stretching and vibrations of O-H, C-H, S-H, and N-H bonds, as well as overall composition (Subramanian and Rodriguez-Saona, 2009). Like other spectroscopic techniques, it has the benefits of no need for reagents, low sample preparation time, and rapid sample analysis.

There are a few shortcomings of NIR. One is a low sensitivity to compounds present at minimal levels, such as salt, soluble nitrogen, and other compounds present at concentrations of 0.1% or lower (Woodcock et al., 2008, Norris, 2009). A second is that water content, temperature, and level of H-bonding present can sometimes overshadow the reliability of the results when predicting other parameters (Woodcock et al., 2008, Norris, 2009). Another is that robust calibrations require large sample sets for reliable correlation methods (Woodcock et al., 2008). The major sources of error in NIR scanning include population error, laboratory error, and packing error (Workman, 2001). Population error relates to the importance of scanning samples that are representative of the greater product population, which is an important consideration in all analysis methods and can be minimized by collecting comprehensive datasets (Workman, 2001). Laboratory error relates to the sample preparation process and can be minimized by precisely reproducing sample preparation procedures (Workman, 2001). Last, packing error is caused when samples may be poorly loaded into the containers and are minimized by using consistent methods and possibly spinning or rotating the sample cups

(Workman, 2001). Overall, consistent methods, a strong understanding of the process, and good training are all important to reduce error.

NIR Dairy product & cheese applications

The use of NIR for characterizing dairy products has grown with applications in mitigating economic adulteration, improving quality control, and ensuring nutritional value, as well as across food formats, from originally liquid, to now solids and pastes (Frankhuizen, 2008). With regards to cheese, NIR methods have already been developed for measuring fat and moisture in process cheese (Kapoor & Metzger, 2008), measuring the quantity of anti-caking agents like cellulose in shredded cheeses (Vazquez, 2019), measuring intact casein in Cheddar cheese (Ma et al., 2019), monitoring the manufacture of PC (Curda and Kukackova, 2004) and many other purposes. Using NIR spectroscopy poses an advantage over other analysis methods due to its rapid analysis time of as little as 30 seconds, little to no sample preparation or reagents needed, non-destructive properties, and ability to analyze samples up to several millimeters in thickness (Buning-Pfaue, 2003, Burns and Ciurczak, 2008). Commercially-available pre-calibrated NIR methods even exist for calculating process cheese formulas based on intact casein content (Goldpeg).

2.6.2.7 Chemometrics

Although spectroscopy methods can provide an abundance of data about a single sample, it is only as useful as our ability to process that data into practical conclusions. It is nearly impossible to evaluate NIR spectra visually, for example, due to small differences in the shift or shape across absorption bands of different samples, broad peaks, and numerous oscillation superimpositions (Büchi, 2016). Chemometrics, or “the interaction of certain mathematical and statistical methods in chemical measurement processes” provides that ability to process the massive quantity of data into a useful method of analysis and prediction (Kumar et al., 2014). Originally coined by the Swedish scientist Svante Wold, its big breakthrough for widespread use came with the advancement of massive data collection and computing in the 21st century (Kumar et al., 2014). Whether developing quantification or identification methods, the various

chemometric tools include qualitative and quantitative calibration methods, validation methods, wavelength selection, and selection of principal components. Chemometric tools can be applied to many of the spectroscopic techniques previously discussed, but its use for FT-NIR applications will be the point of focus below, with a specific focus on the Büchi NIRFlex N-500 FT-NIR spectrometer its associated NIRCal 5.2 Chemometric software. Multivariate regression models help to analyze numerous variables by converting them to new latent variables and using chemometrics to identify relationships between the samples and the latent variables (Kumar et al., 2014). The ultimate function is to find “a statistical correlation between the spectral data and the known property values of the samples used for calibration” (Büchi, 2016).

Qualitative Calibration Methods

Qualitative calibrations are best achieved by using principal component analysis (PCA), which groups samples and spectra by similarities and differences (Büchi, 2016). NIRCal software uses a principal component analysis (PCA) through either the cluster calibrations or the SIMCA method (Büchi, 2016). These can be used to determine identification. However, most dairy and cheese applications involve quantitative analysis so a greater emphasis on those methods is elaborated below.

Quantitative Calibration Methods

Three calibration methods are available in NIRCal software for developing quantitative analyses, including multiple linear regression (MLR), principal component regression (PCR), and partial least squares regression (PLS). Across chemometrics literature, PCR and PLS are the most commonly used methods (Feinberg, 1990, Phatak and De Jong, 1997).

MLR uses multiple variables to predict compositional values. It essentially combines linear regressions in multiple dimensions but is the least useful of the three methods since it only uses a narrow range of wavelengths and discards the rest (Büchi, 2016). As a result, MLR is only recommended when using filter instruments, which are already intended for only partial wavelength ranges (Büchi, 2016).

PCR is the next method and involves a two-step process of PCA with a subsequent MLR (Büchi, 2016). The full spectral range is used for PCA, followed by using those generated principal scores and property values for MLR. One benefit of this process is that “any number of parameters can be simultaneously included in a PCR calibration” (Büchi, 2016). On the other hand, some of those parameters generated from PCA may not describe the biggest spectral variations, so unnecessary data is being used.

PLS, the most robust and updated method, performs multiple iterations to calculate the principal components (PCs) by using spectral information and property values simultaneously (Büchi, 2016). In this method, PCs and scores are calculated similarly to PCR, but the quantitative property values are part of the calculations the whole time. This reduces unnecessary PCs being used, like in PCR, and instead shows the first PCs that lead to the highest correlation (Büchi, 2016). The inclusion of the quantitative property values from the beginning means that separate calibrations should be calculated when the properties are not systematically correlated, while calibrations can be more easily grouped in other methods (Büchi, 2016).

Validation Methods

There are two validation methods: the use of a validation set (VS) and cross-validation (CV). When analyzing a large sample set (~50+ independent samples), it is best to use a VS validation strategy, where two-thirds of samples are assigned to the calibration set and one-third are assigned to the validation set, with the sets having complete independence and no replicates of single samples in both groups (Büchi, 2016). This validation method applies to all qualitative and quantitative calibration methods, and the standard error of prediction (SEP) is used as a metric for validation quality (Büchi, 2016).

When analyzing a smaller sample set (<50 independent samples), it is best to use a cross-validation (CV) strategy (Büchi, 2016). This strategy runs a calibration with all groups except one left out, accomplishing validation by predicting the left out group (Büchi, 2016). A full validation set is created by reiterating the calibration with a different left-out group until all possible groups have been left out. Samples may be grouped in several ways, including leave-one-out, alternate samples, a defined sequence

of samples, random samples, segments along the known property range, segments of equal property values, name of the spectra, or custom groups. CV is ideal for validating small sample sets since it is too time-consuming for larger sets and since small sample sets yield too few samples when split in the two-thirds/one-third grouping for VS methods (Büchi, 2016). Unlike the VS method, CV is only appropriate for PCR and PLS calibration methods, in addition to the standard error of cross-validation (SECV) being used as a validation quality metric instead of SEP (Büchi, 2016).

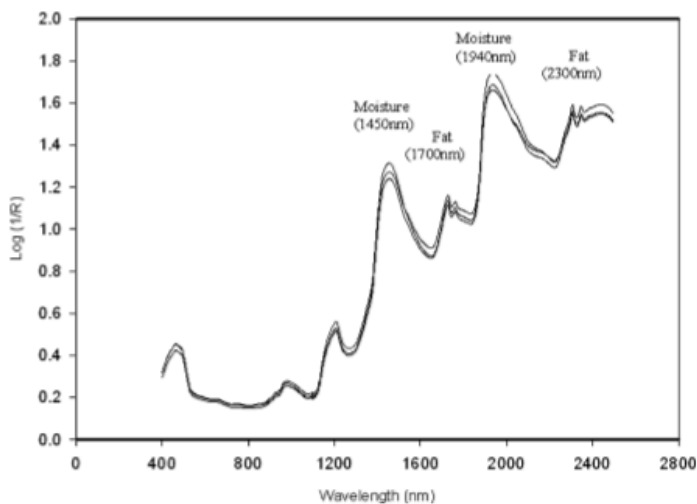


Figure 5. NIR spectra of PC samples (Woodcock et al, 2007)

Wavelengths/Wavenumbers

As previously described, the NIR measurement region is between 750 to 2500 nm, but the exact range depends on the instrument and measuring options (Büchi, 2016). The suggested wavenumber range for solids and liquids when using the NIRFlex N-500 is 4,000 to 10,000 cm^{-1} (Büchi, 2016). When developing calibrations, removing some wavelengths may lead to improved calibrations, although the widest range of wavelengths should be used as possible. An example NIR spectra of PC is shown in **Figure 5**. When adjusting wavelength regions during calibration development, it is important to consider the chemical bonds associated to included or excluded regions and their relevance toward the final calibration. This can sometimes help reduce the

dominating effect of water content or the high presence of H-bonding on the calibration results (Woodcock et al., 2008).

Pretreatments

Data pretreatments are a way to improve spectra by eliminating unwanted effects and emphasizing valuable ones through mathematical transformations that don't change or affect the original spectra (Büchi, 2016). Example detrimental spectra effects that may be worth reducing through pretreatments include overlapping absorption bands, non-linearity, light scattering, and random noise (Büchi, 2016). A few other small variations in spectra may be caused by measurement properties (temperature/humidity of the environment), sample properties (temperature/humidity of the sample, particle size), and changes in the spectrometer (Büchi, 2013). It is suggested to try a calibration without any pretreatments first, then optimize the pretreatments next, since one should understand what does and doesn't need improving from the obtained spectra (Büchi, 2016). NIRCal software offers 34 different pretreatment possibilities within the six groups of normalization, offset, smoothing, derivatives, transformation, and filters (Büchi, 2016). Normalization is used to reduce baseline variations and is best for solids to reduce particle size effects and pressure differences (Büchi, 2016). Offset is used to make baseline corrections that help to adjust for scattering effects (Büchi, 2016). Smoothing is used to reduce noise in spectra, although it affects the spectral resolution and must be chosen carefully so that no loss of spectral information occurs (Büchi, 2016). Like normalization, derivatives also reduce baseline effects but additionally increase smaller absorption peaks. Since derivatives decrease the signal-to-noise ratio, they are often combined with smoothing (Büchi, 2016). Transformations are used to modify the absorption peaks and are recommended for liquids and not for solids (Büchi, 2016). Lastly, linear filters are the most customizable pretreatment and allow for combinations or modified pretreatments defined by the user (Büchi, 2016).

Overall, pretreatments can be used individually or in combinations, with no more than three used at once without leaving data unusable (Büchi, 2013). However, when using combinations of pretreatments, the order in which they are applied is also important and can affect the final results (Büchi, 2013).

Principal Components

Principal components (PCs) are a difficult topic to define clearly and concisely due to highly variable uses in different software and techniques and definitions involving complex mathematical explanations (Mark, 2008). Further confusion occurs due to some literature discussing PCs and other literature discussing PCA, both under the topic of PCs (Mark, 2008). The best concise yet thorough definition is by the American Society for Testing and Materials:

“Principal component analysis – a mathematical procedure for resolving sets of data into orthogonal components whose linear combinations approximate the original data to any desired degree of accuracy. As successive components are calculated, each component accounts for the maximum possible amount of residual variance in the set of data. In spectroscopy, the data are usually spectra, and the number of components is smaller than or equal to the number of variables or the number of spectra, whichever is less” (ASTM).

Ultimately, in the context of spectroscopy and calibration development, PCs represent the sources of variation in the spectra, likely caused by concrete phenomena in the samples that may or may not be known (Mark, 2008).

Furthermore, NIRCal software divides PCs into primary and secondary ones, with primary PCs being used for reconstruction of the spectra and secondary ones being used for separation of compounds present in the sample (Büchi, 2016). When too few primary PCs are used, the calibration is considered under-fitted, resulting in a calibration that isn't selective enough for the samples (Büchi, 2016). On the other hand, too many primary PCs leads to an overfitted calibration, where the calibration spectra may be identified correctly, but the validation spectra will be inaccurate due to irrelevant phenomena being included in the prediction (Büchi, 2016). To determine the right number of PCs, the X-PRESS (predicted residual sum squared) graph (for VS) or CV SECV (standard error of cross-validation) graph (for CV) show which PC quantity is the most influential for a calibration (Büchi, 2016). Two other NIRCal tools that help with primary PC selection are loadings and residuum (Büchi, 2016).

When it comes to secondary PCs, there must be the same or fewer than the quantity of primary PCs (Büchi, 2016). In qualitative calibrations, secondary PC selection impacts the identification of different substances within samples and the allowable range

for accepting those properties (Büchi, 2016). In quantitative calibrations, secondary PCs influence the predicted property values and have the biggest impact on overall calibration quality (Büchi, 2016). The NIRCal tools and guidelines in **Table 3** assist with secondary PC selection for quantitative calibrations.

Ultimately, each calibration will have its ideal quantity of PCs, and choosing the right PCs for a calibration takes multiple attempts and comparisons to compare results before final selection.

Table 3. NIRCal tools for PC selection (BÜCHI, 2016).

Tool		Goal
VS Method	CV Method	
Q-value	Q-value	High (ideally > 0.6)
Regression Coefficients	CV Regression Coefficients	Similar, constant value
SEP Generalized Cross-Validation	--	Low/small
V-Set BIAS	--	Close to zero
C- & V-Set regression coefficients	Calibration & CV regression coefficients	As close to 1 as possible
C- & V-Set PRESS	--	As small as possible
C-Set SEE & V-Set SEP	C-set SEC & CV SECV	As small as possible and similar to each other
C-& V-Set residuum spectra	--	Similar spectra
Consistency	--	As close to 100 (80-110)

Standard Error of Calibration and Cross-Validation

The standard error of calibration (SEC) and standard error of cross-validation (SECV) are two metrics that help to indicate the quality of a chemometric CV calibration model. When creating a C-set/V-set calibration model, SECV is called the standard error of performance or standard error of prediction (SEP) instead (Burns and Ciurczak, 2008). The standard error is generally considered the standard deviation divided by the square root of the number of observations. In the case of a cross-validation model, SECV is computed as the square root of the means square for residuals (Burns and Ciurczak, 2008). The lower and more similar the SEC and SECV are, the better quality the calibration and CV model is (Büchi, 2016).

NIRCal Chemometric applications for natural cheese & PC

One such study that was able to analyze near-infrared (NIR) spectroscopy and use chemometrics to predict final process cheese composition was by Curda & Kukackova (2004). They demonstrated that, after calibration and validation, the properties of dry matter, fat, and crude protein content, pH, and penetration depth of manufactured process cheese samples could be predicted with precision using NIR spectroscopy. This study shows progress towards using chemometrics to determine general process cheese characteristics but still does not meet the need for a rapid test to determine emulsion stability or functional properties such as melt, viscosity, firmness, and oiling off.

Additional NIR studies include those by Adams et al. (1999), who used NIR to determine moisture and fat content in PC; McKenna (2001), who measured moisture in five types of natural cheese; Blazquez et al. (2004), who modeled PC sensory and texture parameters with NIR; Woodcock et al. (2008), who reviewed NIR and MIR techniques for determining cheese quality and authenticity; Ma, Babu, and Amamcharla (2019), who used NIR to predict total protein and intact casein in Cheddar cheese; and Zumbusch (2017) and Vázquez-Portalatín (2019), who developed flow aid, starch, and cellulose quantification methods for shredded and grated cheeses with NIR.

2.7 Conclusion

Process cheese is a complex, continuously changing food product with a large variety of ingredients and processing parameters that determine the final characteristics. Due to the variability of the largest starting ingredient – natural cheese – as well as other processing parameters, methods of predicting final properties or monitoring the steps along the way are challenging but essential. Over the past century, the knowledge and technology surrounding process cheese manufacture have greatly increased, with recent advances in chemometrics and spectroscopy – FT-NIR in particular – showing promising areas for future research. One definite gap in process cheese manufacturing is the existence of a rapid method of analysis to determine emulsion stability prior to cooling, and the combination of chemometrics and FT-NIR spectroscopy may provide the solutions needed.

CHAPTER 3: DEVELOPMENT OF A BENCHTOP METHOD TO PRODUCE PROCESS CHEESE USING A THERMOMIX & OF A RAPID METHOD TO PREDICT PROCESS CHEESE FUNCTIONALITY

3.1 Synopsis

Process cheese (PC) production involves using natural cheese, other dairy and non-dairy ingredients, heating, mixing, and cooling to form a final emulsified product. The properties of natural cheese, in particular, can be difficult to measure or control, leading to process cheese products with undesirable functional properties that may not be apparent until after cooling. Fourier-Transform Near Infrared (FT-NIR) spectroscopy methods exist for measuring fat and moisture in process cheese (Kapoor & Metzger, 2008) and could be a promising tool for predicting PC properties later in shelf life.

In our study, a calibration was developed to correlate spectra of rapidly-cooled PC to 2-week-old PC functional properties (sauce viscosity, melt diameter, and firmness). PC was made at the benchtop level with Cheddar cheese of different ages (1 month & 8 months), butter, instant nonfat dry milk, anhydrous disodium phosphate, cheese salt, and water and processed in a Thermomix using two mixing speeds (approximately 410 and 1015 rpm) and two hold times (0.5 min and 3 min after reaching 80°C final temperature). PC sauce viscosity was measured using a Micro-Visco Amylograph (MVAG), melt diameter was measured using the Schreiber oven melt test, and firmness was measured with a TA.XT texture analyzer. FT-NIR spectra were collected on Petri dishes filled with 50g of molten PC which were rapidly cooled and stored at 4°C and then equilibrated to room temp before scanning. Buchi NIRCAl Chemometric software (V5.6) was used for calibration using partial least squares regression and cross-validation (CV).

When comparing differences in functional properties across the three factors of natural cheese age, mixing speed, and hold time, these findings showed some differences according to age when measuring melted sauce viscosity ($P < 0.01$), but not according to the factors of mixing speed or hold time or when measuring melt area or firmness ($P < 0.05$). To relate the FT-NIR spectra to functional properties, five property calibrations were developed to achieve the highest correlation coefficients and lowest standard errors while adjusting the pretreatments, spectral regions, and principal components. The

calibration with the highest CV correlation coefficient (R^2) was for melt area PC sauce viscosity ($R^2 = 0.9248$), followed by viscosity at 40°C ($R^2 = 0.6046$), firmness ($R^2 = 0.5164$), viscosity at 50°C ($R^2 = 0.2491$), and viscosity at 45°C ($R^2 = 0.1551$).

Despite limited functional property findings relative to manufacturing factors, FT-NIR spectroscopy still showed potential for use as a rapid, nondestructive tool for predicting PC functional properties. Further research into the feasibility of these methods for PC produced at the pilot-scale or full-scale level is still needed.

3.2 Introduction

Process cheese (PC) manufacturers face an ongoing challenge: the ability to produce a final emulsified product within specifications for functional properties despite day-to-day manufacturing variations. The causes of this challenge vary across ingredients, processing conditions, and even storage conditions. Furthermore, the oil-in-water emulsion formed by the end of PC manufacture is not static and can continue to change in the subsequent hours, weeks, and months following manufacture (Kapoor and Metzger, 2008). PC that is produced out of spec leads to inconsistent quality, high amounts of rework, lost profits, and food waste. Many researchers have attempted to solve different parts of the challenge, from stronger ingredient and composition control, improved processing control, and methods of predicting the final properties, but new methods continue to be developed that are faster, more reliable, and lower cost. Fourier-Transform Near Infrared (FT-NIR) spectroscopy combined with chemometrics is one of those new methods and has been used for predicting PC composition but not functionality (Curda and Kuckackova, 2004, Kapoor and Metzger, 2008, Ma et al., 2019). While other rapid methods such as dielectric and front-face fluorescence spectroscopy exist for predicting PC functional properties (Garimella Purna et al., 2005, Amamcharla and Metzger, 2015), we hypothesize that FT-NIR can also be applied to predict PC final functional properties. The objective of this study was to develop a method to predict PC functionality produced at the benchtop level using rapidly-cooled PC samples and FT-NIR spectroscopy. This method would be tested and verified by correlating FT-NIR spectra of PC samples to PC heated sauce viscosity, melt area, and firmness with chemometrics software.

3.3 Materials and Methods

3.3.1 Thermomix Formula & Method

PC spread formulation was created by a collaborator and standardized for identical natural cheese amount, percentage moisture, and percentage fat, and less intact casein in the 3-month versus 8-month formulas. Formulations were developed using proprietary software.

PC spread was made at the benchtop level using a Vorwerk Thermomix blender TM 31-4C (Vorwerk & Co., GmbH, Wuppertal, Germany) at 750-gram sizes using Cheddar cheese of different ages (1 month & 8 months, Land O’Lakes, Arden Hills, MN, US), unsalted butter (Land O’Lakes, Arden Hills, MN, US), instant nonfat dry milk (Maple Island, St. Paul, MN), anhydrous disodium phosphate (Nutricepts, Burnsville, MN, US), Purex all-purpose salt (Morton Salt, Chicago, IL, US), and water (See **Table 4** for formula and target composition). Composition of 3-month versus 8-month Cheddar was not provided by the manufacturer. Cheddar cheese was shredded using the shredding blade of a food processor (3.5qt Waring Commercial by Cuisinart, Stamford, CT, US). Non-water ingredients and shredded cheese were mixed until homogenous but not a complete paste using the chopping blade of a food processor. Cheese mixture and water were then added to the Thermomix to start cooking. Samples were made using two mixing speeds (approximately 410 and 1015 rpm) and two hold times (0.5 min and 3 min after reaching 80°C final temperature).

Table 4. Starting Cheddar composition (left), PC spread target composition (bottom left) standardized for moisture, fat, and protein, and resulting PC formula by percent (bottom right) for Thermomix benchtop level production split by 1-month and 8-month Cheddar.

PC Spread Target Composition	1-month	8-month	1-month		8-month	
			%	g	%	g
Moisture (%)	48.00	48.00	61.55	461.6	61.55	461.6
Fat (g/100g)	24.88	25.25	5.50	41.3	5.50	41.3
Solids-not-fat (%)	27.12	26.75	7.29	54.7	6.27	47.0
Protein (g/100g)	16.82	17.34	2.50	18.8	2.50	18.8
Casein (%)	14.75	14.26	0.60	4.5	0.60	4.5
Intact Casein (%)	87.68	82.24	22.56	169.2	23.58	176.9

3.3.2 Viscosity Analysis

PC sauces were produced by mixing 50g of PC spread with 10g of water and heating in a microwave for 30 sec to mix (approx. 50°C). Two replicates of each sample of melted sauce were analyzed using a Micro-Visco Amylograph (MVAG) (Brabender Instruments, South Hackensack, NJ, US) for cP of sauce heated from 25°C to 50°C over two minutes and held at 50°C for two additional minutes, with a mixing speed of 50 rpm. The average PC sauce viscosity at 45°C is used for calibration development.

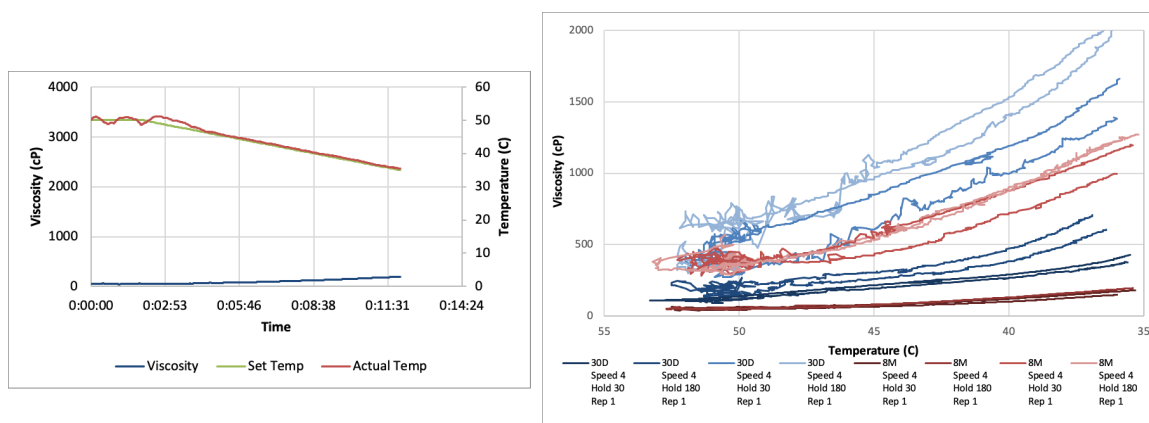


Figure 6. Sample viscosity results as initial MVAG format with both viscosity and temperature on the y-axes and time on the x-axis (left) and adjusted result with time excluded and only viscosity vs temperature (right). Average viscosities at 50C, 45C, and 40C per sample were used for further summaries.

3.3.3 Melt Area Analysis

PC samples were cut to cylinders of 33.5 mm diameter x 7mm tall, melted in covered glass Petri plates in a FREAS mechanical convection oven at 120°C for 7 min, and imaged using a digital imaging system. The melt area of sample images was calculated using Fiji.

3.3.4 NIR Scanning & Chemometric Analysis

FT-NIR spectra were collected with approximately 50 grams of rapidly-cooled PC on glass Petri dishes using the Büchi NIRFlex N-500 (BÜCHI Labortechnik AG) with solids attachment. Three Petri dishes of PC spread were scanned per sample, for a total of 24 spectra per 8-sample manufacturing batch. Based on the functional tests for viscosity,

melt area, and firmness, a total of five properties and values were added to the spectra using the NIRWare Management program.

Büchi NIRCal chemometric software (V5.6) was used for calibration. Calibration development was based on the Büchi NIRCal Chemometric software model for creating a quantitative calibration. Due to the small number of spectra used for calibration (n=16), cross-validation was used instead of assigning spectra to calibration and validation sets. CV Group Selector (V1.9) was used to assign spectra with sequence method into groups with 3 triplicate spectra per group (Figure 7). Calibration Wizard (V5.50 was

used to quickly scan through as many as 56 unique calibrations, adjusting for primary and secondary principal components, wavenumber selection, and pretreatments. The top ten calibrations according to Q-value (a proprietary Büchi calibration quality metric) were compared. The calibration with the lowest standard error (CV SECV graph) and reasonable symmetry in the CV Property Residuum vs Original Property graph was chosen for the final calibration.

3.3.5 Statistics

Two-way analysis of variance (ANOVA) was used to determine the significance of factors and interactions between factors using R (RStudio Version 3.5.1, Boston, MA). A significance level of $P < 0.05$ was used. The exact code can be found in the Appendix (6.2.1 R code for two-way ANOVA of Thermomix sample data).

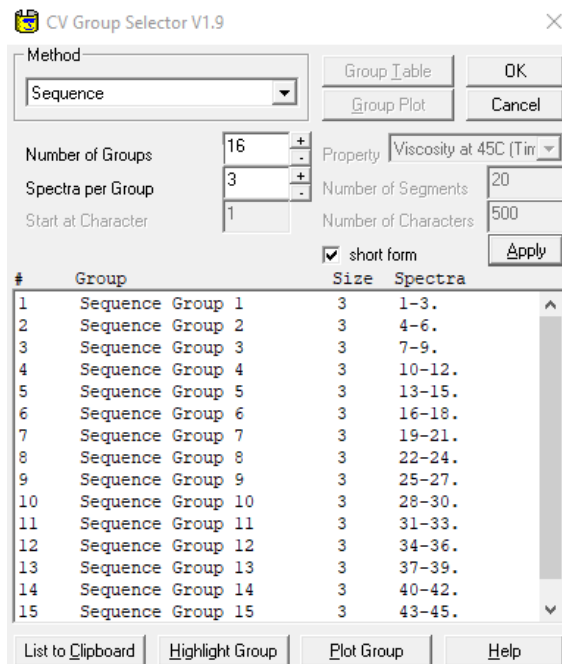


Figure 7. CV Group Selector

3.4 Results and Discussion

3.4.1 Sauce Viscosity Functional Results

Average sauce viscosity results are shown in Table 5. Of the three manufacturing factors of natural cheese age, mixing speed, and hold time, the only one that led to a significant difference in PC sauce viscosity was age ($P < 0.05$) (Table 5 and Table 6). PC sauces made from 1-month-old natural cheese were higher in viscosity than those made from 8-month-old natural cheese. Younger natural cheeses have higher intact casein content, which allows for more protein-water and protein-fat interactions, leading to higher viscosities (Lee et al., 2003b, Thompson, 2016). Some reasoning for finding no significant differences due to mixing speed or hold time factors may be due to not large enough speed change or hold times between samples. Perhaps a 5-min or even 10-min hold time difference would have yielded emulsification and functionality differences. No differences were found when checking for interactions between factors either (Table 6).

Table 5. Average viscosity results (cP) across the three temperature ranges of 40°C, 45°C, and 50°C. Age = natural cheese age, MS = mixing speed, and HT = hold time. Lowercase letters indicate a difference within the temperature range ($P < 0.01$), $n=4$. The only difference found was according to age.

Age	3-month				8-month			
	410 rpm		1015 rpm		410 rpm		1015 rpm	
MS								
HT	0.5 min	3 min	0.5 min	3 min	0.5 min	3 min	0.5 min	3 min
40°C	2091 ^a	2555 ^a	2683 ^a	2636 ^a	1399 ^b	1154 ^b	1290 ^b	1501 ^b
45°C	1524 ^a	1920 ^a	1926 ^a	2035 ^a	841 ^b	766 ^b	925 ^b	1081 ^b
50°C	928 ^a	1198 ^a	1202 ^a	1198 ^a	550 ^b	495 ^b	595 ^b	610 ^b

Table 6. Two-way ANOVA p -value results for average viscosity at 40°C, 45°C, and 50°C across factors and interactions between factors. ** indicates difference ($P < 0.01$). See appendix for exact age p -values. Age = natural cheese age, MS = mixing speed and HT = hold time. $n=32$.

	Age	MS	HT	Age:MS	Age:HT	MS:HT	Age:MS:HT
40°C	<0.01**	0.313	0.669	0.628	0.613	0.950	0.285
45°C	<0.01**	0.184	0.861	0.861	0.531	0.933	0.445
50°C	<0.01**	0.308	0.593	0.787	0.471	0.628	0.417

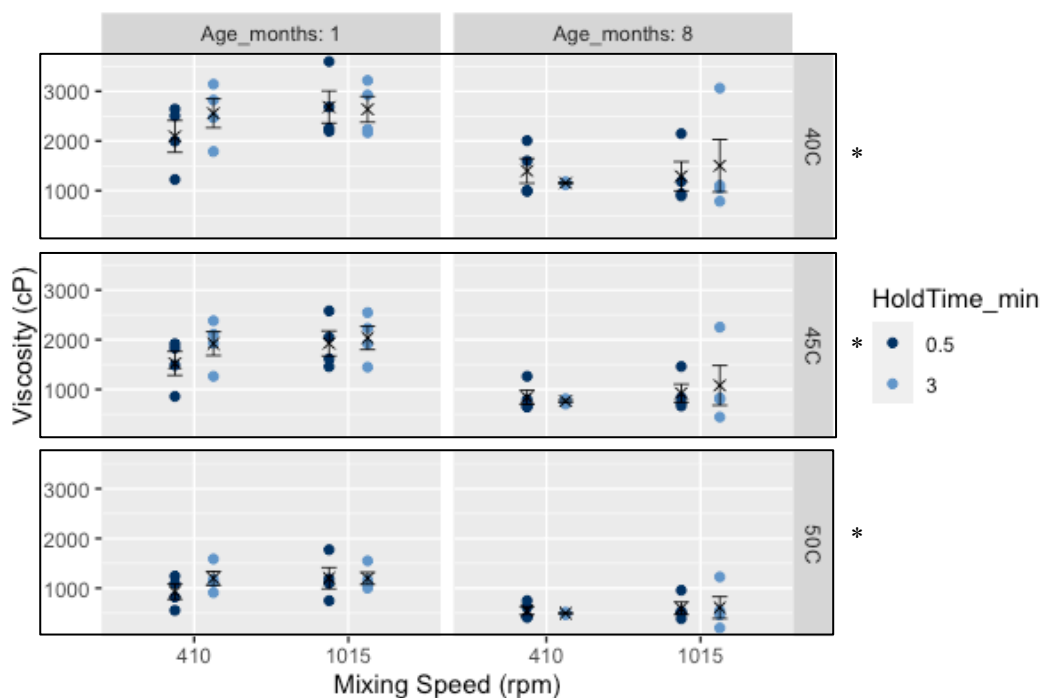


Figure 8. PC sauce viscosity (cP) at 40°C, 45°C, and 50°C (right axis) across samples with different natural cheese age (upper x-axis, 1 & 8 months), mixing speeds (lower x-axis, 410 & 1015 rpm), and hold time (legend, 0.5 & 3 min), $n=32$. x-points represent mean and error bars represent one standard error. Boxes and asterisks indicate rows with differences according to age ($P < 0.05$).

3.4.2 Sauce Viscosity FT-NIR Calibration Results

3.4.2.1 Viscosity at 40°C

The FT-NIR NIRCAl graphs for viscosity cross-validation (CV) at 40°C are shown below (Figure 10, Figure 9, & Figure 11). The best CV calibration was achieved using the pretreatments of first derivative BCAP, followed by normalization by closure (Figure 10). These pretreatments first ran a derivative and then normalization of the spectra. The derivative helps to reduce baseline effects, increase the effect of smaller absorption peaks, and overall reduce signal-to-noise ratio, while the normalization also helps reduce baseline variations (Büchi, 2016). The wavenumbers used for calibration were from 5,000-10,000 cm^{-1} . Although there appears to be some noise in the 8,500-10,000 region, the calibration was still better when including that region than when excluding it. The 4,000-5,000 wavenumber region excluded from the selection is

responsible for NIR combinations region known for NH combinations, NH & OH combinations, NH & CH combinations, CH + CH combinations, and CH + CC combinations (Brüker, 2009)(appendix Figure 81). The peaks in the regression coefficient graph around 6,000, 7,200, and 8,200 cm^{-1} , coincided with wavenumbers known for CH_3 in the first overtone region, CH_3 in the 1st overtone combinations region, and CH_3 in the second overtone region, respectively (Brüker, 2009). Unlike studies that use FT-NIR to correlate to composition, this study places less importance on the specific molecule stretch regions than the overall ability to correlate to the functional properties or finding patterns across similar functional property calibrations. Based on the standard error of cross-validation graph (Figure 9), using 4 principal components (PCs) leads to the lowest standard error of cross-validation, so 4 primary PCs and 4 secondary PCs were used for the final calibration.

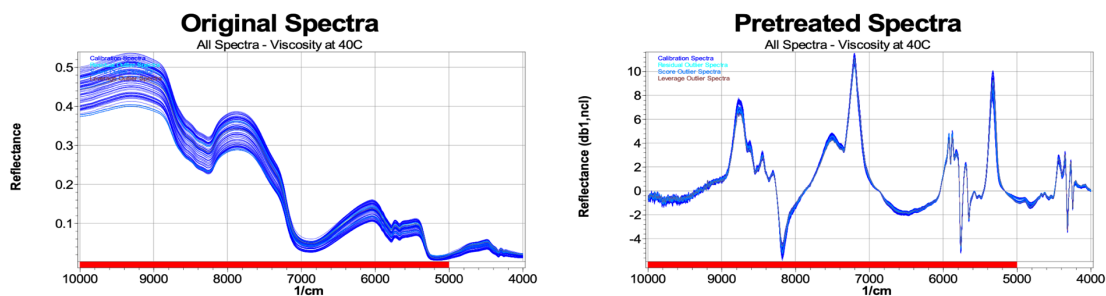


Figure 10. Viscosity at 40°C CV calibration original spectra (left) and pretreated spectra (right). Pretreated spectra used pretreatments 1st BCAP 5 points (db1), followed by normalization by closure (ncl).

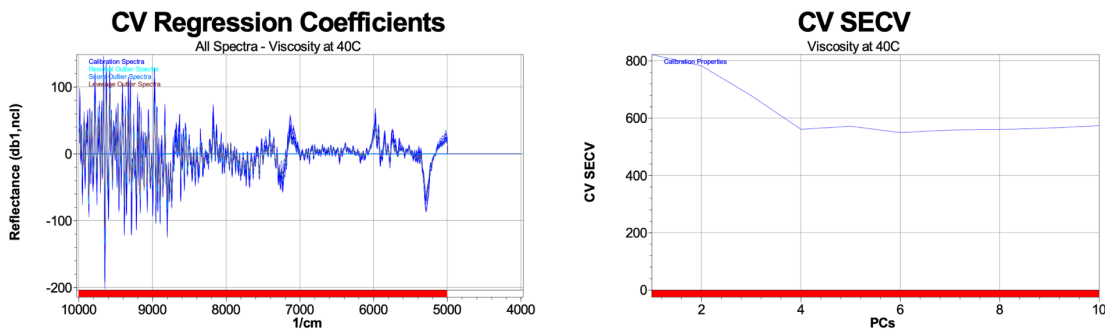
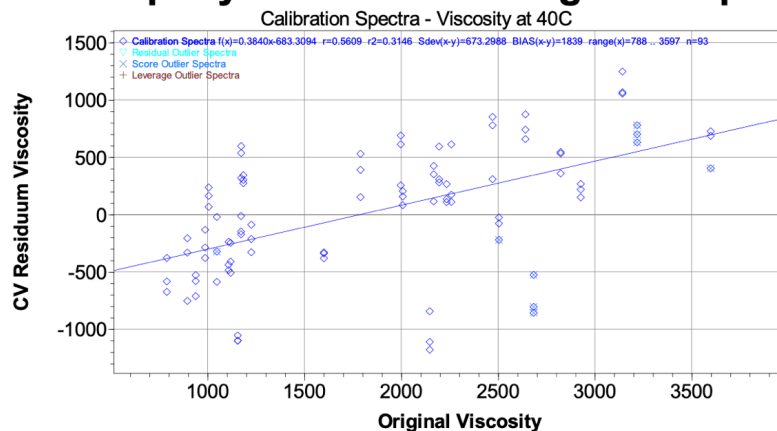


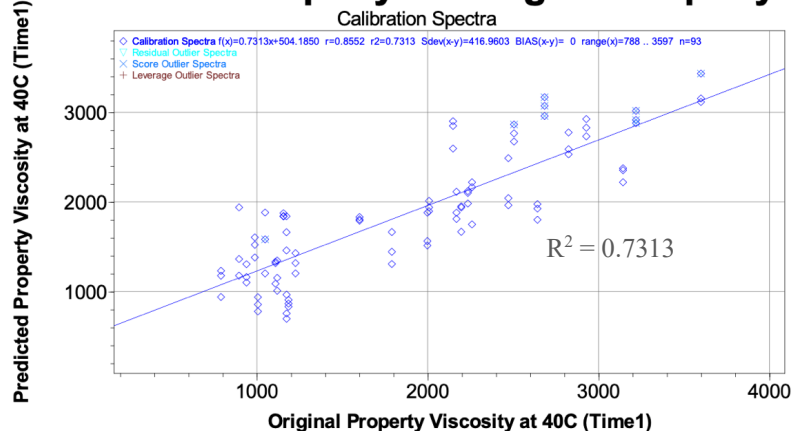
Figure 9. Viscosity at 40°C CV calibration regression coefficients (left) and standard error of cross-validation (SECV, right). Wavenumber region used for calibration was 5,000-10,000 cm^{-1} and 4 PCs were used for primary PC selection.

Figure 11 shows the CV property residuum vs. original property and the predicted property vs the original property of calibration spectra. The first graph represents the difference between the original property and predicted property, so values close to zero for residuum viscosity show a stable calibration (Büchi, 2016). Nine spectra were eliminated from the calibration and designated as score outlier spectra due to the high residuum. The second and third graphs indicate the predicted property vs original property for calibration set and cross-validation set, respectively. For these, a high r^2 value indicates more a reliable calibration. The calibration set r^2 was 0.7313 while the CV set r^2 was slightly lower at 0.6047. Although these are not as high as a statistically relevant 0.800-0.999 correlation coefficient, they still show that a relationship was found between the spectra and the sauce viscosity values at 40°C. The Q-value, a proprietary Büchi quality metric, was 0.4453 for this calibration. This is well below the minimum acceptable calibration Q-values of 0.6, but adding more samples would create a more robust calibration. The moderately low calibration and CV r^2 correlation coefficients indicate that the spectra were poorly related to the functional values. This could mean that the viscosity values measured were more arbitrary to the product's intrinsic properties than we had hoped. Lastly, the standard error of calibration (SEC) showed we were able to determine the viscosity accurately within 416 cP and the standard error of cross-validation (SECV) was able to determine the viscosity within 561 cP (Table 11).

CV Property Residuum vs. Original Property



Predicted Property vs. Original Property



Predicted Property vs Original Property

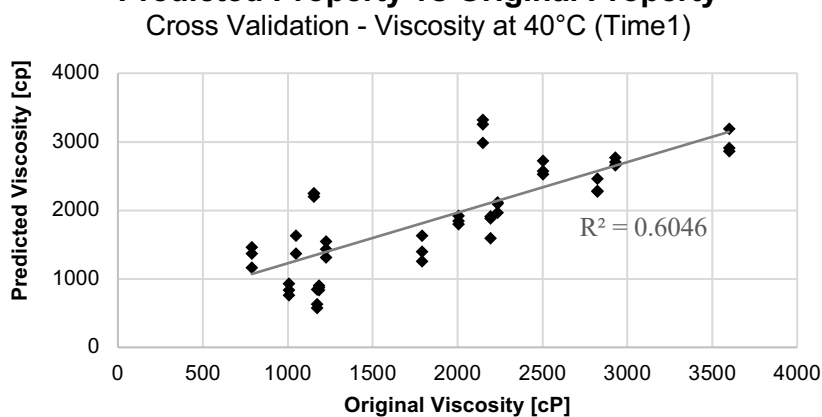


Figure 11. Viscosity (cP) at 40°C CV property residuum vs. original property (top), predicted property vs. original property of calibration (middle), and predicted property vs original property of cross-validation (bottom).

3.4.2.2 Viscosity at 45°C

The CV graphs for viscosity at 45°C are shown below (Figure 12, Figure 13, Figure 14). The best CV calibration was achieved using the pretreatments of first derivative BCAP 5 points (db1), which, as mentioned in the previous calibration, helps to reduce baseline effects, increase the effect of smaller absorption peaks, and reduce the overall signal-to-noise ratio (Büchi, 2016). The full wavenumber region of 4,000-10,000 was used in this final calibration, despite some noise in the 9,000-10,000 wavenumber region (Figure 13). The peaks in the regression coefficient graph around 5400, 5800, 7200, and 8300 cm^{-1} coincided with the wavenumbers known for the water first overtone region, CH_3 first overtone region, CH_3 first overtone combinations region, and CH second overtone region (Appendix **Figure 81**)(Brüker, 2009). As mentioned in the previous calibration, there is less importance on the specific molecule stretch regions than the overall ability to correlate to the functional properties or finding patterns across similar functional property calibrations. The SECV graph indicated 6 primary and 2

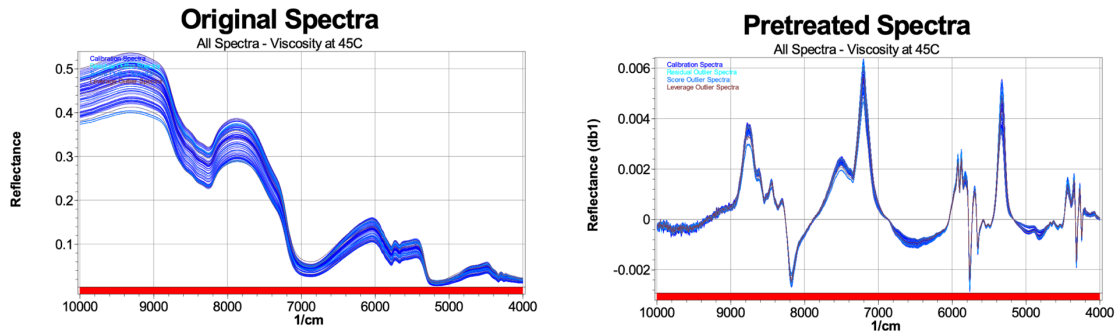


Figure 12. Viscosity at 45°C CV calibration original spectra (left) and pretreated spectra (right). Pretreated spectra used pretreatments first derivative BCAP (db1).

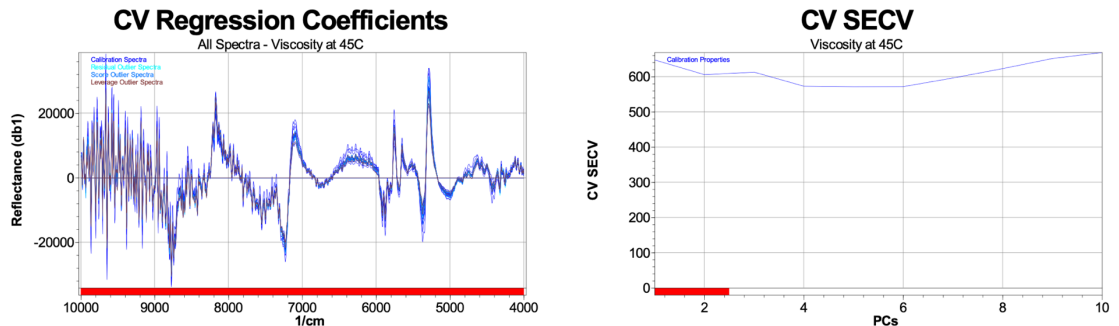
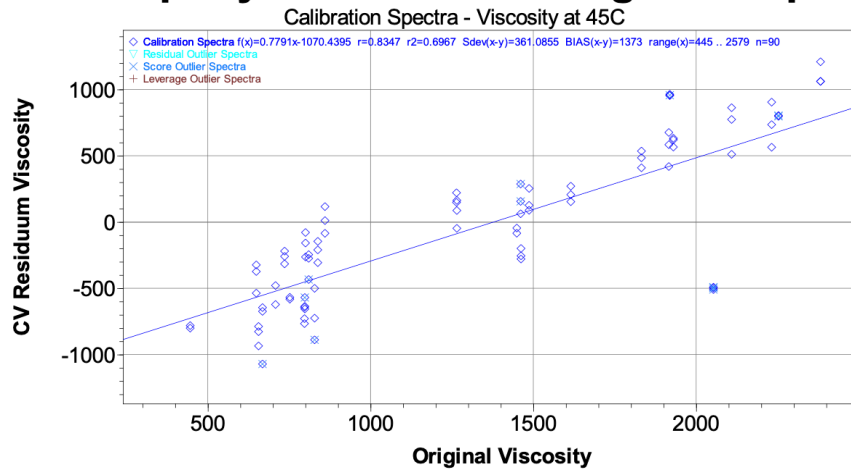
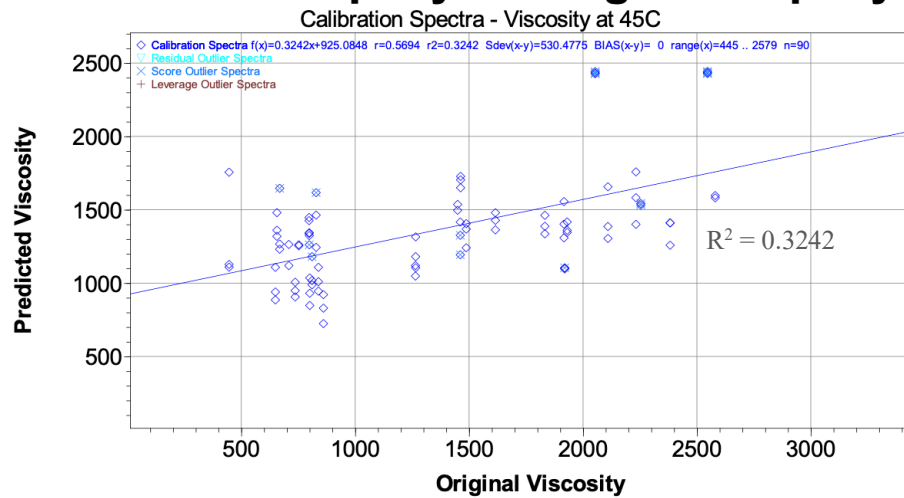


Figure 13. Viscosity at 45°C CV calibration regression coefficients (left) and standard error of cross-validation (SECV, right). Wavenumber region used for calibration was 4,000-10,000 cm^{-1} and 6 primary PCs and 2 secondary PCs used.

CV Property Residuum vs. Original Property



Predicted Property vs. Original Property



Predicted Property vs Original Property

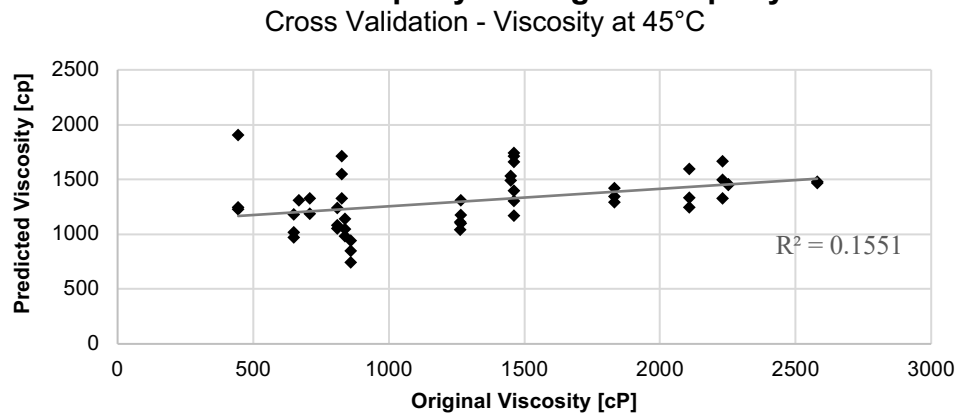


Figure 14. Viscosity at 45°C CV calibration property residuum vs. original property (top) and predicted property vs. original property (bottom).

secondary PCs was the best to achieve minimum standard error.

The final calibration results shown in the three graphs of Figure 14 show residuum ranged symmetrically across the x-axis, with 6 spectra being excluded as score outlier spectra. The second and third graphs indicate that the predicted property vs original property for calibration set and cross-validation set, respectively. The calibration r^2 was 0.3242 and the cross-validation r^2 was 0.1551. Both were very low, indicating that this calibration was not a successful one. Furthermore, the Q-value of 0.4280 from the calibration protocol also indicated it was a poor calibration. Potential reasons for a poor calibration for viscosity at 45°C may be too few samples, inconsistent viscosity analysis, or inconsistent PC production. Lastly, the standard error of calibration (SEC) showed we were able to determine the viscosity within 530 cP and the standard error of cross-validation (SECV) was able to determine the viscosity within 605 cP (Table 11).

3.4.2.3 Viscosity at 50°C

The CV graphs for viscosity at 50°C are shown below (Figure 15, Figure 16, and Figure 17). The final spectra were adjusted using the pretreatments of normalization by closure, followed by first derivative BCAP 5 points (Figure 16). The normalization pretreatment helps to reduce baseline variations, while the derivative helps to reduce baseline effects, increase the effect of smaller peaks, and reduce the overall signal-to-noise ratio (Büchi, 2016). The final calibration used the wavenumber regions of 5,000-7,144 and 7,404-10,000 (Figure 15). The 4,000-5,000 wavenumber region excluded from the selection is responsible for NIR combinations region known for NH combinations, NH & OH combinations, NH & CH combinations, CH + CH combinations, and CH + CC combinations (Brüker, 2009) (see appendix Figure 81). The second region excluded, 7,144-7,404, is responsible for the second overtone region of CH₂, and CH₃ bonds, respectively (Brüker, 2009) (See Appendix Figure 81). Although there was some noise in the 9,000-10,000 wavenumber region, the calibration proved to be stronger by including region than by excluding it. The peaks in the regression coefficient graph around 5300

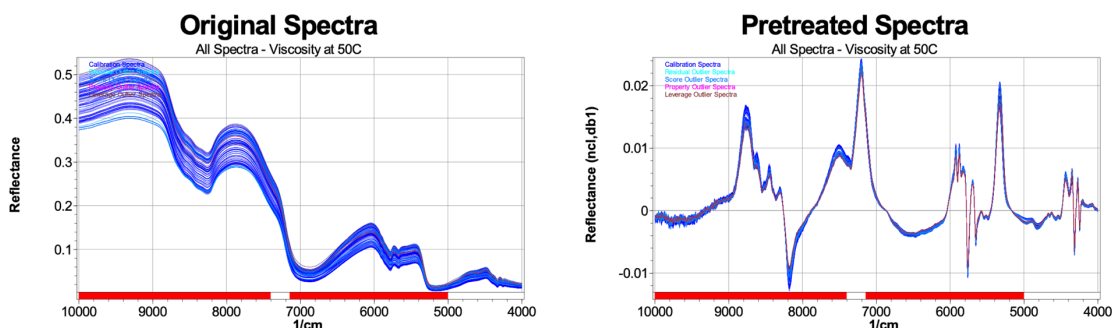


Figure 16. Viscosity at 50°C CV calibration original spectra (left) and pretreated spectra (right). Pretreated spectra used pretreatments normalization by closure (ncl), followed by 1st BCAP 5 points (dbl).

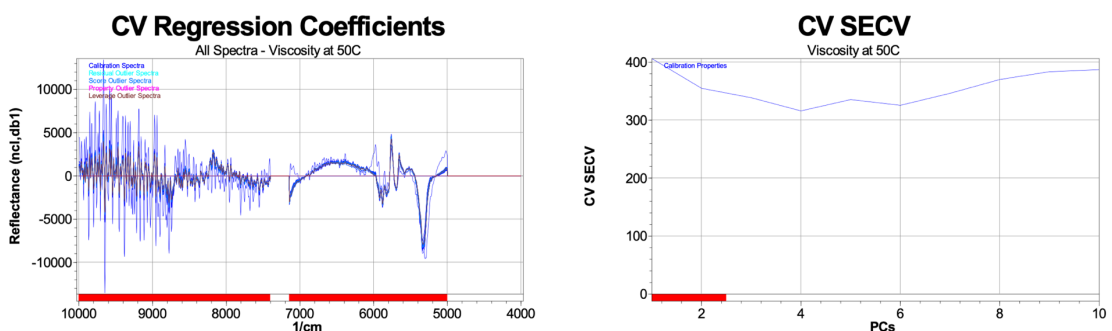
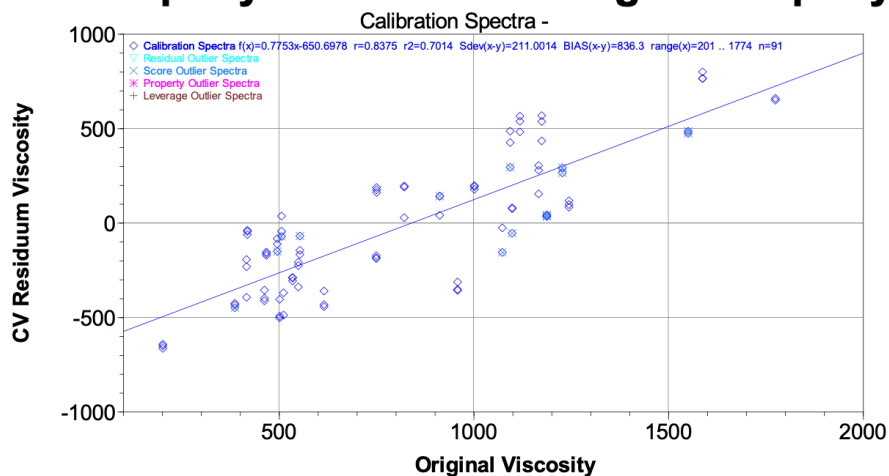


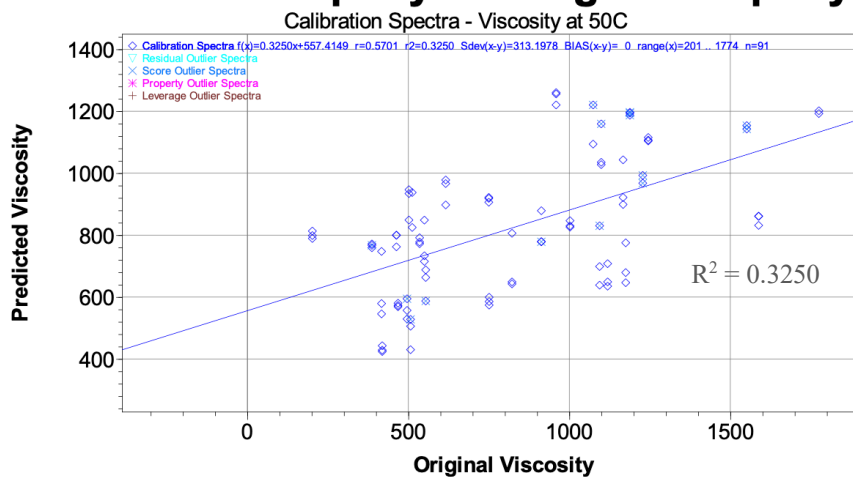
Figure 15. Viscosity at 50°C CV calibration regression coefficients (left) and standard error of cross-validation (SECV, right). Wavenumber region used for calibration was 4,000-7,144 and 7404-10,000 cm^{-1} and 4 PCs were used for primary PC selection.

coincided with the wavenumbers known for the first overtone water region that (Appendix Figure 81)(Brüker, 2009). As mentioned in the previous calibration, there is less importance on the specific molecule stretch regions than the overall ability to correlate to the functional properties or finding patterns across similar functional property calibrations. The SECV graph indicated that 4 primary PCs and 4 secondary PCs were best to achieve minimal standard error (Figure 15). Figure 17 shows the good distribution of residuum values, with 5 spectra excluded as score outlier spectra. It also shows the predicted property vs original property for the calibration set and CV set. The calibration set r^2 was 0.3250 and the CV r^2 was 0.1551. The Q-value for this calibration was 0.4448. Overall, it developed a poor calibration, possibly due to the same reasons provided for the other viscosity sections: too few samples, inconsistent production methods, or inconsistent viscosity analysis methods. Lastly, the standard error of calibration (SEC) showed we were able to determine the viscosity accurately within 313 cP and the

CV Property Residuum vs. Original Property



Predicted Property vs. Original Property



Predicted Property vs Original Property

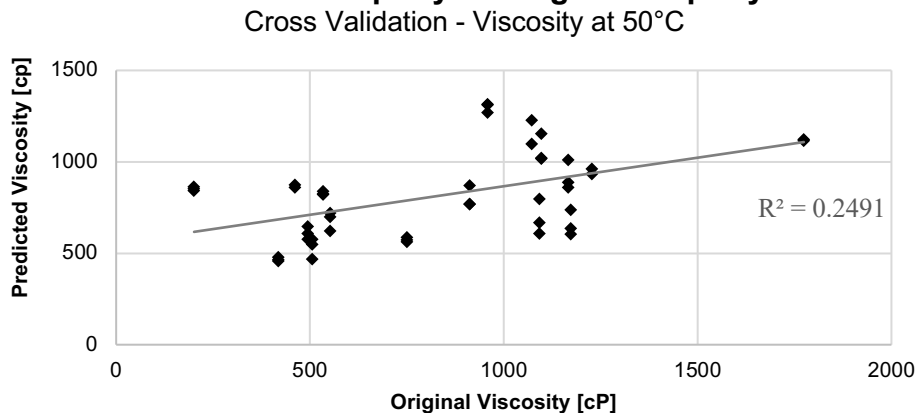


Figure 17. Viscosity at 50°C CV property residuum vs. original property (top), predicted property vs. original property of calibration spectra (middle), and predicted property vs. original property of CV spectra (bottom).

standard error of cross-validation (SECV) was able to determine the viscosity within 355 cP (Table 11).

3.4.3 Melt Area Functional Results

Average melt area results are shown in Figure 18. Of the three manufacturing factors of natural cheese age, mixing speed, and hold time, none led to differences in PC melt area ($P < 0.05$) (Table 8). No differences were found when analyzing interactions between factors either ($P < 0.05$). Although previous literature has shown that PC made with lower levels of intact casein, such as the case in PC made with older natural cheese, are more meltable due to fewer protein-protein and protein-fat interactions and vice versa with younger natural cheese (Templeton and Sommer, 1930, Berger et al., 1989, Garimella Purna et al., 2006, Henderson, 2012), this wasn't as clear in these results. Other literature also suggests that mixing speeds and hold times have effects on meltability (Swenson et al., 2000, Tamime, 2011). The lack of differences found in these samples could be due to too few samples ($n=24$), inconsistencies in PC production on the Thermomix, or melt area analysis. The last possibility of the melt area analysis method is likely the case since one of the three manufacturing runs wasn't able to be tested until a few weeks later in shelf life than the first two runs. This likely led to the set of samples with much higher melt area, as seen in Figure 18.

Table 7. Average melt area results (in^2), $n=3$. Age = natural cheese age, MS = mixing speed, and HT = hold time. No differences were found by age, MS, or HT ($P < 0.05$).

Age	3-month				8-month			
	410 rpm		1015 rpm		410 rpm		1015 rpm	
MS								
HT	0.5 min	3 min	0.5 min	3 min	0.5 min	3 min	0.5 min	3 min
Melt Area	4.92	4.28	3.76	3.63	4.64	4.62	4.41	4.09

Table 8. Two-way ANOVA p -value results for average melt area across factors and interaction between factors. See appendix for exact Age p -values. No differences were found by age, MS, or HT ($P < 0.05$), $n=24$. Age = natural cheese age, MS = mixing speed, and HT = hold.

Age	MS	HT	Age:MS	Age:HT	MS:HT	Age:MS:HT
0.681	0.368	0.694	0.709	0.878	0.938	0.776

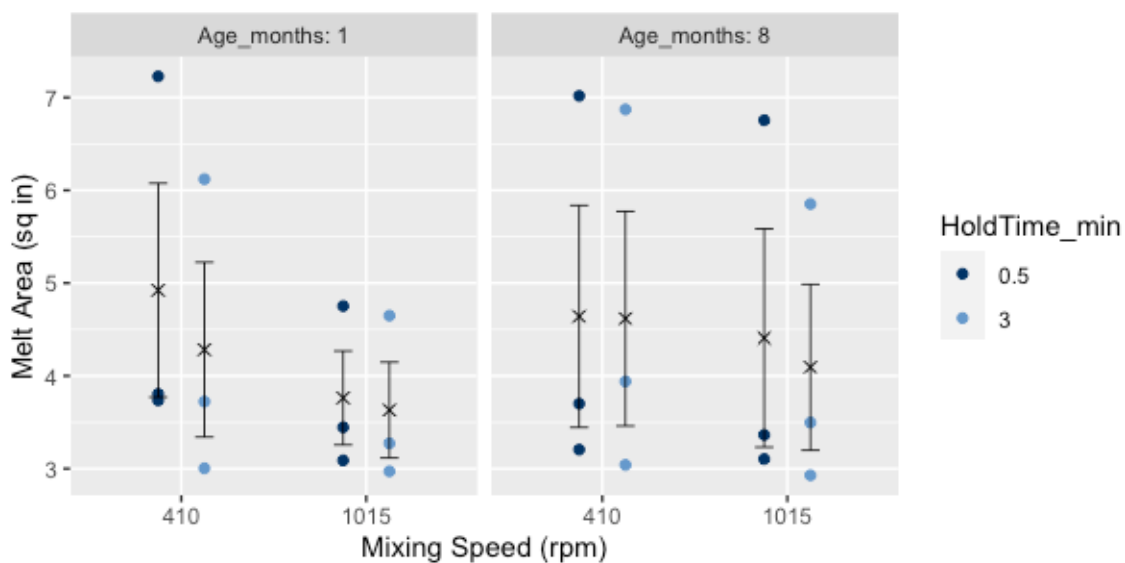


Figure 18. Melt area (sq in) across samples with different natural cheese age (upper x-axis, 1 & 8 months), mixing speeds (lower x-axis, 410 & 1015 rpm), and hold time (legend, 0.5 & 3 min), $n=24$. X-shaped points represent the mean and error bars represent one standard error.

3.4.4 Melt Area FT-NIR Calibration

The FT-NIR NIRCcal graphs for melt area CV are shown below in Figure 19, Figure 20, and Figure 21. The best CV calibration was achieved using the pretreatments of standard normal variate (SNV), followed by first derivative BCAP 5 points (db1) (Figure 19). These pretreatments utilized normalization, which helps reduce baseline variations, and derivative, which helps reduce baseline effects, increase the effect of smaller absorption peaks, and reduce the overall signal-to-noise ratio (Büchi, 2016). Similar to the 50°C viscosity CV calibration, the wavenumber region used for this calibration was 5,000-7,144 and 7,404-10,000 (Figure 20). The 4,000-5,000 wavenumber region excluded from the selection is responsible for NIR combinations regions known for N-H combinations, NH & OH combinations, NH & CH combinations, CH + CH combinations, and CH + CC combinations (Brüker, 2009) (see appendix Figure 81). The second region excluded, 7,144-7,404, is responsible for the second overtone region of CH₂, and CH₃ bonds, respectively (Brüker, 2009) (See Appendix Figure 81). These excluded regions don't necessarily directly relate to the PC chemistry, but instead indicate the broad and complex ability of the chemometric software to correlate to the functional property to the other wavenumber regions. Furthermore, despite showing some

noise in the 8,000-10,000 wavenumber region, the calibration proved to be stronger and have a lower standard error by including that region than by excluding it. The peaks in the regression coefficient graph around 5,400, 5,600, and 5,800 coincided with the wavenumbers known for the first overtone region for water, and the CH, CH₂, and CH₃ first overtone regions (Appendix Figure 81)(Brüker, 2009). The SECV graph (Figure 20) showed that the lowest standard error was achieved with six PCs, so primary and secondary PCs were set to 6 for the final calibration.

The three graphs in Figure 21 show the final calibration values. The top graph shows the distribution of the residuum values, although there are slightly more below the x-axis/0-value than above it and no spectra being assigned as outliers. The second and third graphs show the predicted property for the calibration set and CV set, respectively.

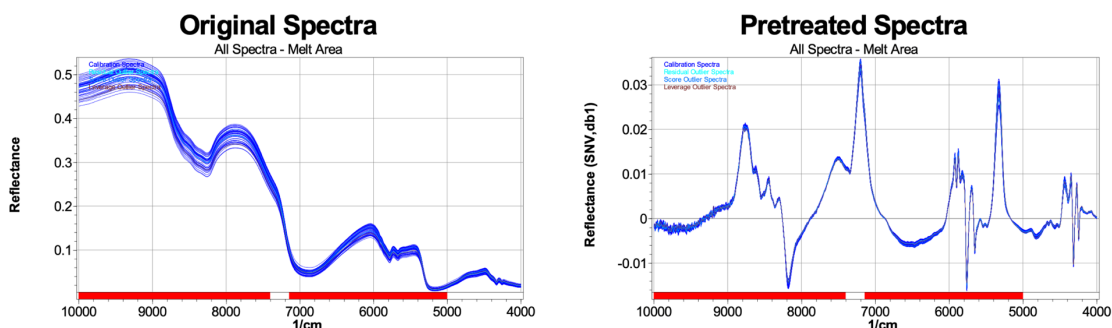


Figure 19. Melt area CV calibration original spectra (left) and pretreated spectra (right). Pretreated spectra used pretreatments of standard normal variate (SNV) and first derivative BCAP (db1).

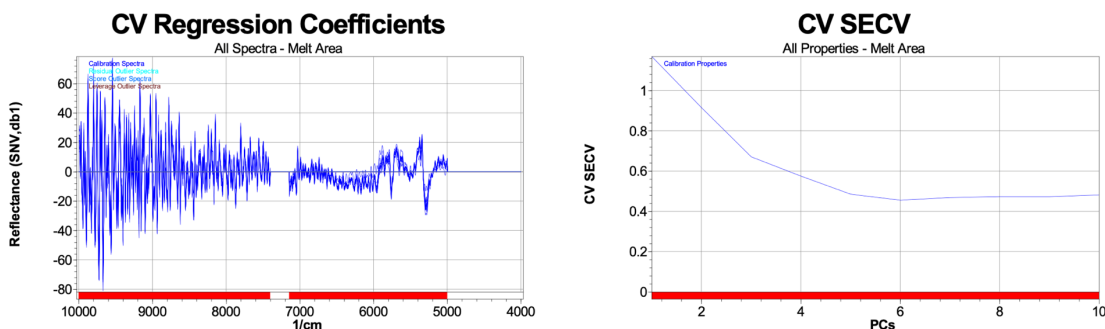
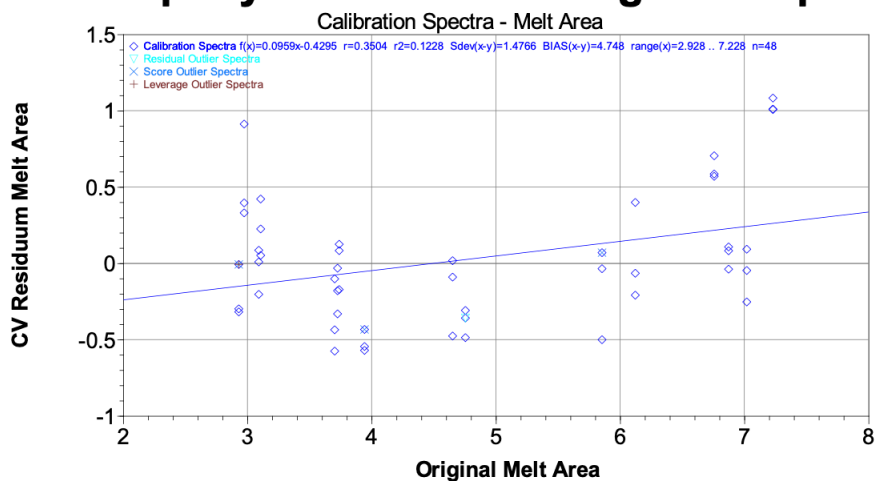
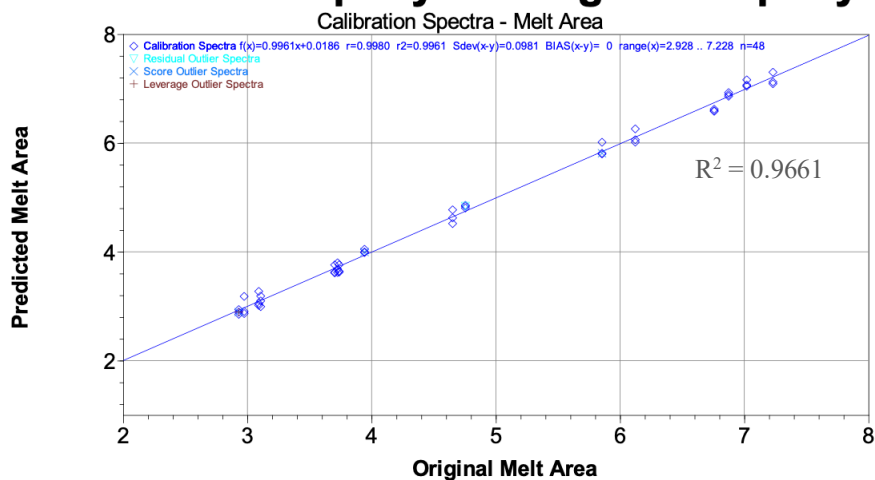


Figure 20. Melt area CV calibration regression coefficients (left) and standard error of cross-validation (SECV, right). Wavenumber region used for calibration was 4,000-7,144 and 7404-10,000 cm^{-1} and 6 PCs used for primary and secondary PC selection.

CV Property Residuum vs. Original Property



Predicted Property vs. Original Property



Predicted Property vs Original Property

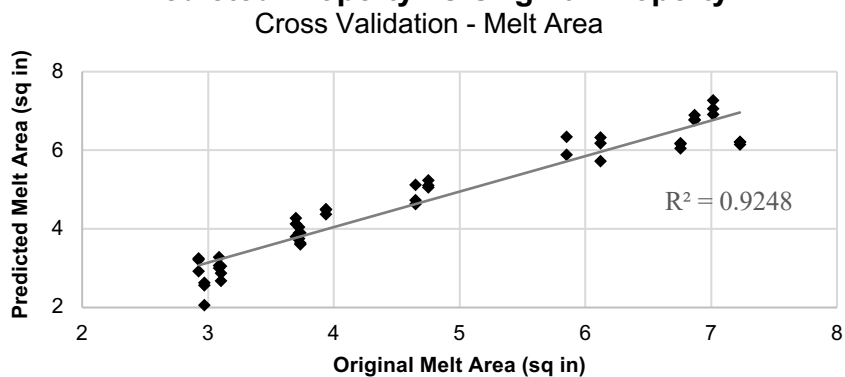


Figure 21. Melt area CV property residuum vs. original property (top), predicted property vs. original property of calibration spectra, $n=48$ (middle), and predicted property vs. original property of CV spectra (bottom).

The calibration set r^2 was 0.9961 and the CV r^2 was 0.9248, which both indicate a high correlation was found between features in spectra to the melt area property values. The Q-value of 0.558 indicates a better calibration than the previous viscosity ones and almost at an acceptable level of 0.6 but still not a high-quality calibration within the 0.8-0.99 Q-value range. Lastly, the standard error of calibration (SEC) showed we were able to determine the melt area accurately within 0.098 in^2 and the standard error of cross-validation (SECV) was able to determine the viscosity within 0.456 in^2 (Table 11).

Another discussion point is the high correlation coefficients found with FT-NIR despite the low ANOVA differences. Perhaps poor consistency across melt runs showed low correlations to effects but NIR could see the intrinsic differences that led to the uneven melt properties, or it could overcome the delayed melt test results that caused high variance and poor ANOVA results.

3.4.5 Firmness Functional Results

Average firmness results are shown in Figure 22. None of the three manufacturing factors of natural cheese age, mixing speed, and hold time led to differences ($P < 0.05$). Since this method was developed later in the study, fewer samples were able to be tested for firmness than for viscosity or melt area. This could have played a part in the lack of differences, despite previous literature showing firmness effects due to the same factors. Examples from literature include that increased cook time led to decreased firmness in fat-free PC, which could correlate to higher hold times (Swenson et al., 2000), and that increased mixing speeds led to higher firmness (Tamime, 2011).

Table 9. Average firmness results (g), $n=2$. Age = natural cheese age, MS = mixing speed, and HT = hold time. No differences were found by age, MS, or HT ($P < 0.05$).

Age	3-month				8-month			
	410 rpm		1015 rpm		410 rpm		1015 rpm	
HT	0.5 min	3 min	0.5 min	3 min	0.5 min	3 min	0.5 min	3 min
Firmness (g)	440.7	545.4	567.2	603.2	487.0	395.6	474.5	520.4

Table 10. Two-way ANOVA *p*-value results for average firmness across factors and interactions between factors. No differences were found by age, MS, or HT ($P < 0.05$). Age = natural cheese age, MS = mixing speed, and HT = hold time, $n=16$.

Age	MS	HT	Age:MS	Age:HT	MS:HT	Age:MS:HT
0.276	0.249	0.700	0.770	0.457	0.781	0.413

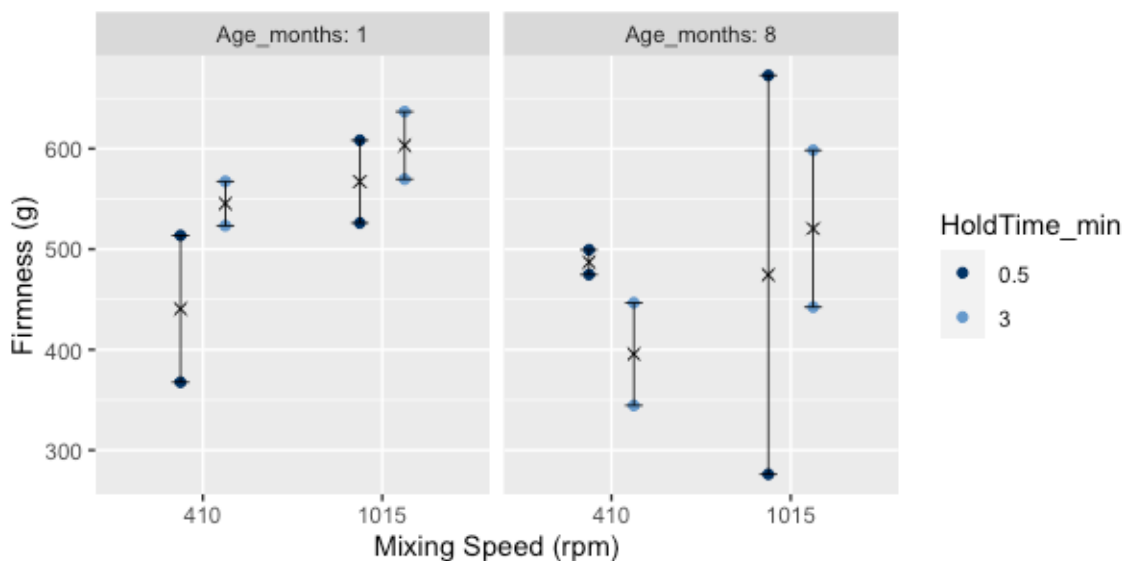


Figure 22. PC firmness (g) across samples with different natural cheese age (upper x-axis, 1 & 8 months), mixing speeds (lower x-axis, 410 & 1015 rpm), and hold time (legend, 0.5 & 3 min), $n=16$. X-shaped points represent the mean and error bars represent one standard error.

3.4.6 Firmness FT-NIR Calibration

The FT-NIR NIRCcal graphs for TA.XT firmness CV are shown below (**Figure 23**, **Figure 24**, and **Figure 25**). The best CV calibration was achieved using the Kubelka Munk pretreatment (**Figure 23**). This pretreatment is a transformation treatment that modifies the absorption peaks and is independent of calibration wavelengths (Büchi, 2016). Although this pretreatment is used more often for liquids than solids (Büchi, 2016), it led to a slightly better calibration than using Savitzky-Golay 9-points or no pretreatment at all. The wavenumber region used was 4,400-4,800, 5,400-6,600, and 7,800-10,000 cm^{-1} (Figure 24). The peaks in the regression coefficient regression graph were around 4,500, 5,500, and 5,900-6,300 cm^{-1} . The 4,500 cm^{-1} peak coincided with the wavenumbers known for several compounds, including the combination regions for

water, RNH₂, CH-O, and C-C (Appendix Figure 81)(Brüker, 2009). The 5,500 and 5,900-6,300 regions are known for the water and CH₃ first overtone regions, respectively (Appendix Figure 81)(Brüker, 2009). The SECV graph indicated that 4 primary PCs and 3 secondary PCs were best to achieve minimal standard error (Figure 24).

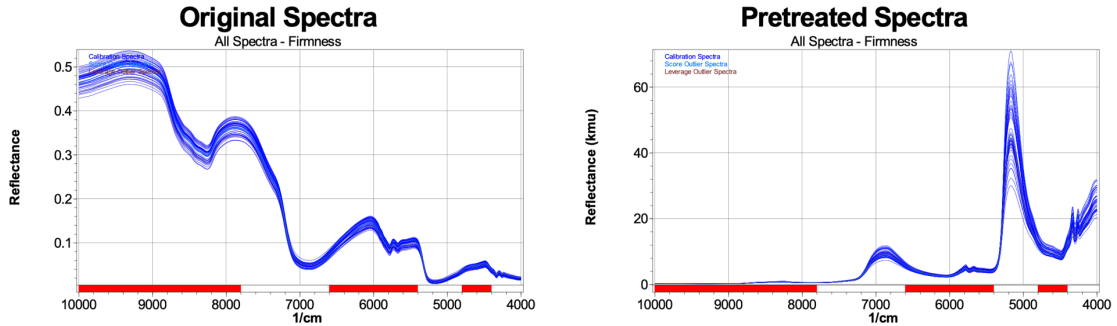


Figure 23. Firmness CV calibration original spectra (left) and pretreated spectra (right). Pretreatment used was Kubelka Munk (kmu).

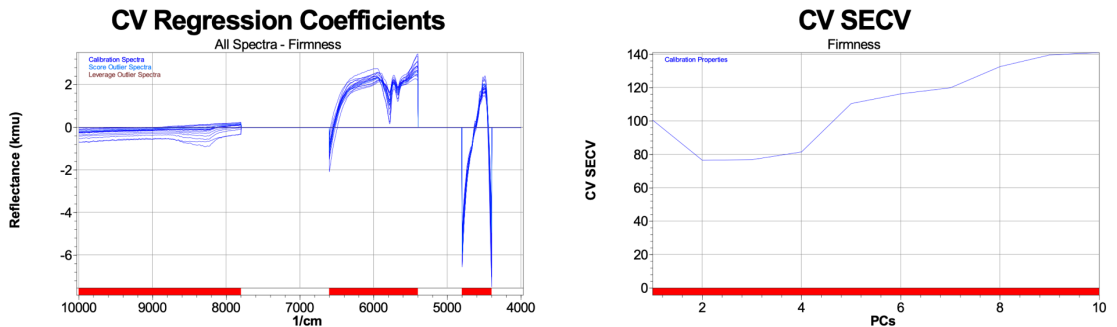
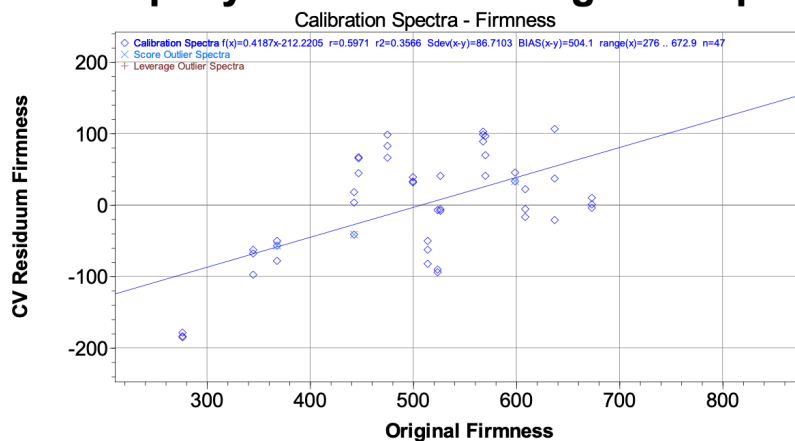


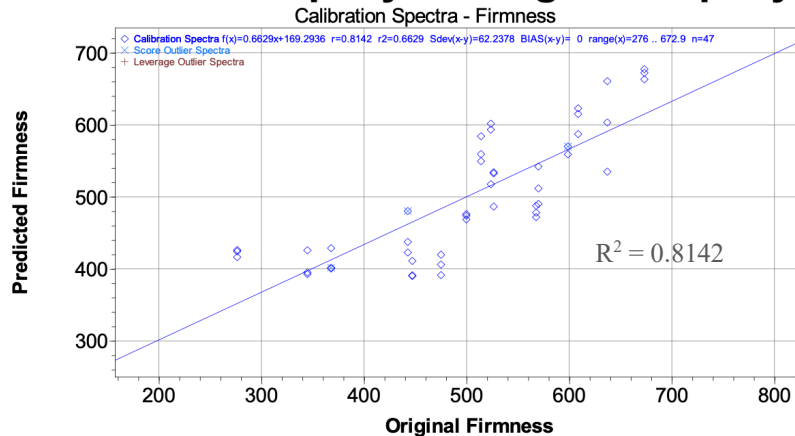
Figure 24. Firmness CV calibration regression coefficient (left) and standard error of cross-validation (SECV, right). Wavenumber region used for calibration was 4,400-4,800, 5,400-6,600, and 7,800-10,000. 4 primary PCs and 3 secondary PCs were used.

The final calibration results shown in the three graphs of **Figure 25** show the residuum values and predicted versus original values for firmness calibration and cross-validation. The residuum values are well-distributed and show one outlier spectra. The calibration set r^2 was 0.5164, the CV r^2 was 0.8142, and the Büchi Q-value was 0.5164.

CV Property Residuum vs. Original Property



Predicted Property vs. Original Property



Predicted Property vs Original Property

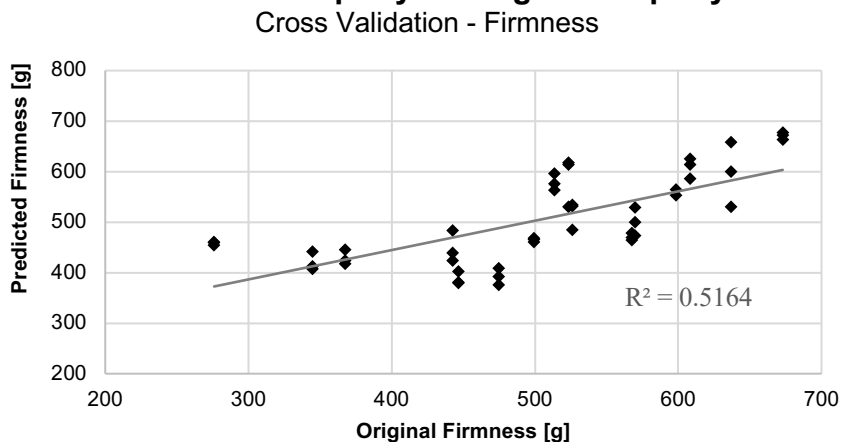


Figure 25. Firmness CV calibration property residuum vs. original property (top), predicted property vs. original property for calibration (middle), and predicted property vs. original property for CV (bottom).

Lastly, the standard error of calibration (SEC) showed we were able to determine the firmness accurately within 62g and the standard error of cross-validation (SECV) was able to determine the viscosity within 77g (Table 11).

One of the shortcomings of this calibration is the limited sample size. With only two manufacturing runs per sample, the 48 spectra only represent 16 samples. As a result, there weren't many values for the calibration to analyze. Curda and Kuckackova also analyzed PC composition and penetration properties, achieving a 0.992 r^2 calibration coefficient and 0.925 r^2 CV coefficient with a sample size of 50 (2004). This suggests a larger sample size would provide improve the calibration found within this research study.

3.4.7 FT-NIR Calibration Summary

The summary of the five NIRCal property calibrations is shown in **Table 11** below. Of the five properties, the melt area achieved the calibration with the highest regression coefficients for calibration and CV. The standard error of calibration (SEC) and standard error of cross-validation (SECV) indicate the difference between the predicted value compared to the original.

Table 11. Calibration equation statistics using cross-validation and regression model for Thermomix PC sample functional properties. Spectra N indicates the number of spectra used, but there were approximately 3 spectra per unique PC sample. 1°/2° PCs = number of primary/secondary PCs used; PT = pretreatment, SEC = standard error of calibration; SECV = standard error of cross-validation; $C r^2$ = calibration regression coefficient, $CV r^2$ = cross-validation regression coefficient; Q-value = Büchi quality value.

Property	Spectra N	1°/2° PCs	PT	Orig-Mean	SEC	SECV	$C r^2$	$CV r^2$	Q-value
Viscosity at 40°C	93	4/4	db1, ncl	1876	416	561	0.7313	0.6046	0.4453
Viscosity at 45°C	90	6/2	ncl	1369	530	605	0.3242	0.1551	0.4280
Viscosity at 50°C	91	4/4	ncl, db1	835	313	355	0.3250	0.2491	0.4448
Melt Area	48	6/6	snv, db1	4.78	0.10	0.46	0.9661	0.9248	0.5580
Firmness	47	4/3	kmu	502	62	76	0.8142	0.5164	0.5164

One explanation for a better calibration and cross-validation model for 40°C than 45°C and 50°C is if more protein-protein and protein-fat interactions could occur at the

slightly cooler temperatures, correlating better to the molecular structures indicated by the spectra.

3.5 Conclusion and Future Research

These findings show that PC samples made on the Thermomix at the benchtop level showed some differences according to natural cheese age when measuring melted sauce viscosity, but not according to the factors of mixing speed or hold time or when measuring melt area or firmness. One gap in this study was the lack of compositional data and pH measurements. These PC samples were originally considered preliminary and so compositional analysis was not completed before samples had reached the end of shelf life. Some pH measurements were taken but measurement was inconsistent across all batches so no results were reported.

Despite limited functional property findings relative to manufacturing factors, FT-NIR spectroscopy still showed some correlations between the rapidly-cooled PC sample spectra and the functional properties of samples later in shelf life. These FT-NIR CV correlations were strongest melt area ($R^2 = 0.9248$), moderate for viscosity at 40°C ($R^2 = 0.6046$) and firmness ($R^2 = 0.5174$), and weakest for viscosity at 45°C ($R^2 = 0.1551$), viscosity at 50°C ($R^2 = 0.2491$). Since previous research using FT-NIR and other spectroscopy for predicting PC functional properties achieved higher quality calibrations with larger sample sizes (Curda and Kukackova, 2004, Amamcharla and Metzger, 2015), increasing sample size would likely increase the robustness of the calibrations and reliability of these conclusions. Manufacturing PC at the benchtop level allowed for a more controlled formulation, but using pilot-level or large-scale, industry-produced samples would allow for more samples to be analyzed and used in a calibration. Although small, the melt area findings in this study suggest that FT-NIR spectroscopy is a feasible nondestructive and rapid tool for determining functional properties of PC produced at the benchtop level. Further research into the feasibility of these methods for PC produced at pilot-scale or full-scale levels is still needed.

CHAPTER 4: DEVELOPMENT OF A RAPID METHOD TO PREDICT PROCESS CHEESE FUNCTIONALITY

4.1 Synopsis

Process cheese (PC) production involves using natural cheese, other dairy and non-dairy ingredients, heating, mixing, and cooling to form a final emulsified product. The properties of natural cheese, in particular, can be difficult to measure or control, leading to process cheese products with undesirable functional properties that may not be apparent until after cooling. Fourier-Transform Near Infrared (FT-NIR) spectroscopy methods exist for measuring fat and moisture in process cheese (Kapoor & Metzger, 2008) and could be a promising tool for predicting PC properties later in shelf life.

In our study, a calibration was developed to correlate spectra of rapidly-cooled PC to 2-week-old and 4-week-old PC functional properties (sauce viscosity, melt diameter, and firmness), as well as fat droplet measurements. PC was made at the pilot level in 1.5kg batches with Cheddar cheese of different ages (3 & 8 months), instant nonfat dry milk, clarified butter oil, salt, anhydrous disodium phosphate, and water and processed in a Blentech using two mixing speeds (150 and 265 rpm) and two hold times (1 min and 3 min after reaching 80°C final temperature). PC sauce viscosity was measured using a Micro-Visco Amylograph (MVAG), melt diameter was measured using the Schreiber oven melt test, firmness was measured with a TA.XT texture analyzer, and fat droplet measurements were found using confocal laser scanning microscopy (CLSM). FT-NIR spectra were collected on Petri dishes filled with 50g of molten PC which were rapidly cooled and stored at 4°C and then equilibrated to room temp before scanning. Buchi NIRCal Chemometric software (V5.6) was used for calibration using partial least squares regression and cross-validation (CV).

When comparing differences in functional properties across the three factors of natural cheese age, mixing speed, and hold time, these findings showed differences according to age when measuring melted sauce viscosity at four weeks past manufacture ($P < 0.05$) and in interactions between the three factors, but not according to the individual factors of mixing speed or hold time or when measuring melt area or firmness ($P < 0.05$).

The only fat droplet measurements that were significant were for interactions between the three factors for average and median Feret diameters ($P < 0.05$).

To correlate the FT-NIR spectra to functional properties, 14 property calibration models were developed using cross-validation methods to achieve the highest correlation coefficients and lowest standard errors while adjusting the pretreatments, spectral regions, and principal components. The calibration models with the highest CV correlation coefficient (R^2) was for melt area (T1, $R^2 = 0.7335$), viscosity at 45°C (T1, $R^2 = 0.6556$; T2, $R^2 = 0.6538$), firmness (T1, $R^2 = 0.6299$), and viscosity at 40°C (T2, $R^2 = 0.6475$). The calibration R^2 were closer to acceptable range (>0.9) for viscosity at 40°C (T1, $R^2 = 0.9041$) and 50°C (T1, $R^2 = 0.9259$).

Despite limited functional property findings relative to manufacturing factors, FT-NIR spectroscopy still showed some potential for use as a rapid, nondestructive tool for predicting PC functional properties. Further research into the feasibility of these methods for PC produced at the full manufacturing level is still needed.

4.2 Introduction

Process cheese (PC) manufacturers face an ongoing challenge: the ability to produce a final emulsified product within specifications for functional properties despite day-to-day manufacturing variations. The causes of this challenge vary across ingredients, processing conditions, and even storage conditions. Furthermore, the oil-in-water emulsion formed by the end of PC manufacture is not static and can continue to change in the subsequent hours, weeks, and months following manufacture (Kapoor and Metzger, 2008). PC that is produced out of spec leads to inconsistent quality, high amounts of rework, lost profits, and food waste. Many researchers have attempted to solve different parts of the challenge, from stronger ingredient and composition control, improved processing control, and methods of predicting the final properties, but new methods continue to be developed that are faster, more reliable, and lower cost. Fourier-Transform Near Infrared (FT-NIR) spectroscopy and chemometrics is one of those new methods, and has been used for predicting compositional properties in PC but not functional ones (Curda and Kukackova, 2004, Kapoor and Metzger, 2008, Ma et al., 2019). While another rapid method, dielectric spectroscopy, exists for predicting PC

functional properties (Amamcharla and Metzger, 2015), we hypothesize that FT-NIR can be applied to rapidly-cooled PC samples made at benchtop level to predict final functional properties. The objective of this study was to develop a method to predict PC functionality produced at the pilot level using rapidly-cooled PC samples and FT-NIR spectroscopy. This method would be tested and verified by correlating FT-NIR spectra of PC samples to PC heated sauce viscosity, melt area, firmness, and fat droplet measurements with chemometrics software.

4.3 Materials and Methods

4.3.1 Experimental Design

To test if FT-NIR spectra can be correlated to functional properties, differences in functional properties in process cheese spreads were necessary. To accomplish that, three factors were utilized – two cheese ages, two mixing speeds, and two hold times – with a factorial design leading to eight unique cheese samples. Manufactured PC spread samples were scanned in FT-NIR, tested for functional properties and droplet size, and those property values were used for developing a calibration.

4.3.2 Process Cheese Spread Formulation and Manufacture

PC spread formulation was adapted from Kapoor et al. (2007), developed using Excel, and standardized for identical natural cheese amount, percentage moisture, and percentage fat, and less intact casein in the 3-month versus 8-month formulas. PC spread was made at the pilot level using a Blentech™ twin-screw cooker (Blentech Corporation, Rohnert Park, CA, USA) at 3 kg “pre-blends” which were split during production steps into two samples of 1.5 kg each (**Figure 26**). Ingredients included Cheddar-type natural cheese of different ages (3 months & 8 months, AMPI Inc., New Ulm, Minn. U.S.A.), clarified butter oil (Mid-America Farms, Springfield, MO), instant nonfat dry milk (Maple Island, St. Paul, MN), anhydrous disodium phosphate (Nutricepts, Burnsville, MN), Purex all-purpose salt (Morton Salt, Chicago, IL), and water (**Table 12**). Ten-pound blocks of Cheddar were shredded using the shredding blade of a food processor (3.5qt Waring Commercial by Cuisinart, Stamford, CT). Three-kilogram double-batch “pre-blends” of all ingredients except water were made using a

food processor, with the resulting mixture having a coarse texture and storing at 4°C until ready to manufacture. They were mixed with water at room temperature in the Blentech at speed 2 (approximately 100 rpm) for 2 min. Next, the speeds were increased to either 4 or 8 (approximately 150 and 265 rpm, respectively) and indirect steam was turned on to heat the steam jacket of the cooker. After reaching 80°C final temperature, samples were held for two hold times (1 min, then 3 min) with the heat off and continuous mixing before pouring into 1-kg plastic-lined cardboard containers for functional tests and three glass Petri plates (~50g each) for FT-NIR scanning. Samples were cooled at room temperature (~22°C) for 15 min before moving to 4°C storage. Within 1-2 days, the samples were transferred to plastic bags and vacuum-sealed and stored at 4°C until further analysis.

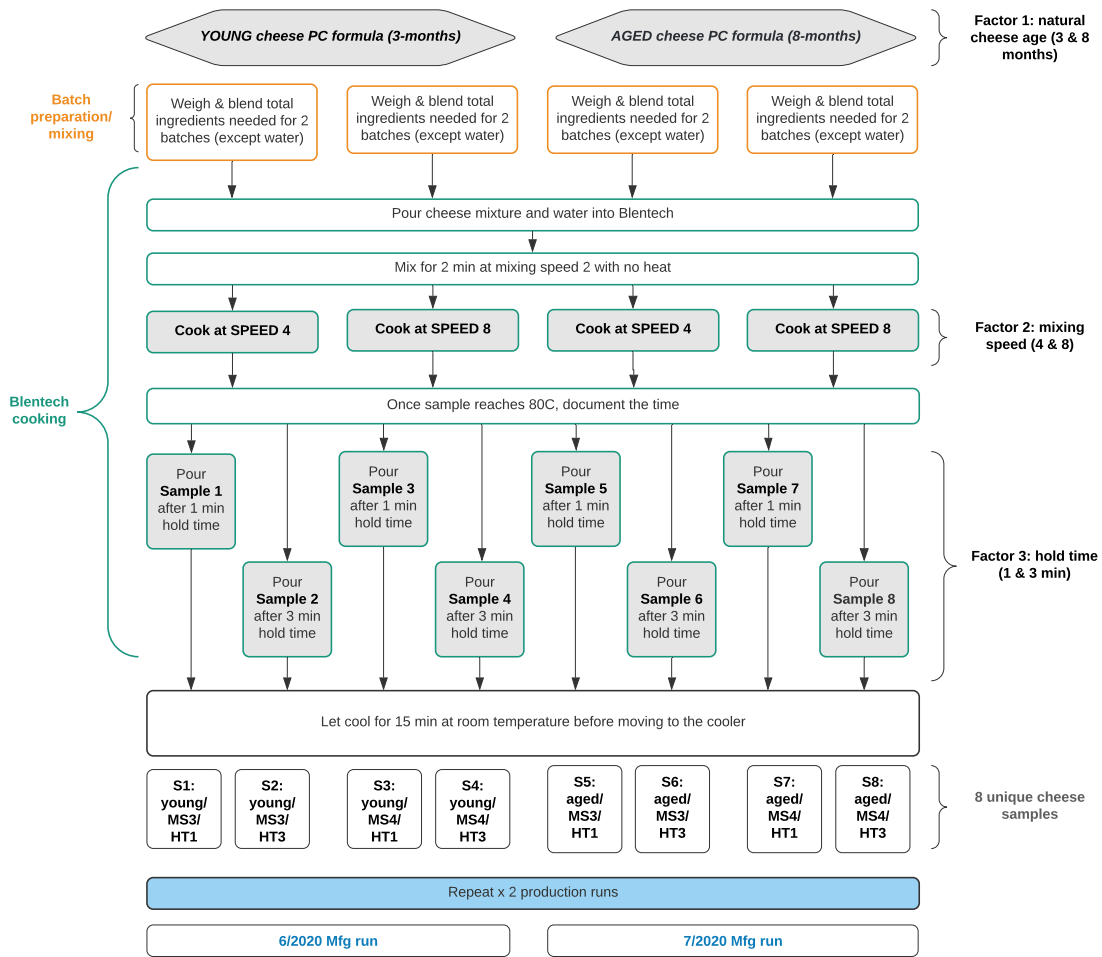


Figure 26. Pilot-scale PC spread manufacturing flowchart. Mixing speed 4 and 8 represent 150 and 265 rpms, respectively.

Cheddar Starting Composition	3-month	8-month
Moisture	38.40	36.90
Fat	33.00	32.00
Total Protein	21.42	22.75
- Casein protein	[19.05]	[18.68]
- % intact casein	[88.94]	[82.11]
Salt	1.68	1.54
pH	5.13	5.30
PC Target Composition	3-month	8-month
Moisture	43.00	43.00
Fat	25.00	25.00
Total Protein	18.01	18.35
- Casein protein	[15.76]	[15.03]
- % intact casein	[87.50]	[81.88]
Salt	1.68	1.58

Table 12. Original Cheddar composition (left), PC spread target composition by percent standardized for moisture, fat, and total protein (below, left), and resulting PC formula by percent (below, right) for Blentech pilot-level production.

PC Formula	3-month	8-month
Natural Cheese	70.00	70.00
NFDM	8.98	7.23
Clarified Butter Oil	1.90	2.60
Salt	0.50	0.50
Disodium Phosphate	2.50	2.50
Water	16.12	17.17

4.3.3 Compositional Analysis

The moisture content of the natural cheese and process cheese spreads was determined using an atmospheric oven method (Case et al., 1985). Fat content was determined using the Mojonnier fat extraction method (Case et al., 2004). Intact casein protein, or insoluble protein, was determined by difference of the soluble protein, which was found using the method by Kosikowski and Mistry (1982). Total protein and soluble protein of the natural cheese was measured by Kjeldahl and total protein of the PC spread was measured by Dumas method with a Leco Tru Spec N analyzer (Leco, St. Joseph, MI, US) (Wiles et al., 1998), both utilizing a conversion factor of 6.36. Salt content and pH of the natural cheese was provided by the manufacturer (AMPI Inc., New Ulm, Minn. US). Ash was determined by a gravimetric method with an adjustment of using a time-ramp heating profile in the muffle furnace as a substitute for the manual carbonization step (Case et al., 2004).

4.3.4 Functional Analysis

All samples (8 PC spread samples x 2 manufacturing runs) were tested for functional tests at two shelf life time points: approximately 2 and 4 weeks after manufacture. Functional tests include sauce viscosity, Schreiber oven melt, and texture profile analysis, along with confocal laser scanning microscopy and FT-NIR spectroscopy.

4.3.4.1 Sauce Viscosity

PC sauces were produced by mixing 45.6g of PC spread with 14.4g of water and heating in a microwave for 30 sec to mix (approx. 45°C final temperature). Two replicates of each sample of melted PC sauce were analyzed using a Micro-Visco Amylograph (MVAG) (Brabender Instruments, South Hackensack, NJ, US). Viscosity (cP) of PC sauce was measured with a mixing speed of 50 rpm while holding samples at 50°C for two minutes and then cooling from 50°C to 35°C over 10 minutes. Each sample was tested in duplicate at 2 and 4 weeks after manufacture. The average PC sauce viscosity at 40°C, 45°C, and 50°C at each time point after manufacture was used for calibration development.

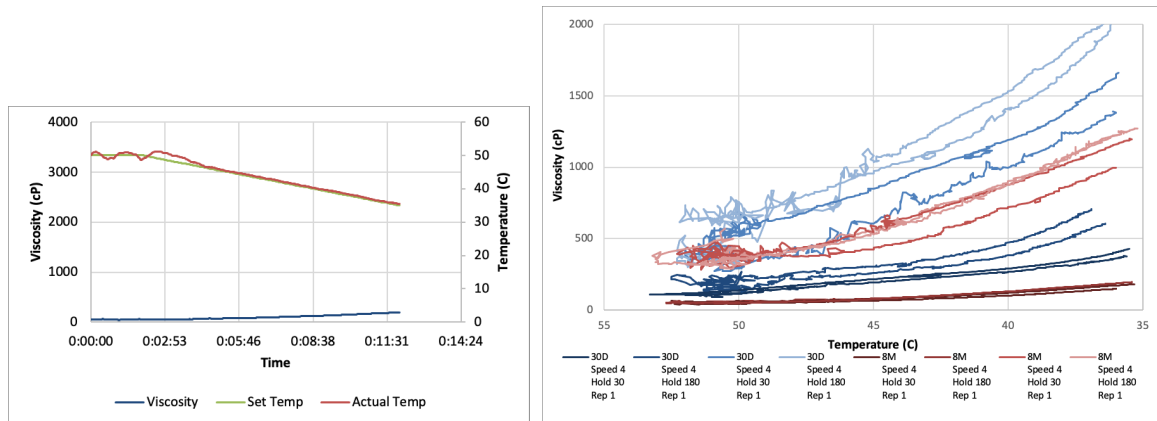


Figure 27. Sample viscosity results as initial output with both viscosity and temperature on y-axes and time on the x-axis (left) and adjusted result with time excluded and only viscosity vs temperature (right). Average viscosities were taken at 50°C, 45°C, and 40°C.

4.2.4.2 Melt Area

The melt area was measured using a modified Schreiber melt test (Amamcharla and Metzger, 2015). PC spread samples were cut to cylinders of 33.5 mm diameter x 7 mm tall using a stainless steel borer and butter slicer and tempered at room temperature

for about 2 hours. Next, they were placed on glass Petri plates and covered with glass lids, melted in a forced draft oven (FREAS precision mechanical convection oven 625, Thermo Scientific, Danville, IN, US) at 130°C for 7 min, cooled to room temperature, and imaged using a digital imaging system (Bio-Rad ChemiDoc XRS+ System, Hercules, CA, U.S.A.). Three replicates per sample were measured. Melt area of sample images was calculated using Fiji by converting to a tiff file, thresholding images, and measuring the area of the cheese sample. Each sample was tested in quadruplicate at 2 and 4 weeks after manufacture. The average area (sq in.) at each time point after manufacture was used for calibration development.

4.2.4.3 Texture Profile Analysis

A modified texture profile analysis was performed using a TA.XT2i texture analyzer (Stable Micro Systems, Godalming, UK; 5 kg load cell) (Amamcharla and Metzger, 2015). PC spread samples were cut to cylinders of 10 mm width and 15 mm height using a #7 metal cork borer and a wire cutter and kept at 4°C before and during testing. A double bite compression was performed with a 75% compression of original height and a 15 s rest period between compressions. PC spread cylinders were compressed with a 25-mm plastic cylindrical probe at a crosshead speed of 0.8 mm/s on a plastic platform base. Samples were tested in triplicate at 2 and 4 weeks after manufacture. A macro was used to generate peak force values for the first and second compression, and the first peak (firmness) was used for calibration development.

4.2.4.4 Fat Droplet Size Analysis - Confocal Laser Scanning Microscopy

Fat droplet size analysis was performed using confocal laser scanning microscopy (CLSM) and involved labeling samples, generating reference spectra, collecting experimental images and unmixing with spectral filters, and analyzing images using Fiji (U.S. National Institutes of Health, Bethesda, Maryland, US).

Labeling

Cheese samples were cut using a razor blade to be approximately 5x5x2 mm. They were fixed in 2% paraformaldehyde and phosphate buffer solution (PBS, see

Appendix for formula) for 15 minutes before staining with Nile Red (72485, Sigma-Aldrich, St. Louis, MO, US) and Fast Green (F-7258, Sigma-Aldrich, St. Louis, MO, US), which were used as fluorescent dyes that bind preferentially to lipids and protein, respectively. Samples were incubated in the NR stain (20% 10 mg/mL NR and 80% PBS) for 20 min, washed in PBS for 3 min twice, incubated in FG stain (1% 10 mg/mL FG, 1% glacial acetic acid, and 98% PBS) for 20 min, and washed in PBS for 3 min twice. All incubations took place at 4°C. Samples for spectral data acquisition were prepared with PBS + fixative only (unlabeled; all samples), PBS + fixative followed by NR only (NR; one sample only), and PBS + fixative followed by FG only (FG; one sample only). All experimental samples were prepared sequentially with PBS + fixative, then FG, then NR.

Reference Spectral Data Acquisition

Images were acquired on a Nikon Eclipse Ti2 inverted fluorescence microscope equipped with an A1si confocal scan head, a 20x Plan Apo objective lens (0.75NA), and a 32-channel PMT spectral detector. Nile Red was excited by a 561-nm laser diode (40 mW), and Fast Green was excited by a 488-nm Argon multiline laser (40mW). Fluorescence emission was split in its component wavelengths with a diffraction grating and simultaneously captured in 326 nm channels between 500-700 nm. The plane of maximum signal intensity was selected, and single plane 512 x 512 pixels images were acquired ($dx = dy = 1.243 \mu\text{m}$) with NIS Elements imaging software (5.02). Reference emission spectra were created by selecting suitable ROI in the images of the individual dyes: unlabeled (background, rectangular ROI), Nile Red (ROI on a fat droplet), and Fast Green (rectangular ROI).

Experimental Image Collection & Spectral Unmixing

Images for experimental samples were collected identically to the reference spectra in addition to multiple z-planes (20-30) being acquired with a $dz = 1.240 \mu\text{m}$. Four images of different areas of each cheese sample were collected. Images were processed using NIS Elements software (5.02) and the reference spectra to unmix the 32 channels collected into 3 channels for unlabeled control, NR, and FG.

Lipid Droplet Image Analysis

The unmixed images were analyzed using ImageJ (model/manufacturer) and a macro made up of the following steps: split channels and duplicate lipid channel; auto-threshold to a binary image using Moments or Default; median filter (2-pixel radius); 3D watershed split (12-pixel radius), Fire LUT. The output image after running macro was analyzed using 3D manager and 3D measure tool to generate a summary of lipid droplet measurements. Measurements were further summarized in Excel to calculate an average and median volume and Feret diameter summaries for each image due to droplet distribution differences, as shown in Figure 33 and Figure 37 in the *4.4.2.4 Fat Droplet Size Analysis with CLSM* section.

4.3.5 Spectroscopic Analysis

FT-NIR spectra were collected with approximately 50 grams of rapidly-cooled PC on glass Petri dishes using the Büchi NIRFlex N-500 (BÜCHI Labortechnik AG) with solids attachment. Three Petri dishes of PC spread were scanned per sample, for a total of 24 spectra per 8-sample manufacturing batch.

Based on the previously-mentioned functional tests, a total of 14 properties and values were added to the spectra using the NIRWare Management program (**Table 13**). Büchi NIRCAl chemometric software (V5.6) was used for calibration. Calibration development was based on the Büchi NIRCAl Chemometric software model for creating a quantitative calibration. Due to the small number of spectra used for calibration (n=16), cross-validation was used instead of assigning spectra to calibration and validation sets. CV Group Selector (V1.9) was used to assign spectra with sequence method, 16 groups, and 3 spectra per group (**Figure 28**). Calibration Wizard (V5.50) was used to quickly scan through as many as 56 unique calibrations, adjusting for primary and secondary principal components, wavenumber selection, and pretreatments. The top ten calibrations according to Q-value (a proprietary Büchi calibration quality metric) were compared. The calibration with the lowest standard error (CV SECV graph) and reasonable symmetry in the CV Property Residuum vs Original Property graph was chosen for the final calibration.

Table 13. NIRCal Calibration Properties

Analysis method	Property	Description
Viscosity (MVAG)	at 40°C (2 weeks)	Heated sauce viscosity (cP) at each temperature along a cooling profile from 50°C to 35°C at two shelf life time points.
	at 45°C (2 weeks)	
	at 50°C (2 weeks)	
	at 40°C (4 weeks)	
	at 45°C (4 weeks)	
	at 50°C (4 weeks)	
Melt Area (Schreiber)	(at 2 weeks)	Melt area (sq. in.) at two shelf life time points
	(at 4 weeks)	
Firmness (TA.XT)	(at 2 weeks)	Firmness (g) at two shelf life time points.
	(at 4 weeks)	
Confocal (CLSM)	Number of fat droplets	Number of isolated fat droplets within a 636µm image
	Average volume	Average fat droplet volume (µm ²)
	Average Feret diameter	Average fat droplet Feret diameter (µm)
	Median Feret diameter	Median fat droplet Feret diameter (µm)

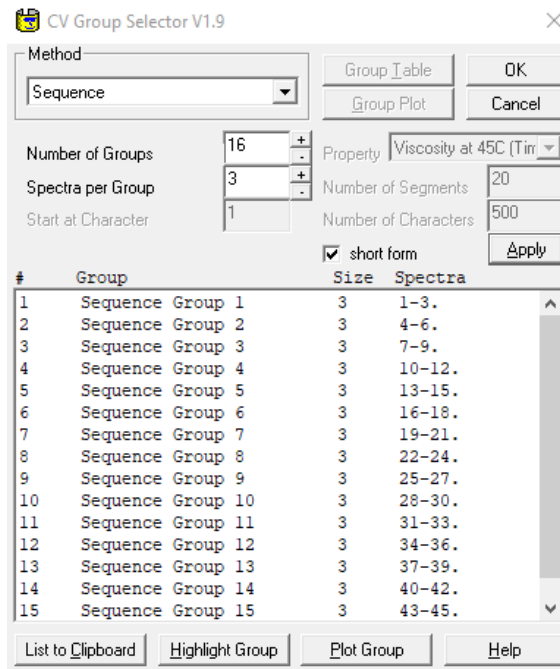


Figure 28. CV Group Selector, with samples grouped by triplicate scans.

4.3.6 Statistics

Split-plot analysis of variance (ANOVA) was used to determine the significance of factors and interactions between factors using R (Rstudio Version 4.0.3, Boston, MA).

A significance level of $P < 0.05$ was used. Two levels of variability were used in ANOVA to reflect the manufacturing treatments. Since ingredients were mixed in 3 kg double-batches, or “pre-blends,” and mixing speeds were applied to 3 kg pre-blends, there were essentially four unique samples for the factors of age and mixing speed per manufacturing run, one for each age-mixing speed combination. The second level of variability is due to the factor of hold time since that was applied at the end of manufacture, leading to eight unique samples per manufacturing run. Two manufacturing runs were completed. See Appendix for R code used to generate ANOVA results (6.2.3 R code for split-plot ANOVA of Blentech sample data).

The significance of NIRCal calibrations was left undetermined. Since so few samples were used, all results are preliminary and suggest outcomes. More samples would be needed for a robust calibration outcome with statistical conclusions.

4.4 Results and Discussion

4.4.1 Compositional Analysis

The target and actual chemical composition of the eight PC spread samples are shown in **Table 14**. One gap in composition analysis was that pH wasn't measured in the final PC. This was an oversight and could have contributed to a deeper understanding of the PC chemistry, but other compositional results showed few differences across the eight samples.

One difference from the target PC composition to the actual composition was in total protein. Although the target was around 18% total protein, all PC eight samples had a final total protein content of around 20%. This may have been due to higher protein contents than expected in the only other protein source, NFDM. Regardless of the difference from target to actual, the consistent protein level across 3-month and 8-month samples allowed for minimal effects due to total protein composition.

The only difference found in compositional values was for ash ($P < 0.05$), where the 3-month-old natural cheese PC was slightly higher in ash (~0.1%) than the 8-month-old natural cheese PC. Since ash analysis measures inorganic compounds, this could mean there was a difference in calcium, phosphorous, or other minerals, and potentially higher calcium or phosphorus content in the 3-month PC versus the 8-month PC could

lead to a weaker emulsion. For example, Kapoor et al. established that as small of a difference as 0.05% calcium and 0.06% phosphorus in PC composition affected the PC hardness, melt area, and dynamic stress rheometry melt temperature (2007). Further studies have confirmed that calcium and phosphorus content of PC affects the rheological and viscoelastic properties (Biswas et al., 2004, Biswas et al., 2008a, 2008b, Biswas et al., 2015). In natural cheese, calcium and phosphorus “act together and form cross-links within and among casein micelles during coagulation during cheese manufacturing” (Biswas et al., 2015). In PC, emulsifying salts displace the calcium and phosphorus cross-links. With higher calcium, more intact calcium phosphate complexes would keep the calcium-paracaseinate-phosphate network more intact, freeing less casein to emulsify the fat droplets in the system, and ultimately increasing firmness (Kapoor and Metzger, 2008). Ultimately, the higher ash in the 3-month versus 8-month PC formula could have confounding effects with the rheological findings discussed in further sections. With no differences found in moisture, fat, or protein, we can conclude that the differences that are found in the FT-NIR spectra are due to either ash or factors outside of composition, such as emulsification and functionality.

Table 14. Summary of composition across eight unique samples of cheese (N=2). 3-month & 8-month indicate natural cheese age used to make PC; MS = mixing speed (rpm); HT = hold time (min). Values within a row not sharing a common superscript significantly differed.

	Target PC Composition		Actual PC Composition							
			Age: 3-month				Age: 8-month			
	3-month	8-month	Low MS		High MS		Low MS		High MS	
			HT 1	HT 3	HT 1	HT 3	HT 1	HT 3	HT 1	HT 3
Moisture	43.00	43.00	44.00 ^a	44.09 ^a	44.18 ^a	44.23 ^a	44.03 ^a	43.76 ^a	44.02 ^a	43.59 ^a
Fat	25.00	25.00	24.80 ^a	25.24 ^a	25.43 ^a	25.51 ^a	25.23 ^a	25.73 ^a	25.47 ^a	26.25 ^a
Protein	18.01	18.35	20.15 ^a	20.38 ^a	20.15 ^a	20.03 ^a	19.98 ^a	20.05 ^a	20.05 ^a	20.25 ^a
Ash	--	--	5.98 ^a	5.99 ^a	5.97 ^a	5.95 ^a	5.91 ^b	5.92 ^b	5.89 ^b	5.93 ^b

4.4.2 Functional Analysis

4.4.2.1 Sauce Viscosity

Average sauce viscosity results across all temperature ranges are shown below (Table 15, Table 16, and Figure 29). Of the three manufacturing factors of natural cheese age, mixing speed, and hold time, age led to a difference ($P < 0.05$) in PC sauce viscosity when measured at the second shelf life time point four weeks after manufacture (Figure 29). Those samples showed higher viscosities in the PC made with younger natural cheese than those made with older natural cheese. Other samples also slightly

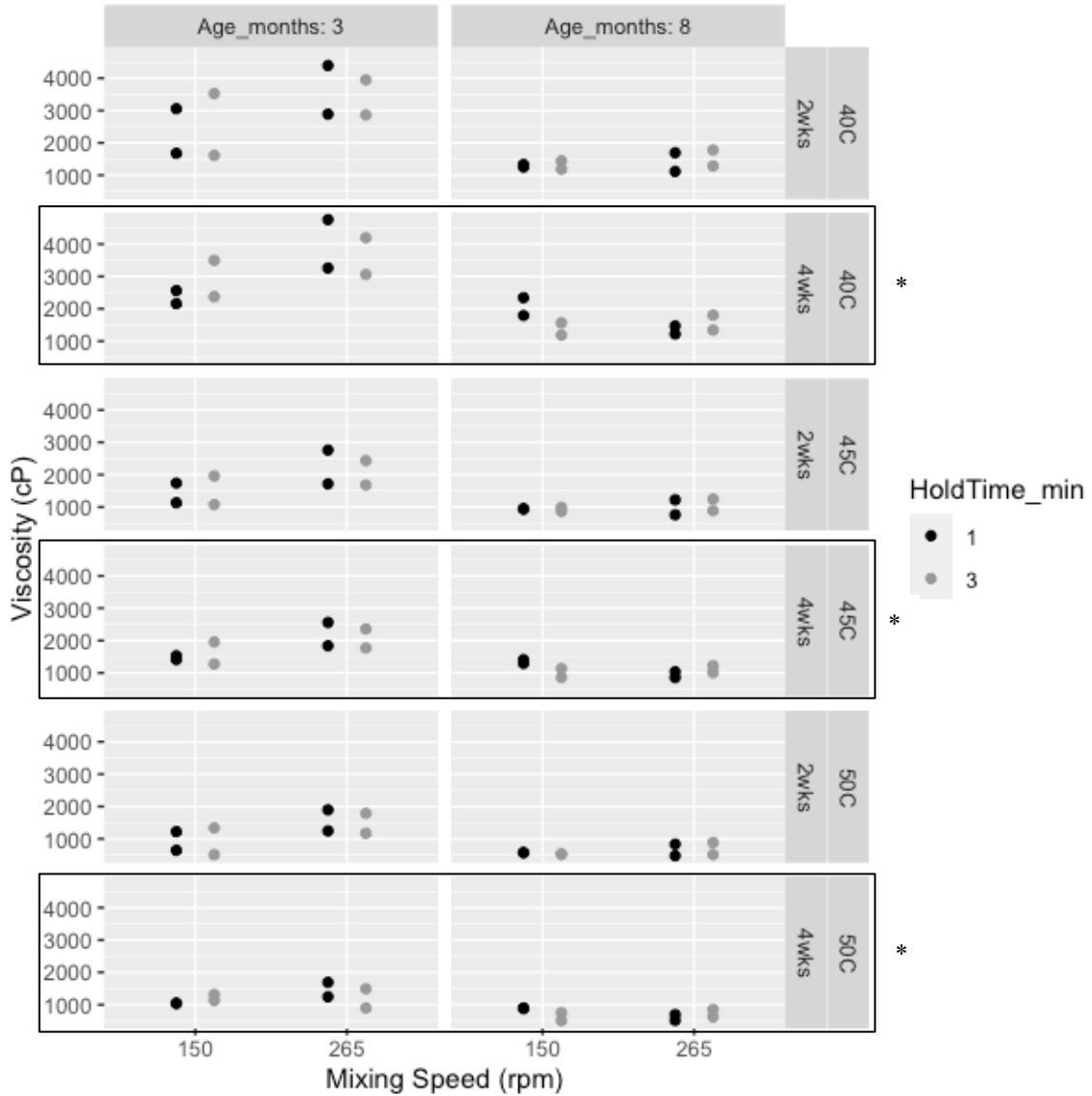


Figure 29. PC sauce viscosity (cP) at three temperatures (right y-axis, 40C, 45C, and 50C), two time points after manufacture (right y-axis, 2 & 4 weeks after mfg) and across samples with different natural cheese age (upper x-axis, 3 & 8 months), mixing speeds (lower x-axis, 150 & 265 rpm), and hold time (legend, 1 & 3 min). Rows surrounded by boxes and an asterisk indicate difference across the factor of age ($P < 0.05$).

showed this trend, but not significantly. The higher viscosity is likely due to the higher intact casein content coming from the younger cheese, which allows for more protein-water and protein-fat interactions (Lee et al., 2003b). However, since these differences were only seen at four weeks past manufacture and not two weeks manufacture, these results suggest that either more interactions formed over time in the younger samples, interactions decreased over time in the older samples, or that they equilibrated and showed smaller differences *between* young samples. Not much literature exists to explain these findings, but it would have helped if pH had been consistently measured across the four weeks of shelf life.

Table 15. Average viscosity results (cP), $n=2$, across three temperatures of 40°C, 45°C, and 50°C and two shelf life time points (T1 = 2 wks past mfg, T2 = 4 wks past mfg). Superscript lowercase letters indicate a difference across the factor of age ($P<0.05$).

Age	3-month				8-month			
	150 rpm		265 rpm		150 rpm		265 rpm	
HT	1 min	3 min	1 min	3 min	1 min	3 min	1 min	3 min
40°C (T1)	2368	2569	3641	3408	1292	1318	1407	1533
40°C (T2)	2361 ^a	2937 ^a	4009 ^a	3630 ^a	2068 ^b	1376 ^b	1345 ^b	1573 ^b
45°C (T1)	1436	1517	2239	2058	943	929	992	1067
45°C (T2)	1471 ^a	1617 ^a	2199 ^a	2066 ^a	1352 ^b	996 ^b	946 ^b	1114 ^b
50°C (T1)	934	922	1570	1479	572	528	656	696
50°C (T2)	1043 ^a	1223 ^a	1468 ^a	1194 ^a	888 ^b	630 ^b	606 ^b	737 ^b

Table 16. Viscosity split-plot ANOVA p -values, with the averaged 4-sample block for Age and MS factor, and second 8-sample block for HT and interactions. Age = natural cheese age, MS = mixing speed, and HT = hold time. Asterisks indicate a significant p -value ($P<0.05$).

	First ANOVA block			Second ANOVA block			
	Age	MS	Age:MS	HT	Age:HT	MS:HT	Age:MS:HT
40°C (T1)	0.080	0.392	0.522	0.752	0.628	0.396	0.205
40°C (T2)	0.036*	0.389	0.211	0.690	0.349	0.959	0.040*
45°C (T1)	0.103	0.362	0.477	0.862	0.488	0.464	0.174
45°C (T2)	0.049*	0.404	0.208	0.640	0.593	0.520	0.081
50°C (T1)	0.121	0.296	0.471	0.446	0.471	0.973	0.261
50°C (T2)	0.048*	0.752	0.437	0.277	0.864	0.729	0.008*

When exploring viscosity interactions between factors, two differences were found in the interaction between age, mixing speed, and hold time ($P<0.05$): one for viscosity at 40°C (T2) and the other at 50°C (T2)(**Table 16**). Interactions indicate that

one

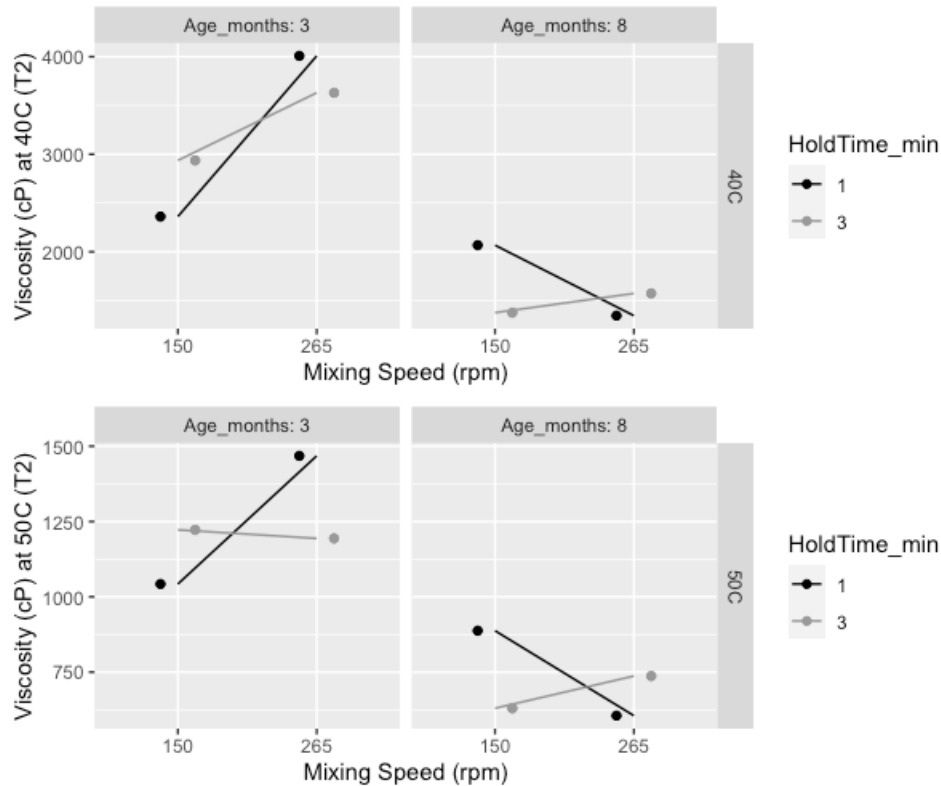


Figure 30. Interaction plots for viscosity at 40°C (T2) (top) and at 50°C (T2) (bottom) across factors of natural cheese age (upper x-axis, 3 & 8 months), mixing speeds (lower x-axis, 150 & 265 rpm), and hold time (legend, 1 & 3 min).

factor's effect depends on another factor. In this case, a three-way interaction between age, MS, and HT mean that an interaction between Age:MS only occurs at one level of HT. Unlike parallel lines, the intersecting lines of the interaction plot (**Figure 30**) show Age:MS:HT interactions for 40°C (T2) and 50°C (T2). At 40°C (T2) and the 3-month age facet, the viscosity is slightly higher at the 150rpm MS for 3-min HT than 1-min HT, but at the 265rpm MS, it's the opposite: 1-min HT leads to a higher viscosity than 3-min HT. If this were a significant interaction, the MS:HT p-value would be <0.05 , but it's *also* the age that makes the interaction significant. This MS:HT interaction pattern continues exists inversely at the 8-month age facet, making this interaction a three-way pattern. The same can be seen for viscosity at 50°C (T2).

These interactions could explain some of the microstructural effects occurring across the different samples and it is important to consider along with the main effects previously discussed. Younger natural cheese provides higher levels of intact casein to

increase the potential for a higher degree of emulsification (Fenelon and Guinee, 2000). However, mixing is necessary to effectively distribute the emulsifying salts and intact casein throughout the system and form the emulsion (Zehren and Nusbaum, 1992). The factor of hold time contributes to these two by lengthening the mixing time and potentially balancing out the effects of a slower mixing speed versus a faster one. As we can see from the interactions at these two temperatures and time points, the individual effects of each of these factors are dependent upon one another; PC samples made with young natural cheese vs. aged natural cheese may lead to a more viscous PC sauce depending on what mixing speed *and* what hold time was used during processing, and so on.

To explain why interactions were significant in only these two viscosity sets and not in the other four sets, we might consider shelf life and temperature. Differences found across age at four weeks shelf life but not at two weeks led to clearer effects of interactions at four weeks but not two weeks as well. In regards to temperature, it's unusual that interactions weren't found at all points across the heating range of 50°C, 45°C, and 40°C (**Figure 27**), but maybe larger effects were visible at the hotter start and cooler end of the heating profile than in the middle. Although an MVAG was used for this research, Prow and Metzger also analyzed PC viscosity using a rapid visco analyzer (RVA) and distinguished different segments of the heating curve into hot viscosity versus apparent viscosity (2005). The viscosity measurement at 40°C may be representing differences in solidification across samples (Prow and Metzger, 2005).

4.4.2.2 Melt Area

Average melt area results across the two shelf life time points are shown in **Table 17** and **Figure 31**. None of the three manufacturing factors of natural cheese age, mixing speed, or hold time led to differences in melt area at either two or four weeks past manufacture or when checking for interactions between factors (**Table 17** and **Table 18**). The meltability change from two weeks to four weeks was also explored by Everard et al., who found no difference when using a sensory analysis method or Olson and Price test but did find a difference when using Schreiber test (2005).

Table 17. Average melt area values (sq. inches), across two shelf life time points. T1 = 2 weeks past manufacture, T2 = 4 weeks past manufacture, Age = natural cheese age, MS = mixing speed, HT = hold time. No differences were found across factors of age, MS, or HT ($P < 0.05$). $N=2$.

Age	3-month				8-month			
	150 rpm		265 rpm		150 rpm		265 rpm	
MS	1 min	3 min	1 min	3 min	1 min	3 min	1 min	3 min
Melt Area (T1)	3.82	3.70	2.28	2.86	4.15	4.06	3.50	3.67
Melt Area (T2)	3.77	3.76	3.31	3.56	4.24	4.06	3.60	3.75

Table 18. Melt area split-plot ANOVA p -values across factors and interaction of factors at two shelf life time points. T1 = 2 weeks past mfg, T2 = 4 weeks past mfg. Age = natural cheese age, MS = mixing speed, HT = hold time. No differences were found ($P < 0.05$).

	First ANOVA block			Second ANOVA block			
	Age	MS	Age:MS	HT	Age:HT	MS:HT	Age:MS:HT
Melt Area (T1)	0.126	0.078	0.376	0.417	0.543	0.184	0.509
Melt Area (T2)	0.223	0.144	0.734	0.439	0.308	0.074	0.788

4.4.2.3 Firmness

Average firmness results across the two shelf life time points are shown in **Table 19** and **Figure 32**. Of the three manufacturing factors of natural cheese age, mixing speed, or hold time, the only difference found was across age at two weeks of shelf life,

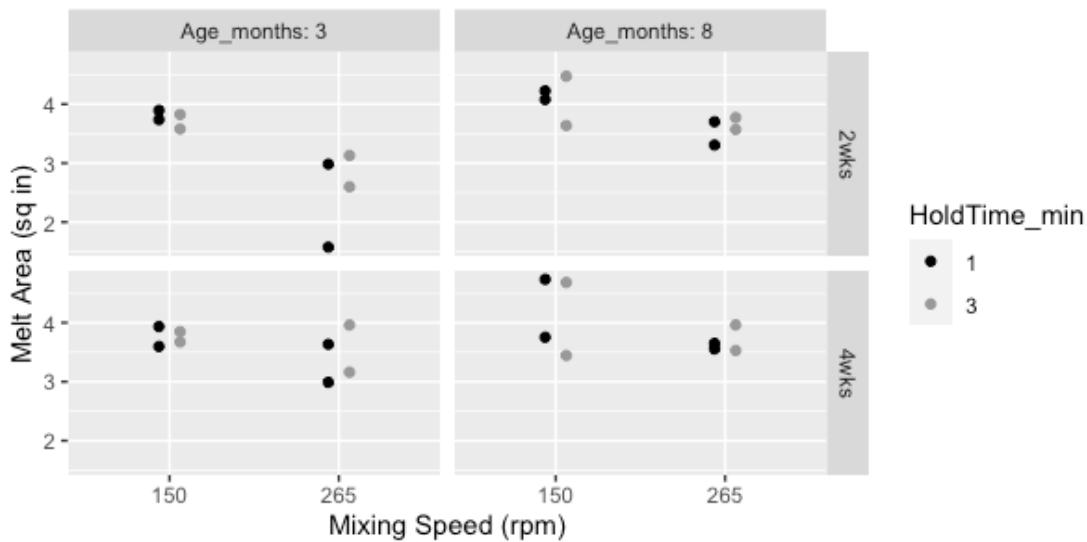


Figure 31. PC oven melt area (sq in) at two time points after manufacture (right y-axis, 2 & 4 weeks after mfg) and across samples with different natural cheese age (upper x-axis, 3 & 8 months), mixing speeds (lower x-axis, 150 & 265 rpm), and hold time (legend, 1 and 3 min)

and no differences were found in interactions between factors (**Table 20**). The single difference across age at two weeks of shelf life showed that a higher firmness was found with the PC made from younger natural cheese than older natural cheese. Similar to viscosity results, this was expected since younger natural cheese contributes higher intact casein content than aged natural cheese, allowing for more protein-protein and protein-fat interactions in PC (Lee et al., 2003a). Those increased interactions can lead to higher firmness.

Table 19. Average firmness values (g of force), across two shelf life time points. T1 = 2 wks past mfg, T2 = 4 wks past mfg, Age = natural cheese age, MS = mixing speed, HT = hold time. Superscript lowercase letters indicate a difference across age for T1, but no other differences were found ($P < 0.05$). $N=2$.

Age	3-month				8-month			
	150 rpm		265 rpm		150 rpm		265 rpm	
MS	1 min	3 min	1 min	3 min	1 min	3 min	1 min	3 min
Firmness (T1)	1104 ^a	1251 ^a	1500 ^a	1313 ^a	932 ^b	852 ^b	1014 ^b	1011 ^b
Firmness (T2)	1086	1012	1384	1424	946	1203	1100	1221

Table 20. Firmness split-plot ANOVA p-values across factors and interaction of factors at two shelf life time points. T1 = 2 weeks past mfg, T2 = 4 weeks past mfg. Age = natural cheese age, MS = mixing speed, HT = hold time. Differences were found ($P < 0.05$) for the factor of Age for T1, but not for T2 or any other factors or interactions.

	First ANOVA block			Second ANOVA block			
	Age	MS	Age:MS	HT	Age:HT	MS:HT	Age:MS:HT
Firmness (T1)	0.016*	0.084	0.484	0.702	0.896	0.438	0.243
Firmness (T2)	0.521	0.239	0.437	0.390	0.315	0.956	0.525

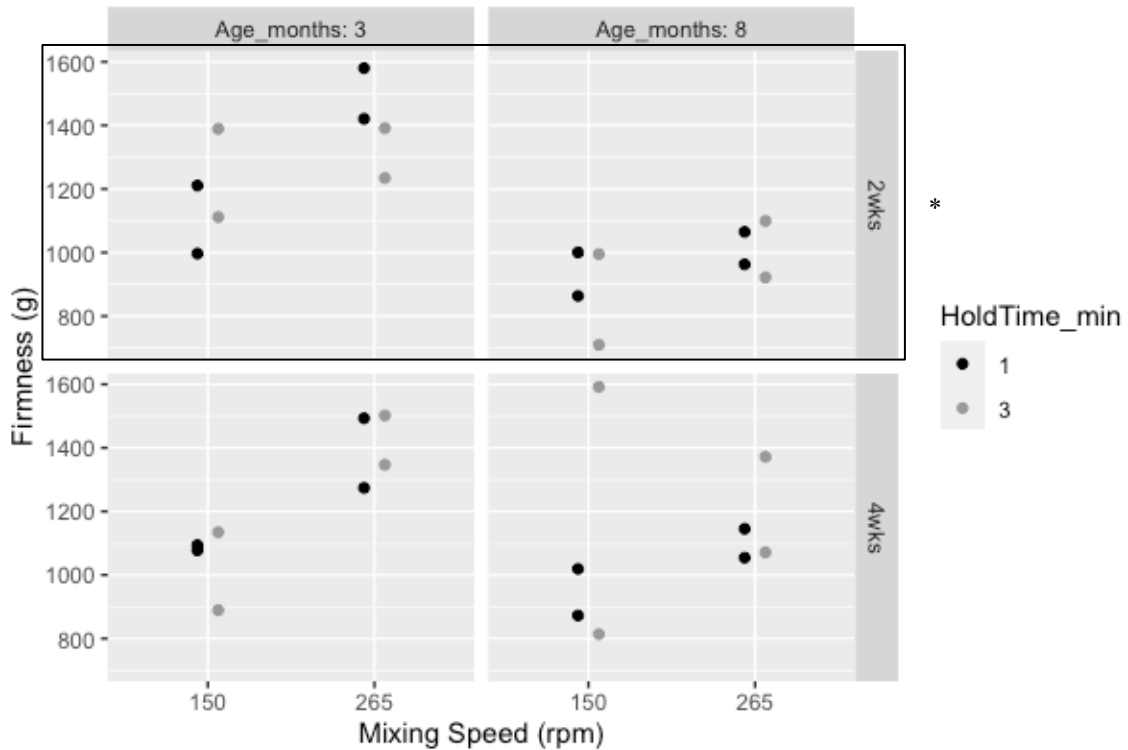


Figure 32. Firmness (g), at two time points after manufacture (right y-axis, 2 & 4 weeks after mfg) and across samples with different natural cheese age (upper x-axis, 3 & 8 months), mixing speeds (lower x-axis, 150 & 265 rpm), and hold time (legend, 1 and 3 min). Asterisk and box indicate a difference ($P < 0.05$) across the factor of age. $N=2$.

4.4.2.4 Fat Droplet Size Analysis with CLSM

Average CLSM fat droplet measurements are shown below, with the number of droplets per $636\mu\text{m}^2$ image and average droplet volume in **Figure 34** and the average and median Feret diameter in **Figure 35**. None of the three factors of natural cheese age, mixing speed, and hold time, or interactions between factors, led to differences across these four fat droplet measurements ($P < 0.05$) (**Table 21**, **Figure 34**, and **Figure 35**). Sample confocal images before and after adjustments are also shown below in **Figure 36**. The droplet diameters found in this study – 15-34 μm – were much larger than those indicated in

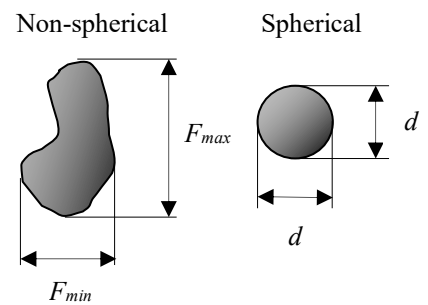


Figure 33. Examples of differences in diameter measurements for non-spherical shapes, such as the difference between maximum Feret diameter (F_{max}) and minimum Feret diameter (F_{min}). Spherical shapes have the same diameter (d) regardless of the angle of measurement.

previous literature, such as PC fat droplet diameters of 0.5-0.92 μm (Cernikova et al., 2018), 0.2-1 μm (Lopez and Briard-Bion, 2007), 2-25 μm (Auty et al., 2001), or 3-6 μm (Pereira et al., 2001). Further studies have found that the diameter of milk fat globules ranged from 0.02-15 μm (Lopez and Briard-Bion, 2007) and natural cheese fat droplet diameter ranged from 1.6-7.6 μm (Everett et al., 1995), which are both moderately smaller ranges than found here. Some other studies have published findings on circularity (Everett et al., 1995) but those trends were left out of the analysis in this study. However, with higher droplet circularity, the diameter can be summarized by one diameter measurement; with lower circularity, Feret diameters are more often used to indicate the minimum or maximum diameter of a non-spherical object (**Figure 33**).

Table 21. Average CLSM fat droplet measurements for the number of droplets per 636 μm^2 image, average volume, average Feret diameter, and median Feret diameter. Age = natural cheese age, MS = mixing speed, HT = hold time. No differences were found ($P < 0.05$). $N=2$.

Age	3-month				8-month			
	150 rpm		265 rpm		150 rpm		265 rpm	
	1 min	3 min	1 min	3 min	1 min	3 min	1 min	3 min
# of Droplets	1408	1286	1466	1171	1534	1277	1224	1342
Avg Vol (μm^3)	1876	1810	1869	1158	2879	3474	1883	2178
Avg FD (μm)	29.6	33.5	33.8	21.4	33.5	31.9	28.4	32.9
Med FD (μm)	28.5	29.6	31.2	15.5	31.7	28.8	25.1	26.5

Table 22. CLSM fat droplet measurement split-plot ANOVA p -values across factors and interactions of factors. Age = natural cheese age, MS = mixing speed, HT = hold time. Asterisk indicates p -value < 0.05 .

	First ANOVA block			Second ANOVA block			
	Age	MS	Age:MS	HT	Age:HT	MS:HT	Age:MS:HT
# of Droplets	0.883	0.362	0.125	0.125	0.390	3.753	0.125
Avg Vol (μm^3)	0.088	0.141	0.887	0.887	0.091	0.277	0.671
Avg FD (μm)	0.438	0.291	0.477	0.477	0.190	0.231	0.036*
Med FD (μm)	0.620	0.226	0.097	0.970	0.154	0.168	0.047*

One study that found fat droplet diameters similar to these results was in the case of lactalbumin-emulsified cheese, where Everett et al. observed “*the presence of two apparent classes of fat – small globules of diameter less than $2\mu\text{m}$ and larger more elongated pools of fat $20\text{-}50\mu\text{m}$ in length*” and hypothesized that the larger globules represented fat “*encapsulated within the casein fibers*” and “*trapped in the protein matrix rather than through emulsification*” (1995). Since the PC formula used in this study wasn’t made with lactalbumin-emulsified milk fat, it is unlikely this was the mechanism for large fat droplet formation. A more likely explanation for larger than usual droplets

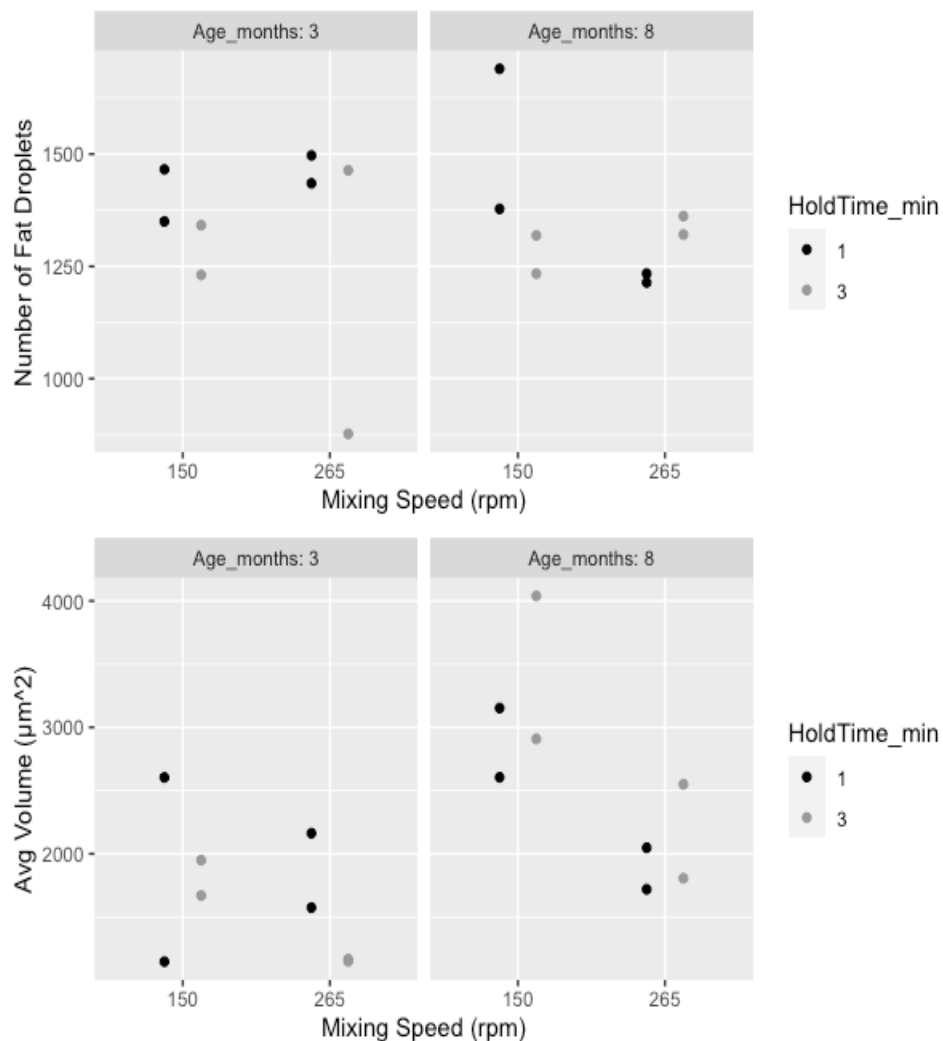


Figure 34. CLSM measurements across samples with different natural cheese age (upper x-axis, 3 & 8 months), mixing speeds (lower x-axis, 150 & 265 rpm), and hold time (legend, 1 and 3 min). Individual graphs represent the number of fat droplets within a $636\mu\text{m}^2$ image (top) and average fat droplet volume (bottom).

being found may lie in the overall confocal analysis process. With so many steps involved in CLSM – sample prep, image acquisition, spectral filter development, image processing, and final quantification – there is a lot of room for error in quantification purposes. The fixation, staining, and washing steps all have the potential to swell or solubilize components of the PC (Dürrenberger et al., 2001). To reduce noise, steps of the Fiji droplet size quantification also may have affected the size distributions by removing potential droplets that were smaller or equal to 1-2 voxels.

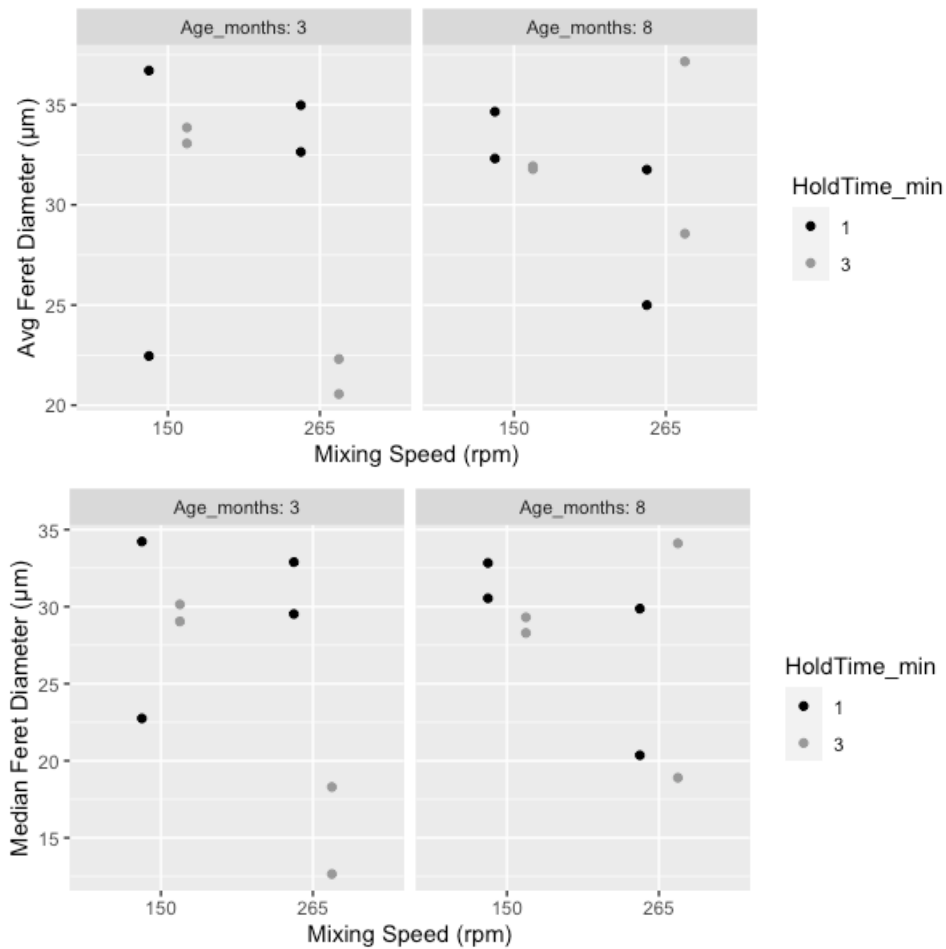


Figure 35. CLSM measurements across samples with different natural cheese age (upper x-axis, 3 & 8 months), mixing speeds (lower x-axis, 150 & 265 rpm), and hold time (legend, 1 and 3 min). Individual graphs represent average Feret diameter (μm , top) and median Feret diameter (μm , bottom).

Since voxels were $1.23\mu\text{m} \times 1.23\mu\text{m} \times 1.24\mu\text{m}$, distinguishing a voxel of singular intensity as noise versus a droplet was impossible without higher resolution. With the majority droplets expected in the size range of $0.2\text{-}5\mu\text{m}$, one processing step that removed isolated pixels may have shifted the average and median diameters much higher.

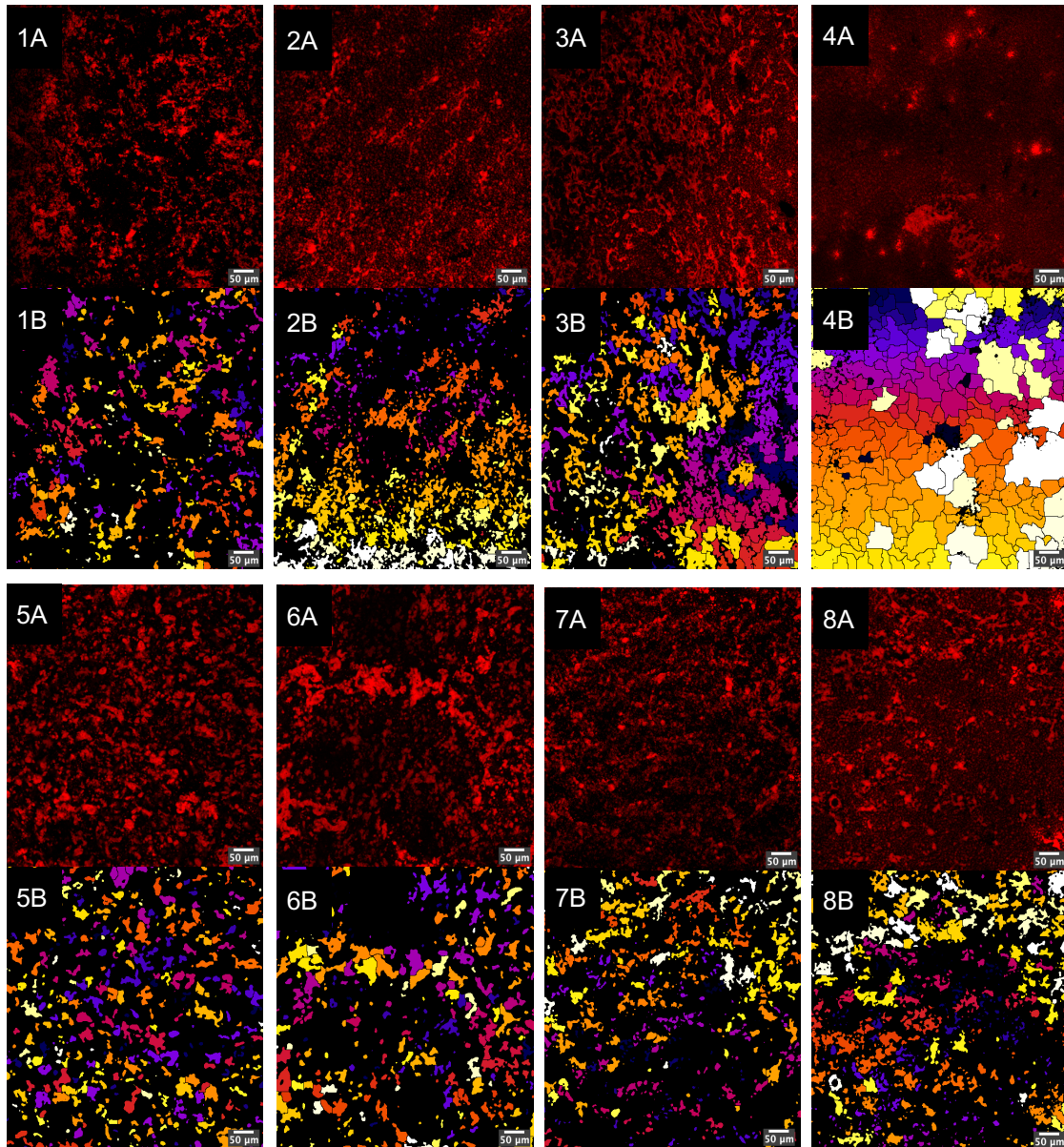


Figure 36. CLSM fat droplet images for 8 unique cheese samples (numbers 1-8), with the red and black original lipid-stained images (A) and multi-color Fiji-adjusted images for fat droplet quantification (B). Images here are of a single z-plane from a collected z-stack of 20-30 images. Full stacks were used for quantification purposes. Scale bar in lower right corners represents $50\mu\text{m}$. Identical samples are grouped vertically (1A + 1B, 2A + 2B, etc).

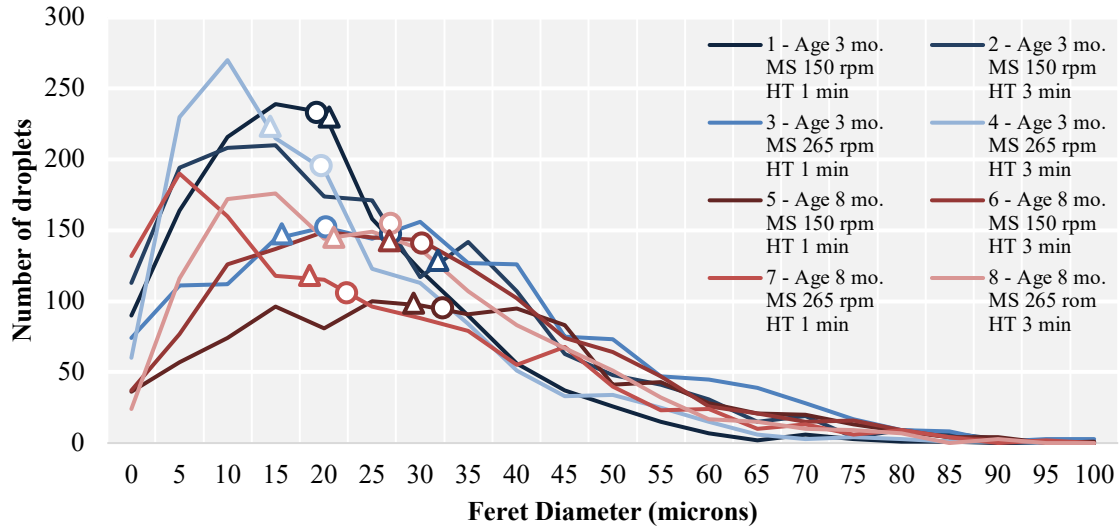


Figure 37. Fat droplet Feret diameter distribution curves across the eight unique PC samples from the one manufacturing run, with the number of droplets (x-axis) across each diameter range (y-axis). Depending on the shape of the distribution curve, the median diameters (triangles) and average diameters (circles) are often different.

Figure 37 shows a greater explanation of why average and median Feret diameter were both used in the ANOVA and subsequent FT-NIR calibration analysis. Since droplets exist in PC across a distribution of size ranges, choosing a single summary value can hide the complexity of representing the droplets throughout the system. As a result, both were used instead of just one.

When exploring interactions between factors, two differences were found in the interaction between age, mixing speed, and hold time: one for average Feret diameter (AFD) and the other for median Feret diameter (MFD) (

Table 22). As described earlier in the 4.3.4.1 *Sauce Viscosity* section, interactions indicate that one factor's effect depends on another factor. In this case, a three-way interaction between age, MS, and HT means that an interaction between Age:MS only occurs at one level of HT. Based on **Figure 38**, the three-way Age:MS:HT interactions of both graphs can be seen by the intersecting lines. Within the 3-month age facet alone, AFD increases with an increasing mixing speed at 1-min HT, but not 3-min HT. The opposite is true at the 8-month facet. Similar findings can be seen in the lower MFD graph as well.

Like the interactions discussed in the 4.4.2.1 *Sauce Viscosity* section, these interactions could indicate similar factor effects of different emulsification development depending on different factors: PC samples made with young natural cheese versus aged natural cheese may lead to a different fat droplet diameter depending on what the mixing speed *and* what hold time was used. Due to the detailed and complex methods involved in CLSM, however, the theoretical mechanisms behind these interactions are a little less certain. A more direct fat droplet analysis method such as NMR would lead to more certain results for this property.

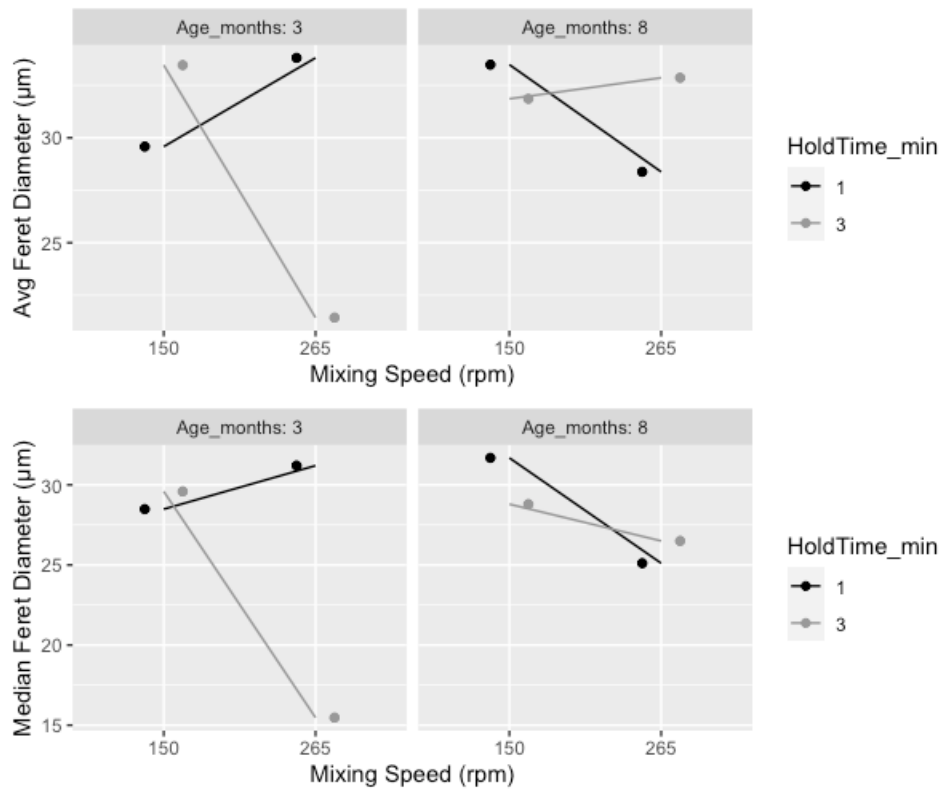


Figure 38. Interaction plots for viscosity at 40°C (T2) (top) and at 50°C (T2) (bottom) across factors of natural cheese age (upper x-axis, 3 & 8 months), mixing speeds (lower x-axis, 150 & 265 rpm), and hold time (legend, 1 & 3 min).

4.4.3 FT-NIR Calibrations

See **Table 13** from the materials and methods section for the full description of properties used for NIRCal calibrations and chemometrics. **Table 23** below shows the summary of calibration results, with further results and discussion in the following sections for each calibration.

Table 23. Calibration equation statistics using cross-validation and regression model for Blentech PC sample functional properties. Spectra *N* indicates the number of spectra used, but there were approximately 3 spectra per unique PC sample. 1°/2° PCs = the quantity of primary and secondary principal components. PT = pretreatments used. SEC = standard error of calibration; SECV = standard error of cross-validation; C r^2 = calibration regression coefficient, CV r^2 = cross-validation regression coefficient.

Property	Shelf life	Spectra <i>N</i>	1°/2° PCs	PT	Mean	SEC	SECV	C r^2	CV r^2
Viscosity at 40°C	2 wks	47	6/6	snv	2201	331	544	0.9041	0.5994
Viscosity at 45°C		47	3/3	none	1401	262	340	0.8016	0.6556
Viscosity at 50°C		46	7/7	ncl	926	217	192	0.9259	0.5348
Viscosity at 40°C	4 wks	48	2/2	none	2412	479	659	0.7949	0.6475
Viscosity at 45°C		47	2/2	db1, ncl	1475	242	301	0.7652	0.6538
Viscosity at 50°C		46	2/2	none	975	174	209	0.7347	0.6251
Melt Area	2 wks	43	3/3	db1, ncl	3.63	0.16	0.25	0.2294	0.7335
	4 wks	45	2/2	db1	3.75	0.27	0.37	0.6598	0.3788
Firmness	2 wks	46	2/2	kmu	1125	117	144	0.7465	0.6299
	4 wks	45	2/2	kmu	1141	174	203	0.3665	0.1861
CLSM # of Droplets	2 wks	43	2/2	ncl, db1	1370	108	143	0.2740	0.0057
CLSM Avg Vol		46	2/2	sg9	2153	596	721	0.4222	0.2052
CLSM Avg FD		44	3/2	snv, db1	30.60	4.15	5.67	0.3357	0.0375
CLSM Med FD		46	3/2	Sg9	27.05	5.29	6.88	0.3074	0.0192

4.4.3.1 Sauce Viscosity – 40°C (Time 1)

The CV graphs for viscosity at 40°C at two weeks past manufacture are shown below in Figure 39, Figure 40, and Figure 41. The final CV calibration was achieved using the standard normal variate (SNV) pretreatment, which helped to reduce baseline variations (Büchi, 2016). The wavenumber region of 5,000-10,000 was used, excluding the region of NH + NH, NH + OH, and NH + CH, CH + CH, and CH + CC combinations (Figure 40)(Brüker, 2009). Further explanations on those regions are covered in the 3.4.4 Melt Area FT-NIR Calibration section. The peaks in the regression coefficient graph around 5,700, 6,500-7,200, 8,300, and 8,800-9,500 cm^{-1} coincided with the wavenumbers known for the first overtone CH region, first overtone combination regions of CH, CH_2 , and CH_3 , second overtone CH region, and second and third overtone regions of CH_2 , CH_3 , and NH (Appendix Figure 81)(Brüker, 2009). As mentioned in Chapter 3 calibrations, there is less importance on the specific molecule stretch regions than the overall ability to correlate to the functional properties or finding patterns across

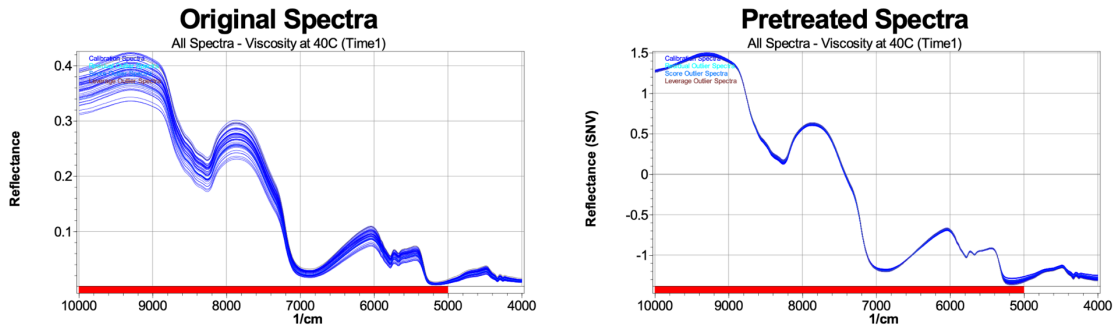


Figure 39. Viscosity at 40°C (Time1) CV calibration original spectra (left) and pretreated spectra (right). Pretreated spectra used pretreatments standard normal variate (snv).

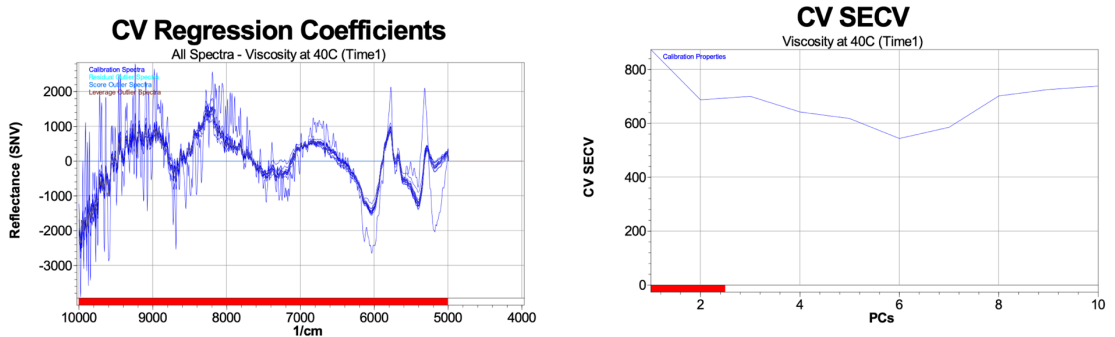
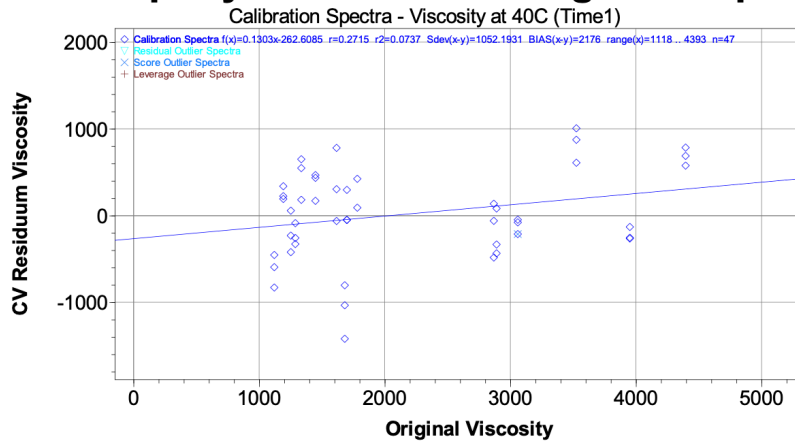
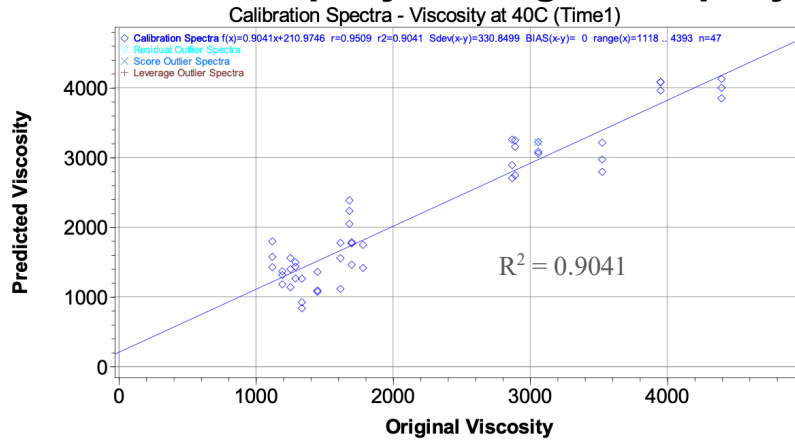


Figure 40. Viscosity at 40°C (Time1) CV calibration regression coefficients (left) and standard error of cross-validation (SECv, right). Wavenumber region used for calibration was 5,000-10,000 cm^{-1} and 6 PCs used for primary and secondary PC selection.

CV Property Residuum vs. Original Property



Predicted Property vs. Original Property



Predicted Property vs Original Property

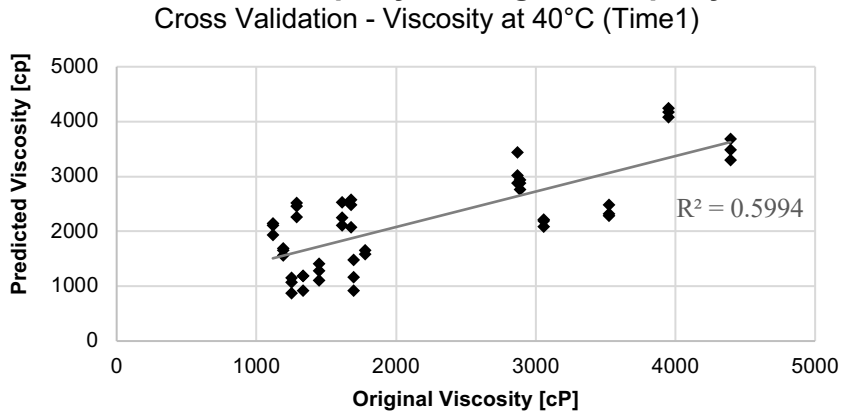


Figure 41. Viscosity at 40°C (Time1) CV calibration property residuum vs. original property (top), predicted property vs. original property of calibration (middle), and predicted property vs original property of CV (bottom).

similar functional property calibrations. The SECV graph (**Figure 40**) indicated that 6 primary PCs and 6 secondary PCs were best to achieve minimal standard error.

The final calibration results shown in the three graphs of **Figure 41** show the distribution of residuum values, the calibration predicted property vs original property, and the CV predicted property vs original property. The residuum values are well distributed above and below the 0-axis, with only one spectrum excluded as score outlier spectra. However, the residuum graph shows more samples grouped toward the lower end of the distribution and not many across the higher values. This could be a reflection of small functional property differences across the factors and therefore the spectra weren't very different either. Overall, the calibration set r^2 was 0.9041, the CV r^2 was 0.5994, and the Büchi Q-value was 0.4078. Lastly, the standard error of calibration (SEC) showed we were able to determine the viscosity accurately within 331 cP and the standard error of cross-validation (SECV) was able to determine the viscosity within 544 cP, given a mean viscosity of 2201 cP (**Table 23**).

4.4.3.2 Sauce Viscosity – 40°C (Time 2)

The CV graphs for viscosity at 40°C at four weeks past manufacture are shown below (**Figure 43**, **Figure 42**, and **Figure 44**). The final CV calibration was achieved without using a pretreatment (**Figure 43**). The wavenumber regions of 5,300-6,800 and 7,200-10,000 were used (**Figure 42**). The peaks in the regression coefficient graph around 5800, 6800, and 8300 cm^{-1} , coincided with the wavenumbers known for the CH/CH₂/CH₃ first overtone region, CH/CH₂/CH₃ first overtone combination region, and CH/CH₂/CH₃ second overtone region (Appendix Figure 81)(Brüker, 2009). The SECV graph indicated that 2 primary PCs and 2 secondary PCs were best to achieve minimal standard error.

The final calibration results shown in the three graphs of **Figure 44** show the distribution of residuum values, the calibration predicted property versus original property, and the CV predicted property vs original property. The residuum values are distributed slightly more below the 0-axis than above but look okay overall and were the best compared to other calibration methods. All spectra were included for the calibration. The calibration set r^2 was 0.7949, the CV r^2 was 0.6475, and the Büchi Q-value was

0.4481. Overall this calibration showed that some correlations between the predicted viscosity and original viscosity exist but weren't that strong. More samples would likely lead to a more robust calibration for this property. Lastly, the standard error of calibration (SEC) showed we were able to determine the viscosity accurately within 479 cP and the standard error of cross-validation (SECV) was able to determine the viscosity within 659 cP, given a mean viscosity of 926 cP (Table 23).

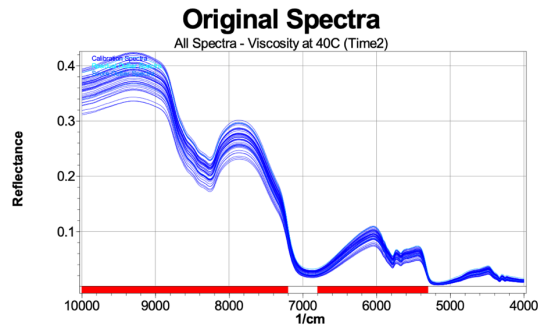


Figure 43. Viscosity at 40°C (Time2) CV calibration original spectra. No pretreatments were used for final calibration.

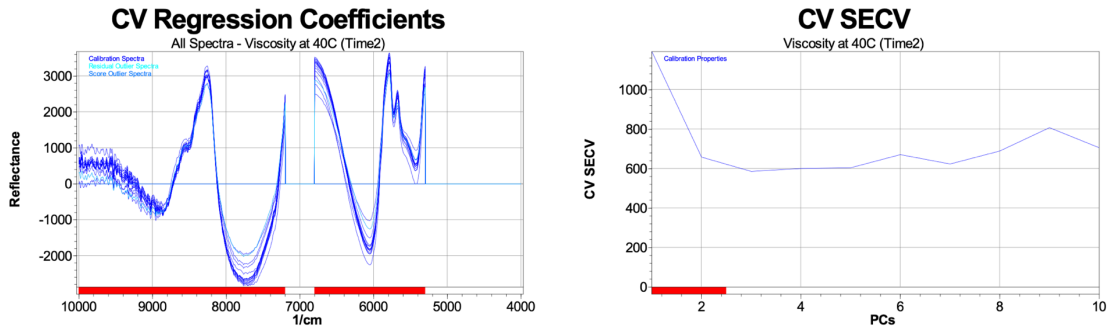
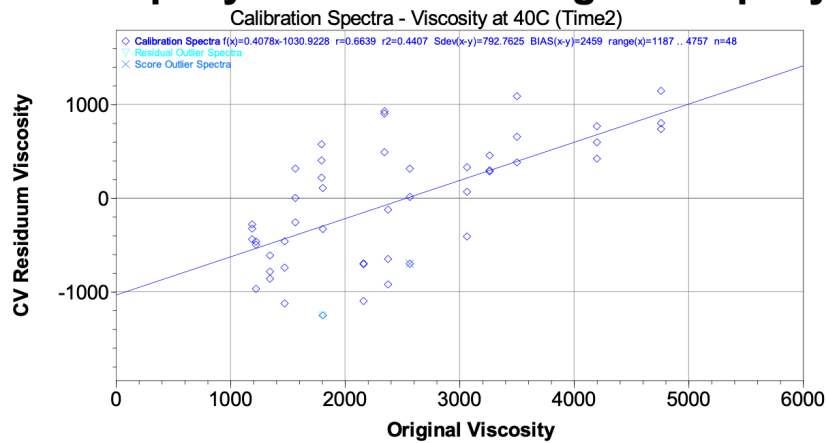
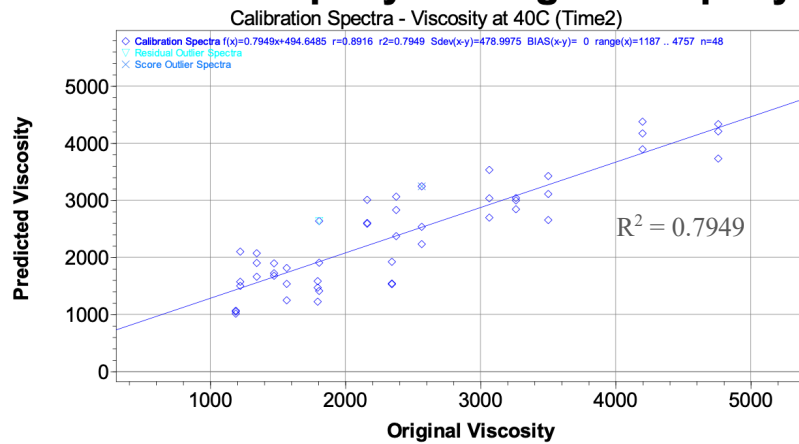


Figure 42. Viscosity at 40°C (Time2) CV calibration regression coefficients (top) and standard error of cross-validation (SECV, bottom). Wavenumber region used for calibration was 4,000-7,144 and 7404-10,000 cm^{-1} and 2 PCs used for primary and secondary PC selection.

CV Property Residuum vs. Original Property



Predicted Property vs. Original Property



Predicted Property vs Original Property

Cross Validation - Viscosity at 40°C (Time2)

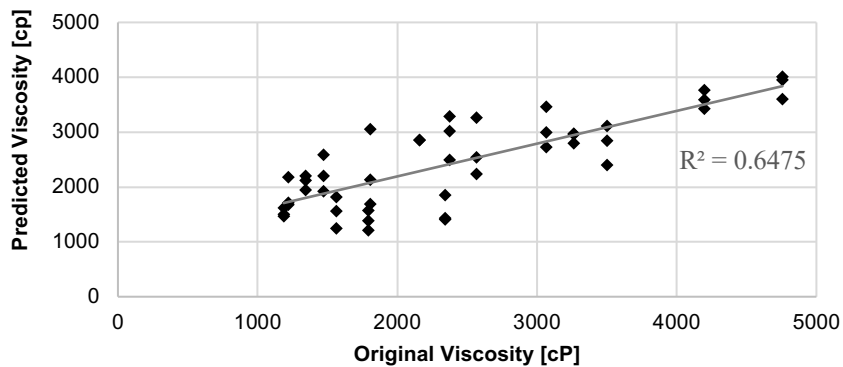


Figure 44. Viscosity at 40°C (Time2) CV calibration property residuum vs. original property (top), predicted property vs. original property of calibration (middle), and predicted property vs original property of CV (bottom).

4.4.3.3 Sauce Viscosity – 45°C (Time 1)

The CV graphs for viscosity at 45°C at 2 weeks past manufacture are shown below (**Figure 46**, **Figure 45**, and **Figure 47**). The final CV calibration was achieved without using a pretreatment (**Figure 46**). The wavenumber regions of 5,300-6,800 and 7,200-10,000 were used, which was the same as for Viscosity at 40°C (Time2)(**Figure 45**). The peaks in the regression coefficient graph around 5800, 6800, and 8300 cm^{-1} , coincided with the wavenumbers known for the CH/ CH₂/CH₃ first overtone region, CH/CH₂/CH₃ first overtone combination region, and CH/CH₂/CH₃ second overtone region (Appendix Figure 81)(Brüker, 2009). These were similar to the 40°C (Time2) calibration. The SECV graph indicated that 3 primary PCs and 3 secondary PCs were best to achieve minimal standard error (**Figure 45**).

The final calibration results shown in the three graphs of **Figure 47** show the residuum good distribution of residuum values, with 5 spectra excluded as score outlier spectra. The other two show the predicted property vs original property for the calibration

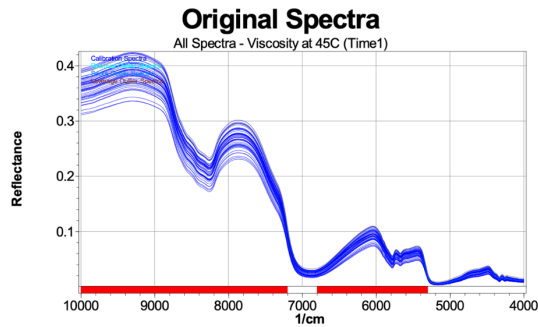


Figure 46. Viscosity at 45°C (Time1) CV calibration original spectra (top) and pretreated spectra (bottom). No pretreatments were used for final calibration.

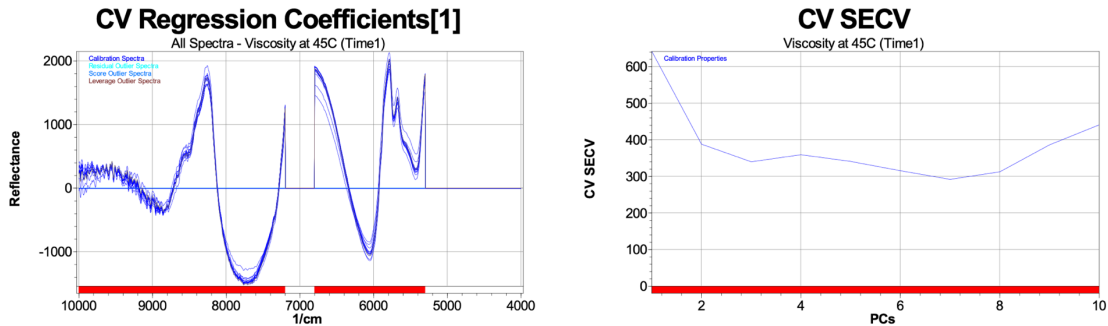
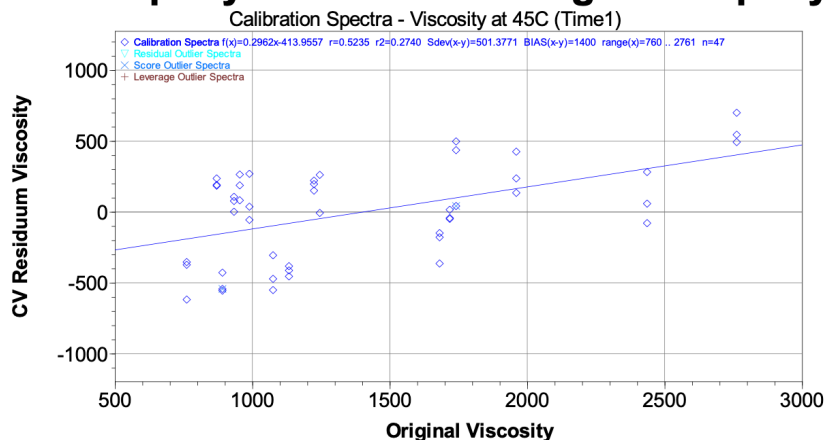
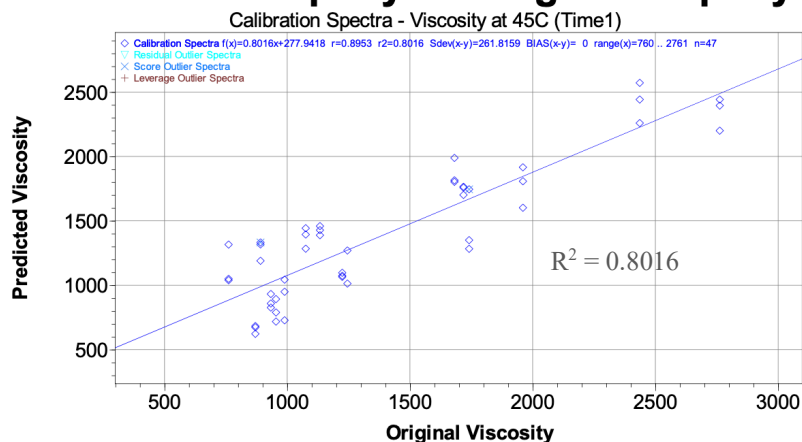


Figure 45. Viscosity at 45°C (Time1) CV calibration regression coefficients (top) and standard error of cross-validation (SECV, bottom). Wavenumber region used for calibration was 4,000-7,144 and 7404-10,000 cm^{-1} and 3 PCs used for primary PC selection.

CV Property Residuum vs. Original Property



Predicted Property vs. Original Property



Predicted Property vs Original Property

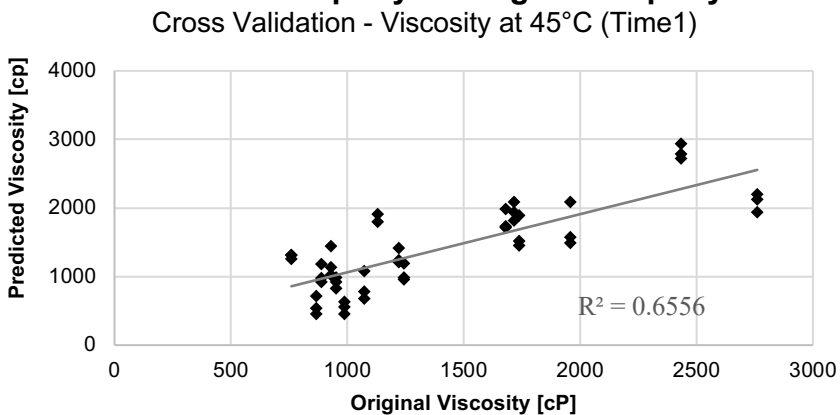


Figure 47. Viscosity at 45°C (Time1) CV calibration property residuum vs. original property (top), predicted property vs. original property of calibration (middle), and predicted property vs original property of CV (bottom).

set and CV set, respectively. There were no outlier spectra, so all spectra were included in the calibration. The calibration set r^2 was 0.8016, the CV r^2 was 0.6556, and the Büchi Q-value was 0.0219. Lastly, the standard error of calibration (SEC) showed we were able to determine the viscosity accurately within 262 cP and the standard error of cross-validation (SECV) was able to determine the viscosity within 340 cP, given a mean viscosity of 1401 cP (Table 23).

4.4.3.4 Sauce Viscosity – 45°C (Time 2)

The CV graphs for viscosity at 45°C at 2 weeks past manufacture are shown below (Figure 48, Figure 49, and Figure 50). The best CV calibration was achieved using the pretreatments of first derivative BCAP, followed by normalization by closure (Figure 48). These pretreatments first ran a derivative and then normalization of the spectra. The derivative helps to reduce baseline effects, increase the effect of smaller

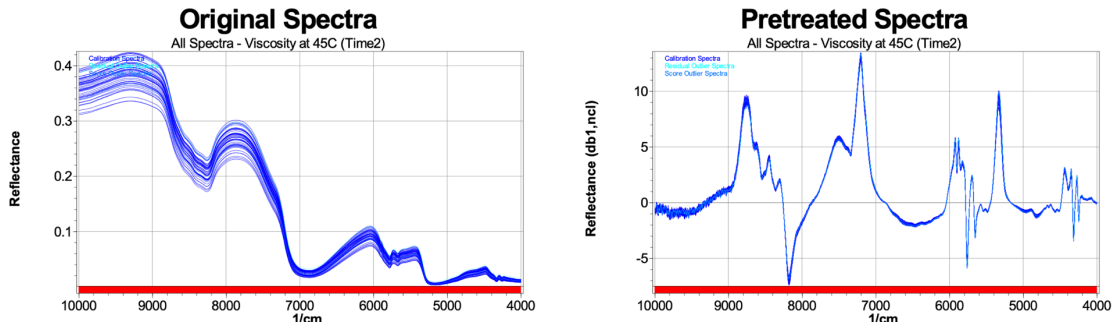


Figure 48. Viscosity at 45°C (Time2) CV calibration original spectra (top) and pretreated spectra (bottom). Pretreated used include 1st BCAP 5 points (db1), followed by normalization by closure (ncl).

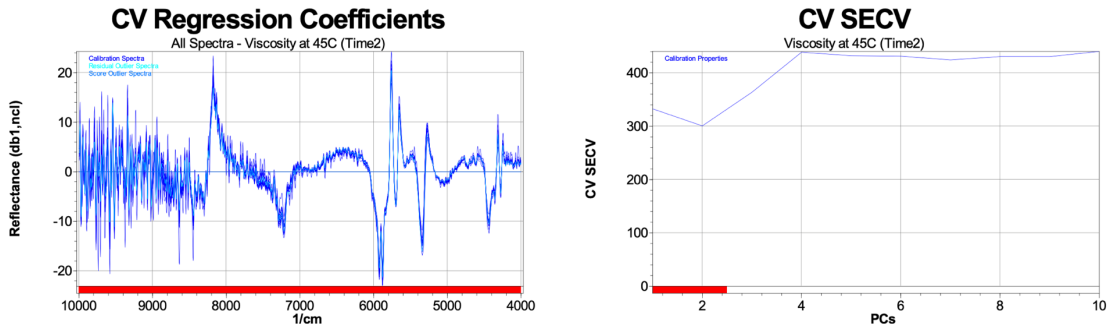
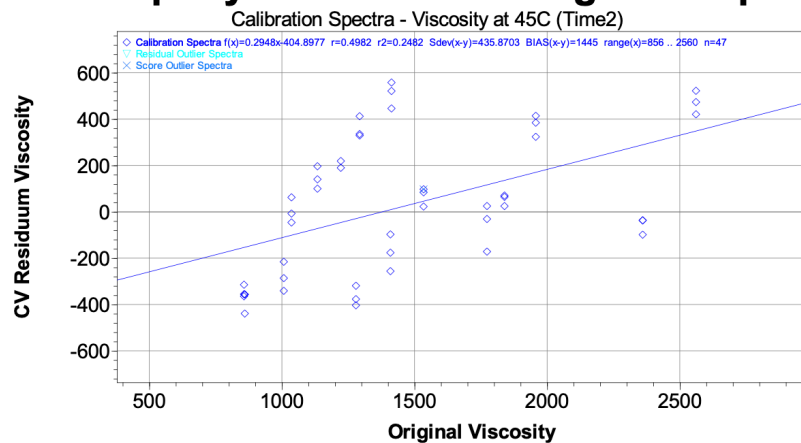
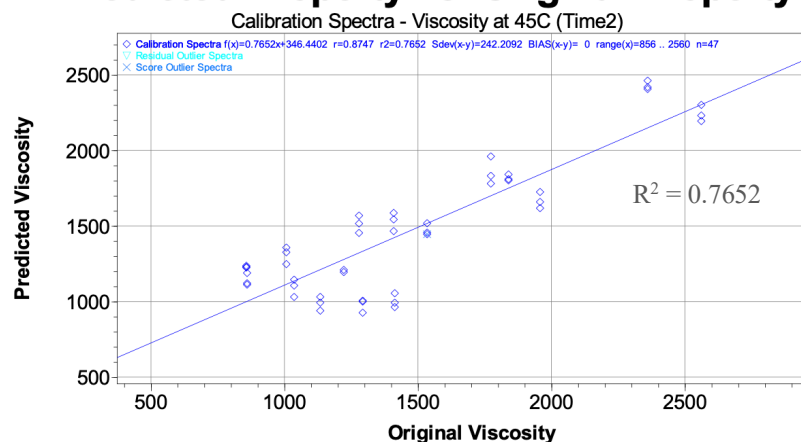


Figure 49. Viscosity at 45°C (Time2) CV calibration regression coefficients (top) and standard error of cross-validation (SECV, bottom). Wavenumber region used for calibration was 4,000-10,000 cm^{-1} and 2 PCs used for primary PC selection.

CV Property Residuum vs. Original Property



Predicted Property vs. Original Property



Predicted Property vs Original Property

Cross Validation - Viscosity at 45°C (Time2)

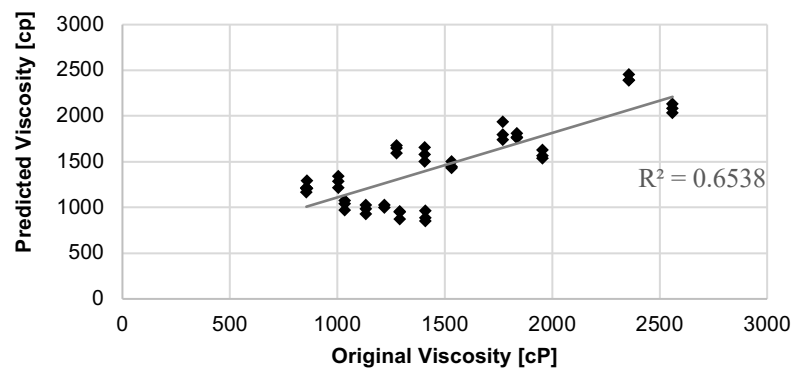


Figure 50. Viscosity at 45°C (Time2) CV calibration property residuum vs. original property (top), predicted property vs. original property of calibration (middle), and predicted property vs original property of CV (bottom).

absorption peaks, and overall reduce signal-to-noise ratio, while the normalization also helps reduce baseline variations (Büchi, 2016). The wavenumber region of 4,000-10,000 was used (**Figure 49**). The main peaks in the regression coefficient graph around 5800 and 8300 coincided with the wavenumbers known for the regions for CH/CH₂/CH₃ first and second overtones (Appendix **Figure 81**)(Brüker, 2009). The SECV graph indicated that 2 primary PCs and 2 secondary PCs were best to achieve minimal standard error (**Figure 49**).

The final calibration results shown in the three graphs of **Figure 47** show the residuum good distribution of residuum values with no outlier spectra, so all spectra were included in the calibration. The other two graphs show the predicted property vs original property for the calibration set and CV set, respectively. The calibration set r^2 was 0.8016, the CV r^2 was 0.6556, and the Büchi Q-value was 0.0219. Lastly, the standard error of calibration (SEC) showed we were able to determine the viscosity accurately within 242 cP and the standard error of cross-validation (SECV) was able to determine the viscosity within 301 cP, given a mean viscosity of 1475 cP (**Table 23**).

4.4.3.5 Sauce Viscosity – 50°C (Time 1)

The CV graphs for viscosity at 50°C at two weeks past manufacture are shown below (**Figure 51**, **Figure 52**, and **Figure 53**). The best CV calibration was achieved using normalization by closure (**Figure 51**). Normalization pretreatments help reduce baseline variations (Büchi, 2016). The wavenumber region of 5,000-10,000 was used (**Figure 52**). The peaks in the regression coefficient graph around 5400, 5800, 8400,

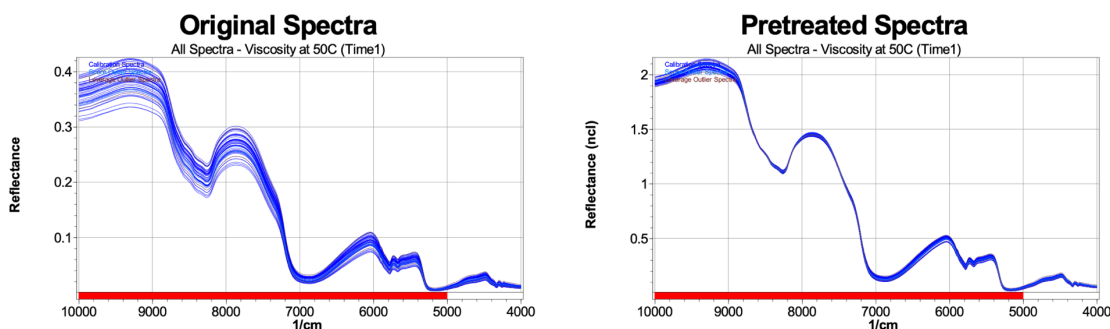


Figure 51. Viscosity at 50°C (Time1) CV calibration original spectra (top) and pretreated spectra (bottom). Pretreated used was normalization by closure (ncl).

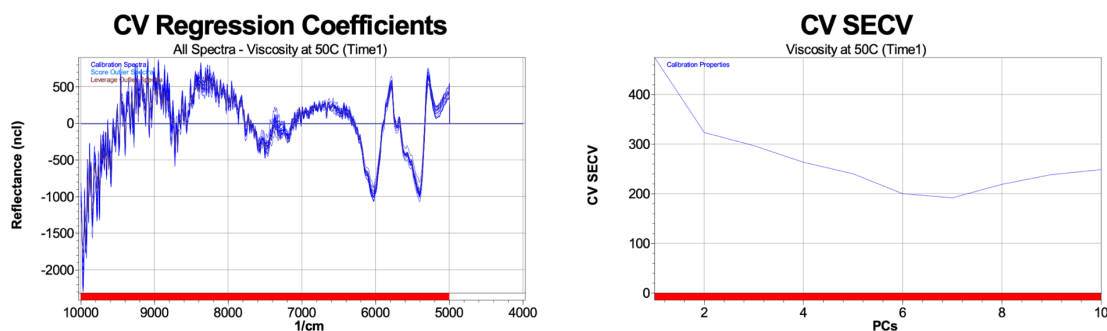
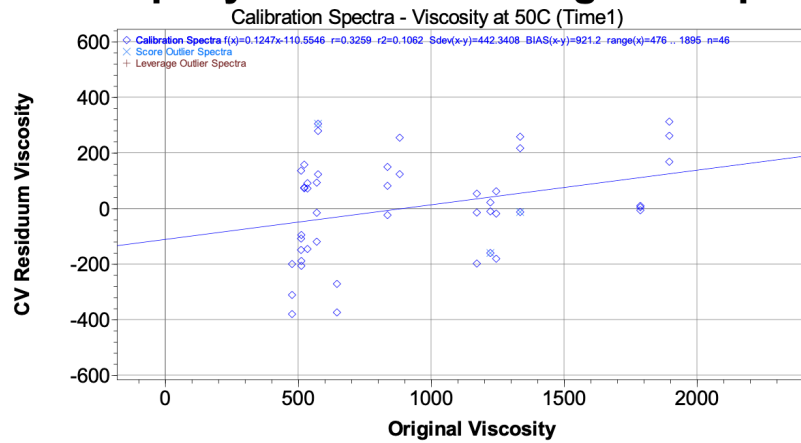


Figure 52. Viscosity at 50°C (Time1) CV calibration regression coefficients (top) and standard error of cross-validation (SECV, bottom). Wavenumber region used for calibration was 5,000-10,000 cm^{-1} and 7 PCs used for primary PC selection.

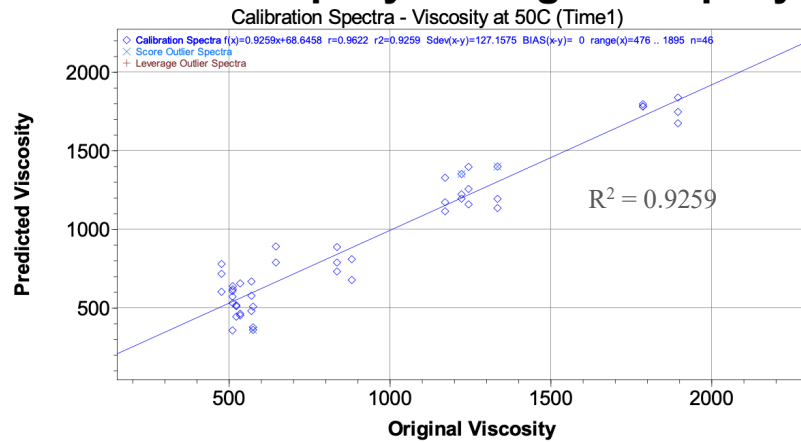
and 8800-9400 cm^{-1} coincided with the wavenumbers known for the H_2O first overtone region and the $\text{CH}/\text{CH}_2/\text{CH}_3$ first and second overtones (Appendix Figure 81)(Brüker, 2009). The SECV graph indicated that 7 primary PCs and 7 secondary PCs were best to achieve minimal standard error (**Figure 52**).

The final calibration results shown in the three graphs of **Figure 53** show the residuum good distribution of residuum values with only two outlier spectra. The other two graphs show the predicted property vs original property for the calibration set and CV set, respectively. The calibration set r^2 was 0.9259, the CV r^2 was 0.5348, and the Büchi Q-value was 0.4878. This large of a gap between calibration and CV r^2 might indicate that more samples are needed to build a CV model with stronger predictive abilities. Lastly, the standard error of calibration (SEC) showed we were able to determine the viscosity accurately within 217 cP and the standard error of cross-validation (SECV) was able to determine the viscosity within 192 cP, given a mean viscosity of 926 cP (**Table 23**).

CV Property Residuum vs. Original Property



Predicted Property vs. Original Property



Predicted Property vs Original Property

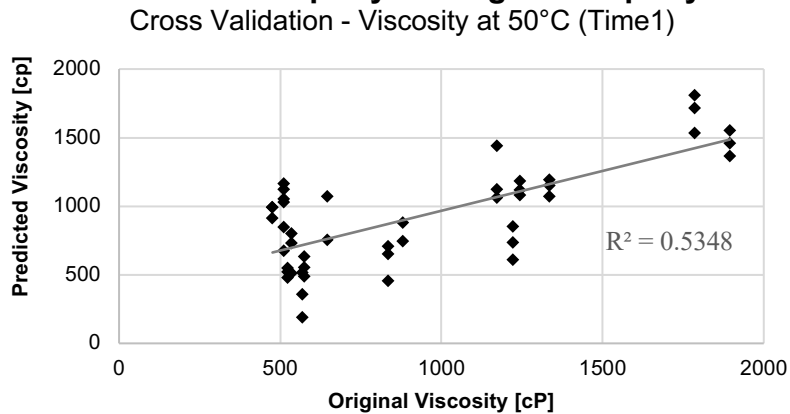


Figure 53. Viscosity at 50°C (Time1) CV calibration property residuum vs. original property (top), predicted property vs. original property of calibration (middle), and predicted property vs original property of CV (bottom).

4.4.3.6 Sauce Viscosity – 50°C (Time 2)

The CV graphs for viscosity at 50°C at four weeks past manufacture are shown below (**Figure 55**, **Figure 54**, and **Figure 56**). The final CV calibration was achieved without using a pretreatment (**Figure 55**). Normalization pretreatments help reduce baseline variations (Büchi, 2016). The wavenumber region of 4,000-10,000 was used (**Figure 54**). The peaks in the regression coefficient graph around 4300, 4800, 5400, 5800, 6800-7200, and 8300 cm^{-1} coincided with the wavenumbers known for the first overtone CH combinations region, NH combinations, H_2O , and $\text{CH}/\text{CH}_2/\text{CH}_3$ regions, as well as the second overtone CH regions (Appendix Figure 81)(Brüker, 2009). The SECV graph indicated that 2 primary PCs and 2 secondary PCs were best to achieve minimal standard error (**Figure 54**).

The final calibration results shown in the three graphs of **Figure 56** show the residuum good distribution of residuum values with only two outlier spectra. The other two graphs show the predicted property vs original property for the calibration set and

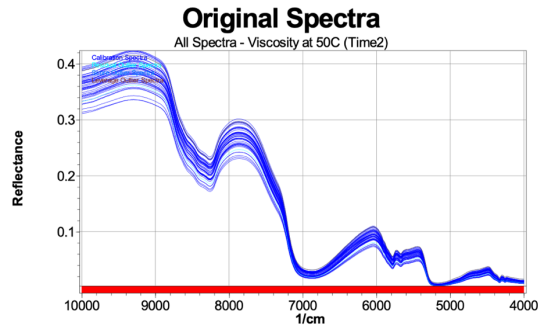


Figure 55. Viscosity at 50°C (Time2) CV calibration original spectra (top) and pretreated spectra (bottom). No pretreatments were used for final calibration.

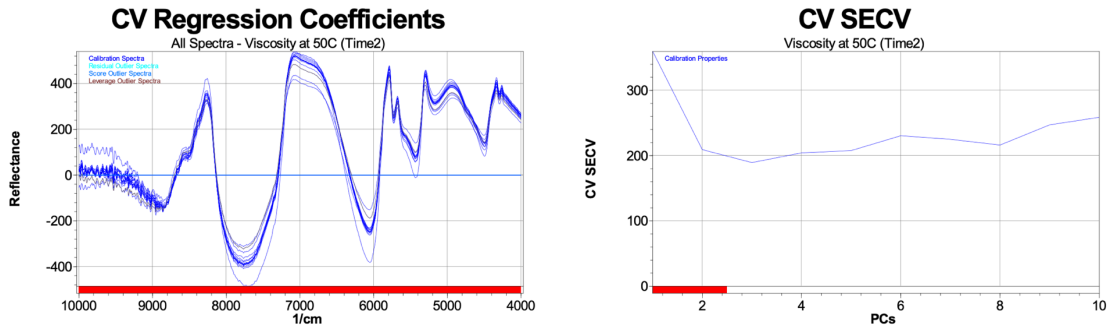
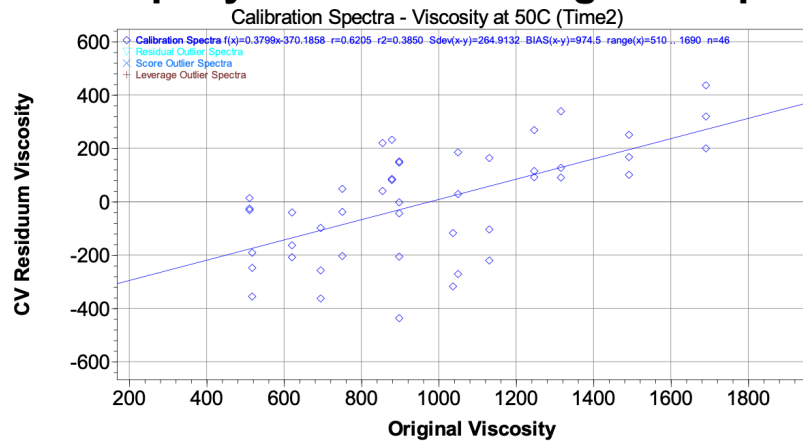
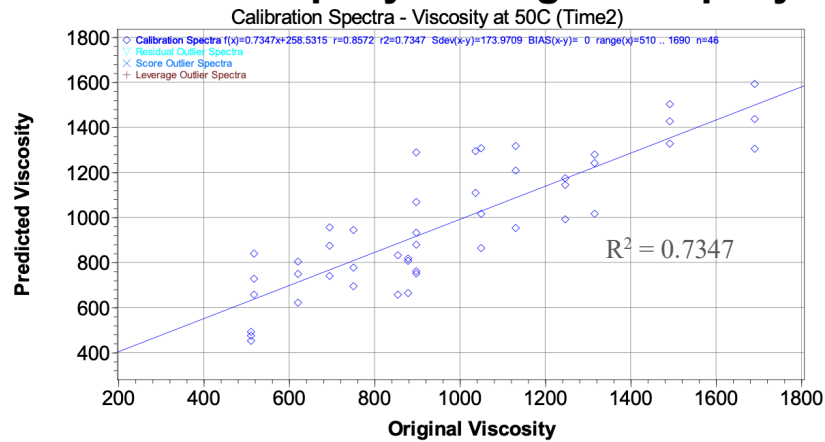


Figure 54. Viscosity at 50°C (Time2) CV calibration regression coefficients (top) and standard error of cross-validation (SECV, bottom). Wavenumber region used for calibration was 4,000-10,000 cm^{-1} and 2 PCs used for primary PC selection.

CV Property Residuum vs. Original Property



Predicted Property vs. Original Property



Predicted Property vs Original Property

Cross Validation - Viscosity at 50°C (Time2)

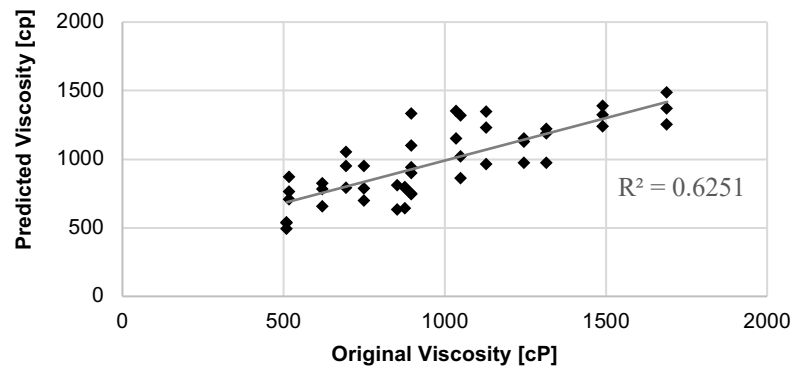


Figure 56. Viscosity at 50°C (Time2) CV calibration property residuum vs. original property (top), predicted property vs. original property of calibration (middle), and predicted property vs original property of CV (bottom).

CV set, respectively. The calibration set r^2 was 0.9259, the CV r^2 was 0.5348, and the Büchi Q-value was 0.5244. Like the previous viscosity at 50°C (Time1) calibration, this large of a gap between calibration and CV r^2 might indicate that more samples are needed to build a CV model with stronger predictive abilities. Lastly, the standard error of calibration (SEC) showed we were able to determine the viscosity accurately within 174 cP and the standard error of cross-validation (SECV) was able to determine the viscosity within 209 cP, given a mean viscosity of 975 cP (**Table 23**).

4.4.3 7 Melt Area (Time 1)

The CV graphs for melt area at two weeks past manufacture are shown below (**Figure 57**, **Figure 58**, and **Figure 59**). The best CV calibration was achieved using the pretreatments of first derivative BCAP, followed by normalization by closure (**Figure 57**). The derivative helps to reduce baseline effects, increase the effect of smaller absorption peaks, and overall reduce signal-to-noise ratio, while the normalization also helps reduce baseline variations (Büchi, 2016). The wavenumber region used was 5,000-7,144 and 7,404-10,000 (**Figure 58**). The peaks in the regression coefficient graph around 5400, 5900, and 8800 cm^{-1} coincided with the wavenumbers known for the H_2O and $\text{CH}/\text{CH}_2/\text{CH}_3$ first overtone region, as well as the CH_3 second overtone region (Appendix Figure 81)(Brüker, 2009). The SECV graph indicated that 3 primary PCs and 3 secondary PCs were best to achieve minimal standard error (**Figure 58**).

The final calibration results shown in the three graphs of **Figure 59** show the residuum good distribution of residuum values with only five spectra excluded as outliers. The other two graphs show the predicted property vs original property for the calibration set and CV set, respectively. The calibration set r^2 was 0.2294, the CV r^2 was 0.7335, and the Büchi Q-value was 0.6551. This Q-value above 0.6 passes the threshold for an acceptable calibration. A much higher in the CV r^2 than C r^2 may indicate that the CV prediction model created a more linear data set than the calibration one, but may lead to different ranges of standard error. This is the best calibration across the 14 properties tested. Lastly, the standard error of calibration (SEC) showed we were able to determine the melt area accurately within 0.16 in^2 and the standard error of cross-validation (SECV)

was able to determine the melt area within 0.25 in², given the mean melt area of 3.63 in² (Table 23).

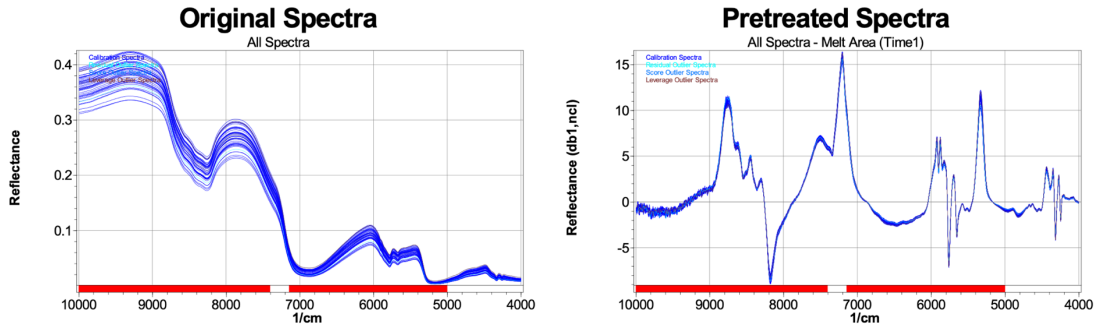


Figure 57. Melt area (Time1) CV calibration original spectra (top) and pretreated spectra (bottom). Pretreated used include 1st BCAP 5 points (db1), followed by normalization by closure (ncl).

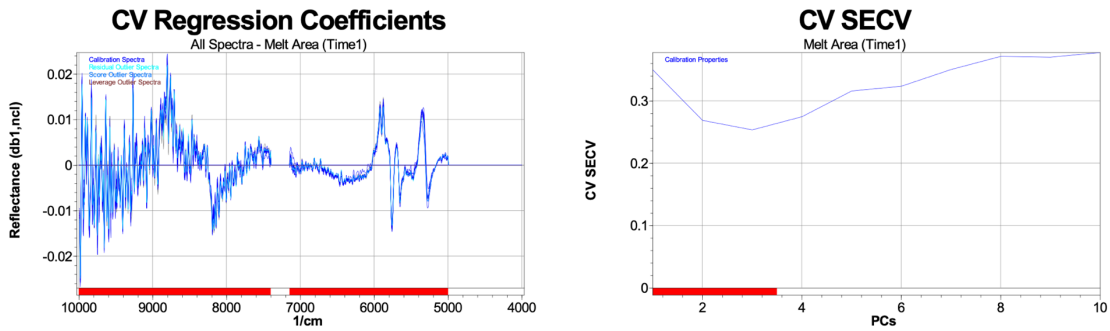
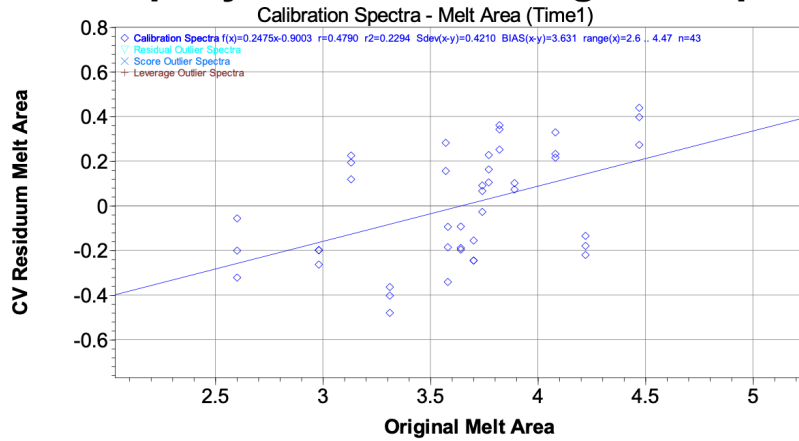
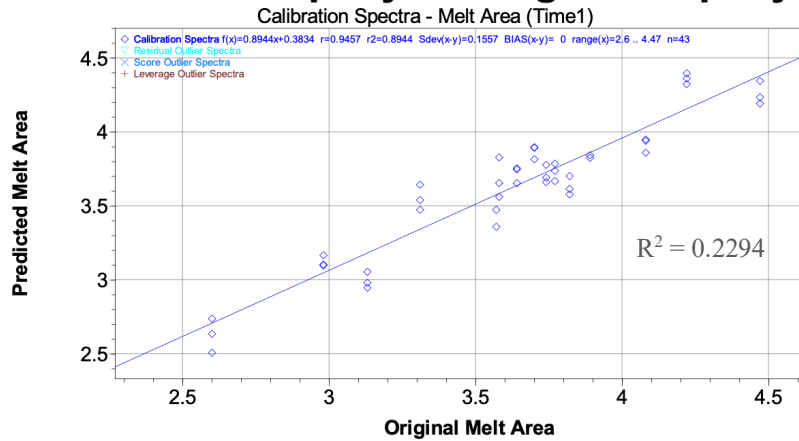


Figure 58. Melt area (Time1) CV calibration regression coefficients (top) and standard error of cross-validation (SECV, bottom). Wavenumber region used for calibration was 4,000-7,144 and 7404-10,000 cm⁻¹ and 3 PCs used for primary PC selection.

CV Property Residuum vs. Original Property



Predicted Property vs. Original Property



Predicted Property vs Original Property

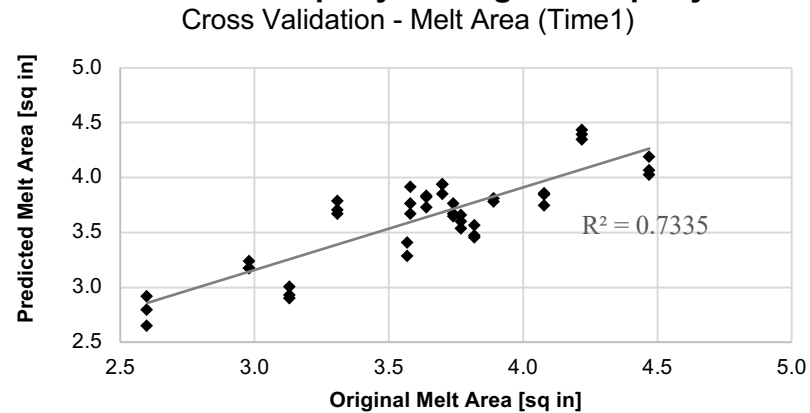


Figure 59. Melt area (Time1) CV calibration property residuum vs. original property (top), predicted property vs. original property of calibration (middle), and predicted property vs original property of CV (bottom).

4.4.3.8 Melt Area (Time 2)

The CV graphs for melt area at four weeks past manufacture are shown below (Figure 61, Figure 60, and Figure 62). The best CV calibration was achieved using the pretreatments of first derivative BCAP, which helps to reduce baseline effects, increase the effect of smaller absorption peaks, and overall reduce the signal-to-noise ratio (Figure 61)(Büchi, 2016). The wavenumber region used was 5,000-10,000 (Figure 60). The peaks in the regression coefficient graph around 5900 cm^{-1} coincided with the wavenumbers known for the CH/CH₂/CH₃ first overtone region (Appendix Figure 81)(Brüker, 2009). The SECV graph indicated that 2 primary PCs and 2 secondary PCs were best to achieve minimal standard error (Figure 60).

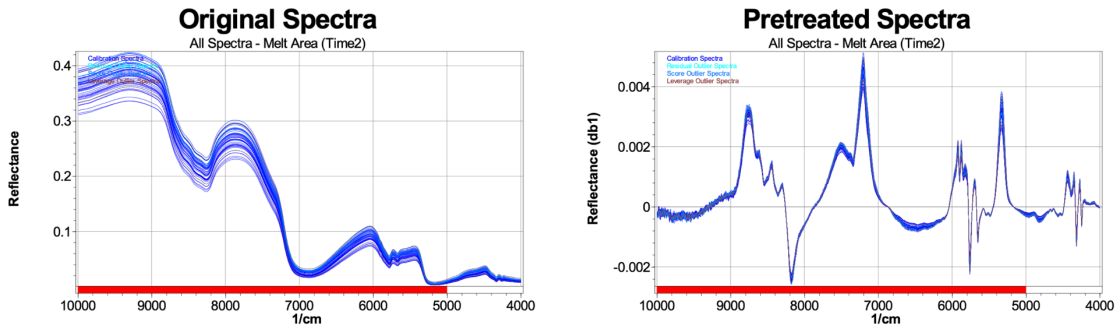


Figure 61. Melt area (Time2) CV calibration original spectra (top) and pretreated spectra (bottom). Pretreatment used was 1st BCAP 5 points (db1).

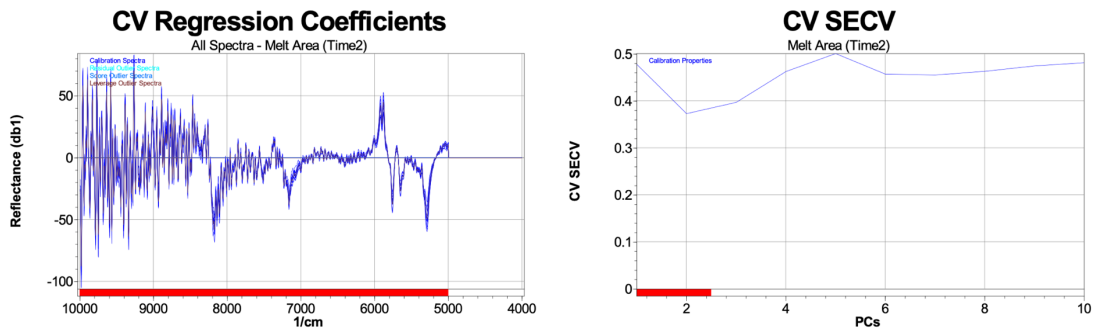
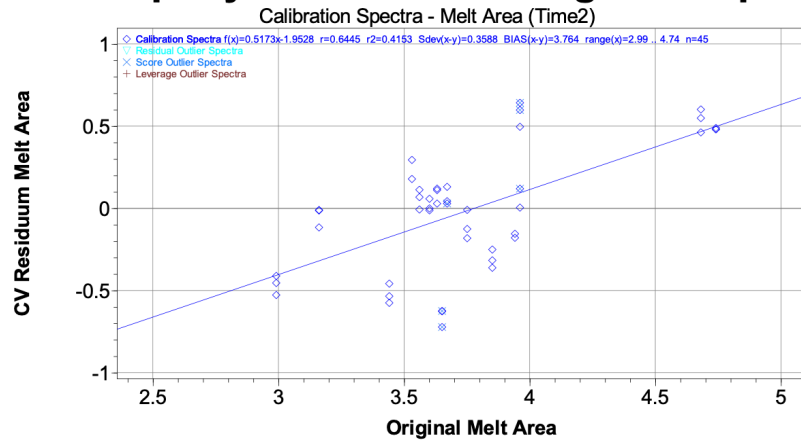


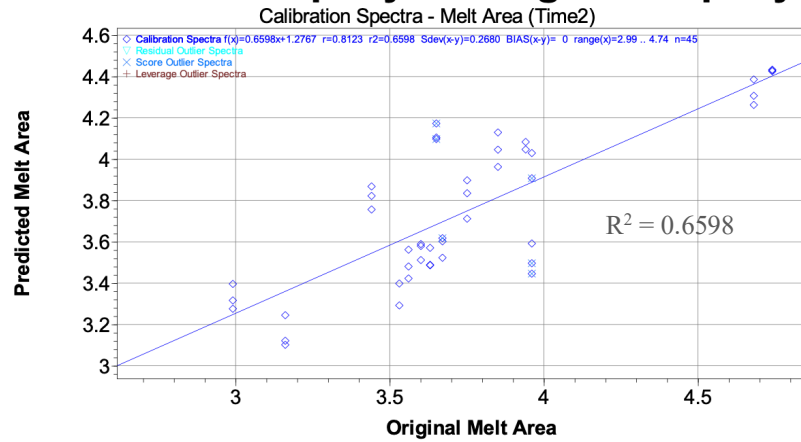
Figure 60. Melt area (Time2) CV calibration regression coefficients (top) and standard error of cross-validation (SECV, bottom). Wavenumber region used for calibration was 5,000-10,000 cm^{-1} and 2 PCs used for primary PC selection.

The final calibration results shown in the three graphs of Figure 62 show the residuum good distribution of residuum values with only three spectra excluded as

CV Property Residuum vs. Original Property



Predicted Property vs. Original Property



Predicted Property vs Original Property

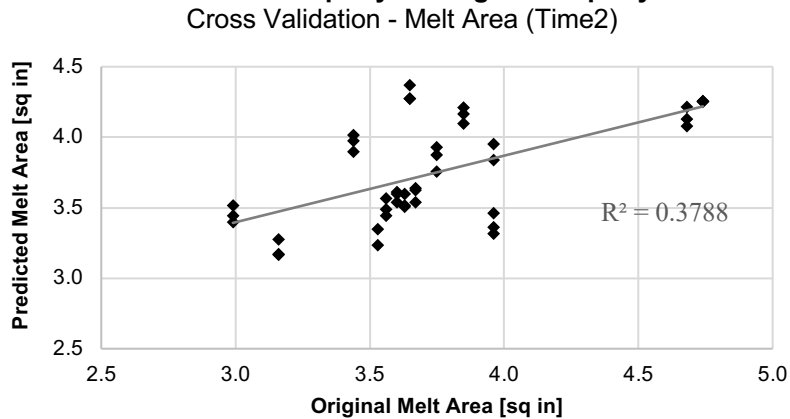


Figure 62. Melt area (Time2) CV calibration property residuum vs. original property (top), predicted property vs. original property of calibration (middle), and predicted property vs original property of CV (bottom).

outliers. The other two graphs show the predicted property vs original property for the calibration set and CV set, respectively. The calibration set r^2 was 0.6598, the CV r^2 was 0.3788, and the Büchi Q-value was 0.5106. Lastly, the standard error of calibration (SEC) showed we were able to determine the melt area accurately within 0.27 in² and the standard error of cross-validation (SECV) was able to determine the melt area within 0.37 in², given the mean melt area of 3.75 in² (**Table 23**).

4.4.3.9 Firmness (Time 1)

The CV graphs for firmness at two weeks past manufacture are shown below (**Figure 64**, **Figure 63**, and **Figure 65**). The best CV calibration was achieved using the pretreatments of Kubelka Munk (**Figure 64b**, kmu). This pretreatment is a transformation treatment that modifies the absorption peaks and is independent of calibration wavelengths (Büchi, 2016). The wavenumber region used was 4,400-4,800, 5,400-6,600, and 7,800-10,000 (**Figure 63**). The peaks in the regression coefficient graph around

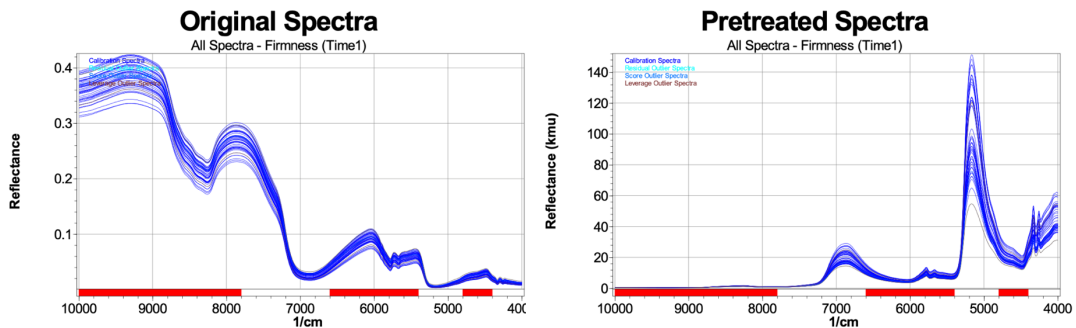


Figure 64. Firmness (Time1) CV calibration original spectra (top) and pretreated spectra (bottom). Pretreatment used was Kubelka Munk (kmu).

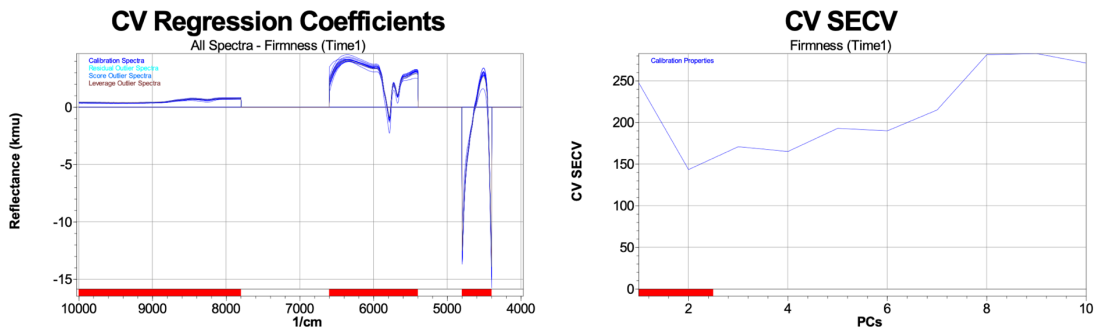
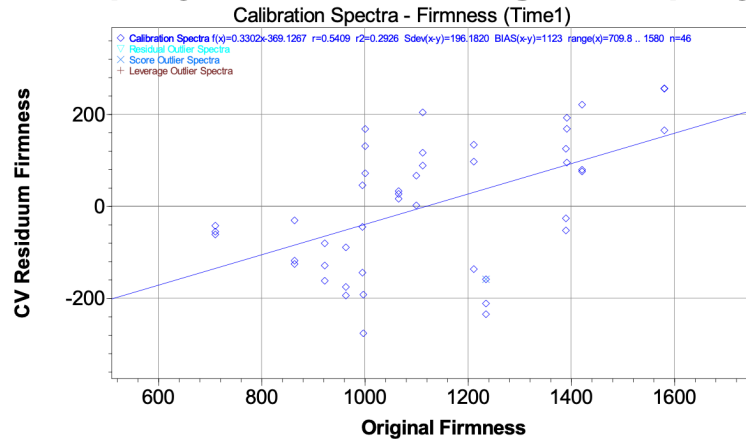
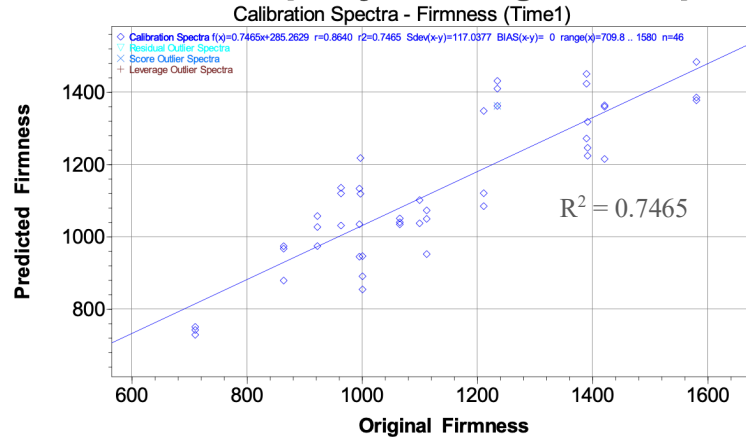


Figure 63. Firmness (Time1) CV calibration regression coefficients (top) and standard error of cross-validation (SECV, bottom). Wavenumber region used for calibration was 4,400-4,800, 5,400-6,600, and 7,800-10,000 cm^{-1} and 2 PCs used for primary PC selection.

CV Property Residuum vs. Original Property



Predicted Property vs. Original Property



Predicted Property vs Original Property

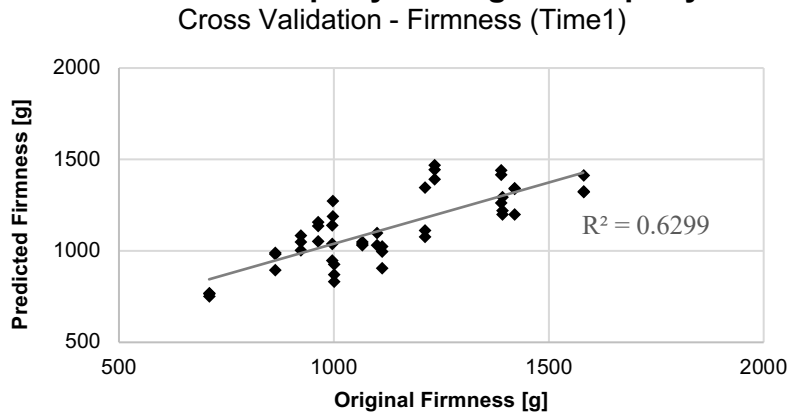


Figure 65. Firmness (Time1) CV calibration property residuum vs. original property (top), predicted property vs. original property of calibration (middle), and predicted property vs original property of CV (bottom).

4500, 5500, and 6000-6500 cm^{-1} coincided with the wavenumbers known for the CHO combination region, CH first overtone region, and NH and OH second overtone region (Appendix Figure 81)(Brüker, 2009). The SECV graph indicated that 2 primary PCs and 2 secondary PCs were best to achieve minimal standard error (**Figure 63**).

The final calibration results shown in the three graphs of **Figure 65** show the good distribution of residuum values with only two spectra excluded as outliers. The other two graphs show the predicted property vs original property for the calibration set and CV set, respectively. The calibration set r^2 was 0.7465, the CV r^2 was 0.6299, and the Büchi Q-value was 0.5358. Lastly, the standard error of calibration (SEC) showed we were able to determine the firmness accurately within 117g and the standard error of cross-validation (SECV) was able to determine the firmness within 144g, given the mean firmness of 1125g (**Table 23**).

Woodcock et al. summarized several studies' findings for NIR and MIR spectroscopy applications for texture, with many different wavelength ranges being used and demonstrating the feasibility for industrial use (2008). The best models according to Woodcock et al. are the ones with only the wavelength ranges of the largest influence as indicated by loading scores (2008). Although loading scores weren't used in the calibration development of this study, they should be included in any further research or exploration of this study's data.

4.4.3.10 Firmness (Time 2)

The CV graphs for firmness at four weeks past manufacture are shown below (**Figure 66**, **Figure 67**, and **Figure 68**). The best CV calibration was achieved using the pretreatments of Kubelka Munk (**Figure 66b**, kmu). As described in the previous firmness calibration, this pretreatment is a transformation treatment that modifies the absorption peaks and is independent of calibration wavelengths (Büchi, 2016). The wavenumber region used was 5,000-10,000 cm^{-1} (**Figure 67**). The peaks in the regression coefficient graph around 5000 and 6500-7000 cm^{-1} coincided with the wavenumbers known for the NH_2 first overtone combinations region and OH/NH first overtone region (Appendix Figure 81)(Brüker, 2009). The SECV graph indicated that 2 primary PCs and 2 secondary PCs were best to achieve minimal standard error (**Figure 67**).

The final calibration results shown in the three graphs of **Figure 68** show the good distribution of residuum values with only two spectra excluded as outliers. The other two graphs show the predicted property vs original property for the calibration set and CV set, respectively. The calibration set r^2 was 0.3665, the CV r^2 was 0.1861, and the Büchi Q-value was 0.4305. Lastly, the standard error of calibration (SEC) showed we were able to determine the firmness accurately within 174g and the standard error of cross-validation (SECV) was able to determine the firmness within 203g, given the mean firmness of 1141g (**Table 23**).

As described in the previous firmness calibration discussion, Woodcock et al. meta-analysis of NIR and MIR spectroscopy studies for rheological parameters of cheese are relevant for this section's findings (2008). Previous studies found correlations

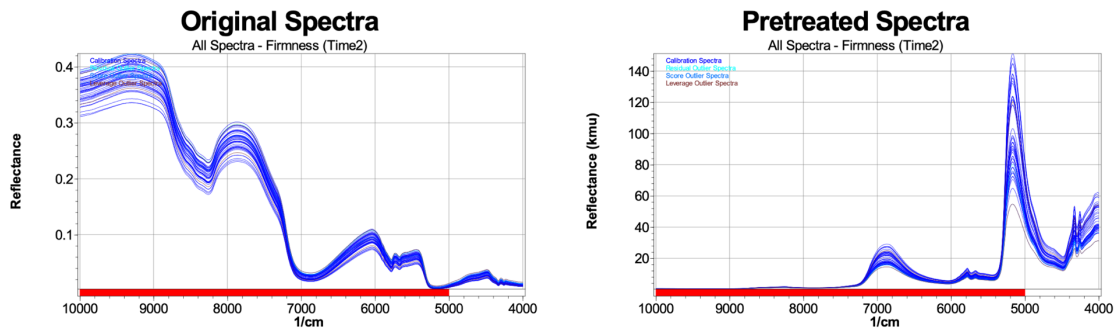


Figure 66. Firmness (Time2) CV calibration original spectra (top) and pretreated spectra (bottom). Pretreatment used was Kubelka Munk (kmu).

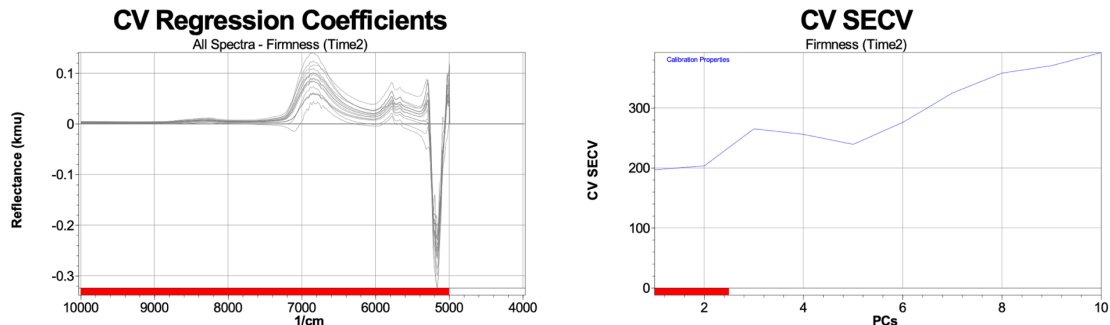
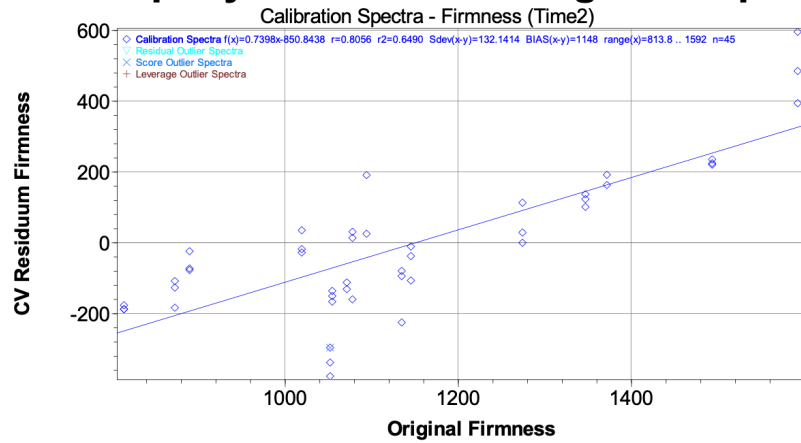
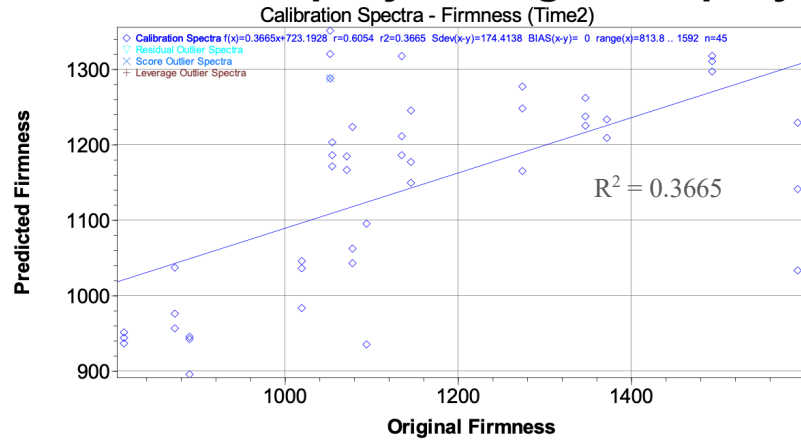


Figure 67. Firmness (Time2) CV calibration regression coefficients (top) and standard error of cross-validation (SECV, bottom). Wavenumber region used for calibration was 5,000-10,000 cm^{-1} and 2 PCs used for primary PC selection.

CV Property Residuum vs. Original Property



Predicted Property vs. Original Property



Predicted Property vs Original Property

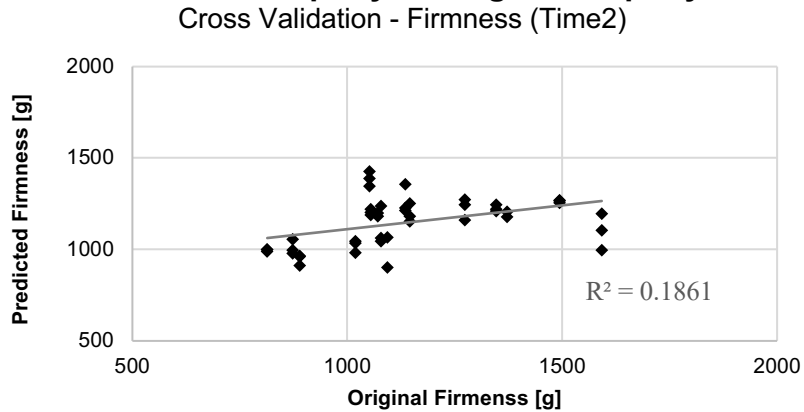


Figure 68. Firmness (Time2) CV calibration property residuum vs. original property (top), predicted property vs. original property of calibration (middle), and predicted property vs original property of CV (bottom).

between spectra to properties at significant enough levels to be applied for industrial use, despite these findings being weaker (Woodcock et al., 2008). Further exploration into the wavenumbers chosen based on the loading scores could be a way to increase the robustness of this study's data.

4.4.3.11 CLSM – Number of Fat Droplets

The CV graphs for CLSM number of fat droplets at two weeks past manufacture are shown below (Figure 69, Figure 70, and Figure 71). The best CV calibration was achieved using the pretreatments of first derivative BCAP (db1), followed by normalization by closure (ncl)(Figure 69). The first derivative helps to reduce baseline effects, increase the effect of smaller absorption peaks, and overall reduce signal-to-noise ratio, while the normalization also helps reduce baseline variations (Büchi, 2016). The wavenumber region used was 4,000-10,000 cm^{-1} (Figure 70). The peaks in the regression coefficient graph around 4400 and 5700 coincided with the wavenumbers

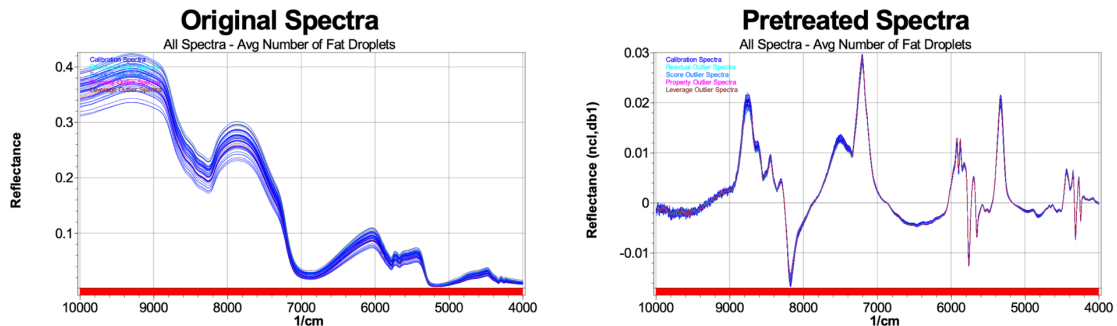


Figure 69. CLSM average number of fat droplets CV calibration original spectra (top) and pretreated spectra (bottom). Pretreated used include normalization by closure (ncl), followed by 1st BCAP 5 points (db1).

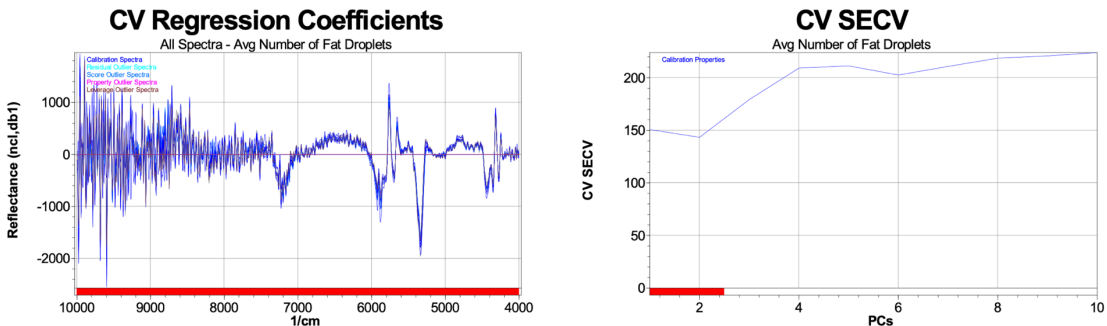
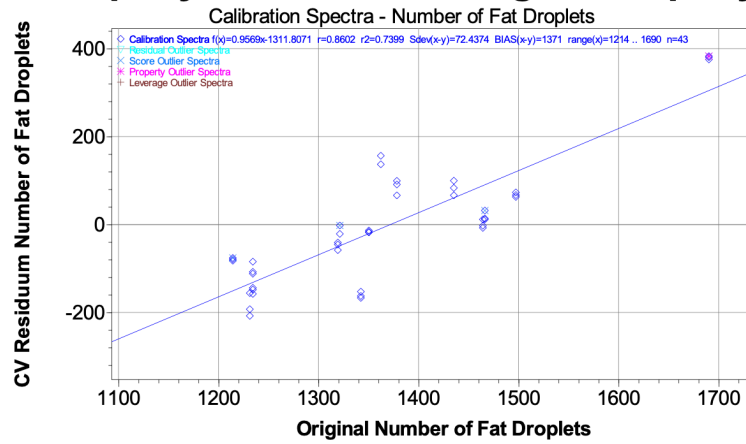
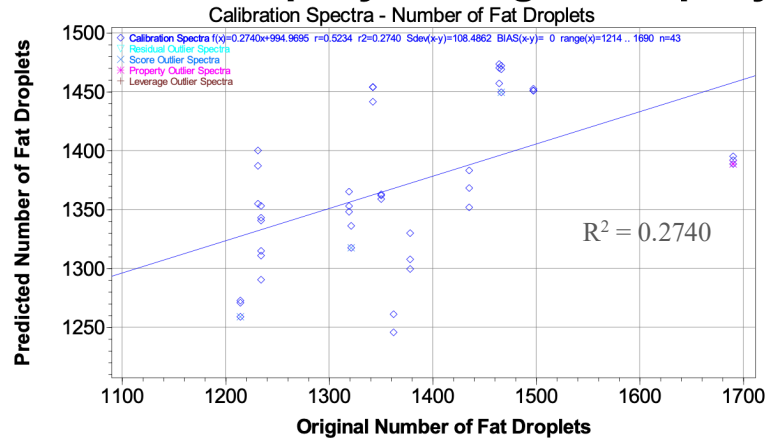


Figure 70. CLSM average number of fat droplets CV calibration regression coefficients (top) and standard error of cross-validation (SECV, bottom). Wavenumber region used for calibration was 4,000-10,000 cm^{-1} and 2 PCs used for primary PC selection.

CV Property Residuum vs. Original Property



Predicted Property vs. Original Property



Predicted Property vs Original Property

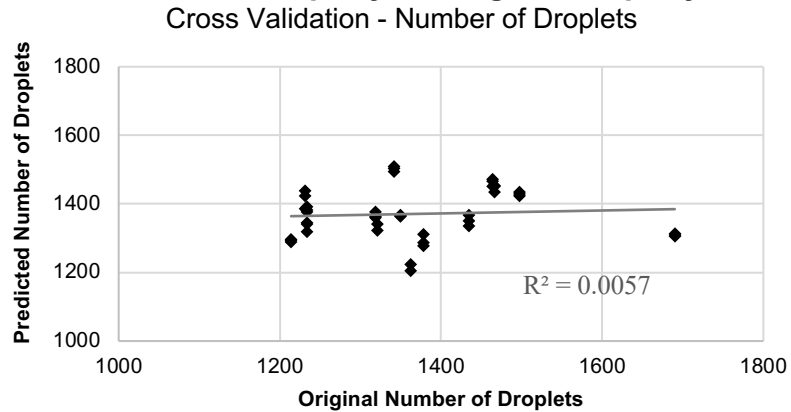


Figure 71. CLSM average number of fat droplets CV calibration property residuum vs. original property (top) and predicted property vs. original property (bottom).

known for the CHO combinations region and the CH first overtone region (Appendix **Figure 81**)(Brüker, 2009). The SECV graph indicated that 2 primary PCs and 2 secondary PCs were best to achieve minimal standard error (**Figure 70**).

The final calibration results shown in the three graphs of **Figure 71** show the good distribution of residuum values with five spectra excluded as outliers. The other two graphs show the predicted property vs original property for the calibration set and CV set, respectively. The calibration set r^2 was 0.2740, the CV r^2 was 0.0057, and the Büchi Q-value was 0.4305. Lastly, the standard error of calibration (SEC) showed we were able to determine the number of fat droplets per 636 μm image accurately within 108 droplets and the standard error of cross-validation (SECV) was able to determine the firmness within 143 droplets, given the mean number of fat droplets of 1370 (**Table 23**).

4.4.3.12 CLSM – Average Fat Droplet Volume

The CV graphs for CLSM average fat droplets volume at two weeks past manufacture are shown below (**Figure 72**, **Figure 73**, and **Figure 74**). The best CV

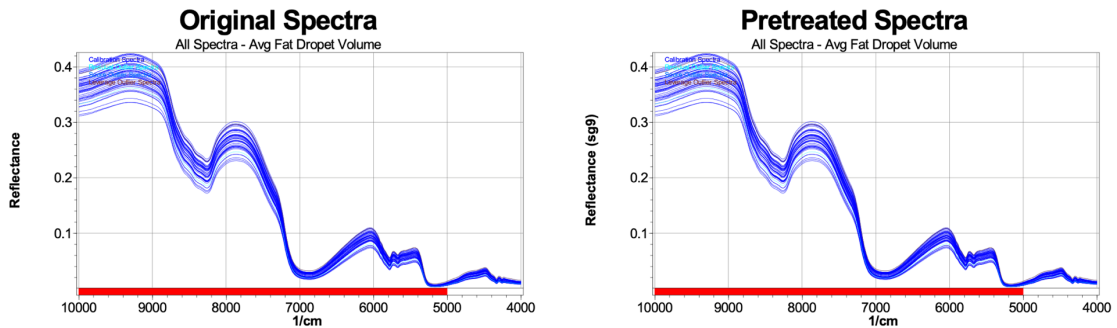


Figure 72. CLSM average fat droplet volume CV calibration original spectra (top) and pretreated spectra (bottom). Pretreatment used was Savitzky-Gola 9 points (sg9).

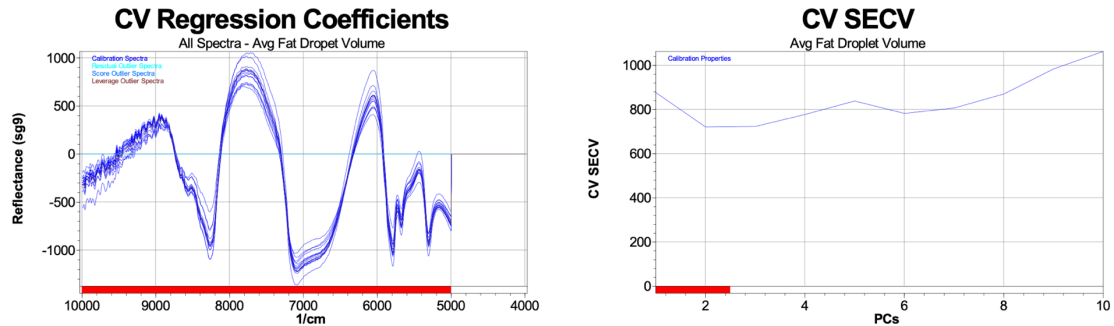
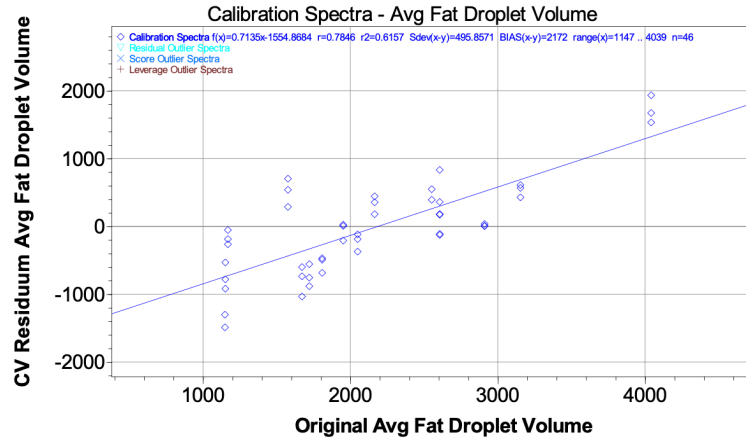
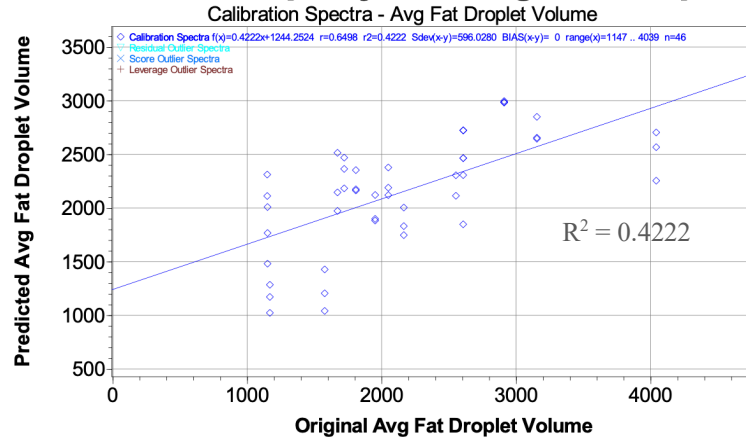


Figure 73. CLSM average fat droplet volume CV calibration regression coefficients (top) and standard error of cross-validation (SECV, bottom). Wavenumber region used for calibration was 5,000-10,000 cm^{-1} and 2 PCs used for primary PC selection.

CV Property Residuum vs. Original Property



Predicted Property vs. Original Property



Predicted Property vs Original Property

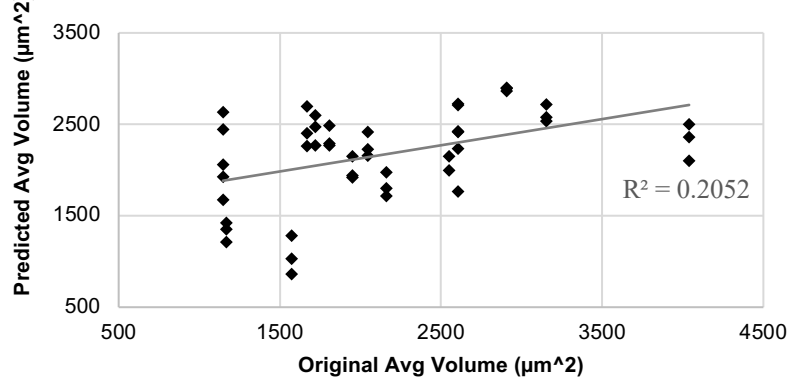


Figure 74. CLSM average fat droplet volume CV calibration property residuum vs. original property (top), predicted property vs. original property of calibration (middle), and predicted property vs original property of CV (bottom).

calibration was achieved using the smoothing pretreatment Savitsky-Golay 9-points (sg9, **Figure 72**). This smoothing pretreatment reduces the noise level in spectra and is a zero-order derivative independent of the calibration wavelengths (Büchi, 2016). The wavenumber region used was 5,000-10,000 cm^{-1} (**Figure 73**). The peaks in the regression coefficient graph around 6100, 7500-8100, and 8800-9200 coincided with the wavenumbers known for the CH first overtone region, CH second overtone region, and the CH/CH₂/CH₃ second overtone region (Appendix **Figure 81**)(Brüker, 2009). The SECV graph indicated that 2 primary PCs and 2 secondary PCs were best to achieve minimal standard error (**Figure 73**).

The final calibration results shown in the three graphs of **Figure 74** show the good distribution of residuum values with two spectra excluded as outliers. The other two graphs show the predicted property vs original property for the calibration set and CV set, respectively. The calibration set r^2 was 0.4222, the CV r^2 was 0.2052, and the Büchi Q-value was 0.4175. Lastly, the standard error of calibration (SEC) showed we were able to determine the average volume of fat droplets within 596 μm^2 and the standard error of cross-validation (SECV) was able to determine the average volume within 721 μm^2 , given the mean number of fat droplets of 2153 μm^2 (**Table 23**).

4.4.3.13 CLSM – Average Fat Droplet Diameter

The CV graphs for CLSM average fat droplet Feret diameter at two weeks past manufacture are shown below (**Figure 75**, **Figure 76**, and **Figure 77**). The best CV calibration was achieved using the normalization pretreatment standard normal variate (SNV) and smoothing pretreatment Savitsky-Golay 9-points (sg9, **Figure 75**). This pretreatment reduces the noise level in spectra and is a zero-order derivative independent of the calibration wavelengths (Büchi, 2016). The wavenumber region used was 5,000-10,000 cm^{-1} (**Figure 76**). The peaks in the regression coefficient graph around 5400 and 7300 coincided with the wavenumbers known for the H₂O first overtone region and CH₃ second overtone region (Appendix **Figure 81**)(Brüker, 2009). The SECV graph indicated that 3 primary PCs and 2 secondary PCs were best to achieve minimal standard error (**Figure 76**).

The final calibration results shown in the three graphs of **Figure 77** show the good distribution of residuum values with four spectra excluded as outliers. The other two graphs show the predicted property vs original property for the calibration set and CV set, respectively. The calibration set r^2 was 0.3357, the CV r^2 was 0.0375, and the Büchi Q-value was 0.4175. Lastly, the standard error of calibration (SEC) showed we were able to determine the average Feret diameter of fat droplets within 4.15 μm and the standard error of cross-validation (SECV) was able to determine the average Feret diameter within 5.67 μm , given the mean number of fat droplets of 30.60 μm (**Table 23**).

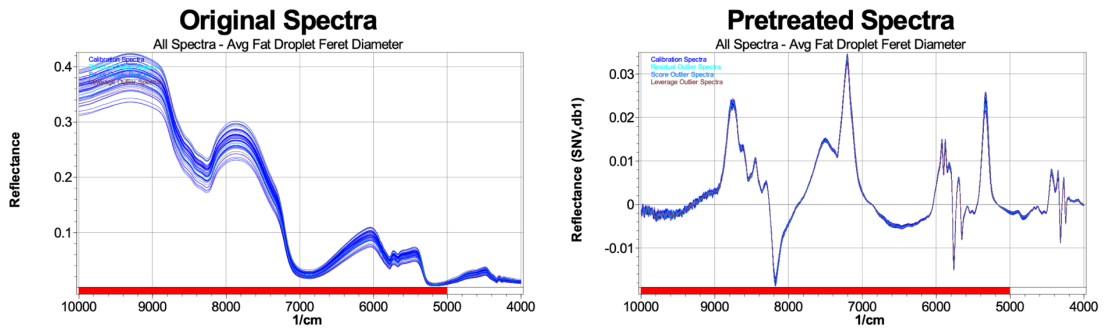


Figure 75. CLSM average fat droplet Feret diameter CV calibration original spectra (top) and pretreated spectra (bottom). Pretreated used include standard normal variate (SNV), followed by 1st BCAP 5 points (db1).6

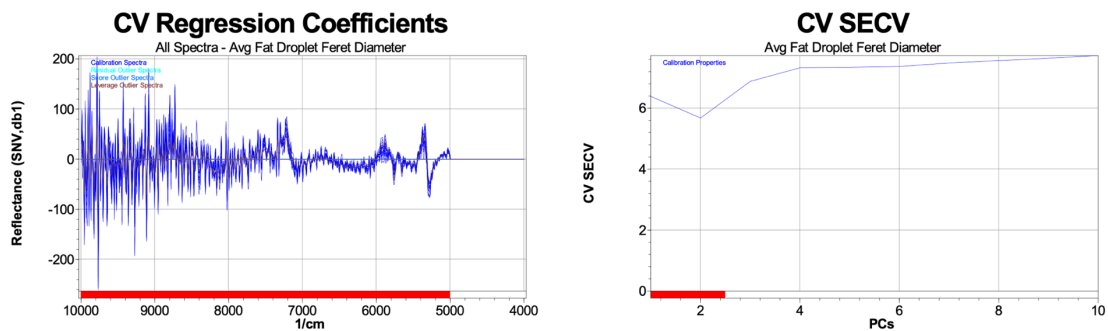
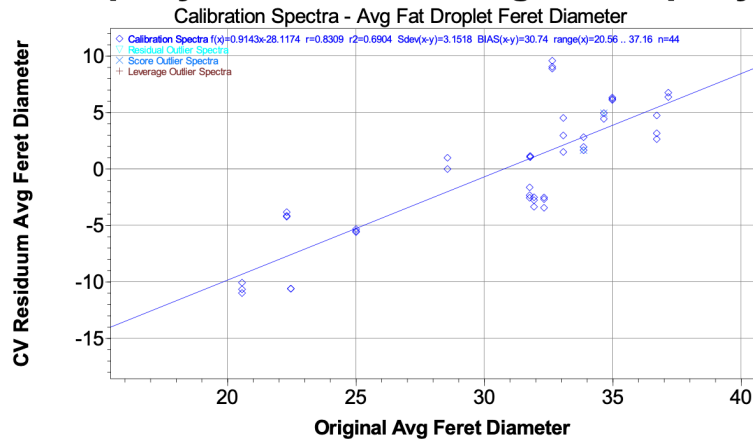
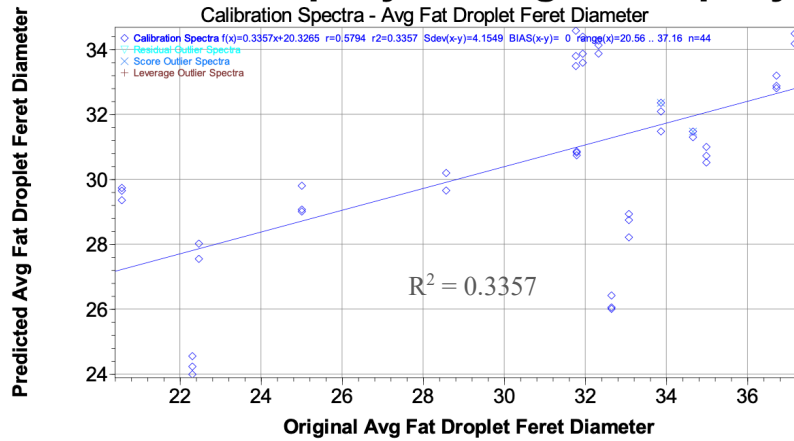


Figure 76. CLSM average fat droplet Feret diameter CV calibration regression coefficients (top) and standard error of cross-validation (SECV, bottom). Wavenumber region used for calibration was 5,000-10,000 cm^{-1} and 3 PCs used for primary PC selection.

CV Property Residuum vs. Original Property



Predicted Property vs. Original Property



Predicted Property vs Original Property

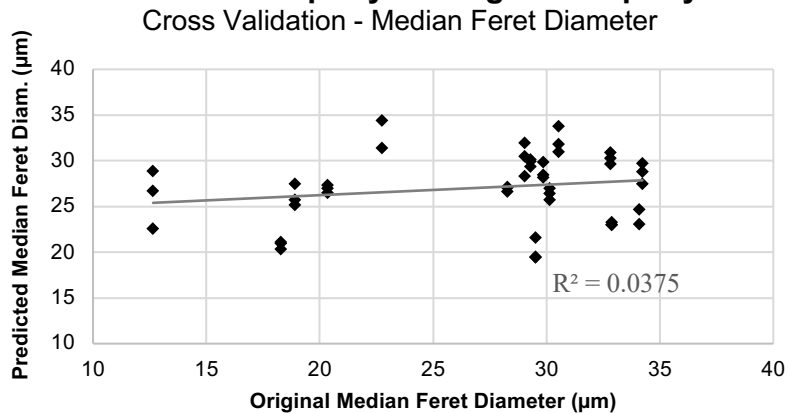


Figure 77. CLSM average fat droplet Feret diameter CV calibration property residuum vs. original property (top), predicted property vs. original property of calibration (middle), and predicted property vs original property of CV (bottom).

4.4.3.14 CLSM – Median Fat Droplet Diameter

The CV graphs for CLSM median fat droplet Feret diameter at two weeks past manufacture are shown below (**Figure 78**, **Figure 79**, and **Figure 80**). The best CV calibration was achieved using the normalization pretreatment standard normal variate (SNV) and smoothing pretreatment Savitsky-Golay 9-points (sg9, **Figure 78**). As previously described, this pretreatment reduces the noise level in spectra and is a zero-order derivative independent of the calibration wavelengths (Büchi, 2016). The wavenumber region used was 5,000-7,144 and 7404-10,000 cm^{-1} (**Figure 79**). The peaks in the regression coefficient graph around 4500, 5400, 6100, 7900, and 9000 cm^{-1} coincided with the wavenumbers known for the H_2O combinations and first overtone regions, CH first, second, and third overtone regions (Appendix **Figure 81**)(Brüker, 2009). The SECV graph indicated that 3 primary PCs and 2 secondary PCs were best to achieve minimal standard error (**Figure 79**).

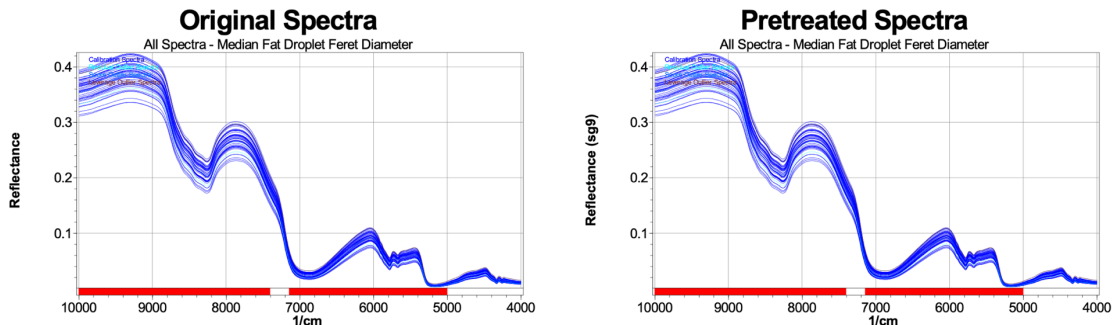


Figure 78. CLSM median fat droplet Feret diameter CV calibration original spectra (top) and pretreated spectra (bottom). Pretreatment used was Savitzky-Golay 9 points (sg9).

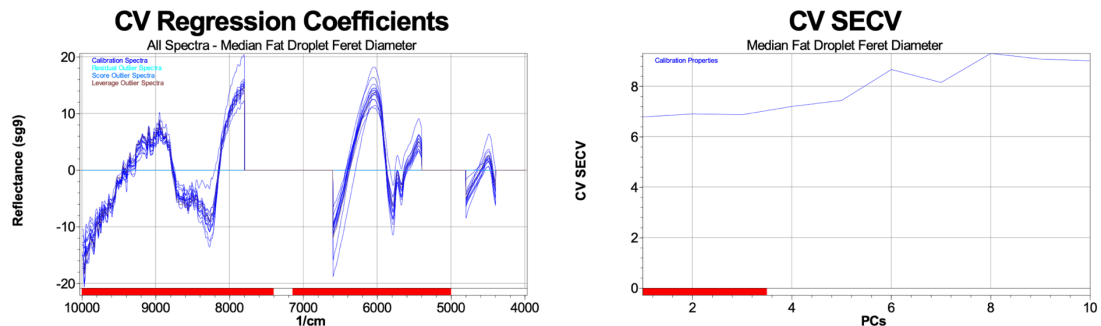
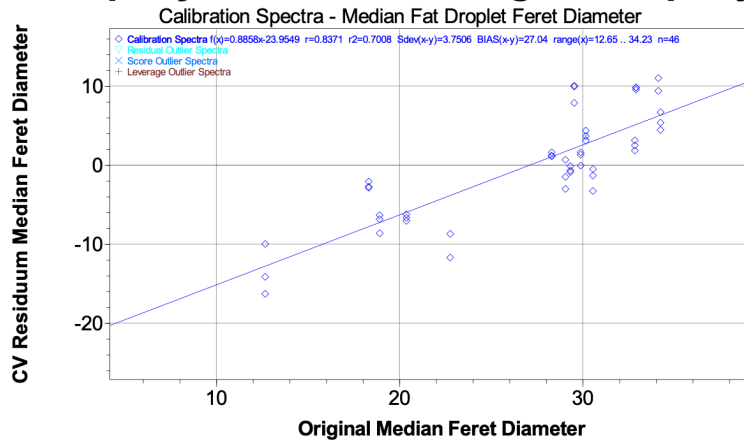
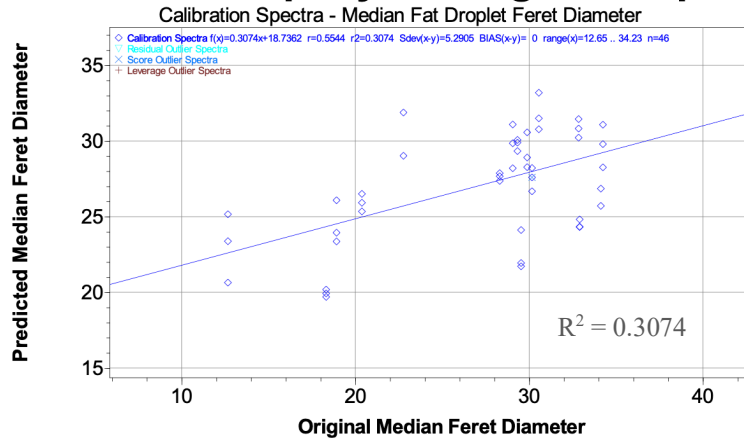


Figure 79. CLSM median fat droplet Feret diameter CV calibration regression coefficients (left) and standard error of cross-validation (SECV, right). Wavenumber region used for calibration was 5,000-7,144 and 7404-10,000 cm^{-1} and 3 PCs used for primary PC select

CV Property Residuum vs. Original Property



Predicted Property vs. Original Property



Predicted Property vs Original Property

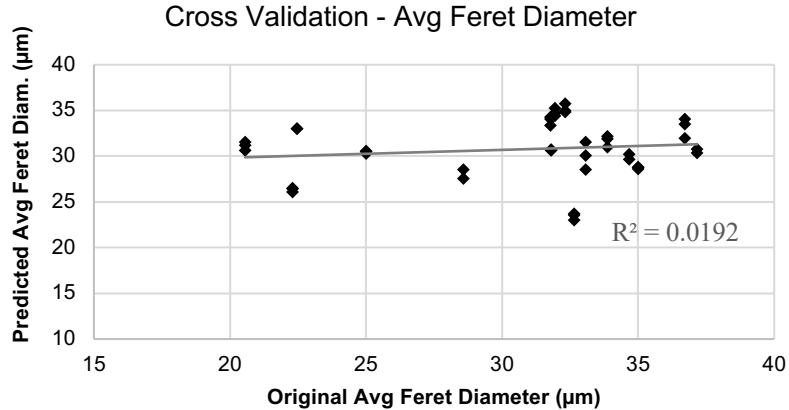


Figure 80. CLSM median fat droplet Feret diameter CV calibration property residuum vs. original property (top), predicted property vs. original property of calibration (middle), and predicted property vs original property of CV (bottom).

The final calibration results shown in the three graphs of **Figure 80** show the good distribution of residuum values with four spectra excluded as outliers. The other two graphs show the predicted property vs original property for the calibration set and CV set, respectively. The calibration set r^2 was 0.3074, the CV r^2 was 0.0192, and the Büchi Q-value was 0.3014. Lastly, the standard error of calibration (SEC) showed we were able to determine the median Feret diameter of fat droplets within 5.29 μm and the standard error of cross-validation (SECV) was able to determine the median Feret diameter within 6.88 μm , given the mean number of fat droplets of 27.05 μm (**Table 23**).

4.4.3.14 FT-NIR Calibrations Calibration Summary

Overall, the best calibrations were found for viscosity properties across both shelf life time points and melt area and firmness at the 2-week time points. One theory for potentially better calibrations for viscosity and melt area could be that the phase transitions demonstrated the protein interactions better than a method of constant temperature. In the viscosity method, hot liquid sauce was gradually cooled, and the melt method gradually heated the sample. Another theory to explain the improved calibrations in the 2-week shelf life than 4-week shelf life in melt area and firmness would be that wider results distributions were found at the earlier time point than the older. A wider range of property values is helpful for generating a predictive model.

4.5 Conclusion

PC produced on the Blentech at the pilot level with two levels of age, mixing speed, and hold times yielded differences in viscosity and firmness according to age, but not according to other factors or for melt area or fat droplet parameters. Despite limited differences in functional properties, FT-NIR spectroscopy of rapidly-cooled samples showed the potential to predict functional properties later in shelf life. The highest correlations were found for viscosity at 40°C (Time1) and 50°C (Time1), followed by other viscosity calibrations (**Table 23**). Melt area at both time points showed a lower correlation than viscosity but the lowest SEC and SECV values proportionally. CLSM and firmness calibrations yielded mediocre to poor results. Analyzing fat droplet structure in a more straightforward method than CLSM, such as NMR, would be suggested for

further research and calibration development. Other areas for improvement would include controlling for lactose and whey protein content and tracking pH throughout the PC shelf life more consistently. Most of all, more samples would be needed than the quantity used in this study to have a more reliable and robust calibration model.

CHAPTER 5: REFERENCES

Adams, M. J., K. Latham, N. W. Barnett, and A. J. Poynton. 1999. Calibration models for determining moisture and fat content of processed cheese using near-infrared spectrometry. *Journal of the Science of Food and Agriculture* 79(10):1232-1236.

Alexander, M. and M. Corredig. 2014. The use of advanced spectroscopic techniques to understand texture in dairy foods. Vol. 9780470672426.

Altan, A., M. Turhan, and S. Gunasekaran. 2005. Short Communication: Comparison of Covered and Uncovered Schreiber Test for Cheese Meltability Evaluation. *Journal of Dairy Science* 88(3):857-861.

Amamcharla, J. and L. Metzger. 2015. Prediction of process cheese instrumental texture and melting characteristics using dielectric spectroscopy and chemometrics. *Journal of Dairy Science* 98(9):6004-6013.

Arnott, D. R., H. A. Morris, and W. B. Combs. 1957. Effect of Certain Chemical Factors on the Melting Quality of Process Cheese. *Journal of Dairy Science* 40(8):957-963.

ASTM. Standard Definitions of Terms and Symbols Relating to Molecular Spectroscopy. Vol. ASTM Vol. 14.01.

Auty, M. A. E., M. Twomey, T. P. Guinee, and D. M. Mulvihill. 2001. Development and application of confocal scanning laser microscopy methods for studying the distribution of fat and protein in selected dairy products. *Journal of dairy research* 68(3):417-427.

Berger, W., H. Klostermeyer, K. Merkenich, and G. Uhlmann. 1989. *Processed Cheese Manufacture - A Joha Guide*. BK Ladenburg GmbH, Ladenburg.

Biswas, A., R. Kapoor, P. Upreti, L. Metzger, and K. Muthukumarappan. 2004. Influence of natural cheese characteristics on process cheese functionality: Dynamic viscoelastic properties. *Journal of Dairy Science* 87:234-234.

Biswas, A. C., K. Muthukumarappan, C. Marella, and L. E. Metzger. 2015. Understanding the role of natural cheese calcium and phosphorous content, residual lactose and salt - in - moisture content on block - type processed cheese functional properties: Cheese hardness and flowability/meltability. *International journal of dairy technology* 68(1):44-53.

Biswas, A. C., K. Muthukumarappan, and L. E. Metzger. 2008a. Dynamic Rheological Properties of Process Cheese: Effect of Ca and P Content, Residual Lactose, Salt-to-

Moisture Ratio and Cheese Temperature. *International journal of food properties* 11(2):282-295.

Biswas, A. C., K. Muthukumarappan, and L. E. Metzger. 2008b. Effect of Ca and P Content, Residual Lactose, and Salt-to-Moisture Ratio on the Model Parameters of Process Cheese Linear Viscoelastic Properties. *International journal of food properties* 11(3):530-543.

Blakemore, E. 2018. How the U.S. Ended Up With Warehouses Full of 'Government Cheese'. Vol. 2019. A&E Television Networks.

Blazquez, C., G. Downey, C. O'Donnell, D. O'Callaghan, and V. Howard. 2004. Prediction of moisture, fat and inorganic salts in processed cheese by near infrared reflectance spectroscopy and multivariate data analysis. *Journal of Near Infrared Spectroscopy* 12(3):149-157.

Bot, A., E. FlöTer, J. G. Lammers, and E. G. Pelan. 2007. 21 - The texture and microstructure of spreads. Pages 575-599. Elsevier Ltd.

Bowland, E. L. and E. A. Foegeding. 1999. Factors Determining Large-Strain (Fracture) Rheological Properties of Model Processed Cheese. *Journal of Dairy Science* 82(9):1851-1859.

Bowland, E. L. and E. A. Foegeding. 2001. Small Strain Oscillatory Shear and Microstructural Analyses of a Model Processed Cheese. *Journal of Dairy Science* 84(11):2372-2380.

Brakenhoff, G. J., H. T. van Der Voort, E. A. van Spronsen, and N. Nanninga. 1988. 3-dimensional imaging of biological structures by high resolution confocal scanning laser microscopy. *Scanning microscopy* 2(1):33-40.

Brandsma, R. 2019. Schreiber.

Brickley, C. A., S. Govindasamy-Lucey, J. J. Jaeggi, M. E. Johnson, P. L. H. McSweeney, and J. A. Lucey. 2008. Influence of Emulsifying Salts on the Textural Properties of Nonfat Process Cheese Made from Direct Acid Cheese Bases. *Journal of dairy science* 91(1):39-48.

Brown, M. 2020a. A Beginner's Guide to FIJI, Pt 1. University of Minnesota-Twin Cities, University Imaging Centers, Minneapolis, MN.

Brown, M. 2020b. A Beginner's Guide to FIJI, Pt 2. University of Minnesota-Twin Cities, University Imaging Centers, Minneapolis, MN.

- Brown, M. E. 2020c. FIJI in 3D: Three-Dimensional Image Processing, Analysis, and Visualization. University of Minnesota-Twin Cities, University Imaging Center, Minneapolis, MN.
- Bruker. 2015. Time-Domain NMR: Basic Principles and Real-World Applications. S. Jehle, ed, Bruker BioSpin.
- Bruker. 2016. Droplet Size Distribution in Food Emulsions. B. BioSpin, ed. Bruker BioSpin.
- Brüker. 2009. Guide for Infrared Spectroscopy. Bruker Optics, Billerica, MA, USA.
- Buning-Pfaue, H. 2003. Analysis of water in food by near infrared spectroscopy. *Food Chemistry* 82(1):107-115.
- Burns, D. A. and E. W. Ciureczak. 2008. Handbook of near-infrared analysis. 3rd ed. Practical spectroscopy. No. 35. CRC Press, Boca Raton, Fla.
- Büchi. 2013. NIRCal 5.5 Operation Manual.
- Büchi. 2016. NIRCal 5.6 Operation Manual. BÜCHI Labortechnik AG.
- Büchi. 2017. N-500 NIRFlex Operation Manual, Version B. Flawil, Switzerland.
- Callaghan, P. T., K. W. Jolley, and R. S. Humphrey. 1983. Diffusion of fat and water in cheese as studied by pulsed field gradient nuclear magnetic resonance. *Journal of colloid and interface science* 93(2):521-529.
- Caric, M., M. Gantar, and M. Kalab. 1985. Effects of emulsifying agents on the microstructure and other characteristics of process cheese - A Review. *Food Microstructure* 4(2):297-312.
- Carter, S. J. Z. 2013. F.U.T.W. in *Magna Carta Holy Grail*. The Island Def Jam Music Group, New York City, NY.
- Caríc, M. and M. Kaláb. 1993. Processed Cheese Products. Pages 467-505 in *Cheese: Chemistry, Physics, and Microbiology*. F. P.F., ed. Springer, Boston, MA.
- Case, R. A., R. L. Bradley Jr., and R. R. Williams. 1985. Chemical and physical methods. Pages 327-404 in *Standard methods for the examination of dairy products*. 15th ed. G. H. Richardson, ed. American Public Health Association, Washington D.C., U.S.A.

Case, R. A., R. L. Bradley Jr., and R. R. Williams. 2004. Chemical and physical methods. in Standard methods for the examination of dairy products. 17th ed. M. H. Wehr and J. F. Frank, ed. Washington etc. : American Public Health Association, Washington [etc.].

Cernikova, M., F. Bunka, M. Pospiech, B. Tremlova, K. Hladka, V. Pavlinek, and P. Brezina. 2010. Replacement of traditional emulsifying salts by selected hydrocolloids in processed cheese production. *International Dairy Journal* 20(5):336-343.

Cernikova, M., J. Nebesarova, R. Salek, R. Popkova, and F. Bunka. 2018. The effect of rework content addition on the microstructure and viscoelastic properties of processed cheese. *Journal of Dairy Science* 101(4):2956-2962.

Cernikova, M., R. Salek, D. Kozackova, H. Behalova, L. Lunakova, and F. Bunka. 2017. The effect of selected processing parameters on viscoelastic properties of model processed cheese spreads. *International Dairy Journal* 66:84-90.

Chalmers, J. M., H. G. M. Edwards, and M. D. Hargreaves. 2012. *Vibrational Spectroscopy Techniques: Basics and Instrumentation*. Pages 9-44. Chichester, UK: John Wiley & Sons, Ltd, Chichester, UK.

Cheese, US. October 2019.

Chen, L. and H. Liu. 2012. Effect of emulsifying salts on the physicochemical properties of processed cheese made from Mozzarella. *Journal of Dairy Science* 95(9):4823-4830.

Creamer, L. K. and A. K. H. MacGibbon. 1996. Some recent advances in the basic chemistry of milk proteins and lipids. Pages 539-568. Vol. 6.

Curda, L. and O. Kukackova. 2004. NIR spectroscopy: a useful tool for rapid monitoring of processed cheeses manufacture. *Journal of Food Engineering* 61(4):557-560.

Dalgleish, D. G. 1997. Structure-function relationship of caseins. Pages 199-223 in *Food proteins and their applications*. S. Damodaran and A. Paraf. M. Dekker, ed. New York : Marcel Dekker, New York.

Deublein, E. J., G. J. W. Goudappel, J. P. M. van Duynhoven, and H. Todt. 2015. *Fast Droplet Size Determination in Food Emulsions by Time Domain-NMR*. Unilever & Bruker.

Dewey, C. 2018. America's cheese stockpile just hit an all-time high. *The Washington Post*.

Donnelly, C. W. 2016. The Oxford companion to cheese. Oxford University Press, New York, NY.

Dufour, E., G. Mazerolles, M. F. Devaux, G. Duboz, M. H. Duployer, and N. Mouhous Riou. 2000. Phase transition of triglycerides during semi-hard cheese ripening. *International dairy journal* 10(1-2):81-93.

Dufour, E. and A. Riaublanc. 1997. Potentiality of spectroscopic methods for the characterisation of dairy products. I. Front-face fluorescence study of raw, heated and homogenised milks. *Lait* 77(6):657-670.

Dürrenberger, M. B., S. Handschin, B. Conde-Petit, and F. Escher. 2001. Visualization of Food Structure by Confocal Laser Scanning Microscopy (CLSM). *LWT - Food Science and Technology* 34(1):11-17.

Everard, C. D., C. P. O'Donnell, C. C. Fagan, E. M. Sheehan, C. M. Delahunty, and D. J. O'Callaghan. 2005. Correlation Between Process Cheese Meltability Determined by Sensory Analysis, Computer Vision Method and Olson and Price Test. *International Journal of Food Properties* 8(2):267-275.

Everett, D. W., K. Ding, N. F. Olson, and S. Gunasekaran. 1995. Applications of confocal microscopy to fat globule structure in cheese. *Advances in Experimental Medicine and Biology* 367:321-330.

Fagan, C. C., C. Everard, C. P. O'Donnell, G. Downey, and D. J. O'Callaghan. 2005. Prediction of inorganic salt and moisture content of process cheese using dielectric spectroscopy. *International Journal of Food Properties* 8(3):543-557.

Fagan, C. C., C. Everard, C. P. O'Donnell, G. Downey, E. M. Sheehan, C. M. Delahunty, and D. J. O'Callaghan. 2007a. Evaluating Mid-infrared Spectroscopy as a New Technique for Predicting Sensory Texture Attributes of Processed Cheese. *Journal of dairy science* 90(3):1122-1132.

Fagan, C. C., C. Everard, C. P. O'Donnell, G. Downey, E. M. Sheehan, C. M. Delahunty, D. J. O'Callaghan, and V. Howard. 2007b. Prediction of processed cheese instrumental texture and meltability by mid-infrared spectroscopy coupled with chemometric tools. *Journal of food engineering* 80(4):1068-1077.

FDA. 2009. US Code of Federal Regulations. in Title 21, Volume 2. Vol. 21 CFR. U. N. A. a. R. Administration, ed. Dept. of Health and Human Services, Washington, D.C.

FDA. 2016. Cheese and Related Cheese Products. in 133.113 Cheddar Cheese. U. S. F. a. D. Administration, ed, Code of Federal Regulations.

FDA. 2018. 21 CFR, Part 133.169 to 133.180. U. S. F. a. D. Administration, ed. Department of Health and Human Services, Washington, D.C.

Feinberg, M. 1990. Multivariate calibration, by H. Martens and T. Naes. *TrAC, Trends in analytical chemistry (Regular ed.)* 9(8):VIII.

Fenelon, M. A. and T. P. Guinee. 2000. Primary proteolysis and textural changes during ripening in Cheddar cheeses manufactured to different fat contents. *International Dairy Journal* 10(3):151-158.

Fox, P. F., T. P. Guinee, T. M. Cogan, and P. L. H. McSweeney. 2017. *Fundamentals of Cheese Science*. 2nd ed. 2017 ed. Boston, MA: Springer US, Boston, MA.

Frankhuizen, R. 2008. NIR Analysis of Dairy Products. in *Handbook of Near-infrared Analysis*. Vol. 35. 3rd ed. D. A. Burns and E. W. Ciurczak, ed. CRC Press, Boca Raton, FL.

Gallier, S., K. C. Gordon, R. Jiménez-Flores, and D. W. Everett. 2011. Composition of bovine milk fat globules by confocal Raman microscopy. *International dairy journal* 21(6):402-412.

Garimella Purna, S., A. Pollard, and L. Metzger. 2006. Effect of formulation and manufacturing parameters on process cheese food functionality - I. Trisodium citrate. *Journal of Dairy Science* 89(7):2386-2396.

Garimella Purna, S. K., L. A. Prow, and L. E. Metzger. 2005. Utilization of Front-Face Fluorescence Spectroscopy for Analysis of Process Cheese Functionality. *Journal of dairy science* 88(2):470-477.

Glass, K. and M. Ellin Doyle. 2013. *Safety of Processed Cheese: A Review of the Scientific Literature*. University of Wisconsin - Food Research Institute.

Glenn, T. A., C. R. Daubert, B. E. Farkas, and L. A. Stefanski. 2003. A statistical analysis of creaming variables impacting process cheese melt quality. *Journal of Food Quality* 26(4):299-321.

Goudappel, G. J. W., J. P. M. van Duynhoven, and M. M. W. Mooren. 2001. Measurement of Oil Droplet Size Distributions in Food Oil/Water Emulsions by Time Domain Pulsed Field Gradient NMR. *Journal of colloid and interface science* 239(2):535-542.

- Guinee, T. P., M. A. E. Auty, and M. A. Fenelon. 2000. The effect of fat content on the rheology, microstructure and heat-induced functional characteristics of Cheddar cheese. *International Dairy Journal* 10(4):277-288.
- Guinee, T. P., M. Caric, and M. Kalab. 2004. Pasteurized processed cheese and substitute/imitation cheese products. *Cheese: chemistry, physics and microbiology* 2(Major cheese groups).
- Gupta, S., C. Karahadian, and R. Lindsay. 1984. Effect of emulsifier salts on textural and flavor properties of processed cheese. *Journal of Dairy Science* 67(4):764-778.
- Hassan, A. N., S. Awad, and V. V. Mistry. 2007. Reduced Fat Process Cheese Made from Young Reduced Fat Cheddar Cheese Manufactured with Exopolysaccharide-Producing Cultures. *Journal of Dairy Science* 90(8):3604-3612.
- Henderson, A. 2012. *The Influence of Intact Casein on Process Cheese*. Goldpeg International, Moorabbin, Australia.
- Herbert, S., N. Mouhous Riou, M. F. o. Devaux, A. Riaublanc, B. Bouchet, D. J. Gallant, and r. Dufour. 2000. Monitoring the identity and the structure of soft cheeses by fluorescence spectroscopy. *Lait* 80(6):621-634.
- Hibbs, A. R. 2004. *Confocal Microscopy for Biologists*. Boston, MA: Springer US, Boston, MA.
- Hirtzer, M., M. Weinraub, T. Watsr, and K. Plume. 2018. USDA's \$12 Billion Farmer Relief Package. in *Reuters Markets Newswire*. Thomson Reuters.
- Horne, D. S. 1998. Casein Interactions: Casting Light on the Black Boxes, the Structure in Dairy Products. *International Dairy Journal* 8(3):171-177.
- Huc, D., F. Mariette, S. Challos, J. Barreau, G. Moulin, and C. Michon. 2013a. Multi-scale investigation of eyes in semi-hard cheese. *Innovative Food Science and Emerging Technologies* 24:106-112.
- Huc, D., G. Moulin, F. Mariette, and C. Michon. 2013b. Investigation of curd grains in Swiss-type cheese using light and confocal laser scanning microscopy. *International Dairy Journal* 33(1):10-15.
- Imoto, E. M., C. H. Lee, and C. Rha. 1979. EFFECT OF COMPRESSION RATIO ON THE MECHANICAL PROPERTIES OF CHEESE. *Journal of food science* 44(2):343-345.

ISO 17996. 2006. in Determination of rheological properties by uniaxial compression at constant displacement rate. International Organization for Standardization.

Johns, M. L. and K. G. Hollingsworth. 2007. Characterisation of emulsion systems using NMR and MRI. *Progress in nuclear magnetic resonance spectroscopy* 50(2-3):51-70.

Joshi, N., R. Jhala, K. Muthukumarappan, M. Acharya, and V. Mistry. 2004. Textural and rheological properties of processed cheese. *International Journal of Food Properties* 7(3):519-530.

Kalab, M., J. Yun, and S. Yiu. 1987. Textural Properties and Microstructure of Process Cheese Food Rework. *Food Microstructure* 6(2):181-192.

Kapoor, R., P. Lehtola, and L. E. Metzger. 2004. Comparison of Pilot-Scale and Rapid Visco Analyzer Process Cheese Manufacture. *Journal of dairy science* 87(9):2813-2821.

Kapoor, R. and L. Metzger. 2005. Small-scale manufacture of process cheese using a rapid visco analyzer. *Journal of Dairy Science* 88(10):3382-3391.

Kapoor, R. and L. Metzger. 2008. Process cheese: Scientific and technological aspects - A review. *Comprehensive Reviews in Food Science and Food Safety* 7(1):194-214.

Kapoor, R., L. E. Metzger, A. C. Biswas, and K. Muthukumarappan. 2007. Effect of natural cheese characteristics on process cheese properties. *Journal of Dairy Science* 90(4):1625-1634.

Karoui, R., A. Laguet, and r. Dufour. 2003. Fluorescence spectroscopy: A tool for the investigation of cheese melting - Correlation with rheological characteristics. *Lait* 83(3):251-264.

Karoui, R., A. Mouazen, É. Dufour, L. Pillonel, E. Schaller, D. Picque, J. Baerdemaeker, and J.-O. Bosset. 2006. A comparison and joint use of NIR and MIR spectroscopic methods for the determination of some parameters in European Emmental cheese. *European Food Research and Technology* 223(1):44-50.

Kokawa, M., S. Ikegami, A. Chiba, H. Koishihara, V. Trivittayasil, M. Tsuta, K. Fujita, and J. Sugiyama. 2015. Measuring Cheese Maturation with the Fluorescence Fingerprint. *Food Science and Technology Research* 21(4):549.

Kosikowski, F. 1982. *Cheese and fermented milk foods*. 2nd ed., 3rd print. with revisions.. ed. Brooktondale, N.Y. : F.V. Kosikowski and Associates, Brooktondale, N.Y. Brooktondale, N. Y.

- Kulmyrzaev, A. A., D. Leveux, and É. Dufour. 2005. Front-Face Fluorescence Spectroscopy Allows the Characterization of Mild Heat Treatments Applied to Milk. Relations with the Denaturation of Milk Proteins. *Journal of agricultural and food chemistry* 53(3):502-507.
- Kumar, N., A. Bansal, G. S. Sarma, and R. K. Rawal. 2014. Chemometrics tools used in analytical chemistry: An overview. *Talanta (Oxford)* 123:186-199.
- Lee, C., E. M. Imoto, and C. Rha. 1978. Evaluation of Cheese Texture. *Journal of food science* 43(5):1600-1605.
- Lee, S., R. Buwalda, S. Euston, E. Foegeding, and A. McKenna. 2003a. Changes in the rheology and microstructure of processed cheese during cooking. *Lebensmittel-Wissenschaft Und-Technologie-Food Science and Technology* 36(3):339-345.
- Lee, S. K., R. J. Buwalda, S. R. Euston, E. A. Foegeding, and A. B. McKenna. 2003b. Changes in the rheology and microstructure of processed cheese during cooking. *Lebensmittel-Wissenschaft Und-Technologie-Food Science and Technology* 36(3):339-345.
- Li-Chan, E. C. Y. 1996. The applications of Raman spectroscopy in food science. *Trends in food science & technology* 7(11):361-370.
- Lichtman, J. 1994. Confocal microscopy. *Scientific American* 271(2):40-45.
- Lopez, C. 2005. Focus on the supramolecular structure of milk fat in dairy products. *Reproduction Nutrition Development* 45(4):497-511.
- Lopez, C., C. Bourgaux, P. Lesieur, S. Bernadou, G. Keller, and M. Ollivon. 2002. Thermal and Structural Behavior of Milk Fat: 3. Influence of Cooling Rate and Droplet Size on Cream Crystallization. *Journal of colloid and interface science* 254(1):64-78.
- Lopez, C. and V. Briard-Bion. 2007. The composition, supramolecular organisation and thermal properties of milk fat: a new challenge for the quality of food products. *Le Lait* 87(4-5):317-336.
- Lopez, C., V. Briard-Bion, B. Camier, and J. Y. Gassi. 2006. Milk Fat Thermal Properties and Solid Fat Content in Emmental Cheese: A Differential Scanning Calorimetry Study. *Journal of dairy science* 89(8):2894-2910.
- Lu, Y., N. Shirashoji, and J. A. Lucey. 2007. Rheological, textural and melting properties of commercial samples of some of the different types of pasteurized processed cheese. *International journal of dairy technology* 60(2):74-80.

- López, A., S. Arazuri, I. García, J. Mangado, and C. Jarén. 2013. A Review of the Application of Near-Infrared Spectroscopy for the Analysis of Potatoes. *Journal of agricultural and food chemistry* 61(23):5413-5424.
- M2-Presswire. 2015. Cheese Ingredients Market by Cheese Type, Ingredients & Geography - Global Trends & Forecast to 2020. Coventry.
- Ma, Y. B., K. S. Babu, and J. K. Amamcharla. 2019. Prediction of total protein and intact casein in cheddar cheese using a low-cost handheld short-wave near-infrared spectrometer. *LWT* 109:319-326.
- Mansfield, J. R., C. Hoyt, and R. M. Levenson. 2008. Visualization of Microscopy - Based Spectral Imaging Data from Multi - Label Tissue Sections. *Current Protocols in Molecular Biology* 84(1):14.19.11-14.19.15.
- Mark, H. 2008. Chapter 8: Data Analysis: Multilinear Regression and Principal Component Analysis. in *Handbook of near-infrared analysis*. 3rd ed.. ed. D. A. Burns and E. W. Ciurczak, ed. Boca Raton : CRC Press, Boca Raton.
- Marqués, G. 2020. Spectral Acquisition and Linear Unmixing. in *The Coronavirus Seminar Series*. University of Minnesota-Twin Cities University Imaging Centers, Dept. of Neuroscience, Minnesota.
- Mazerolles, G. r., M.-F. o. Devaux, G. Duboz, M.-H. l. n. Duployer, N. Mouhous Riou, and r. Dufour. 2001. Infrared and fluorescence spectroscopy for monitoring protein structure and interaction changes during cheese ripening. *Lait* 81(4):509-527.
- McKenna, D. 2001. Measuring moisture in cheese by near infrared absorption spectroscopy. *Journal of AOAC International* 84(2):623-628.
- McSweeney, P. and P. Fox. 1997. Chemical methods for the characterization of proteolysis in cheese during ripening. *Le Lait* 77(1):41-76.
- Metzger, L. E., R. Kapoor, L. A. Rosenberg, and P. Upreti. 2002. RVA: Process cheese manufacture. *Australian journal of dairy technology* 57(2):136.
- Meyer, A. 1973. *Processed Cheese Manufacture*. Food Trade Press Ltd. , London, U.K.
- Mounsey, J. S. and E. D. O'Riordan. 1999. Empirical and Dynamic Rheological Data Correlation to Characterize Melt Characteristics of Imitation Cheese. *Journal of food science* 64(4):701-703.

- Nelson, S. O. 2005. Dielectric spectroscopy in agriculture. *Journal of non-crystalline solids* 351(33-36):2940-2944.
- Norris, K. 2009. Hazards with near Infrared Spectroscopy in Detecting Contamination. Pages 165-166. Vol. 17. *Journal of Near Infrared Spectroscopy*.
- Oliveira, K. D., L. D. Callegaro, R. Stephani, M. R. Almeida, and L. F. C. de Oliveira. 2016. Analysis of spreadable cheese by Raman spectroscopy and chemometric tools. *Food Chemistry* 194:441-446.
- Olson, N. F. and W. V. Price. 1958. A Melting Test for Pasteurized Process Cheese Spreads. *Journal of dairy science* 41(7):999-1000.
- Packer, K. J. and C. Rees. 1972. Pulsed NMR studies of restricted diffusion. I. Droplet size distributions in emulsions. *Journal of colloid and interface science* 40(2):206-218.
- Park, J., J. R. Rosenau, and M. Peleg. 1984. Comparison of Four Procedures of Cheese Meltability Evaluation. *Journal of Food Science* 49(4):1158-1170.
- Pasquini, C. 2018. Near infrared spectroscopy: A mature analytical technique with new perspectives – A review. *Analytica Chimica Acta* 1026:8-36.
- Pereira, R., R. Bennett, Y. Hemar, and O. Campanella. 2001. Rheological and microstructural characteristics of model processed cheese analogues. *Journal of Texture Studies* 32(5-6):349-373.
- Perten Instruments Application Note: RVA Method 30.04. Perten Instruments.
- Phatak, A. and S. De Jong. 1997. The geometry of partial least squares. *Journal of chemometrics* 11(4):311-338.
- Piska, I. and J. Stetina. 2004. Influence of cheese ripening and rate of cooling of the processed cheese mixture on rheological properties of processed cheese. *Journal of Food Engineering* 61(4):551-555.
- Price, W. V. and M. G. Bush. 1974. The process cheese industry in the United States: A review. *Journal of Milk Food Technology* 37(3):135-152.
- Prow, L. A. and L. E. Metzger. 2005. Melt Analysis of Process Cheese Spread or Product Using a Rapid Visco Analyzer. *Journal of dairy science* 88(4):1277-1287.

Roeffaers, M. B. J., X. Zhang, C. W. Freudiger, B. G. Saar, X. S. Xie, M. van Ruijven, G. van Dalen, and C. Xiao. 2011. Label-free imaging of biomolecules in food products using stimulated Raman microscopy. *Journal of Biomedical Optics* 16(2):021118-021118.

Roots, T. 1999. *Double Trouble*. in *Things Fall Apart*. MCA Records, Electric Lady Studios.

Sadlikova, I., F. Bunka, P. Budinsky, V. Barbora, V. Pavlinek, and I. Hoza. 2010. The effect of selected phosphate emulsifying salts on viscoelastic properties of processed cheese. *Lwt-Food Science and Technology* 43(8):1220-1225.

Salek, R., M. Cernikova, S. Maderova, L. Lapcik, and F. Bunka. 2016. The effect of different composition of ternary mixtures of emulsifying salts on the consistency of processed cheese spreads manufactured from Swiss-type cheese with different degrees of maturity. *Journal of Dairy Science* 99(5):3274-3287.

Samples, D. R., R. L. Richter, and C. W. Dill. 1984. Measuring Proteolysis in Cheddar Cheese Slurries: Comparison of Hull and Trinitrobenzene Sulfonic Acid Procedures¹. *Journal of Dairy Science* 67(1):60-63.

Schamberger, G. P. and T. P. Labuza. 2006. Evaluation of Front - face Fluorescence for Assessing Thermal Processing of Milk. *Journal of food science* 71(2):C69-C74.

Shimp, L. A. 1985. *Process Cheese Principles*. *Food Technology* 39(5):63-70.

Shirashoji, N., J. Jaeggi, and J. Lucey. 2006. Effect of trisodium citrate concentration and cooking time on the physicochemical properties of pasteurized process cheese. *Journal of Dairy Science* 89(1):15-28.

Skierucha, W., A. Wilczek, and A. Szyłowska. 2012. Dielectric spectroscopy in agrophysics. *International Agrophysics* 26(2):187-197.

Smith, G., S. Holroyd, D. Reid, and K. Gordon. 2017. Raman imaging processed cheese and its components. *Journal of Raman Spectroscopy* 48(3):374-383.

Sommer, D. 2016. Big isn't always easy - Issues to consider when manufacturing 640 pound blocks of cheese. Pages 4-5 in *Dairy Pipeline*. Vol. 28. 2 ed. Wisconsin Center for Dairy Research, Madison, WI.

Sowoidnich, K. and H.-D. Kronfeldt. 2016. Shifted excitation Raman difference spectroscopy for authentication of cheese and cheese analogues. Pages 98871Z-98871Z-98878. Vol. 9887. SPIE.

Strasburg, G. M. and R. D. Ludescher. 1995. Theory and applications of fluorescence spectroscopy in food research. *Trends in Food Science & Technology* 6(3):69-75.

Subramanian, A. and L. Rodriguez-Saona. 2009. Fourier Transform Infrared (FTIR) Spectroscopy. Pages 146-173 in *Infrared Spectroscopy for Food Quality Analysis and Control*. D.-W. Sun, ed. Academic Press, San Diego, CA.

Subramanian, R., K. Muthukumarappan, and S. Gunasekaran. 2006. Linear Viscoelastic Properties of Regular- and Reduced-Fat Pasteurized Process Cheese During Heating and Cooling. *International Journal of Food Properties* 9(3):377-393.

Swaisgood, H. E. 1996. Characteristics of Milk. in *Food Chemistry*. 3rd ed. O. R. Fennema, ed. Marcel Dekker, New York.

Swenson, B. J., W. L. Wendorff, and R. C. Lindsay. 2000. Effects of Ingredients on the Functionality of Fat - free Process Cheese Spreads. *Journal of food science* 65(5):822-825.

Tamime, A. Y. 2011. Processed cheese and analogues. Society of Dairy Technology series. Wiley-Blackwell, Chichester, West Sussex, U.K.

Tanaka, N., J. M. Goepfert, E. Traisman, and W. M. Hoffbeck. 1979. A Challenge of Pasteurized Process Cheese Spread with *Clostridium botulinum* spores. *Journal of food protection* 42(10):787.

Tanaka, N., E. Traisman, P. Platinga, L. Finn, W. Flom, L. Meske, and J. Guggisberg. 1986. Evaluation of factors involved in antibotulinal properties of pasteurized process cheese spreads. *Journal of Food Protection* 49(7):526-531.

Templeton, H. L. and H. H. Sommer. 1930. Some observations on processed cheese. *Journal of Dairy Science* 13:203-220.

Templeton, H. L. and H. H. Sommer. 1936. Studies on emulsifying salts used in process cheese. *Journal of Dairy Science* 19.

Thapa, T. B. and V. K. Gupta. 1992. Rheology of processed cheese foods prepared with added whey protein concentrates. *Indian Journal of Dairy Science* (45):88-92.

Thompson, J. J. 2016. Effects of Cheese Age on Viscosity of Sauces Made from Process Cheese Loaves and Comparison of Methods Used to Measure Sauce Viscosity. in *Food Science and Nutrition*. University of Minnesota.

- Trivedi, D., R. J. Bennett, Y. Hemar, D. C. W. Reid, S. K. Lee, and D. Illingworth. 2008. Effect of different starches on rheological and microstructural properties of (I) model processed cheese. *International journal of food science & technology* 43(12):2191-2196.
- Tunick, M. H. 2000. Rheology of Dairy Foods that Gel, Stretch, and Fracture. *Journal of dairy science* 83(8):1892-1898.
- Tunick, M. H. 2014. Process Cheeses and Nutrition. in *Science of Cheese*. Oxford University Press, Inc., New York, NY.
- Tunick, M. H., E. J. Nolan, J. J. Shieh, J. J. Basch, M. P. Thompson, B. E. Maleeff, and V. H. Holsinger. 1990. Cheddar and Cheshire Cheese Rheology. *Journal of Dairy Science* 73(7):1671-1675.
- Valm, A. M., R. Oldenbourg, and G. G. Borisy. 2016. Multiplexed Spectral Imaging of 120 Different Fluorescent Labels.(Research Article)(Report). *PLoS ONE* 11(7):e0158495.
- Van Dalen, G. 2002. Determination of the water droplet size distribution of fat spreads using confocal scanning laser microscopy. *Journal Of Microscopy-Oxford* 208:116-133.
- van Duynhoven, J., A. Voda, M. Witek, and H. Van As. 2010. Time-Domain NMR Applied to Food Products. *Annual Reports on NMR Spectroscopy* 69:145-197.
- Van Duynhoven, J. P. M., G. J. W. Goudappel, G. Van Dalen, P. C. Van Bruggen, J. C. G. Blonk, and A. P. A. M. Eijkelenboom. 2002. Scope of droplet size measurements in food emulsions by pulsed field gradient NMR at low field. *Magnetic Resonance in Chemistry* 40(13):S51-S59.
- Van Lent, K., B. Vanlerberghe, P. Van Oostveldt, O. Thas, and P. Van Der Meeren. 2008. Determination of water droplet size distribution in butter: Pulsed field gradient NMR in comparison with confocal scanning laser microscopy. *International Dairy Journal* 18(1):12-22.
- Vazquez, L. 2019. Development of Fourier Transform near Infrared Spectroscopy Methods for the Rapid Quantification of Starch and Cellulose in Mozzarella and Other Italian-Type Cheeses. Page 221 in *ProQuest Dissertations and Theses*. University of Minnesota, Ann Arbor.
- Walstra, P. 2006. *Dairy science and technology*. 2nd ed.. ed. Boca Raton : Taylor & Francis, Boca Raton.

Wang, H.-H. and D.-W. Sun. 2002. Melting characteristics of cheese: analysis of effect of cheese dimensions using computer vision techniques. *Journal of food engineering* 52(3):279-284.

Wiles, P. G., I. K. Gray, R. C. Kissling, C. Delahanty, J. Evers, K. Greenwood, K. Grimshaw, M. Hibbert, K. Kelly, H. Luckin, K. McGregor, A. Morris, M. Petersen, F. Ross, and M. Valli. 1998. Routine Analysis of Proteins by Kjeldahl and Dumas Methods: Review and Interlaboratory Study Using Dairy Products. *Journal of AOAC International* 81(3):620-632.

WITec. Food Analysis with Confocal Raman Microscopy. WITec, GmbH, Germany.

Wold, J. P., K. Jørgensen, and F. Lundby. 2002. Nondestructive Measurement of Light-induced Oxidation in Dairy Products by Fluorescence Spectroscopy and Imaging. *Journal of dairy science* 85(7):1693-1704.

Woodcock, T., C. C. Fagan, C. P. O'Donnell, and G. Downey. 2008. Application of Near and Mid-Infrared Spectroscopy to Determine Cheese Quality and Authenticity. *Food and Bioprocess Technology* 1(2):117-129.

Workman, J. J. 2001. NIR Spectroscopy Calibration Basics. Pages 123-149 in *Handbook of Near-Infrared Analysis*. 3rd Ed. ed. D. A. Burns and E. W. Ciurczak, ed. CRC Press, New York, NY.

Zaïdi, F., H. Rouissi, S. Dridi, M. Kammoun, J. De Baerdemaeker, and R. Karoui. 2007. Front-Face Fluorescence Spectroscopy as a Rapid and Non-Destructive Tool for Differentiating Between Sicilo-Sarde and Comisana Ewe's Milk During Lactation Period: A Preliminary Study. *Food and bioprocess technology* 1(2):143-151.

Zehren, V. L. and D. D. Nusbaum. 1992. *Processed Cheese*. 1st ed. Cheese Reporter Publishing Co. Inc., Madison, WI.

Zhong, Q. 2003. Cooling effects on the functionality and microstructure of processed cheese. ProQuest Dissertations Publishing.

Zhong, Q., C. Daubert, and B. Farkas. 2004. Cooling effects on processed cheese functionality. *Journal of Food Process Engineering* 27(5):392-412.

Zimmermann, T., J. Marrison, K. Hogg, and P. O'Toole. 2014. Clearing Up the Signal: Spectral Imaging and Linear Unmixing in Fluorescence Microscopy. Pages 129-148 in *Confocal Microscopy: Methods and Protocols*. S. W. Paddock, ed. Springer New York, New York, NY.

Zumbusch, A. 2017. Quantification Of Flow Aids In Shredded Cheese Blends Using Enzymatic Starch Analysis And Fourier Transform Near-Infrared Spectroscopy.

CHAPTER 6: APPENDIX

6.1 Functional Analysis Method SOPs

6.1.1 MVAG Viscosity Analysis

Adapted from the Jason Thompson's thesis (2016).

Updated 10-1-2020

I. Cheese sauce prep

Prepare cheese sauces by mixing 50g of 48% moisture process cheese samples with 10g of water. Once mixed with water, use a metal spatula to break process cheese into small pieces (1-2 cm chunks) until ready to test. Immediately before testing each sample, heat in a 1300W microwave for 30 seconds and stir until smooth using a fork (10-15 seconds) with a final temp of 50 C. Pour immediately into MVAG cup and begin method

Final cheese sauce temp: approximately 50°C

II. MVAG method

Add full amount of cheese sauce (~60g) from sauce container into MVAG test cylinder. Measurement begins once sample reaches 50C, hold at 50C for 2 min, and cool to 35C over 10 min. Analyze samples by averaging each sample's viscosity (cP) when it reaches 40°C, 45°C, and 50°C. (original unit is torque in mPas, but it's a 1:1 conversion from mPas to cP)

6.1.2 Schreiber Oven Melt Method

Adapted from Muthukumarappan, Wang, & Gunaskeran (1999)

I. Cutting samples

Cut a square block of process cheese out of the tray or block. Use a wire butter slicer to slice the block into 7 mm thick slices (Figure 1). Use the cylinder cutter to cut the slices into circle disks with diameter 33.45 mm (Figure 1). If not testing the samples on the same day, store the disks on a cutting board covered in plastic wrap to prevent drying out. Allow the samples to equilibrate to room temperature 1 hour before analysis.

II. Melting samples

Preheat the forced air oven (FREAS mechanical convection oven 625) in the teaching lab or lab 95 to 130C and set fan speed to speed 1 (preheating takes approx. 30 min). Place each disk on a glass Petri plate, cover with glass lid, and place in the oven. Follow the diagram (Figure 2) for the plate placement with the most even heating profile. Remove samples after 7 minutes of heating and allow to cool to room temperature.

III. Imaging samples in BioRad

After cooling, measure the area using the BioRad Imaging Tool in lab 107. Turn on the BioRad and the attached computer. Open GelDoc XR program within the BioRad program. Select EPI WHITE button on the BioRad panel. Place black piece of plastic on imaging area for contrast. Using a ruler, double check that the imaging area is set at zoom level where the width and height are 12cm x 9cm. Adjust zoom on panel if needed. Place Petri plate in the BioRad on the black plastic (Figure 3). In the BioRad software sample window, select Auto Exposure. Once the image stabilizes, select Save Image. Remove sample and place next sample on black plastic. Repeat until all sample images have been collected and saved. The default file format is .lsc, but the Fiji software works better with .tif format. To change format, open each image on the BioRad software, select Export, and select .tif. Transfer all files to another storage device for Fiji analysis.

IV. Measuring area of images

Download the free Fiji software from the website <https://imagej.net/Fiji/Downloads>

To measure the area of one sample:

- Open the TIFF (.tif) format of the photo in Fiji by dragging and dropping image onto the Fiji window. Using the TIFF format of the image transfers the area calibration from the BioRad to Fiji and provide results in units of square inches. If the .lsc format is used, results are in microns. JPEG format doesn't work at all.
- Select Image → Adjust → Threshold (or use command+shift+T). Check the box called "Dark background". Adjust the threshold until the perimeter of the sample matches the pixels set as the threshold for area.
- Select Analyze → Analyze Particles. It sometimes helps Fiji to measure only the cheese area if you adjust Circularity to 0.50-1.00. Select Ok.
- Document the area (in sq. in.) for the cheese sample.
- Repeat for all other photos

V. Analyzing results in RStudio

(See Rmarkdown files called 'melt test stats' for exact RStudio steps.)

Copy duplicate or triplicate values into a tidy file and save in Rstats folder. Open tidy file for one batch in RStudio. Mutate data from character to factor if needed. Run ANOVA relative to age, mixing speed, and hold time. Use `gf_boxplot` to plot the areas relative to each sample. Print off data table, boxplot, and ANOVA results and add to lab notebook.

6.1.3 TA.XT Firmness Analysis Method

Method: Based off ISO/TS 17996 Cheese – Determination of rheological properties by uniaxial compression at constant displacement rate

1. File located under Google Drive Schoenfuss Lab Documents folder → Lab Equipment and Methods → Rheology → “TPA IDF RM 201 Cheese Method”

Equipment

1. Ta.XT2i Texture Analyzer (Texture Technologies Corp., Scarsdale, NY/Stable Microsystems Godalming, UK)
2. Cheese probe: 25.4 mm (1 inch) diameter
3. Cheese base

Cheese sample prep – cutting a 10mm diameter x 15mm height sample

1. Use a #7 corkborer to cut a 10 mm diameter cylinder out of the block. Cut slowly to avoid narrowing of cylinder with too much pressure on cheese block. If it is difficult to obtain a good cylindrical form, use mineral oil of low viscosity (e. g. Vaseline oil) to lubricate the cork borer.
2. Use wire cheese cutter to cut 3-5 mm off of the top surface of the chunk (to adjust for any drying out) and to cut the bottom off to create a sample with height of 15mm
 - a. the height to diameter ratio should fall between 1.1-1.5; $15\text{mm} / 10\text{mm} = 1.5$
3. Cut at least 4 samples from each block and wrap with saran wrap to prevent moisture loss and store at 4°C until testing

Analysis method

1. Move the TPA device into the cooler on a rolling cart and complete all testing in a walk-in cooler at 4°C to minimize warming of samples or temperature variability across samples.
2. Use a double bite compression with a rest period of 2s between the 2 bites
3. Use 25% strain crosshead with 5kg load cell down a vertical column to 75% of their original height using a 25.4 mm cylindrical flat probe (TA-3) with a crosshead speed of 50 mm/min (0.83 mm/s)

Force curve analysis using TA.XT macro

1. Firmness = max force during the first
2. Adhesiveness = Area under the x-axis after first compression (Gunasekaran & Ak, 2002)
3. Springiness = distance recovered by the sample during the time between the end of the first bite and the start of the second bite (originally known as “elasticity”)

Revision history

4/12/19

- changed the size of the cheese cylinder because 1st size (#11 corkborer/15 mm wide x 20mm tall) tried was too big for the probe after it was compressed. The compressed cheese cylinder was wider than the probe, making the force reading by the probe inaccurate. See photo
- eliminated 12-hour room temp equilibration step: samples got too warm overnight
- store samples in cooler until exact sample needs to be tested

6/19/19: test samples in the walk-in cooler

11/15/19: Added “analyzing samples in RStudio” section

6.1.4 CLSM Method

Sample staining

Cheese Protein and Fat Fluorescence Imaging Using Confocal Double Labeling- Nile Red, Fast Green (from UMN University Imaging Centers)

SOLUTION (S):

A: Phosphate Buffer Saline (PBS, Lab Stock)

0.01 M phosphate:	
KH ₂ PO ₄ (monobasic stock, 0.4 M)	3.5 ml
K ₂ HPO ₄ (dibasic stock, 0.4 M)	9.0 ml
150 mM NaCl (4.0 M stock) for PBS only	18.75 ml
Q. S. with n- H ₂ O, pH 7.2	500 ml

B: 1mg/ml Nile Red (Nile Red, Sigma 72485, Lab Stock)

Nile Red	25 mg
100% Methanol	25 ml

C: 10mg/ml Fast Green FCF (Sigma-Aldrich F-7258, Lab Stock)

Fast Green	400 mg
n- H ₂ O, pH 7.2	40 ml

PROTOCOL:

One set of samples control (unstained), and one set experimental (stained). All experiments performed at or below 4°C. Bulk quantities of the FG+AA+PBS and NR+PBS were prepared to add more quickly to each PC sample.

- To experimental set add 10 µl acetic acid, 10 µl Fast Green (protein stain) and 980 µl PBS. Put samples on rocker at 4°C slow speed, 1-3 RPM, for 15 minutes.
- Wash with ice cold PBS twice.
- Remove PBS.
- To experimental and set add 100 µl Nile Red and 900 µl PBS. Put samples on rocker at 4°C slow speed, 1-3 RPM, for 15 minutes.
- Wash with ice cold PBS twice.
- Observe and collect images using confocal microscope.

Sample scanning steps for spectral filters and final image acquisition

Purpose: collecting the 488 laser + 561 laser along each step of prep to ultimately generate background filters for all 8 samples and 1 NR only filter and 1 FG only filter (see 01/07/20 Spectral Filter Development Flow Chart as a reference)

Outline of Method:

- I. Prep samples, fixatives, and stains**
- II. Collect z-scans for spectral filter development**
 - a. Of all 8 fixed samples from this batch**
 - b. Of one fixed + FG-labeled sample (any sample is ok to use)**
 - c. Of one fixed + NR-labeled sample (any sample is ok to use)**
- III. Collect z-series of 8 normally-stained samples x 2 reps each (fixative + FG + NR)**

Detailed Method:

- I. Prep samples, fixatives, and stains**
 - a. Cut samples
 - i. Rinse razor blade with 50-75% EtOH to clean off oils
 - ii. Cut samples to approx. 5mm wide x 5mm long x 2mm tall and store in covered container until ready for use within 1 hour
 - b. Fill insulated ice bucket from ice machine in autoclave room on 2nd floor to use for storing stains and PBS outside of the fridge at ice-cold temps.
 - c. Prep fixative
 - i. (book 2, pg 15; about 1.5 mL needed per sample)
 - ii. To make 5mL of 2% PFA fixative, mix 4.375mL of PBS with 0.625mL of 16% PFA
 - iii. Store in fixative fridge only
 - d. Prep stains
 - i. Fast Green; about 1.5 mL needed per sample; see Book 2, pg 38
 1. Mix 50 μ L acetic acid + 50 μ L FG + 4900 μ L PBS and store in main fridge to keep as cold as possible
 - ii. Nile Red; about 1.5 mL needed per sample; see Book 2, pg 38
 1. Mix 500 μ L of NR (at 10mg/mL conc.) with 4500 μ L PBS and store in main fridge to keep as cold as possible
- II. Collect z-scans of fixed unlabeled samples of all 8 batches**
 - a. Sample prep
 - i. Cut small rectangular sample
 - ii. Incubate in fixative (2% PFA solution + PBS) for 15 min in fixative fridge
 - iii. Wash in PBS for 5 min
 - b. Sample imaging (see Book 2, pg 54)
 - i. Open the *NRFG_spectral* optical configuration
 - ii. Adjust the z-series knob on microscope to find the brightest spot, then adjust gain until spectra lies between 2500-4000 units

- iii. Before collecting image, make sure the collection is only of a z-scan (X & Y lateral plane only) and that the laser is set to channel series, not normal series (might take slightly longer, but better for final spectral development)
- iv. Click “collect” button and double check that a good image was collected (no oversaturated areas)
- v. Repeat steps ii-iv 2-3 times on different areas (X-Y) of same sample
- vi. Repeat steps ii-v on the rest of the 7 different samples

III. Collect z-scan of fixed + FG-labeled sample (any batch is ok to use)

- a. Sample prep
 - i. Cut small rectangular sample
 - ii. Incubate in fixative (2% PFA solution + PBS) for 15 min in fixative fridge
 - iii. Wash in PBS for 5 min
 - iv. Incubate in FG for 20 min
 - v. Wash in PBS for 2.5 min
 - vi. Wash in fresh PBS for 2.5 min again
- b. Sample imaging
 - i. **important** to use 488nm laser for this one

IV. Collect z-scan of fixed + NR-labeled sample (any batch is ok to use)

- a. Sample prep
 - i. Cut small rectangular sample
 - ii. Incubate in fixative (2% PFA solution + PBS) for 15 min in fixative fridge
 - iii. Wash in PBS for 5 min
 - iv. Incubate in NR for 20 min
 - v. Wash in PBS for 2.5 min
 - vi. Wash in fresh PBS for 2.5 min again
- b. Sample imaging
 - i. **important** to use 561nm laser for this one

V. Collect z-series of 8 normally-stained samples x 2 reps each (fixative + FG + NR)

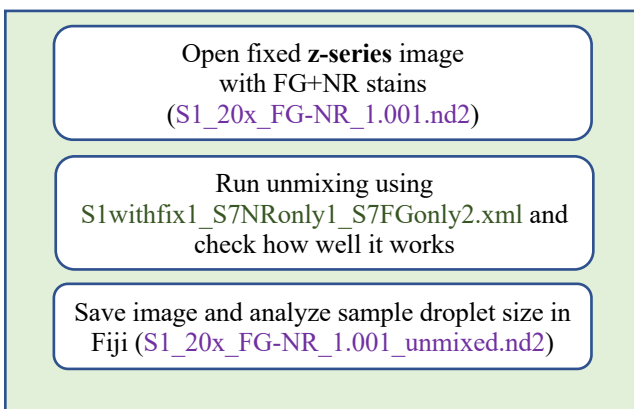
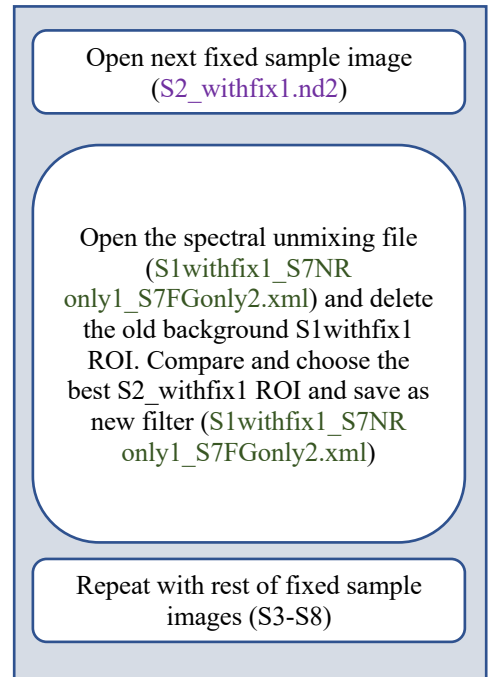
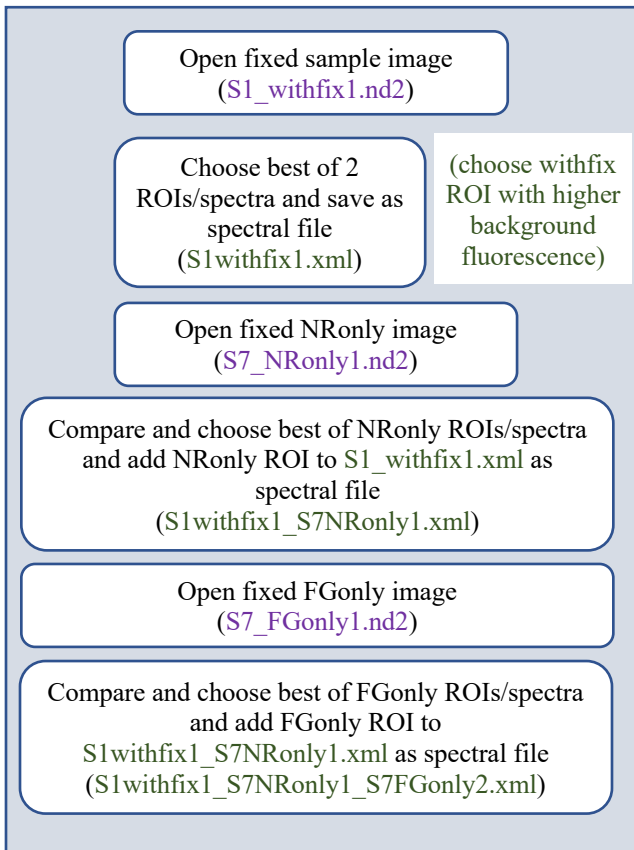
- a. Sample prep
- b. Sample imaging

Flow chart for spectral filter development

(see lab notebook 2, pg 61 for detailed example)

Background info:

3 sections of spectral filter: (z-scans only)	Fixed sample	FG only	NR only
	X 8 cheese samples	X 1 cheese sample	X 1 cheese sample
	X 2 images per sample	X 2 images per sample	X 2 images per sample
	X 1 ROI/spectra per image	X 1 ROI/spectra per image	X multiple ROI/spectra per image



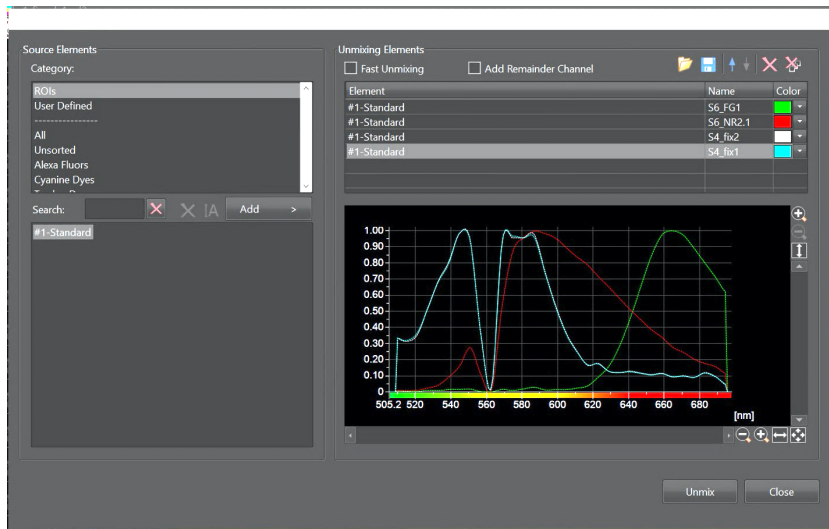
Spectral filter development and application steps

Develop new spectral filters & run filters on 8 normally-stained samples

Develop new spectral filters – see flow chart

Unmix 8 normally-stained samples using new spectral filters

Example combined spectral filter with background, NR, and FG filters.



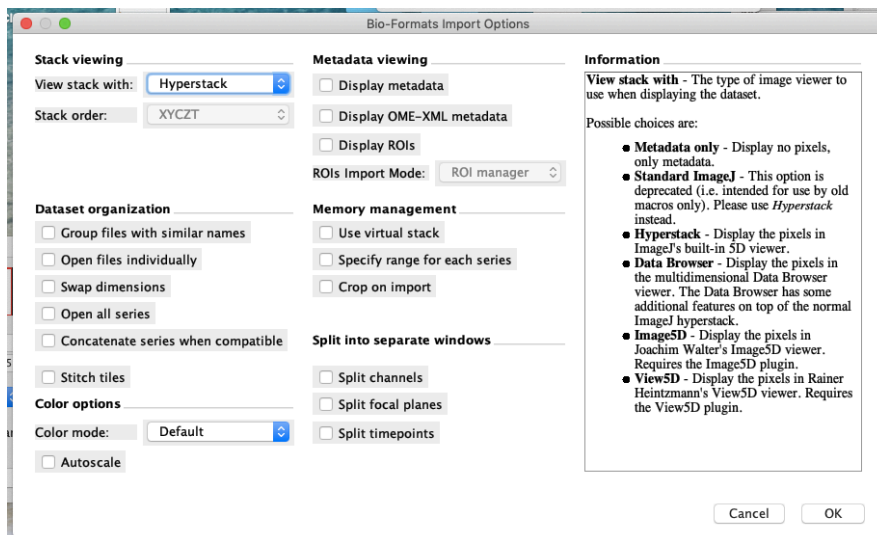
Fiji image adjustment & droplet quantification

General steps:

1. Open original nd2 file
2. Save the lipid channel stack as a tif file with the same name
3. Duplicate the stack, set the threshold to Triangle, and save the image as a new tif with “_ Triangle” added to the end of the file name
4. Duplicate the stack, use the BAR > Remove Individual Pixels tool, and save the image as a new tif with “_RIP” added to the end of the file name
5. Duplicate the stack and change the name to have a 0 in the front to make it easier to select on the watershed split drop-down menu. Run the 3D watershed split tool on the file with “0” at the start of the name using Automatic for seeds and 12 pixels as the radius and save the image as a new tif with “_12pxSplit” added to the end and the “0” removed from the front.
6. Duplicate the stack and use the LUT > Fire filter, save the image as a new tif with “_Fire” added to the end, and verify that the droplets were characterized effectively
7. With the Fire file open, use 3D Objects Counter tool with the Threshold set at 1 and only Objects, Statistics, and Summary boxes checked

Steps for running the macro:

1. Open Fiji/ImageJ
2. Drag the macro into the drag & drop panel
3. Click Run on the macro panel
 - a. The first prompt is to select the directory/folder where you want the output images to go
 - b. The second prompt is to select the original image you want to run (mine is an .Nd2 file)
4. Select *Hyperstack* and uncheck *split channels* on the BioFormats Imports Options
5. All windows remain open and have been saved through the macro until it completes all steps and closes all windows when finished.



Macro code (saved in .ijm file format for Fiji use):

```
/*
 * Macro template to process multiple images in a folder
 */

#@ File (label = "Input directory", style = "directory") input
#@ File (label = "Output directory", style = "directory") output
#@ String (label = "File suffix", value = ".tif") suffix

// See also Process_Folder.py for a version of this code
// in the Python scripting language.

processFolder(input);

// function to scan folders/subfolders/files to find files with correct suffix
function processFolder(input) {
    list = getFileList(input);
    list = Array.sort(list);
    for (i = 0; i < list.length; i++) {
        if(File.isDirectory(input + File.separator + list[i]))
            processFolder(input + File.separator + list[i]);
        if(endsWith(list[i], suffix))
            processFile(input, output, list[i]);}
}

function processFile(input, output, file) {
    // Do the processing here by adding your own code.
    // Leave the print statements until things work, then remove them.
    //@ File(style="directory") outputDirectory
    open();
    name1 = getTitle();
    name2 = "0_File.nameWithoutExtension";
    run("Properties...", "global");
    run("Split Channels");
    selectWindow("C2-" + name1);
        rename(File.nameWithoutExtension);
    saveAs("Tiff", output + "/" + File.nameWithoutExtension + "_488nm" + ".tif");
    run("Duplicate...", "duplicate");
    setAutoThreshold("Default dark stack");
    setOption("BlackBackground", true);
    run("Convert to Mask", "method=Default background=Dark black");
    run("Scale Bar...", "width=100 height=4 font=14 color=White background=None location=[Lower
Right] bold overlay");
    saveAs("Tiff", output + "/" + File.nameWithoutExtension + "_488nm_Default" + ".tif");
    run("Duplicate...", "duplicate");
    run("Remove Isolated Pixels");
    run("Scale Bar...", "width=100 height=4 font=14 color=White background=None location=[Lower
Right] bold overlay");
    saveAs("Tiff", output + "/" + File.nameWithoutExtension + "_488nm_Default_RIP" + ".tif");
    run("Duplicate...", "duplicate");
    run("Median...", "radius=2 stack");
    run("Scale Bar...", "width=100 height=4 font=14 color=White background=None location=[Lower
Right] bold overlay");
    saveAs("Tiff", output + "/" + File.nameWithoutExtension + "_488nm_Default_RIP_MedFilter2" +
".tif");
```



```

run("Duplicate...", "duplicate");
rename("0_ ");
run("3D Watershed Split", "binary=0_ seeds=Automatic radius=12");
saveAs("Tiff", output+"/"+ File.nameWithoutExtension +
"_488nm_Default_RIP_MedFilter2_12pxSplitAuto" + ".tif");
run("Duplicate...", "duplicate");
run("Fire");
rename(File.nameWithoutExtension);
run("Scale Bar...", "width=100 height=4 font=14 color=White background=None location=[Lower
Right] bold overlay");
saveAs("Tiff", output+"/"+ File.nameWithoutExtension +
"_488nm_Default_RIP_MedFilter2_12pxSplitAuto_Fire" + ".tif");
//run("3D Objects Counter", "threshold=1 min.=3 max.=50000000 exclude_objects_on_edges
objects statistics summary");
//rename(File.nameWithoutExtension + "ObjMap.tif");
//saveAs("Tiff", output+"/"+ File.nameWithoutExtension + "ObjMap" + ".tif");
//saveAs("Results", output+"/"+ File.nameWithoutExtension + "Stats.csv");
run("Close All");
print("Processing: " + input + File.separator + file);
print("Saving to: " + output);}

```

6.2 Statistical Analysis R code

6.2.1 R code for two-way ANOVA of Thermomix sample data

```
## opening tidy files & mutating data

Thmx_tidy1 <- read_excel("All_tests_Thmonly_tidy.xlsx", na="na")
Thmx_tidy1 <- mutate_at(Thmx_tidy1, c("MixSpeed_rpm", "HoldTime_min", "Age_months"), factor)
inspect(Thmx_tidy1)

## Running two-way ANOVA of all Viscosity values relative to Age/MS/HT

V40 <- aov(cP_40C_T1 ~ Age_months*MixSpeed_rpm*HoldTime_min, data=Thmx_tidy1)
summary(V40)
##              Df    Sum Sq Mean Sq F value    Pr(>F)
## Age_months    1 10677976 10677976  27.351 2.33e-05 ***
## MixSpeed_rpm  1   414278   414278   1.061  0.313
## HoldTime_min  1    73249    73249   0.188  0.669
## Age_months:MixSpeed_rpm  1    94070    94070   0.241  0.628
## Age_months:HoldTime_min  1   102265   102265   0.262  0.613
## MixSpeed_rpm:HoldTime_min  1    1554     1554   0.004  0.950
## Age_month:MixSpd_rpm:HoldTime_min  1   467786   467786   1.198  0.285
## Residuals    24  9369882   390412
## ---
## Signif. codes:  0 '***' 0.001 '**' 0.01 '*' 0.05 '.' 0.1 ' ' 1

V45 <- aov(cP_45C_T1 ~ Age_months*MixSpeed_rpm*HoldTime_min, data=Thmx_tidy1)
summary(V45)
##              Df    Sum Sq Mean Sq F value    Pr(>F)
## Age_months    1 7191410 7191410  32.178 7.66e-06 ***
## MixSpeed_rpm  1  418984  418984   1.875  0.184
## HoldTime_min  1  171899  171899   0.769  0.389
## Age_months:MixSpeed_rpm  1    6958    6958   0.031  0.861
## Age_months:HoldTime_min  1    90166   90166   0.403  0.531
## MixSpeed_rpm:HoldTime_min  1    1605    1605   0.007  0.933
## Age_months:MixSpeed_rpm:HoldTime_min  1  134664  134664   0.603  0.445
## Residuals    24 5363640  223485
## ---
## Signif. codes:  0 '***' 0.001 '**' 0.01 '*' 0.05 '.' 0.1 ' ' 1

V50 <- aov(cP_50C_T1 ~ Age_months*MixSpeed_rpm*HoldTime_min, data=Thmx_tidy1)
summary(V50)
##              Df    Sum Sq Mean Sq F value    Pr(>F)
## Age_months    1 2590088 2590088  29.822 1.3e-05 ***
## MixSpeed_rpm  1   94178   94178   1.084  0.308
## HoldTime_min  1   25425   25425   0.293  0.593
## Age_months:MixSpeed_rpm  1    6498    6498   0.075  0.787
## Age_months:HoldTime_min  1   46665   46665   0.537  0.471
## MixSpeed_rpm:HoldTime_min  1   20910   20910   0.241  0.628
## Age_months:MixSpeed_rpm:HoldTime_min  1   59340   59340   0.683  0.417
## Residuals    24 2084409   86850
## ---
## Signif. codes:  0 '***' 0.001 '**' 0.01 '*' 0.05 '.' 0.1 ' ' 1
```

```

## running ANOVA of all melt area values relative to age/MS/HT

Area <- aov(Area_T1 ~ Age_months*MixSpeed_rpm*HoldTime_min, data=Thmx_tidy1)
summary(Area)

##
##           Df Sum Sq Mean Sq F value Pr(>F)
## Age_months      1    0.50   0.5046   0.175  0.681
## MixSpeed_rpm     1    2.48   2.4766   0.858  0.368
## HoldTime_min     1    0.46   0.4625   0.160  0.694
## Age_months:MixSpeed_rpm      1    0.42   0.4167   0.144  0.709
## Age_months:HoldTime_min      1    0.07   0.0704   0.024  0.878
## MixSpeed_rpm:HoldTime_min     1    0.02   0.0179   0.006  0.938
## Age_months:MixSpeed_rpm:HoldTime_min  1    0.24   0.2406   0.083  0.776
## Residuals          16  46.16   2.8848
## 8 observations deleted due to missingness

## running ANOVA of all firmness values relative to age/MS/HT

Firmness <- aov(Firmness_T1 ~ Age_months*MixSpeed_rpm*HoldTime_min, data=Thmx_tidy1)
summary(Firmness)

##
##           Df Sum Sq Mean Sq F value Pr(>F)
## Age_months      1  19463  19463   1.369  0.276
## MixSpeed_rpm     1  21989  21989   1.547  0.249
## HoldTime_min     1   2265   2265   0.159  0.700
## Age_months:MixSpeed_rpm      1   1302   1302   0.092  0.770
## Age_months:HoldTime_min      1   8677   8677   0.610  0.457
## MixSpeed_rpm:HoldTime_min     1   1178   1178   0.083  0.781
## Age_months:MixSpeed_rpm:HoldTime_min  1  10616  10616   0.747  0.413
## Residuals          8 113738  14217
## 16 observations deleted due to missingness

## mutating code for making new block for age (all 3 properties)

tmpvisc <- Thmx_tidy1 %>% select(Prod_Date, Age_months, MixSpeed_rpm, HoldTime_min, starts_with("cP")) %>%
  mutate(Sample=1:n()) %>%
  pivot_longer(starts_with("cP"), names_to=c("X")) %>%
  select(-X)

tmpmelt <- Thmx_tidy1 %>% select(Prod_Date, Age_months, MixSpeed_rpm, HoldTime_min, starts_with("Area")) %>%
  mutate(Sample=1:n()) %>%
  pivot_longer(starts_with("Area"), names_to=c("X")) %>%
  select(-X)

tmpfirmness <- Thmx_tidy1 %>% select(Prod_Date, Age_months, MixSpeed_rpm, HoldTime_min, starts_with("Firmness")) %>%
  mutate(Sample=1:n()) %>%
  pivot_longer(starts_with("Firmness"), names_to=c("X")) %>%
  select(-X)

```

6.2.2 R code for graphs of Thermomix sample data

```
## final graphs to use

## viscosity
ggplot(tmpvisc) + aes(MixSpeed_rpm, value, color=HoldTime_min, group=HoldTime_min) +
  facet_grid(Temp ~ Age_months, labeller = labeller(Age_months = label_both))
+
  geom_point(position=position_dodge(width=0.5)) +
  xlab("Mixing Speed (rpm)") + ylab("Viscosity (cP)") +
  scale_color_manual(values=c("#003366", "#6699CC")) +
  stat_summary(position=position_dodge(width=0.5), fun.data=mean_se, fun.args=
list(mult=1),
  geom="errorbar", color="#000000", width=0.2, size=0.3) +
  stat_summary(position=position_dodge(width=0.5), fun=mean, geom="point",
  color="#000000", size=2, shape=4)

## melt area
ggplot(tmpmelt) + aes(MixSpeed_rpm, value, color=HoldTime_min, group=HoldTime_min) +
  facet_grid(MixSpeed_rpm ~ Age_months) +
  geom_point(position=position_dodge(width=0.5)) +
  xlab("Mixing Speed (rpm)") + ylab("Melt Area (sq in)") +
  facet_grid(cols = vars(Age_months), labeller = label_both) +
  scale_color_manual(values=c("#003366", "#6699CC")) +
  stat_summary(position=position_dodge(width=0.5), fun.data=mean_se, fun.args=
list(mult=1),
  geom="errorbar", color="#000000", width=0.2, size=0.3) +
  stat_summary(position=position_dodge(width=0.5), fun=mean, geom="point",
  color="#000000", size=2, shape=4)

## Warning: Removed 8 rows containing non-finite values (stat_summary).
## Warning: Removed 8 rows containing non-finite values (stat_summary).
## Warning: Removed 8 rows containing missing values (geom_point).

## firmness
ggplot(tmpfirmness) + aes(MixSpeed_rpm, value, color=HoldTime_min, group=HoldTime_min) +
  facet_grid(MixSpeed_rpm ~ Age_months) +
  geom_point(position=position_dodge(width=0.5)) +
  xlab("Mixing Speed (rpm)") + ylab("Firmness (g)") +
  facet_grid(cols = vars(Age_months), labeller = label_both) +
  scale_color_manual(values=c("#003366", "#6699CC")) +
  stat_summary(position=position_dodge(width=0.5), fun.data=mean_se, fun.args=
list(mult=1),
  geom="errorbar", color="#000000", width=0.2, size=0.3) +
  stat_summary(position=position_dodge(width=0.5), fun=mean, geom="point",
  color="#000000", size=2, shape=4)

## Warning: Removed 16 rows containing non-finite values (stat_summary).
## Warning: Removed 16 rows containing non-finite values (stat_summary).
## Warning: Removed 16 rows containing missing values (geom_point).
```

6.2.3 R code for split-plot ANOVA of Blentech sample data

```
## Opening tidy files & mutating data

Bl_tidy2 <- read_excel("All_tests_Blentechonly2020_tidy.xlsx", na="na")
Bl_tidy2 <- mutate_at(Bl_tidy2, c("MS", "HoldTime_min", "Age_months"), factor)
inspect(Bl_tidy2)

## Running split-plot ANOVA of all Viscosity values relative to Age/MS/HT/preblend

V402wks <- aov(cP_40C_2wks ~ Age_months*MS*HoldTime_min + Error(Mfg_Date/Preblend), data=Bl_tidy2)
summary(V402wks)

##
## Error: Mfg_Date
##           Df Sum Sq Mean Sq F value Pr(>F)
## Residuals  1 127985  127985
##
## Error: Mfg_Date:Preblend
##           Df  Sum Sq Mean Sq F value Pr(>F)
## Age_months  1 10353915 10353915  6.807 0.0797 .
## MS          1  1490231  1490231  0.980 0.3952
## Age_months:MS  1  793436  793436  0.522 0.5223
## Residuals    3  4563034  1521011
## ---
## Signif. codes:  0 '***' 0.001 '**' 0.01 '*' 0.05 '.' 0.1 ' ' 1
##
## Error: Within
##           Df Sum Sq Mean Sq F value Pr(>F)
## HoldTime_min  1  3570  3570  0.115 0.752
## Age_months:HoldTime_min  1  8510  8510  0.274 0.628
## MS:HoldTime_min  1  27973  27973  0.900 0.396
## Age_months:MS:HoldTime_min  1  70889  70889  2.281 0.205
## Residuals    4 124300  31075

V452wks <- aov(cP_45C_2wks ~ Age_months*MS*HoldTime_min + Error(Mfg_Date/Preblend), data=Bl_tidy2)
summary(V452wks)

##
## Error: Mfg_Date
##           Df Sum Sq Mean Sq F value Pr(>F)
## Residuals  1  8603  8603
##
## Error: Mfg_Date:Preblend
##           Df  Sum Sq Mean Sq F value Pr(>F)
## Age_months  1 2754770 2754770  5.403 0.103
## MS          1  586373  586373  1.150 0.362
## Age_months:MS  1  334373  334373  0.656 0.477
## Residuals    3 1529532  509844
##
## Error: Within
##           Df Sum Sq Mean Sq F value Pr(>F)
```

```

## HoldTime_min          1    390    390  0.034  0.862
## Age_months:HoldTime_min  1   6602   6602  0.581  0.488
## MS:HoldTime_min        1   7439   7439  0.655  0.464
## Age_months:MS:HoldTime_min  1  30888  30888  2.719  0.174
## Residuals              4  45434  11358

V502wks <- aov(cP_50C_2wks ~ Age_months*MS*HoldTime_min + Error(Mfg_Date/Preblend), data=Bl_tidy2)
summary(V502wks)

##
## Error: Mfg_Date
##           Df Sum Sq Mean Sq F value Pr(>F)
## Residuals  1  44838   44838
##
## Error: Mfg_Date:Preblend
##           Df Sum Sq Mean Sq F value Pr(>F)
## Age_months  1 1503689 1503689  4.606  0.121
## MS          1  521645  521645  1.598  0.296
## Age_months:MS  1  221135  221135  0.677  0.471
## Residuals    3  979484  326495
##
## Error: Within
##           Df Sum Sq Mean Sq F value Pr(>F)
## HoldTime_min  1   2783    2783  0.713  0.446
## Age_months:HoldTime_min  1   2475    2475  0.634  0.471
## MS:HoldTime_min  1     5     5  0.001  0.973
## Age_months:MS:HoldTime_min  1   6683    6683  1.712  0.261
## Residuals     4  15619    3905

V404wks <- aov(cP_40C_4wks ~ Age_months*MS*HoldTime_min + Error(Mfg_Date/Preblend), data=Bl_tidy2)
summary(V404wks)

##
## Error: Mfg_Date
##           Df Sum Sq Mean Sq F value Pr(>F)
## Residuals  1   2970    2970
##
## Error: Mfg_Date:Preblend
##           Df Sum Sq Mean Sq F value Pr(>F)
## Age_months  1 10807656 10807656 13.255 0.0357 *
## MS          1  824464  824464  1.011 0.3887
## Age_months:MS  1  2053489  2053489  2.518 0.2107
## Residuals    3  2446162  815387
## ---
## Signif. codes:  0 '***' 0.001 '**' 0.01 '*' 0.05 '.' 0.1 ' ' 1
##
## Error: Within
##           Df Sum Sq Mean Sq F value Pr(>F)
## HoldTime_min  1  17822   17822  0.183 0.6904
## Age_months:HoldTime_min  1 109230  109230  1.125 0.3487
## MS:HoldTime_min  1    289    289  0.003 0.9591
## Age_months:MS:HoldTime_min  1 877969  877969  9.039 0.0397 *
## Residuals     4 388508   97127

```

```

## ---
## Signif. codes:  0 '***' 0.001 '**' 0.01 '*' 0.05 '.' 0.1 ' ' 1

V454wks <- aov(cP_45C_4wks ~ Age_months*MS*HoldTime_min + Error(Mfg_Date/Preblend), data=B1_tidy2)
summary(V454wks)

##
## Error: Mfg_Date
##           Df Sum Sq Mean Sq F value Pr(>F)
## Residuals  1  4422     4422
##
## Error: Mfg_Date:Preblend
##           Df  Sum Sq Mean Sq F value Pr(>F)
## Age_months  1 2168256 2168256  10.327 0.0488 *
## MS          1  197136  197136   0.939 0.4040
## Age_months:MS  1  537289  537289   2.559 0.2080
## Residuals    3  629888  209963
## ---
## Signif. codes:  0 '***' 0.001 '**' 0.01 '*' 0.05 '.' 0.1 ' ' 1
##
## Error: Within
##           Df Sum Sq Mean Sq F value Pr(>F)
## HoldTime_min  1   7656     7656   0.255 0.6402
## Age_months:HoldTime_min  1  10100     10100   0.336 0.5931
## MS:HoldTime_min  1  14884     14884   0.496 0.5203
## Age_months:MS:HoldTime_min  1 161604    161604   5.380 0.0812 .
## Residuals     4 120142     30035
## ---
## Signif. codes:  0 '***' 0.001 '**' 0.01 '*' 0.05 '.' 0.1 ' ' 1

V504wks <- aov(cP_50C_4wks ~ Age_months*MS*HoldTime_min + Error(Mfg_Date/Preblend), data=B1_tidy2)
summary(V504wks)

##
## Error: Mfg_Date
##           Df Sum Sq Mean Sq F value Pr(>F)
## Residuals  1 26406     26406
##
## Error: Mfg_Date:Preblend
##           Df  Sum Sq Mean Sq F value Pr(>F)
## Age_months  1 1068122 1068122  10.431 0.0482 *
## MS          1  12321   12321   0.120 0.7516
## Age_months:MS  1   81796   81796   0.799 0.4373
## Residuals    3  307196  102399
## ---
## Signif. codes:  0 '***' 0.001 '**' 0.01 '*' 0.05 '.' 0.1 ' ' 1
##
## Error: Within
##           Df Sum Sq Mean Sq F value Pr(>F)
## HoldTime_min  1  12100     12100   1.582 0.27696
## Age_months:HoldTime_min  1    256     256   0.033 0.86376
## MS:HoldTime_min  1   1056     1056   0.138 0.72907
## Age_months:MS:HoldTime_min  1 177662    177662  23.221 0.00853 **

```

```

## Residuals          4  30604   7651
## ---
## Signif. codes:  0 '***' 0.001 '**' 0.01 '*' 0.05 '.' 0.1 ' ' 1

## Running split-plot ANOVA of all Melt Area values relative to Age/MS/HT/preblend

A2wks <- aov(Area_2wks ~ Age_months*MS*HoldTime_min + Error(Mfg_Date/Preblend), data=B1_tidy2)
summary(A2wks)

##
## Error: Mfg_Date
##           Df Sum Sq Mean Sq F value Pr(>F)
## Residuals  1 0.01257 0.01257
##
## Error: Mfg_Date:Preblend
##           Df Sum Sq Mean Sq F value Pr(>F)
## Age_months  1 1.8499  1.8499   4.414 0.1264
## MS          1 2.8978  2.8978   6.914 0.0784 .
## Age_months:MS 1 0.4513  0.4513   1.077 0.3757
## Residuals   3 1.2573  0.4191
## ---
## Signif. codes:  0 '***' 0.001 '**' 0.01 '*' 0.05 '.' 0.1 ' ' 1
##
## Error: Within
##           Df Sum Sq Mean Sq F value Pr(>F)
## HoldTime_min  1 0.0737  0.07369   0.818 0.417
## Age_months:HoldTime_min  1 0.0397  0.03972   0.441 0.543
## MS:HoldTime_min  1 0.2318  0.23180   2.573 0.184
## Age_months:MS:HoldTime_min  1 0.0474  0.04736   0.526 0.509
## Residuals     4 0.3604  0.09009

A4wks <- aov(Area_4wks ~ Age_months*MS*HoldTime_min + Error(Mfg_Date/Preblend), data=B1_tidy2)
summary(A4wks)

##
## Error: Mfg_Date
##           Df Sum Sq Mean Sq F value Pr(>F)
## Residuals  1  1.382   1.382
##
## Error: Mfg_Date:Preblend
##           Df Sum Sq Mean Sq F value Pr(>F)
## Age_months  1 0.3945  0.3945   2.342 0.223
## MS          1 0.6505  0.6505   3.862 0.144
## Age_months:MS 1 0.0234  0.0234   0.139 0.734
## Residuals   3 0.5053  0.1684
##
## Error: Within
##           Df Sum Sq Mean Sq F value Pr(>F)
## HoldTime_min  1 0.01068 0.01068   0.737 0.4391
## Age_months:HoldTime_min  1 0.01977 0.01977   1.364 0.3077
## MS:HoldTime_min  1 0.08373 0.08373   5.776 0.0741 .
## Age_months:MS:HoldTime_min  1 0.00120 0.00120   0.083 0.7878

```



```

## Residuals          4 0.05799 0.01450
## ---
## Signif. codes:  0 '***' 0.001 '**' 0.01 '*' 0.05 '.' 0.1 ' ' 1

## Running split-plot ANOVA of all Firmness values relative to Age/MS/HT/preblend

F2wks <- aov(Firmness_2wks ~ Age_months*MS*HoldTime_min + Error(Mfg_Date/Preblend), data=Bl_tidy2)
summary(F2wks)

##
## Error: Mfg_Date
##           Df Sum Sq Mean Sq F value Pr(>F)
## Residuals  1 10809  10809
##
## Error: Mfg_Date:Preblend
##           Df Sum Sq Mean Sq F value Pr(>F)
## Age_months  1 461415  461415  24.484 0.0158 *
## MS          1 122232  122232   6.486 0.0842 .
## Age_months:MS  1  11933   11933   0.633 0.4843
## Residuals    3  56537   18846
## ---
## Signif. codes:  0 '***' 0.001 '**' 0.01 '*' 0.05 '.' 0.1 ' ' 1
##
## Error: Within
##           Df Sum Sq Mean Sq F value Pr(>F)
## HoldTime_min  1   3819    3819   0.170 0.702
## Age_months:HoldTime_min  1    441    441   0.020 0.896
## MS:HoldTime_min  1 16669  16669   0.740 0.438
## Age_months:MS:HoldTime_min  1 42128  42128   1.871 0.243
## Residuals     4  90088   22522

F4wks <- aov(Firmness_4wks ~ Age_months*MS*HoldTime_min + Error(Mfg_Date/Preblend), data=Bl_tidy2)
summary(F4wks)

##
## Error: Mfg_Date
##           Df Sum Sq Mean Sq F value Pr(>F)
## Residuals  1 28779  28779
##
## Error: Mfg_Date:Preblend
##           Df Sum Sq Mean Sq F value Pr(>F)
## Age_months  1  47517   47517   0.525 0.521
## MS          1 194670  194670   2.152 0.239
## Age_months:MS  1  72249   72249   0.799 0.437
## Residuals    3 271321   90440
##
## Error: Within
##           Df Sum Sq Mean Sq F value Pr(>F)
## HoldTime_min  1  29840   29840   0.927 0.390
## Age_months:HoldTime_min  1 42360  42360   1.316 0.315
## MS:HoldTime_min  1   110    110   0.003 0.956

```

```

## Age_months:MS:HoldTime_min 1 15611 15611 0.485 0.525
## Residuals 4 128775 32194

## Running split-plot ANOVA of all Confocal values relative to Age/MS/HT/preblend
end

Con1 <- aov(Cf_Number_of_droplets ~ Age_months*MS*HoldTime_min + Error(Mfg_Date/Preblend), data=Bl_tidy2)
summary(Con1)

##
## Error: Mfg_Date
## Df Sum Sq Mean Sq F value Pr(>F)
## Residuals 1 97906 97906
##
## Error: Mfg_Date:Preblend
## Df Sum Sq Mean Sq F value Pr(>F)
## Age_months 1 511 511 0.026 0.883
## MS 1 22922 22922 1.151 0.362
## Age_months:MS 1 8761 8761 0.440 0.555
## Residuals 3 59743 19914
##
## Error: Within
## Df Sum Sq Mean Sq F value Pr(>F)
## HoldTime_min 1 77618 77618 3.753 0.125
## Age_months:HoldTime_min 1 19210 19210 0.929 0.390
## MS:HoldTime_min 1 10120 10120 0.489 0.523
## Age_months:MS:HoldTime_min 1 75295 75295 3.641 0.129
## Residuals 4 82726 20682

Con2 <- aov(Cf_Avg_Vol ~ Age_months*MS*HoldTime_min + Error(Mfg_Date/Preblend), data=Bl_tidy2)
summary(Con2)

##
## Error: Mfg_Date
## Df Sum Sq Mean Sq F value Pr(>F)
## Residuals 1 180735 180735
##
## Error: Mfg_Date:Preblend
## Df Sum Sq Mean Sq F value Pr(>F)
## Age_months 1 3426367 3426367 6.246 0.0878 .
## MS 1 2174522 2174522 3.964 0.1406
## Age_months:MS 1 666484 666484 1.215 0.3509
## Residuals 3 1645762 548587
## ---
## Signif. codes: 0 '***' 0.001 '**' 0.01 '*' 0.05 '.' 0.1 ' ' 1
##
## Error: Within
## Df Sum Sq Mean Sq F value Pr(>F)
## HoldTime_min 1 3244 3244 0.023 0.8870
## Age_months:HoldTime_min 1 694145 694145 4.904 0.0912 .
## MS:HoldTime_min 1 223279 223279 1.577 0.2775
## Age_months:MS:HoldTime_min 1 29564 29564 0.209 0.6714
## Residuals 4 566186 141546

```

```

## ---
## Signif. codes:  0 '***' 0.001 '**' 0.01 '*' 0.05 '.' 0.1 ' ' 1

Con3 <- aov(Cf_Avg_FeretDiam ~ Age_months*MS*HoldTime_min + Error(Mfg_Date/Pre
blend), data=Bl_tidy2)
summary(Con3)

##
## Error: Mfg_Date
##           Df Sum Sq Mean Sq F value Pr(>F)
## Residuals  1  51.81   51.81
##
## Error: Mfg_Date:Preblend
##           Df Sum Sq Mean Sq F value Pr(>F)
## Age_months  1  17.22   17.22  0.795  0.438
## MS          1  35.45   35.45  1.637  0.291
## Age_months:MS  1   3.43    3.43  0.158  0.717
## Residuals    3  64.96   21.65
##
## Error: Within
##           Df Sum Sq Mean Sq F value Pr(>F)
## HoldTime_min  1   7.95    7.95  0.614  0.477
## Age_months:HoldTime_min  1  32.21   32.21  2.485  0.190
## MS:HoldTime_min  1  25.76   25.76  1.988  0.231
## Age_months:MS:HoldTime_min  1 125.10  125.10  9.652  0.036 *
## Residuals     4  51.84   12.96
## ---
## Signif. codes:  0 '***' 0.001 '**' 0.01 '*' 0.05 '.' 0.1 ' ' 1

Con4 <- aov(Cf_Median_FeretDiam ~ Age_months*MS*HoldTime_min + Error(Mfg_Date/
Preblend), data=Bl_tidy2)
summary(Con4)

##
## Error: Mfg_Date
##           Df Sum Sq Mean Sq F value Pr(>F)
## Residuals  1  62.91   62.91
##
## Error: Mfg_Date:Preblend
##           Df Sum Sq Mean Sq F value Pr(>F)
## Age_months  1  13.49   13.49  0.303  0.620
## MS          1 102.79  102.79  2.309  0.226
## Age_months:MS  1   1.60    1.60  0.036  0.862
## Residuals    3 133.57   44.52
##
## Error: Within
##           Df Sum Sq Mean Sq F value Pr(>F)
## HoldTime_min  1  65.01   65.01  4.664 0.0969 .
## Age_months:HoldTime_min  1  43.10   43.10  3.092 0.1535
## MS:HoldTime_min  1  39.45   39.45  2.830 0.1678
## Age_months:MS:HoldTime_min  1 111.51  111.51  7.999 0.0474 *
## Residuals     4  55.76   13.94
## ---
## Signif. codes:  0 '***' 0.001 '**' 0.01 '*' 0.05 '.' 0.1 ' ' 1

```

6.2.4 R code for graphs of Blentech data

```
## opening files and mutating data

Bl_tidy2 <- read_excel("All_tests_Blentechonly2020_tidy.xlsx", na="na")
Bl_tidy2 <- mutate_at(Bl_tidy2, c("MS", "MS_rpm", "HoldTime_min", "Age_months"), factor)
inspect(Bl_tidy2)

## mutating code for ggplots

tmpvisc <- Bl_tidy2 %>% select(Mfg_Date, Preblend, Age_months, MS_rpm, HoldTime_min, starts_with("cP")) %>%
  mutate(Sample=1:n()) %>%
  pivot_longer(starts_with("cP"), names_to=c("X", "Temp", "ShelfLife"), names_sep="_") %>%
  select(-X)

tmpmelt <- Bl_tidy2 %>% select(Mfg_Date, Preblend, Age_months, MS_rpm, HoldTime_min, starts_with("Area")) %>%
  mutate(Sample=1:n()) %>%
  pivot_longer(starts_with("Area"), names_to=c("X", "ShelfLife"), names_sep="_") %>%
  select(-X)

tmpfirmness <- Bl_tidy2 %>% select(Mfg_Date, Preblend, Age_months, MS_rpm, HoldTime_min, starts_with("Firmness")) %>%
  mutate(Sample=1:n()) %>%
  pivot_longer(starts_with("Firmness"), names_to=c("X", "ShelfLife"), names_sep="_") %>%
  select(-X)

tmp2confocal <- Bl_tidy2

## making ggplots with tmp datasets / final graph to use

## Viscosity
ggplot(tmpvisc) + aes(MS_rpm, value, color=HoldTime_min, group=HoldTime_min) +
  facet_grid(Temp + ShelfLife ~ Age_months, labeller = labeller(Age_months = label_both)) +
  geom_point(position=position_dodge(width=0.5)) +
  xlab("Mixing Speed (rpm)") + ylab("Viscosity (cP)") +
  scale_color_manual(values=c("#000000", "#999999"))

## MeltArea
ggplot(tmpmelt) + aes(MS_rpm, value, color=HoldTime_min, group=HoldTime_min) +
  facet_grid(ShelfLife ~ Age_months, labeller = labeller(Age_months = label_both)) +
  geom_point(position=position_dodge(width=0.25)) +
  xlab("Mixing Speed (rpm)") + ylab("Melt Area (sq in)") +
  scale_color_manual(values=c("#000000", "#999999"))

## Firmness
ggplot(tmpfirmness) + aes(MS_rpm, value, color=HoldTime_min, group=HoldTime_min) +
  facet_grid(ShelfLife ~ Age_months, labeller = labeller(Age_months = label_both)) +
```

```

geom_point(position=position_dodge(width=0.25)) +
xlab("Mixing Speed (rpm)") + ylab("Firmness (g)") +
scale_color_manual(values=c("#000000", "#999999"))

## CONFOCAL graphs

## Number of droplets
ggplot(tmp2confocal, aes(x=MS_rpm, y=Cf_Number_of_droplets, color=HoldTime_min
)) + facet_grid(MS_rpm ~ Age_months) +
geom_point(position=position_dodge(width=0.5)) +
xlab("Mixing Speed (rpm)") + ylab("Number of Fat Droplets") +
facet_grid(cols = vars(Age_months), labeller = label_both) +
scale_color_manual(values=c("#000000", "#999999"))

## Average Fat Droplet Volume
ggplot(tmp2confocal, aes(x=MS_rpm, y=Cf_Avg_Vol, color=HoldTime_min)) +
facet_grid(MS_rpm ~ Age_months) +
geom_point(position=position_dodge(width=0.5)) +
xlab("Mixing Speed (rpm)") + ylab("Avg Volume ( $\mu\text{m}^2$ )") +
facet_grid(cols = vars(Age_months), labeller = label_both) +
scale_color_manual(values=c("#000000", "#999999"))

## Average Fat Droplet Feret Diameter
ggplot(tmp2confocal, aes(x=MS_rpm, y=Cf_Avg_FeretDiam, color=HoldTime_min)) +
facet_grid(MS_rpm ~ Age_months) +
geom_point(position=position_dodge(width=0.5)) +
xlab("Mixing Speed (rpm)") + ylab("Avg Feret Diameter ( $\mu\text{m}$ )") +
facet_grid(cols = vars(Age_months), labeller = label_both) +
scale_color_manual(values=c("#000000", "#999999"))

## Median Fat Droplet Feret Diameter
ggplot(tmp2confocal, aes(x=MS_rpm, y=Cf_Median_FeretDiam, color=HoldTime_min))
+
facet_grid(MS_rpm ~ Age_months) +
geom_point(position=position_dodge(width=0.5)) +
xlab("Mixing Speed (rpm)") + ylab("Median Feret Diameter ( $\mu\text{m}$ )") +
facet_grid(cols = vars(Age_months), labeller = label_both) +
scale_color_manual(values=c("#000000", "#999999"))

## Graphs of significant interactions

## viscosity 40C T2
tmpvisc_40ct2 <- tmpvisc %>% filter(Temp == "40C", ShelfLife == "4wks")
tmpvisc_40ct2.1 <- tmpvisc_40ct2 %>% group_by(Preblend, HoldTime_min) %>% muta
te(meanvalue = mean(value))

ggplot(tmpvisc_40ct2.1) + aes(MS_rpm, meanvalue, color=HoldTime_min, group=Hol
dTime_min) +
facet_grid(Temp ~ Age_months, labeller = labeller(Age_months = label_both))
+
geom_line() +
geom_point(position=position_dodge(width=0.5)) +
xlab("Mixing Speed (rpm)") + ylab("Viscosity (cP) at 40C (T2)") +
scale_color_manual(values=c("#000000", "#999999"))

```

```

## viscosity 50C T2
tmpvisc_50ct2 <- tmpvisc %>% filter(Temp == "50C", ShelfLife == "4wks")
tmpvisc_50ct2.1 <- tmpvisc_50ct2 %>% group_by(Preblend, HoldTime_min) %>% muta
te(meanvalue = mean(value))

ggplot(tmpvisc_50ct2.1) + aes(MS_rpm, meanvalue, color=HoldTime_min, group=Hol
dTime_min) +
  facet_grid(Temp ~ Age_months, labeller = labeller(Age_months = label_both))
+
  geom_line() +
  geom_point(position=position_dodge(width=0.5)) +
  xlab("Mixing Speed (rpm)") + ylab("Viscosity (cP) at 50C (T2)") +
  scale_color_manual(values=c("#000000", "#999999"))

## CLSM avg feret diam
tmp2confocal2.1 <- tmp2confocal %>% group_by(Preblend, HoldTime_min) %>% mutat
e(meanAFD = mean(Cf_Avg_FeretDiam))

ggplot(tmp2confocal2.1, aes(x=MS_rpm, y=meanAFD, color=HoldTime_min)) +
  facet_grid(MS_rpm ~ Age_months) +
  geom_line(aes(group=HoldTime_min)) +
  geom_point(position=position_dodge(width=0.5)) +
  xlab("Mixing Speed (rpm)") + ylab("Avg Feret Diameter (µm)") +
  facet_grid(cols = vars(Age_months), labeller = label_both) +
  scale_color_manual(values=c("#000000", "#999999"))

## CLSM median feret diam
tmp2confocal2.2 <- tmp2confocal %>% group_by(Preblend, HoldTime_min) %>% mutat
e(meanMFD = mean(Cf_Median_FeretDiam))

ggplot(tmp2confocal2.2, aes(x=MS_rpm, y=meanMFD, color=HoldTime_min)) +
  facet_grid(MS_rpm ~ Age_months) +
  geom_line(aes(group=HoldTime_min)) +
  geom_point(position=position_dodge(width=0.5)) +
  xlab("Mixing Speed (rpm)") + ylab("Median Feret Diameter (µm)") +
  facet_grid(cols = vars(Age_months), labeller = label_both) +
  scale_color_manual(values=c("#000000", "#999999"))

```

6.3 Supplemental NIR tools

● Near Infrared Table

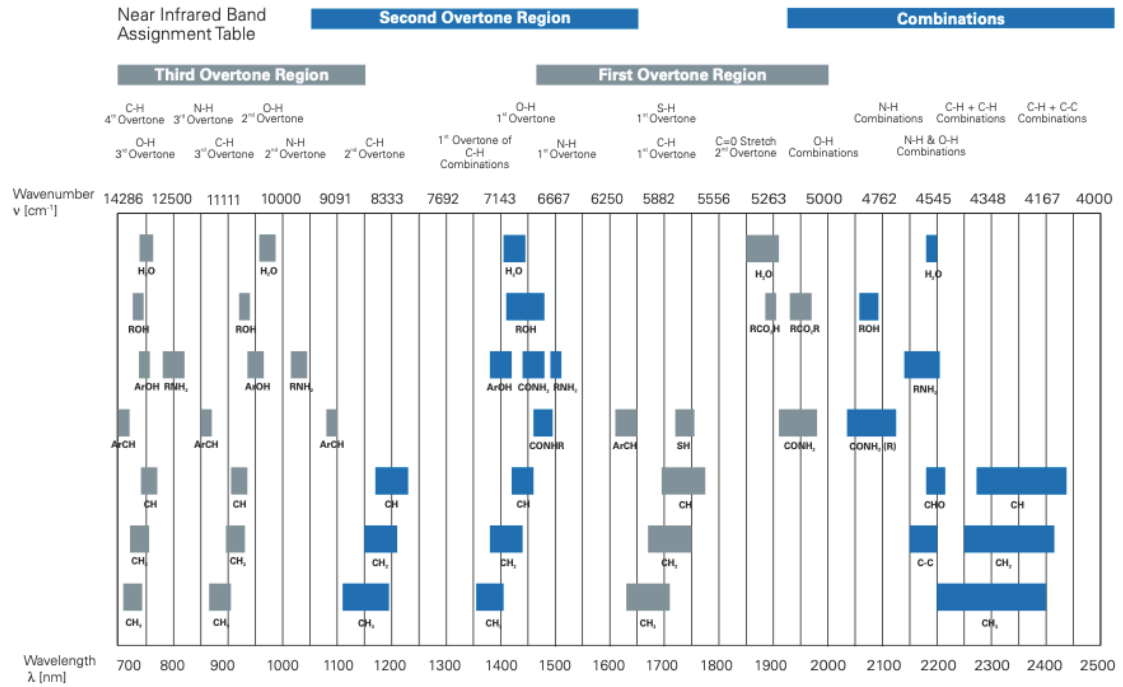


Figure 81. NIR Band Assignment Table (Bruker, 2009)